Behaviour of Fibre Composite Sandwich Structures: *A case study on railway sleeper application*

By

Allan Manalo

Supervised by

Assoc. Prof. Thiru Aravinthan

Assoc. Prof. Karu Karunasena

A dissertation submitted for the award of

DOCTOR OF PHILOSOPHY

Centre of Excellence in Engineered Fibre Composites

Faculty of Engineering and Surveying

University of Southern Queensland

Toowoomba, Queensland, Australia

February 2011

Abstract

Timber is the most widely used material for railway sleepers; however, as a sleeper material it deteriorates with time and needs appropriate replacement. Hardwood timber for railway sleepers is becoming more expensive, less available and of inferior quality compared to the timber previously available. This problem is accentuated in railway turnouts where larger, longer, stronger and more expensive timber is required. Research has therefore focused on the possibility of fibre composites replacing timber as the many issues related to the currently used sleeper materials could be simulated using this material.

This study is the first to investigate the concept of glue-laminated composite sandwich beams for railway turnout sleepers. The building block of this innovative beam is a novel composite sandwich structure made up of glass fibre composite skins and modified phenolic core material that has been specifically developed for civil engineering applications. The beam is produced by gluing layers of composite sandwich structure together in different orientations, i.e. flatwise (horizontal) and edgewise (vertical). This experimental beam enabled the author to determine the more effective use of this composite material for structural beam applications. In this way, a detailed understanding was achieved of the behaviour of the constituent materials and composite sandwich structures to determine the suitability of this construction system for railway sleepers.

An experimental study of the flexural and shear behaviour of the individual sandwich structures in the flatwise and the edgewise positions was conducted. The sandwich structures in the edgewise position possessed better structural performance compared to the flatwise position due to the introduction of the vertical fibre composite skins. The sandwich structure with the same dimensions in the edgewise position displayed almost 20% and 70% higher failure load in bending and shear respectively, than the sandwich structures in the flatwise position suggesting more effective utilisation of the fibre composite material. This structure also exhibited ductile failure behaviour which is important in the civil engineering perspective.

The effects of the number and the orientation of sandwich laminations on the strength and failure behaviour of glue-laminated composite sandwich beams were also examined. The glued sandwich beams with edgewise laminations have at least 25% higher flexural strength and over 20% in shear strength, compared to the

individual sandwich beams. Gluing the sandwich beams in the edgewise position could offer up to 25% increase in flexural strength, a similar bending stiffness, and almost double the shear strength over beams in the flatwise position.

Theoretical prediction and numerical simulations were performed to gain a better understanding of the structural behaviour of the composite sandwich structures. Simplified Fibre Model Analysis (FMA) provides a preliminary indication of the flexural behaviour, while the shear prediction equation gives a good estimation of the shear strength of the sandwich structures. The Strand7 finite element program predicted the behaviour up to failure load of the sandwich structures reasonably well. This confirms that the behaviour and failure modes of composite sandwich structures can be well predicted by simplified analysis procedures and by using the currently available finite element software packages provided a good understanding of the constituent materials and the individual sandwich lamination is known. These can be important tools for design engineers permitting the design and development of fibre composite sandwich structures with a higher degree of confidence.

A grillage beam analogy was implemented to investigate the behaviour of sleepers and to obtain critical design parameters in a typical railway turnout system. The effects of the elastic modulus of sleeper, support modulus, and spot replacement were studied. All these factors have significant influences on the behaviour of turnout sleepers. An elastic modulus of 4 GPa was found optimal for a fibre composite turnout sleeper from the consideration of sleeper/ballast pressures and the vertical deflection. It was established that the turnout sleeper has a maximum bending moment of 19 kN-m and a shear force of 158 kN under service conditions.

Finally, the behaviour of the full-scale glue-laminated composite sandwich beams in three different layouts was evaluated to determine their suitability as railway turnout sleepers. The glued sandwich beams with edgewise laminations presented appropriate strength and stiffness for replacement turnout timber sleeper. The mechanical properties of these glue-laminated sandwich beams are comparable with the existing timber turnout sleepers demonstrating that the innovative composite sandwich beam is a viable alternative sleeper material for railway turnouts.

From this study, it is concluded that the glue-laminated composite sandwich structures can be effectively used for replacement railway turnout sleepers. An enhanced understanding of the behaviour of fibre composite sandwich structures for potential civil engineering applications is an outcome of this investigation.

Certification of Dissertation

I certify that the ideas, experimental work, results, analysis and conclusions reported in this dissertation are entirely my own effort, except where otherwise acknowledged. I also certify that the work is original and has not been previously submitted for any award, except where otherwise acknowledged.

--   /   /

Signature of Candidate

Endorsed:

--   /   /

Signature of Supervisor/s

--   /   /

Signature of Supervisor/s

Acknowledgements

I would like to extend my deepest gratitude to my supervisor Assoc. Prof. Thiru Aravinthan for giving me the opportunity to do a PhD at the University of Southern Queensland (USQ). I am greatly indebted to him for his continuing confidence in me as well as for giving me constant support throughout these years. He has been involved in all the studies included in this dissertation and I have learnt many things from his rich academic and practical experience. I am also thankful to my associate supervisor, Assoc. Prof. Karu Karunasena. The discussions with him helped me better understand numerical modelling; all his valuable suggestions were essential in improving the quality of this research.

I greatly appreciate the academic, financial and technical support of the Faculty of Engineering and Surveying and the Centre of Excellence in Engineered Fibre Composites (CEEFC), which made this research possible. I would like to acknowledge the USQ postgraduate scholarships awarded me to pursue my PhD study. I especially thank Assoc. Prof. David Buttsworth, Associate Dean of Research, for his continuous support that facilitated my work through the Faculty. Thanks to Dr. Md. Mainul Islam, for all the helpful discussions and suggestions. I am very thankful for the technical and administrative support from Wayne Crowell, Martin Geach and Atul Sakhiya and to all the staff and postgraduate students at CEEFC for the suggestions, support and friendship.

I would also like to thank Dr. Gerard Van Erp and the staff of LOC Composites Pty. Ltd., Australia for the technical and materials support. The technical assistance of Mr. Steve Douglas and Dr. Nick Stevens in the design and analysis of fibre composite turnout railway sleepers is gratefully acknowledged.

The most important "*thank you*" goes to my dear wife, Jen. Thank you for your love, for your endless patience, for comforting and encouraging me during the challenging periods. Without your support I would not have been able to complete this undertaking. I also want to thank my family who has always believed in my capabilities. Thanks also to the Inocentes family who made our stay in Toowoomba more enjoyable and memorable. To Almighty God for giving me the knowledge and strength, thank you very much.

To those whom I failed to mention but have been a great part of this endeavour, thank you very much.

Associated Publications

Journal

Manalo, A.C., Aravinthan, T., Karunasena, W., and Ticoalu, A. (2010). A review on alternative materials for replacement railway sleepers. Composite Structures, 92(3), 603-611.

Manalo, A.C., Aravinthan, T., Karunasena, W., and Islam, M. (2010). Flexural behaviour of structural fibre composite sandwich beams in flatwise and edgewise positions. *Composite Structures*, 92(4), 984-995.

Manalo, AC, Aravinthan, T. and Karunasena, W. (2010). In-plane shear behaviour of structural fibre composite sandwiches using asymmetrical beam shear test. *Construction and Building Materials*, 24(10), 1952-1960.

Manalo, A.C., Aravinthan, T. and Karunasena, W. (2010). Flexural behaviour of glue-laminated fibre composite sandwich beams. *Composite Structures*, 92(11), 2703-2711.

Manalo, A.C., Aravinthan, T. and Karunasena, W. 2010. Shear behaviour of glued structural fibre composite sandwich beams. *Journal of Construction and Building Materials* (*under review*)

Manalo, A.C., Aravinthan, T., Karunasena, W., and Stevens, N. Analysis of a typical turnout sleeper system with a low modulus of elasticity using grillage beam analogy. *Journal of Engineering Structures* (*under review*)

Refereed Conference Proceedings

Manalo, A.C., Aravinthan, T. & Karunasena, W. (2009). Behaviour of laminated beams from fibre composite sandwiches. *Asia-Pacific Conference on FRP in Structures (APFIS 2009)*, 9-11 December, Seoul, Korea, pp. 407-412.

Karunasena, W., Aravinthan, T., and Manalo, A.C. (2009). Vibration of debonded laminated fibre composite sandwich beams. *Asia-Pacific Conference on FRP in Structures (APFIS 2009)*, 9-11 December, Seoul, Korea, pp. 457-462.

Manalo, A.C., Aravinthan, T., Karunasena, W., and Islam, M. (2009). Flexural behaviour of composite sandwich for structural applications. *The 9th International Symposium on Fibre Reinforced Polymer Reinforcement for Concrete Structures (FRPRCS9)*, 13-15 July, Sydney, Australia, pp. 26 (full paper in CD).

Manalo, A.C., Aravinthan, T. and Karunasena, W. (2010). Behaviour of structural glulam beams from sustainable fibre composite sandwich panels. *Proceedings of the 5th Civil Engineering Conference in the Asian Region and Australasian Structural Engineering Conference (CECAR 5/ASEC)*, 8-12 August, Sydney, Australia, pp. 62 (full paper in USB).

Aravinthan, T., Manalo, A.C. and Douglas, S. (2010). Development of a fibre composite turnout sleeper. *Proceedings of the 5th Civil Engineering Conference in the Asian Region and Australasian Structural Engineering Conference (CECAR 5/ASEC)*, 8-12 August, Sydney, Australia, pp. 34 (full paper in USB)

Manalo, A.C., Aravinthan, T. and Karunasena, W. (2010). Shear behaviour of glue-laminated composite sandwich beams. *The 5th International Conference on FRP Composites in Civil Engineering (CICE 2010)*, 27-29 September, Beijing, China, pp. 139-143.

Manalo, A.C., Aravinthan, T. and Karunasena, W. (2010). A comparison of the shear behaviour of a fibre composite sandwich structure in the transverse and in-plane directions. *Proceedings of the 21st Australasian Conference on the Mechanics of Structures and Materials (ACMSM21)*, 7-10 December, Victoria University, Melbourne, Australia, pp. 421-426.

Manalo, A.C., Aravinthan, T., Karunasena, W., and Stevens, N. (2010). The effect of modulus of elasticity on the behaviour of railway turnout sleepers. *Proceedings of the 21st Australasian Conference on the Mechanics of Structures and Materials (ACMSM21)*, 7-10 December, Victoria University, Melbourne, Australia, pp. 427-432.

Manalo, A.C., Aravinthan, T., and Karunasena, W. (2010). Evaluation of the strength and stiffness of glue-laminated fibre composite sandwich panels for structural beam application. *Proceedings of the 6th Australasian Congress on Applied Mechanics (ACAM 6)*, 12-15 December, Perth, Western Australia, 10 p. (Conference proceedings in digital USB)

Manalo, A.C., Aravinthan, T., Karunasena, W., and Douglas, S. (2010). Fibre composite sandwich beam: An alternative to railway turnout sleeper? *Proceedings of the 2010 Southern Region Engineering Conference*, 12 November, University of Southern Queensland, Toowoomba, Queensland, 8 p. (Paper no. F1-2, Conference proceedings in website: http://www.usq.edu.au/engsummit/proceedings)

Table of Contents

Chapter 4   Flexural behaviour of fibre composite sandwich structures in flatwise and in edgewise positions

List of Figures

Chapter 4   Flexural behaviour of fibre composite sandwich structures in flatwise and in edgewise positions

Chapter 5   Shear behaviour of fibre composite sandwich structures with high strength core material

Chapter 6   Behaviour of glue-laminated fibre composite sandwich beams

Chapter 7   Analysis of a typical turnout sleeper system for critical design parameters

Chapter 8   Behaviour of a full-scale fibre composite turnout sleeper

Appendix B   Effect of plate width on the shear strength

Appendix C   Behaviour of glued sandwich beam with fibre wraps

Appendix D   Bond quality between sandwich laminations

Appendix E   FE model for glue-laminated sandwich beams

Appendix F   Influence of train route and steel distance blocks

Appendix G   Behaviour of new composite sandwich panels

Appendix H   Screw holding capacity of glued sandwich beams

List of Tables

Chapter 8   Behaviour of a full-scale fibre composite turnout sleeper

Appendix B   Effect of plate width on the shear strength

Appendix D   Bond quality between sandwich laminations

Appendix E   FE model for glue-laminated sandwich beams

Appendix G   Behaviour of new composite sandwich panels

Appendix H   Screw holding capacity of glued sandwich beams

Notations

General notation

Roman alphabets

Notation	Description
A	Cross-sectional area
A_c	Shear area of the core
A_s	Shear area of the fibre composite skin
$A_{c(c)i}$	Area of core layer in compression
$A_{c(t)i}$	Area of core layer in tension
$A_{s(c)i}$	Area of skin layer in compression
$A_{s(t)i}$	Areas of skin layer in tension
a	Shear span
a/D	Shear span-to-depth ratio
B	Width of the composite sandwich structures
c	Neutral axis depth of the sandwich beam section
D	Thickness/depth of the composite sandwich structures
DF	Axle load distribution factor
d	Distance between the centre of the skins
d_c	Distance from the centre of the core to the neutral axis
d_s	Distance from the centre of the skin to the neutral axis
E_{app}	Apparent bending modulus of elasticity
E_c	Modulus of elasticity of the core
E_s	Modulus of elasticity of the skin
$E_{sleeper}$	Design modulus of elasticity parallel to the grain
EI	Flexural stiffness
EI_{edge}	Flexural stiffness in the edgewise position
EI_{eff}	Effective bending stiffness of the sandwich structures
EI_{flat}	Flexural stiffness in the flatwise position
$f_{c(c)i}$	Stress at the layer of the core in compression
$f_{c(t)}$	Cracking strength in tension of the core material
$f_{c(t)i}$	Stress at layer core in tension
$f_{s(c)i}$	Stress at the layer of skin in compression
$f_{s(t)i}$	Stress at layer of skin in tension
$f_b^{'}$	Characteristic bending strength of structural timber
$f_c^{'}$	Characteristic compressive strength parallel to grain
$f_s^{'}$	Characteristic shear strength of structural timber
$f_t^{'}$	Characteristics tensile strength parallel to grain of structural timber
G_{ave}	Apparent shear modulus
G_c	Shear modulus of the core
G_s	Shear modulus of the skin

$G_{sleeper}$	Characteristic modulus of rigidity
G_{sw}	Effective modulus of rigidity of the sandwich structures
GA_{edge}	Shear stiffness of composite sandwich beam in the edgewise position
GA_{flat}	Shear stiffness of composite sandwich beam in the flatwise position
j	Combined vertical design load factor
k	Shear correction factor
L	Support span
L_f	Test span in flexure
L_T	Total length of the specimen
L_v	Test span in shear
M_L	Bending moments due to actual load
M_{max}	Maximum bending moment
M_n	Nominal flexural capacity of the composite sandwich section
M_u	Bending moments due to unit
n	Number of sandwich laminations
n_G	Transformation factor based on shear modulus of materials
n_i	Number of layers that the sandwich beam section was subdivided
n_r	Number of rails supported by the sleeper
P	Applied load
P_c	Shear capacity of the sandwich structures due to core shear failure
$P_{cs(flat)}$	Failure load due to core shear of beams in the flatwise position
$P_{cf(flat)}$	Failure load of sandwich beams due to tensile/compressive failure of the core in the flatwise position
$P_{cf(edge)}$	Failure load of sandwich beams due to tensile/compressive failure of the core in the edgewise position
$P_{cs(edge)}$	Failure load due to core shear of beams in the edgewise position
$P_{csG(flat)}$	Failure load due to core shear of sandwich beams in the flatwise position considering the shear moduli of the skin and core
$P_{csG(edge)}$	Failure load due to core shear of sandwich beams in the edgewise position considering the shear moduli of the skin and core
P_{E_G}	Shear capacity of the glued sandwich beams in the edgewise position transformed into an equivalent skin material using the ratio of the shear moduli
P_f	Basic equation for shear strength of composite sandwich structures
P_{F_G}	Shear capacity of the glued sandwich beams in the flatwise position transformed into an equivalent core material using the ratio of the shear moduli
P_{lc}	Load to cause local crushing failure
P_{id}	Load to cause indentation failure
P_{max}	Maximum applied load
P_{sf}	Failure mode of the sandwich beam due to skin failure
P_s	Shear capacity of the sandwich structure due to shear failure of the skins
P_{sw}	Shear capacity of the sandwich structure
P_{sw_c}	Shear capacity of the sandwich beams due to core shear
P_{sw_s}	Shear capacity of the sandwich beams due to shear of skin
Q	Equivalent design static wheel load

R	Rail seat load
t_c	Thickness of the core
t_i	Thickness of layers in the sandwich beam element
t_s	Thickness of the skin
U_s	Sleeper support modulus
V_L	Shear due to actual load
V_u	Shear due to unit load
$\tilde{y}$	Centre of the composite sandwich section

Greek letters

Notation	Description
Δ_b	Deflection of the sandwich beam due to bending
Δ_s	Deflection of the sandwich beam due to shear
Δ_{total}	Total deflection of the sandwich beam
$\Delta_{4FSW\text{-}I}$	Deflection at midspan for specimen 4FSW-I
$\Delta_{4FSW\text{-}II}$	Deflection at midspan for specimen 4FSW-II
$\Delta P/\Delta v$	Slope of the load-deflection curve
ε_{+45}	Strain measured by the $+45^o$ strain gauge
ε_{-45}	Strain measured by the -45° strain gauge
$\varepsilon_{c(c)}$	Compressive strain of the core
$\varepsilon_{c(t)}$	Cracking strain of the core material
ε_i	Strain at sandwich beam element
$\varepsilon_{s(c)}$	Strain in the extreme fibre composite skin in compression
$\varepsilon_{s(t)}$	Strain in the extreme fibre in tension
γ_{ave}	Average shear strain
γ_c	Failure shear strain of the core
γ_f	Failure shear strain of the sandwich structures
γ_s	Failure shear strain of the fibre composite skins
φ	Curvature of the composite sandwich beam
$\sigma_{b,exp}$	Maximum bending strength of sandwich beam from experiment
σ_{cb}	Bending strength of the core
σ_{cc}	Compressive strength of the core
σ_{cs}	Compressive strength of skin
τ_{ave}	Average shear stress
τ_c	Shear strength of the core
τ_s	Shear strength of the skin

Chapter 1

Introduction

1.1 General

Railway sleepers are one of the most important elements of the railway track system. They are the beams laid underneath the rails to support the track (Ellis, 2001). Their functions are to transfer and distribute the transported rail loads to the ballast, transversely secure the rails to maintain the correct gauge-width and to resist the cutting and abrading actions of the bearing plates and the ballast material (Zhao et al., 2007). Sleepers also resist the lateral and the longitudinal movement of the rail system. The other structural elements needed to take into consideration in a railway track foundation are the rail, the ballast and the subgrade (Kohoutek and Campbell, 1989). The rail made of steel provides smooth and hard running surfaces for the train wheels and guide the wheel sets in the direction of the track (Iwnicki, 2006). Railpads are placed between the rails and sleepers to protect the sleepers from wear and impact damage. The coarse aggregate where the sleepers are laid is called ballast and the surface where the ballast rest is the subgrade (Gonzales-Nicieza et al., 2008). These main components of a rail track system are illustrated in Figure 1.1.
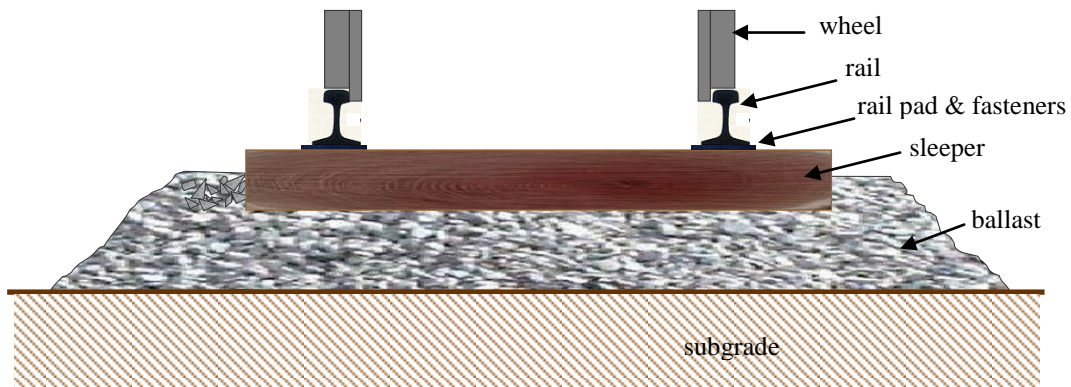
Figure 1.1 Components of a typical railway track system

Hardwood timber has been the preferred material for railway sleepers, and the maintenance work on existing timber sleeper tracks continued to be provided by hardwood. Currently, there are more than 2.5 billion timber sleepers installed in the

railway track throughout the world (Ets Rothlisberger, 2008). In totality, it was estimated that 75% of the world's railway track are on timber sleepers (Adams, 1991). Within Australia, the state of Queensland alone has over 8 million timber sleepers in service (Miller, 2007). Most of these railway sleepers are deteriorating and becoming less capable of meeting performance requirements. In order to maintain the track quality to a specified service level and ensure a safe track operation, damaged and deteriorated sleepers are being replaced with new ones. Over the last decade, it has been increasingly difficult to get good quality hardwood to keep up with the demand for railway maintenance. This trend is set to continue in the future, hence the need to develop a sleeper product from renewable resources.

The problem of supply of quality hardwood for sleeper application is greater in specific location of a railway track such as turnouts where stronger, bigger and longer timber is required. A railway turnout is the mechanical installation that enables a train to be guided from one track to another (Pfeil and Broadley, 1991). Elkins et al. (1989) indicated that the railway turnout sleepers are becoming an increasingly significant cost in track structure maintenance. Kassa and Nielsen (2008) suggested that the maintenance cost of turnout sleepers can be reduced by using a more durable material. Thus, several attempts have been carried out to investigate the most durable, the strongest and the most cost-effective material for replacing deteriorated and damaged timber sleepers in a railway turnout. Some of these approaches attempted to optimise the use of the already existing materials for sleepers such as plantation timber, steel and pre-stressed concrete (Adams, 1991; Hearsch, 2008; Stevens and Dux, 2008; BHP, 2008). However, these maintenance strategies have gained limited success as these materials have not been proven as reliable alternatives because they have mechanical properties incompatible with the existing timber turnout sleepers.

1.2 Background on hardwood timber sleepers

A large number of timber structures such as road and rail bridges, railway sleepers, and marine and fender piles remain in service in rural and regional Australia (Dutton and Cartwright, 2001). The important components of these timber structures have deteriorated to a point where they are no longer considered safe and needs immediate replacement. With limited resource for maintenance, it is significantly less expensive to replace only the deteriorated components on these existing timber structures than

to demolish and build a new one. Managing these structures is very challenging as it has been increasingly difficult to get large section of good quality hardwood in quantities to replace the deteriorating timber components. For well over a decade, Engineers Australia has been calling for a new approach to the maintenance of existing infrastructure promising results as long-term solutions (Hardwicke, 2005).

Railway infrastructure is one of the industries that have a considerable pressure on finding a suitable alternative to hardwood timber. The Australian railway lines require in excess of 1.5 million timber sleepers per year for railway maintenance (Van Erp et al., 2006). As much as they want to eliminate the use of timber sleepers, the Queensland Rail (QR) is still purchasing more than 80,000 timber sleepers per year including 5,000 for turnout sleepers for track maintenance and development as there are still no viable alternative for timber sleepers (Miller, 2007). In the US, the railway industry replaces two percent of the 700 million timber sleepers annually (Lampo, 2002). Furthermore, India imports 7 million timber sleepers per year to solve its railway maintenance problems (Van Erp et al., 2006). Railway industries in Germany on the other hand are in need of 11 million timber sleepers for replacement (Woidasky, 2008). This figure still does not include other European countries and China where the railway industries are almost exclusively using timber sleepers.

The Australian railway industry spends approximately 25-35 percent of its annual budget on rail track maintenance (Yun and Ferreira, 2003). According to Hagaman and McAlpine (1991), sleeper replacement represents the most significant maintenance cost for the railways, exclusive of the rail cost. This has cost the US railway industries more than US$1 billion per year (Optimat Ltd. and MERL Ltd., 2003). Thus, several railway industries have adopted the spot replacement strategy to lessen the cost of track maintenance. This is also the maintenance program being implemented by most Australian railway industries (Baggot et al., 2006). The spot replacement strategy embraces the component replacement of failing timber sleepers with new sleepers to maintain the railway tracks. A prerequisite of this maintenance strategy is that replacement sleepers should have properties compatible with that of existing timber sleepers. Furthermore, the method of installation in-situ should also be relatively easy. Due to the vast number of deteriorating timber sleepers in the railway track and restriction on the supply of new timber sleepers of approved quality, the demand requirements cannot be matched to replace deteriorated timber sleepers. In addition, there have been intensified pressures for limiting the use of

timber sleepers from durable hardwood species because of the various environmental concerns. These problems have resulted in many railway industries throughout the world investigating alternative materials for replacement timber sleepers.

Hardwood timber continues to be the most widely used sleeper material in a railway turnout (Zarembski, 1993). The special sleepers laid on a turnout are called turnout sleepers (Andersson and Dahlberg, 1998). The structure of a turnout is complicated and requires special sleepers with varying lengths and fastening locations (AS1085.14, 2003). Figure 1.2 is an example of a right-hand railway turnout structure. In a railway turnout, the sleepers are subjected to a complicated mixture of flexural and shear loads due to the wheel-rail impact force caused by the crossing train. Remennikov and Kaewunruen (2008) found that the extreme impact conditions on the tracks cause the sleeper's failure and the severity of the impact loading at the railway turnout depends strongly on the train speed (Andersson and Dahlberg, 1998). In order to cope with the complex loading, the turnout sleepers are produced with larger dimensions than the mainline sleepers. Because of the special nature of turnout sleepers, its manufacturing procedure is different from that of mainline sleepers which makes its maintenance more costly. The use of prestressed concrete and steel sleepers for these special sleepers is more expensive and difficult. A footprint of every single sleeper to be replaced had to be made as sleepers in a railway turnout have varying lengths and fastening locations. The replacement sleepers need to be pre-measured on the site and then fabricated at the factory with accurate bolt holes. Thus, an alternative material with similar usability and design characteristics to that of hardwood sleepers is more suitable.

Figure 1.2 Right-hand railway turnout structure

1.3 Fibre composites as an alternative for sleeper applications

Fibre composites are very appropriate for replacement railway timber sleeper as this material can be engineered based on the required structural applications (Bank, 2006). The sleepers produced from fibre composites could be manufactured with almost the same size/depth and weight to that of hardwood timber and to any specified lengths. It also has excellent durability requiring less maintenance. Like timber sleepers, fibre composite railway sleepers can be inserted under the track and provide flexibility to be drilled in-situ for the attachment of rail fasteners. Being lightweight, it offers easy installation and great flexibility in construction. The high proportion of replacement sleepers required for railway turnouts could further benefit from the development of fibre composite sleepers.

Significant efforts have been provided towards the development of fibre composite sleeper alternatives. Several researchers have applied fibre composites as reinforcement for existing railway sleepers (Qiao et al., 1998; Humpreys and Francey, 2004; Shokrieh and Rahmat, 2006; Ticoalu, 2008). Other approaches focused on the replacement of deteriorated timber sleepers using alternative materials such as polymer concrete, reinforced plastics, rubber, and fibre composites (Miura et al., 1998; Hoger, 2000; Lampo, 2002; Jordan and Morris, 2006). These composite railway sleeper technologies have evolved from concept development to the construction and deployment of full-scale prototypes for trial testing. However, these earlier developments are only for standard applications which are not cost competitive with conventional sleeper materials. Currently, there are no significant research and development on fibre composite sleepers for railway turnout applications. The premium benefit of fibre composite sleepers could make this material a viable alternative to existing timber sleepers in a railway turnout as they are more environmentally sustainable than steel and concrete and the cost of special timber sleepers for this type of application is higher than that of the standard ones.

1.4 Fibre composite railway sleepers using sandwich structures

A structural sandwich is a special form of a laminated composite fabricated by attaching two thin but stiff skins to the lightweight but thick core (ASTM C274, 1999). The main benefit of using the sandwich concept in structural components is its high bending stiffness and its high strength to weight ratios (Belouettar et al., 2009). In addition, composite sandwich structures are preferred over conventional

materials because of its high corrosion resistance (Russo and Zuccarello, 2007). This material has been widely used in the automotive, aerospace, marine and other industrial applications due to its many advantages (Bakis et al., 2002). Fibre composite sandwich structure is gaining a lot of interest in the construction industry and is now beginning to be in use for civil engineering applications (Keller, 2006).

The many advantages of fibre composite sandwich structure favour its application to railway turnout sleepers. Although engineers have access to a wide range of composite sandwich panels, very limited attempts have been done so far to use these materials for this type of structural application. The main reason could be that most of the currently used core materials are not appropriate for this type of structural application. Moreover, a thicker composite sandwich is usually used in structural applications than in industrial applications (Styles et al., 2007) where the shear strength of the core material is a critical parameter to efficiently transfer the shear between the top and bottom skins. It is also indicated in most literature that the core shear is the dominant failure mode of most sandwich construction under flexural loading (Shenhar et al., 1996; Kampner and Grenestedt, 2007). Accordingly, many have used high density core material to improve the structural performance of the composite sandwich panel.

A new type of composite sandwich panel made up of glass fibre-reinforced polymer skins and a modified phenolic core material has been developed recently for structural applications (Van Erp and Rogers, 2008). The significant improvement in strength of the core of this sandwich structure presents an ideal opportunity to increase the use of this material for civil engineering applications. As these composite sandwich panels are produced in limited thickness, the structural beam section can be manufactured by gluing several sandwich panels together. Gluing a number of elements of limited dimension to manufacture large structural members in any shapes and sizes has been used many years in the construction industry (Hernandez et al., 1997). However, little is known about the performance of the structural elements made from laminated composite sandwich beams even though the benefits of this type of construction have been highlighted in many applications. In this study, the potential of glue-laminated composite sandwich beams for structural applications was explored specifically for replacement railway turnout sleepers.

The development of new and innovative structural systems using fibre composite materials should always be accompanied by scientific studies within the

overall concept. The current study is the first to investigate the application of glue-laminated composite sandwich beam concept for railway turnout sleeper in a systematic manner. Accordingly, a number of important aspects had to be addressed starting from understanding the behaviour of a fibre composite sandwich structure, validating the concept and investigating the suitability of this construction system for replacement railway sleepers. The results of this study will provide valuable information necessary to facilitate the actual application of this innovative beam concept in a railway turnout sleeper.

1.5 Objectives

The evaluation of the behaviour of a fibre composite structure is very important to demonstrate its construction and performance capacity. The aim of this study is to investigate the behaviour of a novel fibre composite sandwich structure and determine its potential application for a replacement railway timber sleeper. The main objectives of the study are the following:

(a) Characterise the mechanical behaviour of the glass fibre composite skin and the phenolic core material of the novel fibre composite sandwich structure;

(b) Evaluate the mechanical behaviour of individual fibre composite sandwich structure in the flatwise and in the edgewise positions experimentally, theoretically, and numerically;

(c) Investigate the flexural and shear behaviour of the glue-laminated composite sandwich structures experimentally and numerically;

(d) Determine the effects of material properties, loading conditions and the subgrade modulus on the performance of fibre composite railway turnout sleepers using a simplified finite element model; and,

(e) Experimentally and numerically investigate the structural behaviour of the full-scale glue-laminated fibre composite sandwich beams and evaluate its behaviour for railway turnout sleeper application.

1.6 Scope of the thesis

The study focused on understanding the behaviour of a novel fibre composite sandwich structure and investigates its potential for railway turnout sleeper application. There are no significant material developments conducted and only the existing composite sandwich panels that suit the proposed structural system are used. The accompanying intellectual patent of this new material would not permit the author to divulge any information related to the chemical composition and microstructure of the modified phenolic foam core material nor the plant based resin used to develop the composite sandwich panels. During the course of the study, particular attention is given to the following:

- Review on fibre composite railway sleeper developments;
- Material properties and characterisation;
- Testing and evaluation of the behaviour and failure mechanisms of fibre composite sandwich structures;
- Numerical simulations of the composite sandwich beam behaviour;
- Development of simplified calculation method to describe the approximate behaviour and failure mechanisms of the composite sandwich structure;
- Development of simplified FE model to simulate the behaviour of a complex railway turnout system;
- Comparison of the experimental, theoretical and numerical results; and,
- Evaluation of the glue-laminated fibre composite sandwich beams for railway turnout sleeper application.

A broader approach was taken in order to ascertain the validity of the innovative composite sandwich beam concept and understanding its fundamental mechanical behaviour, providing a base knowledge from which further research could continue. As a result of this adopted broad approach, the following issues are beyond the scope of this study:

- Characterisation of the long-term behaviour of the composite sandwich beams;
- Dynamic and fatigue effects on the composite sandwich beam behaviour;
- Durability and environmental effects; and,
- Non-linear behaviour of fibre composite sandwich structures.

1.7 Outline the thesis

This thesis is divided into 9 chapters which describe the different investigations conducted in this study.

- The first chapter is an introduction and objectives of this study.

- Chapter 2 gives an overview on the existing materials for railway sleepers and the consequent issues on using these materials for replacement railway sleepers. An important review on composite sandwich structure focused on the several challenges needed to be overcome by this composite material to become a suitable alternative for railway turnout sleeper application is also presented.

- Chapter 3 is concerned with the intensive characterisation of the mechanical properties of the glass fibre composite skin and the phenolic core of the novel sandwich panel for its effective utilisation as a structural material.

- Chapter 4 characterizes the flexural behaviour of the individual composite sandwich structure in the flatwise and in the edgewise positions through experimental, theoretical and numerical investigations to determine the most effective configuration of this material for structural beam applications.

- Chapter 5 focuses on the characterisation of the shear behaviour of a composite sandwich structure with high strength core material. The contribution of the skin and the core material in resisting shear forces in a composite sandwich structure is characterised in this chapter.

- Chapter 6 discusses the evaluation of the behaviour of the glue-laminated composite sandwich beams in flexure and shear. The effects of the number and the orientation of laminations on the overall behaviour of the sandwich beams are determined through experiment and finite element simulations.

- Chapter 7 covers the parametric investigation on the behaviour of sleepers in a railway turnout. A simplified grillage beam model simulating the railway turnout system was developed to facilitate the optimisation process of an alternative fibre composite turnout sleeper.

- Chapter 8 covers a testing program to determine the structural behaviour of the full-scale fibre composite sandwich beams. The mechanical properties of this composite sandwich structure were evaluated for a typical timber railway turnout sleeper application.

- The main body of the thesis ends with Chapter 9 which presents the main conclusions of the research and the recommendations for future work.

1.8 Summary

Many of the world's railway lines are supported by timber sleepers that do not meet the requirements of the modern railway traffic. The reduced availability of hardwood timber for sleeper replacement is a serious problem affecting most railway industries in Australia and around the world. It is getting harder and harder to find hardwood timber especially the longer and bigger beams for railway turnout sleepers. Recent developments have focused on fibre composites as an alternative material for railway sleepers as this material can be made to have similar usability and design characteristics to hardwood timber with the added advantages. This has been the key motivation for this research.

Chapter 2

A review of alternative materials for timber sleepers

2.1 General

This chapter provides an overview on the existing materials for railway sleepers and the consequent issues in using these materials for replacement railway sleepers. This chapter also reviews the on-going research conducted throughout the world directed towards finding suitable alternatives for replacing timber sleepers. The research and developments on fibre composite railway sleepers are highlighted and the necessary background on the need to develop an alternative fibre composite sleeper for railway turnout application. An important review on fibre composite sandwich structure and the several challenges needed to be overcome by this composite material to become a suitable alternative sleeper material are also included.

2.2 Sleeper replacement strategies

Railway maintenance is necessary to keep the track quality to a specified service level and ensure a safe track operation. Grimes and Barkan (2006) indicated that the largest portion of the annual capital program for railway maintenance is for rails and sleepers; with the sleeper maintenance given a slightly higher budget. At the same time, sleepers in a railway turnout are becoming an increasingly significant cost element in the track structure maintenance (Elkins et al., 1989). Kassa and Nielsen (2008) indicated that the track defects per km of turnout are 16.52 times higher than the mainline railway lines. Due to budget constraints and the vast number of deteriorating sleepers in existing railway track, proper measures need to be undertaken to ensure the most cost effective utilisation of this limited resource. Accordingly, the railway industries use different proportions of ordinary maintenance and periodic renewal for the most cost-effective railway maintenance. Kohoutek (1991) suggested that interspersing timber sleepers seems a feasible way to upgrade an existing track. Zhang et al. (2000) indicated that some railway systems do not replace failed sleepers unless a cluster of failed sleepers is considered unacceptable. Yun and Ferreira (2003) developed a simulation model to assess

alternative railway sleeper replacement strategies to lessen the cost of track maintenance. The model showed that replacement could be delayed until 10% of the sleepers have failed. This model considers only two-consecutive sleeper failure as replacement but not the isolated and failed ones to reduce costs. Zhao et al. (2007) proposed a model to further optimise sleeper maintenance by considering the reliability of a railway system even with three consecutive failed sleepers and carried out maintenance only when a reliable and safe sleeper operation could not be met. In all these models, spot replacement strategy was adopted to minimise track maintenance cost. This strategy embraced the localised or component replacement of failing timber sleepers in maintaining railway tracks. However, due to a vast number of deteriorating timber sleepers in the railway track and the restriction on the supply of new timber sleepers of approved quality, the demand requirement cannot be matched to replace deteriorated timber sleepers. This has resulted in many railway industries searching for alternative materials to replace deteriorating timber sleepers in existing railway lines.

2.3 Existing materials for railway sleepers

There has already been a vast research and development effort into materials for sleepers since railways were introduced. Timber sleepers are still the most common; however, the use of pre-stressed concrete and steel sleepers is also increasing. The advantages and disadvantages of these railway materials are discussed in the following sections.

2.3.1 Hardwood timber

Timber sleepers have a long history of effective and reliable performance in the railway environment (Zarembski, 1993). The major advantage of timber sleepers is their adaptability. They can be fitted with all types of railway track. Timber sleepers are workable, easy to handle, easy to replace and needs no complicated assembly equipment. Thus, local problem sites can be repaired or replaced without the need for outside support in the form of either manpower or equipment. This is particularly attractive in high speed or high density lines where track time is both limited and constrained by the ability to bring in large scale production gangs (Ets Rothlisberger, 2008). In addition, timber sleepers can flex repeatedly with minimal fatigue (Smith, 2006). In can absorb severe impact with limited damage, as results when a train

derails. Such impact shatters concrete sleepers. Furthermore, timber sleeper provides electrical isolation, an important factor for track signalling which cannot be matched by other alternative sleeper materials except maybe by plastics or fibre composites (Zarembski, 1993).

The main disadvantage in using timber for sleepers is their susceptibility to mechanical and biological degradation leading to failure (Qiao et al., 1998). Most common failure modes in timber sleepers are shown in Figure 2.1. In Queensland, fungal decay (Figure 2.1a) is the most predominant form of timber sleeper failure (Hagaman and McAlpine, 1991). The splitting of timber at the ends (Figure 2.1b) is also common as railway sleepers support very large transverse shear loadings (Hibbeler, 2004). There are also several cases reported where timber sleepers were attacked and damaged by termites as shown in Figure 2.1c (Miller, 2007). However, the most difficult problem that the railway industry is now facing is the declining availability of quality timber for railway sleepers. In addition, various conservation groups are outraged over the use of native timber for railway sleepers (Morris, 2008).

(a) Fungal decay   (b) Splitting at ends   (c) Termite attack
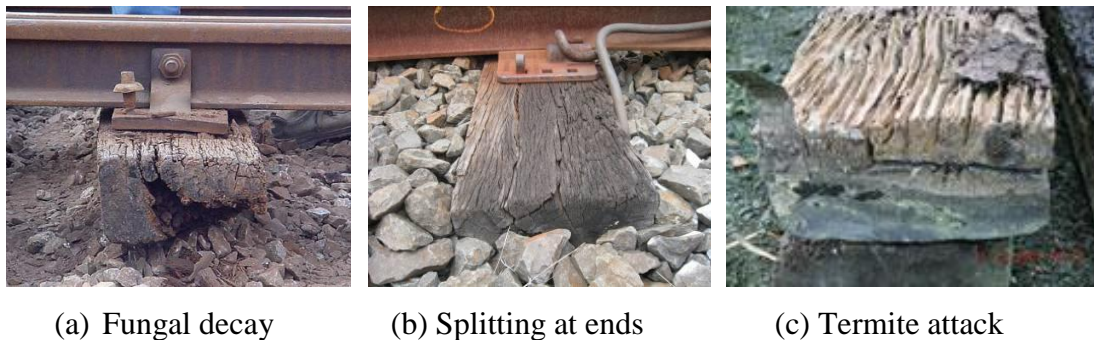
Figure 2.1 Common types of timber sleeper failure

Another growing concern is the environmental and health impact of the use of chemical preservatives to timber sleepers. The railway industry has historically almost exclusively used *creosote* impregnated timber sleepers (Pruszinski, 1999). This industry is still relying on these sleepers in the absence of satisfactory substitutes to timber (European Rail Infrastructure Managers, 2008). In the near future, it is more likely that the chemical impregnated timber sleepers will require specific disposal procedures as timber sleepers are gradually being removed and replaced with new ones. Moreover, newer research has suggested that many of the timber sleepers exceed the creosote critical limit set by the European Union

environmental regulations and should be treated as hazardous waste when they are disposed (Thierfelder and Sandstrom, 2008). Thus, efforts have been made in various countries to restrict the use of *creosote* impregnated timber sleepers and to tighten regulations on the production process due to environmental concerns (Pruszinski, 1999). Morris (2008) reported that there is a need for a set of rules on how the old *creosote* impregnated sleepers are to be stored and disposed off to prevent potential health hazards. Reports worldwide suggest that the disposal to landfill of preservative-treated timber sleepers is at present an acceptable option. It is unlikely that existing landfills will be able to accept increasing loads of preservative-treated timber sleepers without impacting the environment. In Australia, the New South Wales Environmental Protection Agency (2004) requires that treated timber be disposed off to engineered landfills with currently operating leachate management systems. Although options for the re-use of sleepers exist such as in home garden applications, these are only for untreated timber sleepers. Industries are also reluctant to recycle chemically-impregnated timber products due to concerns over workers safety and environmental problems (Smith and Shiau, 1998). Combustion or incineration is also not an acceptable option due to the toxicity of the ash (Norton, 1998). This process is expensive and impractical on an economic basis. Clearly, an environment-friendly material should be developed as an alternative to chemical impregnated timber railway sleepers.

2.3.2 Softwood and engineered timber

Research at Forest Products Laboratory in the US has shown that reconstituted laminated railway sleepers could be fabricated from old timber sleepers (Geimer, 1982). Laboratory tests of the developed sleepers from recycled timber exhibited an average effective modulus of elasticity of around 5.7 GPa and a bending strength of 21 MPa. The low strength of the reconstituted sleepers is due to the poor flake bonding as it is very difficult to remove all the grits and stones embedded in deep splits and cracks in the used timber sleepers. Moreover, the reconstituted timber sleepers swelled as much as 35% after soaking in water for 24 hours. Although the author concluded that the target design properties for sleeper application can be attained with proper fabricating equipment, no further development was conducted to suggest the economic feasibility of developing new sleepers from old timber sleepers. In a report by Vermaak and Quinn (1983), a series of tests was conducted

by the South African Forestry Research Institute to determine the performance of laminated pine railway sleepers. Service tests showed that the laminated pine sleepers have an average service life of only 15 years even when properly impregnated with creosote.

Softwood timber does not offer the resistance to gauge spreading and spike hole enlargement as that of hardwood timber sleeper (AREMA, 2003a). In addition, softwood sleepers are not as effective in transmitting the loads to the ballast as the hardwood sleepers do, thus they should not be mixed with hardwood sleepers on the railway track. However, since softwood timber is sourced mostly from plantations and is a renewable resource, a research project is being implemented by the Queensland University of Technology in Australia to transform softwood into timber suitable for railway sleepers (Hearsch, 2008). A series of tests have already been completed which have proven the technical suitability of softwood timber for railway sleepers. However, it should be noted that this test was conducted only for more lightly used secondary rail networks.

Plantation grown softwood timber for railway sleeper must be impregnated with preservatives to have high durability (McCarthy and Cookson, 2008). In most cases, the large cross section of the sleeper and the smaller diameter of plantation logs allow only one sleeper from a sleeper length log, therefore, the overwhelming majority of the sleepers have a percentage of heartwood. The heartwood has low permeability and is very difficult to impregnate. Vinden et al. (2010) investigated the use of microwave technique modification of Radiata pine railway sleepers for preservative treatment. The results of their study show that this modification technique increases heartwood permeability enabling the treatment to achieve the required quality of sleeper preservative treatment. However, the microwave modification ruptures some elements of the wood structure and leads to timber strength reduction. Similarly, end splits, internal checks and surface cracks were observed in some modified sleepers which are more than the allowable limit for quality sleepers as specified in AS 3818.2 (2004). Moreover, the proper modification using microwave technique requires energy consumption of around 75-110 kWh/m^3 which further increases the cost of a sleeper material of around AU$27-43/m^3.

2.3.3 Prestressed concrete

Prestressed concrete sleepers have become widely and successfully accepted for railway sleeper use especially in high speed lines. Their economic and technical advantages are the results of longer life cycles and lower maintenance costs. With their great weight, concrete sleepers assure optimal position permanence and stability even for traffic at high speeds. In fact, many prestressed-concrete sleeper technologies have now been developed and successfully tested. Monobloc prestressed concrete sleepers are the most commonly used (AREMA, 2003a). Twin-bloc, on the other hand, is gaining popularity because it weighs less compared to monoblock sleepers. Twin-bloc sleeper is made up of two concrete parts supported by steel reinforcements. However, handling and placing of twin-bloc sleepers can be difficult due to the tendency to twist when lifted. '*Ladder sleepers*' are another development (Miura et al., 1998). These sleepers consist of a 12-m long pre-stressed longitudinal concrete member bound by lateral steel tubes like a ladder. The rails are supported continuously on the concrete members which distribute the load lengthwise thereby reducing the need for ballast maintenance.

Further developments in the technology of concrete sleepers have since seen the introduction of low profile concrete sleepers. Researchers at the University of Queensland, Australia have designed the world's first pre-stressed concrete railway sleeper specifically aimed at replacing timber sleepers (Stevens and Dux, 2006). Unlike existing concrete sleeper designs, the new sleeper has similar dimensions to a timber sleeper. This is of great benefit to the railway infrastructure owners who want the long term benefits of concrete but because of size restrictions cannot use the traditionally designed concrete sleepers. These sleepers are similar to the partial replacement sleepers shown in Figure 2.2. This sleeper is specifically designed to be interspersed with timber sleepers in existing timber tracks or to replace timber sleepers that have reached the end of their useful life. However, this sleeper is limited only to mainline replacement as it has specific pattern to hold track gauge.

The problem with concrete sleepers is their heavy weight which requires specialised machinery during laying and installation. Concrete sleepers also require more ballast and heavier rails than timber sleepers but can be placed with wider spacing resulting to a slightly fewer sleepers (Smith, 2006). The initial cost of concrete sleepers is almost double that of hardwood timber sleepers. Studies conducted by Kohoutek (1991) confirmed that the sleepers manufactured from

concrete performed differently to those made from timber. Concrete sleepers have high stiffness characteristics and the design requires higher depth than the existing timber sleepers which means they cannot safely be inserted into sections of rail with timber sleepers. Concrete sleepers are also vulnerable to rail seat corrosion resulting from the absence of a resilient rail pad and the concrete (Cope and Ellis, 2001). In addition, the low profile concrete sleepers trialled being relatively inflexible and with little damping showed poor results requiring good standard rails and ballast to avoid damage (Baggot et al., 2006).

Figure 2.2 Partial replacement concrete sleepers

2.3.4 Steel

Australia has developed a world reputation in technology related to the design and performance of steel railway sleepers. The Institute of Railway Technology at Monash University is working to minimise cost and ensure the superior performance of steel sleepers (BHP, 2008). Currently, steel sleepers account for over 13% of the railway sleepers used within Australia. Figure 2.3 shows a schematic illustration of steel sleepers commonly used in the Australian railway lines. Steel sleepers can be interspersed with the existing track but in a fixed interspersing pattern to reduce the variation in the track geometry and prevent the early in-service failure of sleepers (Birks et al., 1989). A steel sleeper weighs similar to timber sleeper which makes it easy to handle as well as having a life expectancy known to be in excess of 50 years. However, steel sleepers are being used only on more lightly travelled tracks and are regarded as suitable only where speeds are 160 km/h or less (Railway Track and Structures, 2008).
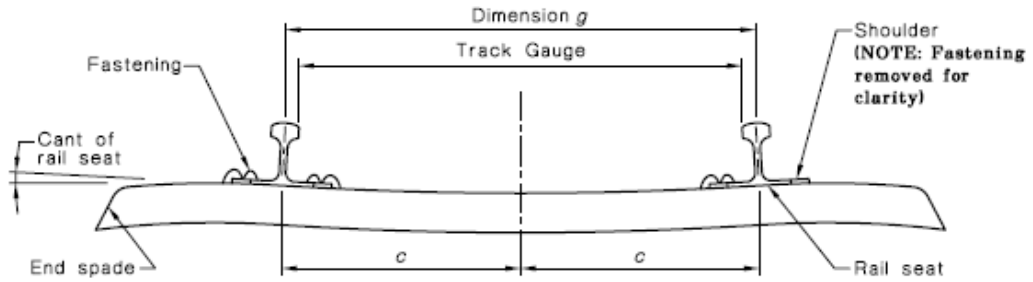
(a) Elevation along sleeper
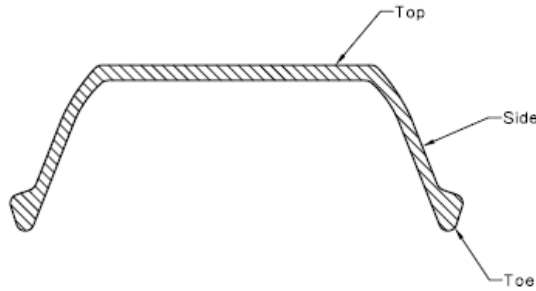
(b) Typical cross-section of steel sleeper

Figure 2.3 Schematic illustration of steel sleepers (AS1085.17-2003)

A modern Y-shaped steel sleeper (Figure 2.4) was developed to replace the traditional steel sleeper (Quante, 2001). The name itself implies that the Y-steel-sleeper is shaped like a '*Y'* in its horizontal layout. Compared to the usual steel sleeper, the Y-steel-sleeper possesses much greater resistance against cross movements due to the greater amount of ballast contained between the two parts of the Y-fork. However, due to its form, laying of the Y-steel-sleepers follow strict guidelines that require high output renewal trains. Practical experiences have proven that it is not possible to adjust or pull the sleepers in the ballast subsequently by means of a simple laying device.

Figure 2.4 Y-steel sleepers (http://www.efrtc.org)

Conventional steel sleepers require extra care during installation and tamping due to their inverted through profile which makes them difficult to satisfactorily pack with ballast. The observations on rail deflections under imposed vehicle track loading have shown that the steel sleepers settle a greater amount than the timber sleepers, indicating that the steel and the adjacent timber sleepers are not carrying an even proportion of the imposed wheel loading (Mitchell et al., 1987). Furthermore, steel sleepers are expensive and are only used in minimal number because of the risk of corrosion. Another problem with steel sleepers is fatigue cracking in the fastening holes caused by the moving trains (Cope and Ellis, 2001).

2.4 The need for alternatives

Many railway infrastructure companies have long been trialling concrete and steel for replacing timber sleepers in existing railway tracks. However, this maintenance strategy has gained limited success. These materials did not prove to be a viable alternative to timber sleepers. Gruber (1998) stated that over 90% of maintenance and construction of railway tracks still utilised timber sleepers despite the increasing reliability and effectiveness of alternatives such as steel and concrete. It is often more financially viable or convenient in the short term to replace sleepers with new timber sleeper (Humpreys and Francey, 2004). In 2006 alone, QR in Australia purchased 80,000 timber sleepers for track maintenance and development (Miller, 2007). In North America, the approximate market share for traditional timber sleepers was 91.5% compared to about 8.5% for concrete, steel and plastic composite sleepers combined as of January 2008.

Concrete sleepers have the ability to provide better line and gauge-holding characteristics than timber sleepers, but they are relatively expensive, heavy and are often incapable of providing a projected 50-year service life (Howe, 1996). Sleepers made of steel, on the other hand, can offer superior strength over that of wood and concrete, but steel sleepers are being used in moderate quantities because of their high cost (Qiao et al., 1998). Frequent replacement and tightening of fastenings are also required. Similarly, replacement of timber sleepers with concrete or steel sleepers will be both difficult and costly. Both concrete and steel sleepers have mechanical properties incompatible with the existing timber sleepers. The higher structural stiffness of the concrete means a higher load is transferred to the concrete

sleepers which could lead to greater deterioration due to flexural cracks (Gonzalez-Nicieza, 2008). Similarly, steel sleepers should not be mixed with timber sleepers because of their differential settlement (Health and Safety Executive, 2006). The shape and size of steel sleepers result in a tendency to settle more quickly than timber sleepers. This problem can only be overcome by completely replacing all the timber sleepers in a rail track with concrete or steel sleepers making it even more expensive. The manufacturing of concrete and steel sleepers requires considerably more energy and is one of the largest producers of atmospheric carbon. The Australian Greenhouse Office (2006) reported that the carbon dioxide emissions during the production of concrete and steel are 10 and 200 times higher than that of hardwood timber, respectively. Table 2.1 summarises the advantages and disadvantages of the currently used materials for railway sleepers.

Table 2.1 Comparison of existing materials for railway sleepers

Properties	Hardwood	Softwood	Concrete	Steel
Adaptability	Easy	Difficult	Difficult	Difficult
Workability	Easy	Easy	Difficult	Difficult
Handling and installation	Easy	Easy	Difficult	Difficult
Durability	Low	Low	High	Low
Maintenance	High	High	Low	High
Replacement	Easy	Easy	Difficult	Difficult
Availability	Low	High	High	High
Cost	High	Low	Very high	Very high
Fasteners	Good	Poor	Very good	Poor
Sleeper ballast interaction	Very good	Good	Very good	Poor
Electric conductivity	Low	Low	High	Very high
Impact	High	High	Low	Medium
Weight[a], kg	60-70	60-70	285	70-80
Service life, years	20-30	20	50	50

[a] Based on the weight of a standard mainline sleepers

It is evident that timber has been the material of choice for railway sleepers, especially for the replacement of damaged and deteriorated timber sleepers. However, the main problem with timber sleepers is their tendency to rot, particularly near the points where they are fastened to the rails. Timber needs to be treated with preservatives; some of which are toxic chemicals that are of concern for various environmental protection authorities (Zarembski, 1993). Similarly, replacement

timber sleepers are now being cut from less desirable species due to the declining availability of quality hardwoods. Some of these species have poor resistance to decay and are more susceptible to mechanical degradation (Qiao et al., 1998). These problems have resulted in more premature failures and higher replacement rates of timber sleepers. The current supply of quality hardwood could not meet the significant demand of existing timber sleepers that require replacement hence an alternative material for sleeper replacement to reduce maintenance cost and overcome problems encountered using timber is both desirable and necessary.

2.5 Fibre composite alternatives

The recent developments on fibre composites now suggest their use as an alternative material for railway sleepers. These developments can be subdivided into new railway sleepers produced by combining other materials with composites and the strengthening of existing sleeper materials with fibre composite wraps.

2.5.1 Combinations with other materials

Early developments have shown that railway sleepers made of polymer materials combined with fibre composites could enhance both physical and mechanical properties. Pattamapron et al. (2005) have investigated the possibility of using natural rubber for railway sleepers. The mechanical properties of natural rubber were engineered and resulted in a better compressive modulus and hardness. However, the engineered rubber is excessively stiff and inelastic. In Japan, synthetic sleepers made of hard polyethylene foam and glass fibre are a unique development (Miura et al., 1998). These sleepers are designed for long service life (more than 60 years) while maintaining the physical properties of timber sleepers. These sleepers are also used in railway sections where maintenance or replacement is difficult. Furthermore, Hoger (2000) investigated the use of bulk recycled plastic as material for railway sleepers. This material showed increased strength but is not competitive in terms of cost.

Table 2.2 summarizes the recent developments on fibre composite railway sleepers in different countries around the world. Railway sleepers manufactured from recycled plastic bottles with glass fibre reinforcements have been introduced in the US over the past ten years (Lampo, 2002). This sleeper possesses physical and mechanical properties that are comparable to those of timber sleepers. This

sleeper is lightweight, can be screwed together and sawed using conventional woodworking tools. The performance of these sleepers in the field is now being investigated. The Indian railways adopted these materials for use in bridge sleepers (Jacob, 2004). In South Africa, composite polymer sleepers are being used in the mining industry to support underground railway lines (Cromberge, 2005). Another recycled plastic sleeper (Figure 2.5a) was developed by the Transport Research Laboratory (TRL) in the UK (Jordan and Morris, 2006). This sleeper exhibited similar stiffness to softwood sleepers but has greater strength and better resistance to the removal of the screw spikes. In Germany, an on-going study is being conducted by Woidasky (2008) to develop railway sleepers from mixed plastics post consumer waste (RailWaste) along with glass fibre wastes and other auxiliary agents. The RailWaste sleeper is expected to meet the mechanical requirements for sleepers and expected to show superior weather resistance than timber sleepers.

A number of companies are now selling railway sleepers manufactured using recycled plastic materials and fibre composites. These sleepers are said to have high strength, be more durable and weigh similar to timber sleepers while exhibiting properties similar to their wooden counterparts in terms of damping impact loads, lateral stability and sound absorption. Dynamic Composites, LLC is the manufacturer and distributor of a revolutionary composite railway sleeper made from recycled materials (http://www.dynamic-cci.com/product.htm). These sleepers are made from recycled high density polyethylene, recycled rubber, steel and concrete. The superior design provides a significantly stronger sleeper, with an improved life cycle and excellent track characteristics. The IntegriCo composite sleeper boosts to have an exceptional physical characteristics and longevity (Chow, 2007). This composite sleeper is manufactured using rectangular wood beam coated with plastic and rubber mixture (Figure 2.5b). TieTek^{TM} has developed a high-performance, long lasting composite sleeper made from recycled materials - plastic, rubber from used tires and waste fibreglass - and are combined with various mineral fillers to create sleepers that are strong, durable and highly-resistant to harsh environmental conditions (Evans and Evans, 2006). Tietek^{TM} sleepers are now being used by a number of railway industries in the US and the UK.

Table 2.2 Recent developments on fibre composite railway sleepers

Country	Description	Type of application	Level of development
Australia	Polymer concrete with glass fibres	Standard sleepers	Trial application
	Composite sandwich with carbon fibre strips	Transoms	Trial application
	LVL with glass fibre wraps	Turnout sleepers	R & D
Austria	Hard polyurethane foam and glass fibres	Transoms	Actual application
Germany	Mixed plastic consumer waste	Standards sleepers	R & D
India	FRP sleepers and Composite plastic sleepers	Standard sleepers Bridge transoms	Trial application
Japan	Hard polyurethane foam and glass fibres	Standard sleepers Turnout sleepers	Actual application
South Africa	Composite polymer	Underground railway	Trial application
Thailand	Engineered natural rubber	Standard sleepers	R & D
UK	Recycled plastic sleeper	Standard sleepers	R & D
US	Glass fibre reinforced recycled-plastic	Standard sleepers	Actual application

(a) TRL plastic sleeper (www.trl.co.uk)   (b) IntegriCo sleeper (www.integrico.com)

Figure 2.5 Commercially available fibre composite railway sleepers

Eslon Neo Lumber FFU (Fibre reinforced Foamed Urethane) from Sekisui Chemical Co. Ltd., a synthetic wood developed for use as railway sleepers in 1978 has since then been widely applied in Japan's railroad infrastructure (Koller, 2009). The production of the Sekisui sleepers uses the pultrusion process where the reinforcing glass fibres are impregnated with a polyurethane foam system and the composite is then cured at elevated temperature. So far, more than 870 km of track have been laid with this sleeper where the main areas of application are turnouts, open steel girder structures and tunnels. Following several successful applications in Japan, the year 2004 marked the European premiere for Sekisui sleeper when it was used in the renovation project of the railway track in Zollamt Bridge in Vienna, Austria as shown in Figure 2.6.

    (a) Mainline railway track   (b) Railway track in Zollamt Bridge

Figure 2.6 Actual applications of Sekisui composite sleepers

Table 2.3 compares the mechanical properties of some of the commercially available fibre composite sleepers and the minimum performance requirements recommended by the Subcommittee on Engineered Composite Ties formed under the American Railway Engineering and Maintenance-of-way Association (AREMA, 2003b) Committee 30 on crossties. In the table, the $E_{sleeper}$, σ_b, SSW and σ_c correspond to the modulus of elasticity, bending strength, screw-spike withdrawal resistance, and compressive strength of the fibre composite railway sleepers, respectively. The comparison with the AREMA recommendations showed that the commercially available fibre composite sleepers have mechanical properties suitable for sleeper application. The information listed in the table also indicates that most of the developed fibre composite sleepers have a bending stiffness of only around 1.2

GPa. This information is very appropriate in the development of an alternative sleeper as fibre composites have relatively lower stiffness compared to conventional structural materials. Further investigation is however warranted to determine if these mechanical properties are suited for railway turnout sleeper application.

Table 2.3 Mechanical properties of fibre composite railway sleepers

Composite sleeper	$E_{sleeper}$, GPa	σ_b, MPa	SSW, kN	σ_c, MPa
AREMA	1.17	13.83	22.21	6.23
Dynamic Composites LLC	1.73	17.92	17.81	310.15
IntegriCo	2.00	24.23	16.62	15.26
Tietek™	1.24	13.79	17.83	206.74
Eslon Neo Lumber	8.10	142.00	65.03	58.06
RailWaste	1.36	18.92	--	--

There have been many developed fibre composite technologies for railway sleepers. However, most of them are for replacement of standard sleepers and construction of new ones and very few development for turnout sleepers. Another major concern is that these composite products have gained limited acceptance by the railway industry due to their prohibitive cost, which is approximately 3 times the current cost of timber sleepers. These sleepers are imported technologies and importing these will entail higher cost for the Australian railway industry which could further increase track maintenance cost. These fibre composite sleepers might have limited application to Australian railways because of the differences in vehicle and track characteristics. Nevertheless, fibre composites showed the highest potential among the alternative sleeper materials for replacement of timber sleepers in the existing railway lines. A new fibre composite sleeper technology that suits local conditions and is made from locally produced construction materials should therefore be developed for a more cost competitive and a more adoptive sleeper technology.

2.5.2 Strengthening of existing sleepers

Another successful application of fibre composites in railway maintenance is the strengthening of existing sleepers. Quaio et al. (1998) evaluated the performance of timber sleepers wrapped in glass fibre reinforced polymer or GFRP (Figure 2.7). The results of their study demonstrated that the GFRP-wood beams exhibited significant improvement in performance. The composite reinforcement increases the stiffness

and the ultimate load capacity of the timber sleeper while decreasing stresses and providing a tough surface to resist plate cutting and ballast abrasion. The GFRP wrap also improved the resistance of the sleepers to moisture. The Transportation Technology Centre in Colorado, USA (2005) evaluated the performance of fibreglass fabric wrapped solid-sawn timber sleepers and discovered that the fibreglass wraps improved the durability of the timber sleepers. However, metal cover plates were provided to prevent damage to the fibreglass wrap under high loads. Furthermore, Humpreys and Francey (2004) in Australia made a preliminary study on the rehabilitation of timber railway sleepers with fibre-reinforced materials. The results of their study indicated that the load carrying capacity of timber sleepers externally reinforced with carbon can significantly increase if delamination of the carbon reinforcement did not occur prematurely. In another study, Shokrieh and Rahmat (2006) investigated the effect of reinforcing concrete sleepers with carbon and glass fibre composites (Figure 2.8). The results show that reinforcing concrete sleepers with two layers of glass fibres is more economical than one layer of carbon fibres as the increase in the load capacity of the concrete sleepers reinforced with carbon and with glass fibres is almost equal.
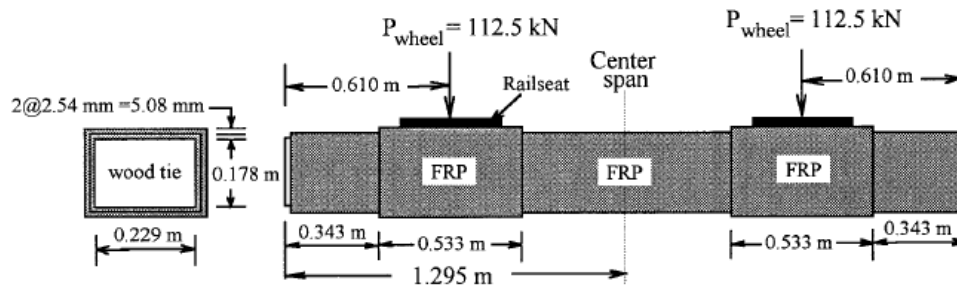
Figure 2.7 Timber sleepers wrapped in GFRP

Figure 2.8 Strengthening of concrete sleepers with fibre composites

2.6 R&D on innovative fibre composite sleepers

Recent developments in the railway industry have focused on the use of fibre composite alternatives for innovative railway sleepers. The Centre of Excellence in Engineered Fibre Composites (CEEFC) at the University of Southern Queensland Toowoomba, in collaboration with the different railway industries in Australia, has been involved in a number of research and development projects involving innovative fibre composite railway sleepers to replace deteriorated hardwood sleepers in existing railway lines.

One of the earliest technologies developed by CEEFC is a composite railway sleeper (Figure 2.9) that can be used as replacement for timber, steel and concrete sleepers in existing or new railway tracks (Van Erp et al., 2005). The sleeper is made of polymer concrete and glass fibre reinforcement and weighs only 61 kg. This sleeper has excellent electrical insulation properties and can be fitted with standard fasteners. The revolutionary shape of the sleeper provides it with excellent resistance against lateral movement. A trial section of track was manufactured to determine if the rail clips could be installed with sufficient accuracy in a production trial. The trial test has shown that the sleeper performs well under actual service conditions. However, this composite sleeper has not entered the market to date as its cost is not competitive with that of the existing sleeper materials.

Another development is the fibre composite (FC) railway transom (Figure 2.10) which is now being trialled on an actual railway bridge in Australia (Prasad, 2008). The FC railway transom is made up of fibre composite sandwich panel with additional fibre reinforcements. The core material of the sandwich panel is made up of fly-ash with low density polystyrene beads. The research and testing program have shown that the FC transom behaved similarly, or even better than the hardwood transoms. The trial test also confirmed its very good ability to hold rail fasteners. The first FC transoms were installed on top of a steel railway bridge located on a heavy and busy haulage line in November 2007. The trial investigation verified that the FC transoms are performing to expectations and estimated that its serviceable life should be well in excess of 50 years. However, the FC transoms are specifically designed for railway bridge applications and are not flexible for turnout applications.

The continuous effort of CEEFC in providing innovative solutions to the problems of the railway industry, a research project was implemented in collaboration with an Australian railway industry to develop an optimised fibre

composite railway turnout sleeper. Ticoalu (2008) began the investigation on the development of fibre composite turnout sleepers. The results of her study suggested that a sleeper with a modulus of 10 GPa showed no significant difference in bending moment, shear and deflection. In her work, laminated veneer lumber (LVL) with carbon fibre laminates on top and bottom, wrapped with tri-axial glass fibres (Figure 2.11) were prepared and tested. Although the results suggested that the concept is feasible for replacement railway sleepers, the use of LVL has some maintenance issues as timber is not eliminated. Timber is a biodegradable material and requires continued maintenance. While wrapping the LVL with fibre composites provided structural enhancement and environmental protection, the drilling of holes for spikes enables moisture and surface water to penetrate which can cause degradation of the LVL. The development of a replacement railway sleeper made from fibre composite materials which requires low maintenance cost is promising.

Figure 2.9 Sleeper made of polymer concrete and fibre composites

Figure 2.10 Fibre composite railway transoms

Figure 2.11 Composite sleepers made of LVL wrapped with tri-axial glass fibres

2.7 Properties of existing timber railway sleepers

One of the ways to reduce the cost of railway maintenance is replacing only the damaged and deteriorated timber sleepers. Thus, alternative materials with strength and performance characteristics similar to that of timber sleepers are more suitable. The replacement sleeper should be produced with almost the same size/depth and weight to that of existing hardwood sleepers because the material and geometric properties have a significant effect on the design and performance of railway sleepers. In Australian railway systems, timber sleepers need to satisfy specific requirements such as strength, durability and stiffness properties. The structural design properties of timber used for railway sleepers are listed in Table 2.4 (AS 1720.1-1997). For special sleepers like turnout, it is specified to use only stress-grade F17 or higher (AS 3818.2-2004). In addition, it should be within the specified dimensions to meet the standard for railway track timber.

The increasing difficulty of sourcing quality hardwood with large cross-section for replacement railway sleepers and the certainty that the hardwood timber nowadays have inferior quality compared to the timber previously available, several investigations were conducted to determine the bending strength and modulus of the currently used timber for railway sleepers. Davalos et al. (1999) tested 40 samples of 45 x 45 x 914 mm of Northern Red Oak using a 4-point bending set-up with a test span of 762 mm and 254 mm between loads. Hoger (2000) on the other hand tested a total of 10 narrow mainline sleepers with nominal dimensions of 115 x 230 x 2150 mm. The results of these investigations show that the strength of timber sleepers in the existing railway lines ranges from 57.41 MPa to 123.20 MPa while the bending

modulus is between 8.33 GPa and 17.87 GPa. In their attempt to improve the properties of old timber sleepers, Humpreys and Francey (2004) conducted a 3-point bending test to determine the strength and stiffness of old hardwood timber sleepers. The results of their test suggest that the average strength and stiffness of old hardwood timber sleepers is around 103.75 MPa and 10.6 GPa, respectively. These researchers concluded that the high variation in the properties of timber can be explained by the inherent properties of timber secondary to its type and species, its moisture content, its grain direction, the presence of internal defects, and environment effects. They also found out that that it is now possible to use timber sleeper with a stress grade of F8 to F34 in actual practice.

Table 2.4 Structural design properties for F-grades timber *(Table 2.4 AS1720.1-1997)*

Stress grade	Characteristic strength (MPa)					$E_{sleeper}$ (GPa)	$G_{sleeper}$ (GPa)
	f_b'	f_t'		f_s'	f_c'		
		Hardwood	Softwood				
F34	100	60	50	7.2	75	21.5	1.43
F27	80	50	40	6.1	60	18.5	1.23
F22	65	40	35	5.0	50	16.0	1.07
F17	50	30	26	4.3	40	14.0	0.93
F14	40	25	21	3.7	30	12.0	0.80
F11	35	20	17	3.1	25	10.5	0.70
F8	25	15	13	2.5	20	9.1	0.61
F7	20	12	10	2.1	15	7.9	0.53
F5	16	9.7	8.2	1.8	12	6.9	0.46
F4	13	7.7	6.5	1.5	9.7	6.1	0.41

where:

f_b' = characteristic bending strength;

f_t' = characteristics tensile strength parallel to grain;

f_s' = characteristic shear strength;

f_c' = characteristic compressive strength parallel to grain;

$E_{sleeper}$ = design modulus of elasticity parallel to the grain;

$G_{sleeper}$ = characteristic modulus of rigidity.

In the development of an alternative material for railway sleeper, it is desirable that the fibre composite turnout sleepers be produced to have similar modulus of elasticity to that of the existing timber turnout sleepers. Ticoalu (2008) considered therefore it essential to conduct further testing, specifically for timber turnout sleepers as there is no data available on these. In her experimental investigation, eight timber sleepers with nominal dimensions of 230 mm x 150 mm and lengths varying from 3000 mm to 4100 mm were subjected under four-point bending test to evaluate the strength and stiffness properties of the existing timber turnout sleepers. Figure 2.12 shows the bending test set-up for timber turnout sleeper. The load and deflection were measured to calculate the bending stiffness. The timber turnout beams were tested up to failure to determine their strength.

Figure 2.12 Testing of full-size turnout timber sleepers

The results of the test show that the bending strength of the existing railway timber turnout sleepers vary between 64 and 160 MPa with the modulus of elasticity ranging from 7 to 26 GPa. This gave an average modulus of rupture value of 130.9 MPa and a modulus of elasticity value of 8.1 GPa with a variation of coefficient of 31.5% and 20.5%, respectively. These values showed that the timber sleepers are strong enough to be used in the railway lines but some have stiffness lower than the recommended value. The large variation in bending strength and stiffness of the existing timber turnout sleepers suggests that it is very difficult to maintain uniformity in the mechanical properties of timber sleepers in a railway turnout. From the test results, it is also difficult to conclude a desirable strength and modulus of elasticity for the development of an alternative fibre composite railway turnout

sleeper. However, the results indicate that the existing timber turnout sleepers in the Australian railways can have an elastic modulus as low as 7 GPa. This modulus value can easily be achieved using fibre composite materials which is very advantageous as producing fibre composite turnout sleepers with high modulus of elasticity can be expensive. It is also of high importance that the behaviour of sleepers with a lower range of elastic modulus in a turnout system be examined to ascertain an optimal elastic modulus for fibre composite sleeper alternatives. At the same time, it is important that new and innovative fibre composite structure be investigated as it could provide a more cost-effective option and innovative solution for replacement railway sleeper. This has provided the motivation to continue the research and development on understanding the behaviour of fibre composite sandwich structures to come up with an optimised sleeper section.

2.8 Fibre composite sandwich structures

Fibre composites could be an ideal material for the development of railway sleepers. This composite material typically consists of strong fibres embedded within a light polymer matrix offering high strength, lightweight, durability and low-life maintenance costs (Bank, 2006) which is a suitable material for the replacement of deteriorated timber sleepers. In composites, the fibres provide strength and stiffness and generally carry most of the applied loads. On the other hand, the matrices which are commonly made-up of epoxies, polyester, vinyl esters, or phenolics act to bond and protect the fibres, and provide transfer of stress from fibre to fibre through shear stresses (ACI 440R, 2007). Fibre composite materials are anisotropic or its properties vary with direction. Typically, the most favourable mechanical properties are in the direction of the fibre placement (Barbero, 1999).

Fibre composites provide many advantages compared to the traditional construction materials. It is gaining popularity because of its low unit weight, ease of handling and application, and cheaper installation and maintenance costs. Fibre composites are not only superior to other materials in harsh environments, they are also non-magnetic and have good electrical insulating properties (Hollaway and Head, 2001). The main disadvantage of fibre composites is its high material cost. The relatively lower bending stiffness compared to traditional structural materials is also one of the issues on fibre composites when used as a reinforcement material. In most of the demonstration projects constructed to date, the design of structure using

fibre composites has been driven by the stiffness requirement rather than strength (GangaRao et al., 2007). These drawbacks of fibre composites have been overcome with the development of innovative structures utilising the inherent advantages of this material. An example of this efficient structure is the composite sandwich construction. The main benefit of using a sandwich concept in structural components is its high bending stiffness and high strength to weight ratios (Belouttar et al., 2009).

Composite sandwich structures provide an efficient method to increase bending rigidity without a significant increase in weight. Sandwich structure is composed of the top and bottom skins which are separated by core material (He and Hu, 2008). Because of this special feature, the sectional area is increased and consequently an increase in its flexural rigidity. The strength of this type of construction results from the combination of properties from the skin, core and interface (Mai et al., 2007). Composite sandwich structures can be designed so that each component is utilised to its ultimate strength. Fibre composites are commonly used for the skin due to its high mechanical performance and low density (Shenhar et al., 1996) however sheet metal laminated directly onto the core may also be used (Karlsson and Astrom, 1997). The skins are subject to either tension or compression and are largely responsible for the flexural strength and stiffness of the sandwich structure. On the other hand, the core material provides most of the shear rigidity (Galletti et al., 2008). It also plays an important role in enhancing the flexural rigidity without increasing the weight and thereby controlling the failure mechanisms (Feichtinger et al., 2006). In a sandwich structure, the faces resemble the flanges and the core acts as the web. Similar to an I-beam, a structural sandwich will transmit loads to their top compression skin down to the bottom tension skin through the core in shear. In order to act efficiently, the core material of a sandwich structure should have good shear stiffness and strength.

A great variety of core materials, such as balsa wood, foam core, honeycombed and trussed core, have been bonded to fibre composite skins to manufacture sandwich panels and structures (Vinson, 1999). Figure 2.13 shows some of the commonly used core materials. Traditional sandwich structure is generally formed by a simple foam core structure with low mechanical properties shown in Figure 2.13a (Torre and Kenny, 2000). However, the low compressive strength of foam core limits its use in structural applications. Brocca et al. (2001) found that composite sandwich structure with light weight foam core material usually fails due to core indentation and crushing. In addition, the low shear stiffness of the foam core leads to early skin-

core delamination failure (Russo and Zuccarello, 2007). This premature delamination failure in the soft-core sandwich beams decreases the capacity by more than 40% (Sokolinsky et al., 2003). Foam core tends to absorb and retain moisture often reducing the structure's mechanical properties and increasing its weight (Moody and Vizzini, 2000). Another challenge has been to improve the behaviour of foam core material in fires (Marsh, 2007). Balsa wood (Figure 2.13b) is another common core material in sandwich structures because of its light weight and good mechanical properties (Grenestedt and Bekisli, 2003). The major problem with balsa wood is its susceptibility to water penetration leading to swelling, debonding and rotting.

Honeycombed cores (Figure 2.13c) have received much attention in recent years to meet compression requirements of sandwich structures. Honeycombed core sandwich panel is formed by adhering two high-rigidity thin-face sheets with a low density honeycomb core possessing less strength and stiffness (He and Hu, 2008). A sandwich composite with honeycomb core increases the low through thickness compressive strength of commonly used composite sandwich structure. These core materials can perform better in compression and shear at equivalent weight, if designed properly. However, the closed cell of the honeycombed core is susceptible to entrapped moisture causing potential for delamination of the core and skins (Kooistra and Wadley, 2007). The continued high cost of this core structure has also restricted their applications predominantly to the aerospace industry (Reis and Rizkalla, 2008). The shortcomings of honeycomb core lead to the development of an open-cell lattice truss structure core (Figure 2.13d). Composite sandwich structures with trussed cores are highly efficient from a weight standpoint and have a good compression performance (Wicks and Hutchinson, 2001). However, these sandwich panels are weak at bearing concentrated loads and very difficult to join (Demelio et al., 2001). The presence of cavities between the skins of honeycomb and truss cores materials reduces the capacity of these composite sandwich structures to hold mechanical connectors. These studies showed that the performance of a sandwich structure depends largely on the properties of its core. The nature of the core of existing sandwich structure also limits its application for civil infrastructures. Thus, the evolution of a composite sandwich structure with lightweight, high strength core material and with good holding capacity for mechanical connections could provide an opportunity to develop this material for railway turnout sleepers.
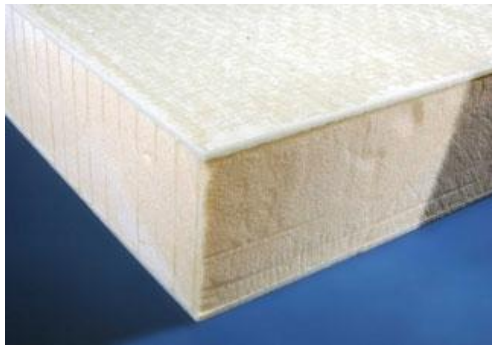
(a) Foam core

(b) Balsa wood

(c) Honeycomb core
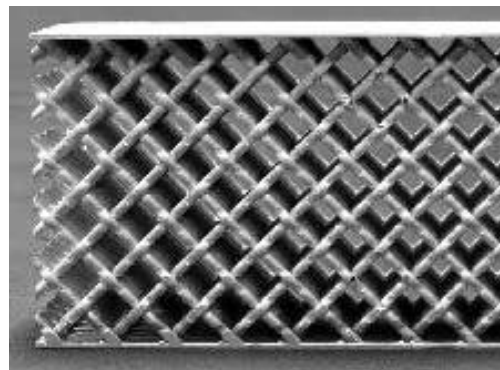
(d) Trussed core

Figure 2.13 Commonly used core materials

2.9 Recent developments in composite sandwich structures

Composite sandwich structure has been identified as a very interesting alternative to traditional construction materials. Consequently, several researchers have contributed towards the research and development of composite sandwich for structural purposes. The desired stiffness and strength characteristics of the sandwich structures can be modified by varying the materials for the skin and the core (Daniel and Abot 2000). Mouritz and Thomson (1999) investigated the edgewise compression, shear and flexural properties of GFRP and polyvinyl chloride (PVC) foam core sandwich panels to find the damage tolerance of a large mine hunter ship. It was found that the edgewise compression strength decreases with increasing length and the failure mechanisms changes suddenly from compressive fracture of face-sheet to shear crimping of the core. Dai and Thomas Hahn (2003) found similar results on the flexural behaviour of sandwich beams with different core materials. A higher shear strength was measured for heavier H-250 PVC foam core than the lighter D-100 end grain balsa wood core. However, this advantage disappears as the span becomes longer as both beams failed due to skin failure. The results of the study conducted by

Borsellino et al. (2004) showed that the presence of different fibre composite skins does not significantly affect the stiffness of the sandwich structure but heavily influences the fracture mechanism, while the core material greatly influences the compressive strength. The results of their numerical modelling also showed that the composite sandwich behaviour can be predicted using the material data obtained from experimental test. Mahfuz et al. (2004) showed that the stiffness and strength of the sandwich beams increased with increasing core density. Russo and Zuccarello (2007) investigated the mechanical behaviour of fibre glass laminate skins over PVC foam employed in the marine construction. The results showed that the low shear stiffness of the core material resulted to an early skin-core delamination failure under three and four point loading. The shorter specimens have failed due to shear failure of the core while the longer specimens have failed after the lower skin tensile failure.

Styles et al. (2007) investigated the effect of core thickness on the flexural behaviour of aluminium foam core sandwich structures. Results of the 4-point bending test showed a number of failure mechanisms in the sandwich specimens with different core thicknesses. The specimens with thinner cores exhibited skin wrinkling while samples with thicker cores failed due to core indentation. Shear cracking of the core became the dominant failure mode for samples with a thick core and an increased skin thickness. Cabrera et al. (2008) designed and manufactured sandwich panels with polypropylene (PP) skins and core. The all-PP sandwich panels showed superior flexural stiffness and buckling performance but low compressive strength. Mamalis et al. (2008) developed a new hybrid concept for sandwich structures. This new concept uses metal sheets at the outer surfaces adhesively bonded to lightweight cores to maximise rigidity while introducing an intermediate plywood layers between the skins and the core. The results showed that the introduction of an intermediate plywood layers improve the impact resistance of the composite sandwich structure. The failure of the hybrid composite sandwich structure is due to the indentation on the low-strength core material. Jen and Chang (2008) showed that the bending and fatigue strengths of the aluminium honeycomb sandwich beam increases with the relative density of the core.

A thorough investigation on the failure behaviour of composite sandwich beams made up of unidirectional carbon/epoxy skins and a PVC closed-cell foam core under three- and four-point bending was undertaken by Gdoutos and Daniel (2008a). Based on the results of their study, they concluded that the failure modes of

sandwich beams depend on the type of loading, constituent materials and geometrical dimensions. The failure modes observed of the sandwich beams that they have tested includes core failure, compressive skin wrinkling and indentation failure. Belouttar et al. (2009) investigated the effects of core densities on the static and fatigue behaviours of honeycomb composite sandwich under four-point bending. The results showed that the stiffness and the failure load of composite sandwich increases with increasing core density. They have also observed that the failure modes of the sandwich structure depend largely on the nature of the core material. Failure is essentially due to wrinkling of the compressive skin for high density core materials.

In recent years, there have been considerable attempts to improve the performance of core materials for composite sandwich structure. Marsh (2007) suggested that cellular manipulation could be made to achieve a high strength core material for composite sandwich structures. Accordingly, Daniel and Abot (2000) filled the cells of the honeycomb core with epoxy to prevent premature shear failure of the composite sandwich structure at the load application. The results of their 4-point flexural testing showed that filling the cells of the honeycomb core with epoxy at the shear span prevented the premature shear failure of the core and the flexural failure was ensured at the constant moment region. In another study, Sokolinsky et al. (2003) altered the sandwich beam structure by reinforcing the outer core sections with another layer of fibres in order to prevent shear failure of the core and to ensure compression failure of the skin under four-point bending tests. Similarly, Dai and Thomas Hahn (2003) measured higher shear strength for H-250 polyvinyl chloride (PVC) foam core than the D-100 balsa wood core for short beams. However, such advantage disappeared as the test span becomes longer. On the other hand, Mahfuz et al. (2004) improved the performance of a sandwich structure under flexure by infusing titanium dioxide (TiO_2) nanoparticles into the parent polyethylene foam material to strengthen the core structure. The results showed that a 53% increase in the flexural stiffness and about 26% in strength could be attained by infusing 3% loading of TiO_2 nanoparticles in the core compared to a neat polyurethane.

Another approach to improve the performance of sandwich structure is to reinforce the core with fibre composites. Karlsson and Astrom (1997) suggested that three-dimensional reinforcing fabrics that integrate the faces and the core have the potential of significantly improving structural integrity of composite sandwich structures. Stoll et al. (2001) developed the fibre-reinforced foam (FRF) core for

composite sandwich panel construction. This core material is composed of closed-cell foam mechanically combined with composite fibres which takes the form of angled struts oriented in a truss or lattice-like webs. The standardised sandwich panel tests performed have shown that the FRF core can surpass the structural performance of the common structural core materials, however, the greater amount of fibre reinforcement in the core increases the amount of resin pickup during moulding which adds to the weight and cost of a panel. Lascoup et al. (2006) studied the mechanical effect of stitching the top and bottom skins of the composite sandwich panels with glass fibres (Figure 2.14). They found that stitching added mass to the composite sandwich panel, although this prevented the delamination between the skins and the core and enhance its mechanical performance. The stitching causes the sandwich panel to become more brittle and fragile compared to an unstitched panel.
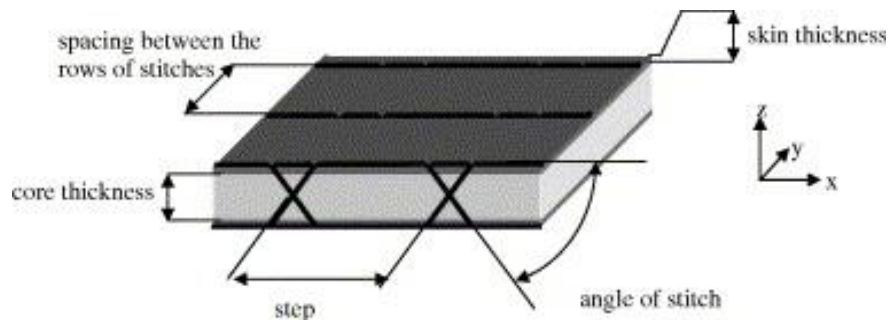
Figure 2.14 Stitched sandwich panel (Lascoup et al., 2006)

The concept of stitched sandwich panel is similar to the "tied-core" sandwich structure introduced by Pitarresi et al. (2007) to prevent the debonding failure between the skin and the core. In this design, some form of additional reinforcement is integrated within the core. The extra reinforcement provided increased stiffness and strength to the foam-cored sandwich panels. Not contradictory to this finding, Feichtinger et al. (2006) found that resin-filled kerfs slightly augmented the shear strength of foam core structure. Furthermore, Reis and Rizkalla (2008) developed a 3-D fibre reinforced polymer sandwich panel with the top and bottom skins connected with through the thickness unidirectional glass fibres to overcome delamination problems typically encountered in traditional sandwich systems. The results of their experimental investigation showed that by increasing the quantity of 3-D fibres, a significant increased in the shear modulus and compressive strength was obtained. However, there is a decrease in the tensile strength of the skins due to

the waviness created by the stitched fibres. Kampner and Grenestedt (2007) found that the introduction of corrugated skin improved the shear carrying capacity and offered weight savings in the composite sandwich structure (Figure 2.15). The corrugated skin also increases the wrinkling strength of compression loaded sandwich structures. As a result, the corrugated sandwich beams showed similar strength but weigh 10-20% lighter than their plain counterparts.

Figure 2.15 Sandwich with corrugated skin (Kampner and Grenestedt, 2007)

Studies have shown that the enhancement of the core material significantly improved the performance of the composite sandwich structures. However, the methods of enhancement to core structure involve a complex process such as weaving or injection technology which may further increase the cost of production. The combined use of flatwise and edgewise sandwich laminations in the beam might contribute towards the improvement of the structural performance while maintaining the simplicity of the production process. This presents an ideal opportunity to increase the use of composite sandwich structures for civil engineering applications.

2.10 Applications of composite sandwich structures in civil engineering

The recent applications have demonstrated that composite sandwich construction can be effectively and economically used in the civil infrastructure. A unitary construction or "*monocoque*" fibre composite truss concept which uses two planer skins that contain the fibre separated by a core material was designed and developed by Humpreys et al. (1999). The Advanced Composite Construction System (ACCS), undertaken by Maunsell Structural Plastics, London, made from pultruded FRP composite with polyethylene foam core was developed for use in walls and floors of

a two-storey building structure (Holloway and Head, 2001). An all natural composite sandwich beams for structural applications was developed by Dweib et al. (2004). The 89 x 203 mm composite sandwich beam which is made up of skins from recycled paper combined with chicken feathers and foam core exhibited flexural stiffness and strength comparable to that of 38.1 x 88.9 mm Cedar timber. An FRP composite sandwich deck was used to replace the deteriorated concrete slab on a bridge over Bennet's creek in Steuben County, New York (Aref et al., 2005). Prior to this, Kalny et al. (2003) has investigated the behaviour of FRP bridge deck system made up of sandwich panels with a honeycomb core. This system is now installed in bridges in several states in the US including Kansas, Missouri and West Virginia. Rocca and Nanni (2005) investigated the structural performance of a low-profile bypass roadway made up of sandwich panels which are comprised of GFRP skins and fibre reinforced foam core. Omar (2008) developed a deployable shelter using modular fibre composite truss panel as the main structural system. The diagonal members of the truss are made of composite sandwich structures as shown in Figure 2.16.
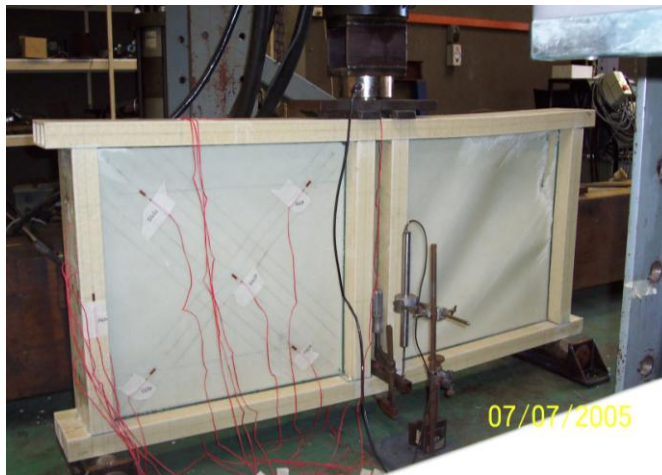
Figure 2.16 Modular fibre composite truss panel (Omar, 2008)

The inherent advantages in strength and stiffness per unit weight as compared to traditional steel reinforced concrete decks make the composite sandwich bridge decks a good alternative. Several variants of fibre composite bridge decks comprise sandwich profiles, spanning transversely or longitudinally between supporting elements (such as concrete, steel and timber beams) or suspended from tension cables have been developed (Karbhari and Seible, 2000). Kumar et al. (2003; 2004)

studied the flexure performance under static loading of an all-composite bridge deck made of pultruded GFRP tubes. The unidirectional glass fibre tubes were bonded together using epoxy adhesive to build a four-layered tube bridge deck assembly. The experimental results showed that the stiffness of the tubes and their assemblies demonstrate that they can be used in the building of an all-composite bridge decks and for other infrastructure applications. The other structures constructed using fibre composite sandwich profiles are highway bridge deck systems (Davalos et al., 2001) and temporary bypass roadways (Rocca and Nanni, 2005).

Many studies have shown that fibre composite sandwich structures are now commonly used in many areas of civil engineering. Composite sandwich materials are now commonly used as structural panel for roofs, floors, walls and bridge decks. However, very limited attempt has been done so far to use these materials for structural beam application although engineers have access to a wide range of composite sandwich panels. The only available report known to the authors on sandwich construction for beam application was when it was used as a web of an innovative hybrid box section proposed by Canning et al. (1999). The web of the beam section is made up of sandwich construction to prevent buckling with an upper layer of concrete in the compression side. A similar structural concept was used by Primi et al. (2009) to construct a new FRP bridge in Spain. The webs of this hybrid fibre composite bridge beam are sandwich panels with polyurethane core and glass-fibre skins produced by hand lay-up process. The main reason for the lack of composite sandwich application for structural beams could be that most of the currently used core materials are not appropriate for this type of application.

2.11 Novel composite sandwich structures for replacement railway sleepers

The LOC Composites Pty. Ltd. in Toowoomba, Queensland, Australia is now producing a novel fibre composite sandwich panel with lightweight but high-strength core material (Figure 2.17). The composition of the skin and core of this composite sandwich structure is discussed in the next chapter. In addition to being moisture proof, this composite sandwich panel is also strong, lightweight, termite proof, and with excellent thermal insulation properties. Most importantly, this sandwich structure uses less than 1/7th the energy to produce and maintain, creates $1/10^{th}$ the volume of polluted water and about $1/5^{th}$ the air pollution (Van Erp and Rogers, 2008). The structural application of this composite material has been demonstrated in

several building and residential projects within Australia and its use has already been explored for bridge infrastructure. Figure 2.18 shows some of the structural applications of the composite sandwich panel. There is no systematic study on the behaviour and failure mechanisms of this novel sandwich structure although actual construction applications now exist. Neither are there reports on the behaviour of glue-laminated beams from composite sandwich structures. Therefore, understanding its behaviour could lead to a safer and more efficient use of this material and the possibilities for the development of new structural forms and components.

Figure 2.17 The fibre composite sandwich panels produced by LOC Composites
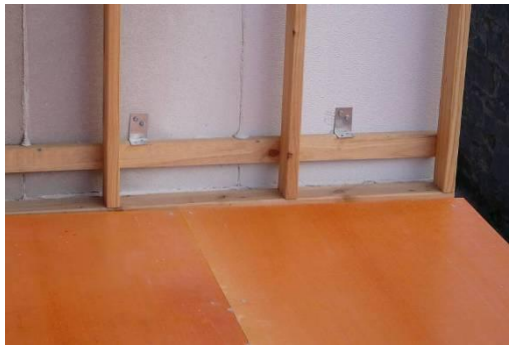
(a) Wet areas and balconies   (b) Pedestrian decks

Figure 2.18 Structural applications of fibre composite sandwich panels

The development of structural beams made completely from this composite panel for railway turnout sleeper application is highly practical. As these composite sandwich panels are produced in limited thickness for reasons of cost effectiveness and efficiency, the structural beam can be manufactured by gluing several sandwich panels together either in the flatwise (horizontal) or edgewise (vertical) positions.

The glue lamination construction technique has been gaining popularity in structural applications due to the increasing difficulty of sourcing large cross-section of timber with approved quality (Hernandez et al., 1997). This type of construction provides flexibility to tailor different properties of the structural member using smaller elements to achieve strength and stiffness requirements. A good understanding of the behaviour of structural sections manufactured using this type of construction technique and the individual sandwich laminations is important in order to develop an optimised railway sleeper section and guarantee its structural performance.

2.12 Conclusions

The widespread deterioration of most timber sleepers combined with an intensified pressure to limit its use as a result of environmental concerns are the main drivers for research throughout the world aimed at finding a suitable alternative for timber sleepers. While many railway infrastructure companies have long been trialling materials like concrete and steel, this has gained limited success as these materials have not proven reliable alternatives to existing timber sleepers. Research and development have now focused on fibre composites, as the many issues related to the currently used sleeper material could be simulated using this material.

Fibre composite alternatives for railway sleepers have the ability to compete effectively with conventional sleeper materials. This material can be engineered based on the required structural applications and has excellent durability requiring less maintenance. Fibre composite sleepers have shown that this alternative sleeper material has physical and mechanical properties comparable or even better than that of timber sleepers. Although most fibre composite sleeper developments are more expensive compared to traditional sleeper materials, fibre composites remains a viable alternative for specific applications such as railway turnouts where larger, longer, stronger and more expensive timber sleepers are required. Currently, there is no significant research and development on fibre composite sleepers for railway turnout, a case study on the application of fibre composites to railway turnout sleepers should therefore be conducted

The many advantages of fibre composite sandwich structure support the development of a low weight, high strength and more durable railway sleepers. The significant improvement on the strength of the core material of a novel fibre composite sandwich structure presents an ideal opportunity to use this material in the

development of railway turnout sleepers. However, little is known about the performance of the structural elements made from laminated composite sandwich beams even though the structural benefit of this sandwich construction have been highlighted in many applications. A good understanding of the complicated behaviour of the individual sandwich structure and their failure mechanisms is necessary before this material can be used in the development of railway turnout sleepers. The overall behaviour of the full-scale composite sandwich beams should be determined and the validity of this novel composite sandwich beam concept for railway turnout sleeper application should be investigated. These topics are systematically studied in the succeeding chapters.

In Chapter 3, an extensive investigation into understanding the behaviour of the basic materials constituting the composite sandwich section is presented.

Chapter 3

Characterisation of the constituent materials of a novel composite sandwich structure

3.1 Introduction

The development of a novel fibre composite sandwich structure presents an ideal opportunity to increase the use of fibre composites for civil infrastructure. As discussed in Chapter 2, this composite material has a high potential for the development of a timber replacement railway turnout sleeper. A detailed knowledge of the mechanical behaviour and the failure mechanisms of the basic materials which constitute this sandwich structure is however necessary, for its effective utilisation as a structural material. This chapter focuses on the intensive experimental investigations onto the characterisation of the mechanical properties of the fibre composite skins and the core material of such composite sandwich structure.

The overall performance of composite sandwich structure depends on the mechanical properties of its constituent materials, thus a detailed knowledge of the behaviour of the skin and the core is a fundamental requirement for the effective utilisation of a fibre composite sandwich structure. This information is important to predict the behaviour of structural components made from this composite material. It is also important to establish failure limits of the basic materials that constitute the composite sandwich structure in order to size them appropriately both for strength and serviceability requirements.

It is generally preferred to determine the material properties of fibre composites for structural engineering applications experimentally and not rely only on theoretical models (Bank, 2006). This is because the result from theoretical model relations may not always agree with experimental values since the fibres themselves exhibit some degree of anisotropy and fibre properties are very sensitive to the fabrication conditions (Gay and Hoa, 2007). Similarly, the individual properties of fibres and resin, the fibre volume fraction, and the composition of all the laminae within the sandwich profile must be known for the estimation of the mechanical properties (Santos-Neto and La Rovere, 2007). In most cases however, not all the

details of the composite materials in a laminate are known, which is the case in this study. Consequently, several experimental studies using coupon specimens have been conducted to determine the effective mechanical properties of the structural components made from fibre composite materials (Herakovich and Mirzadeh, 1991; Wang and Zureick, 1994; Bank et al., 1996; Davalos et al., 1996). The results of these studies have shown that the structural response of a fibre composite section can be predicted accurately using the material properties obtained from coupon test data. In 2003, Bank et al. proposed a model specification that provided a procedure for material characterization, methods for prediction of material properties, and performance and acceptance criteria of fibre composite materials for civil engineering structures through test of coupon specimens. For this reason, properly designed and carefully conducted experiments are important in order to determine the mechanical behaviour of the constituent materials of a composite sandwich structure in order to advance this material for the civil infrastructure use.

The characterisation of the mechanical properties of the fibre composite skins and the modified phenolic core material was conducted using coupon specimens following the ISO and the ASTM standards. These mechanical properties are then utilised as material input into the analytical and numerical investigations for the verification of the behaviour of the fibre composite sandwich structures.

3.2 Material under study

The structural composite sandwich panels tested in this study are manufactured by LOC Composites, Pty. Ltd. Australia using proprietary formulations. This highly sustainable fibre composite structure is made up of bi-axial (0/90) glass fibre composite skins co-cured onto the modified phenolic core material using a toughened phenol formaldehyde resin (Figure 3.1). The composite sandwich panel has an overall density of around 990 kg/m^3. The top and bottom skins of this composite sandwich structure is made up of 2 plies of stitched bi-axial (0/90) E-CR glass fibre fabrics manufactured by Fiberex Corporation and has a nominal thickness of 1.792 mm. The 0-degree glass fibres have a density of 400 g/m^2 and a thickness of 0.512 mm while the 90-degree glass fibres have a density of 300 g/m^{2}and a thickness of 0.384 mm. The modified phenolic foam core of the structural composite sandwich panel is a proprietary formulation by LOC Composites. This material comes from

natural plant products derived from vegetable oils and plant extracts and chemically bonded within the polymer resin (Van Erp and Rogers, 2008).
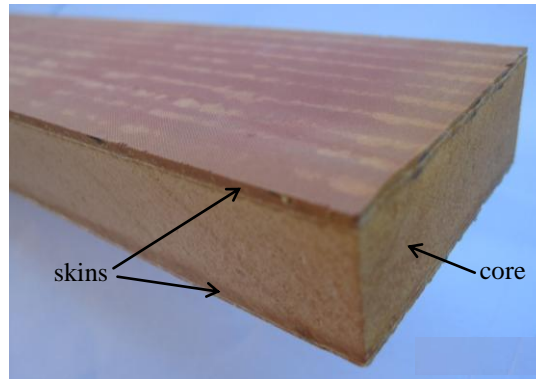
Figure 3.1 Cross-sectional view of the novel composite sandwich panel

3.3 Characterisation of the fibre composite skin

The test specimen for the fibre composite skin is cut from the laboratory size panel, which was fabricated by hand lay-up process. The same toughened phenol formaldehyde resin was used for the laminate matrix. The burnout tests conducted following ISO Standard 1172 (1996) revealed that the fibre composite skin has a glass fibre content of around 45% by weight. This proportion is similar to the glass fibre content of the skin obtained from the actual sandwich panel. The experimental characterisation of the fibre composite skins has been performed using flexure, tensile, compressive and shear tests. The details of the specimen for characterisation of the behaviour of the fibre composite skin are listed in Table 3.1. Six specimens of each, cut in the longitudinal (0°) and the transverse (90°) directions of the test laminate were prepared and tested to determine the constitutive behaviour of the fibre composite skin. Each specimen was labelled with an identifying number in preparation for the test.

Table 3.1 Details of specimens for skin characterisation

Type of test	Test standard	No. of coupons	Dimensions (mm)		
			length	width	thickness
Flexural	ISO 14125:1998(E)	6	60	15	1.792
Tensile	ISO 527-1:1995	6	300	25	1.792
Compressive	ISO 14126:1999	6	140	12.75	1.792
Shear	ASTM D5379:1993	6	76	20	1.792

3.3.1 Flexural test

The flexural test of the fibre composite skin was conducted following the ISO 14125 (1998) standard. The specimen was simply supported and was tested under 3-point loading with the span set at approximately 16 times the thickness of the laminate (Figure 3.2). The supports are made up of a roller and a pin to allow the specimen to rotate minimising the membrane stresses. The load was applied at midspan of the specimen at a constant rate of 1 mm/min using a 10 kN MTS testing machine. The load and midspan deflection were recorded up to failure to determine the strength and elastic properties in bending. The failure mode was also observed after each test.

The typical flexural stress-strain relationship at the bottom of the fibre composite skin is shown in Figure 3.3. In the figure, F2-0 represents the specimen tested in longitudinal direction while F2-90 represents the specimen tested in the transverse direction. Based on the experimental results, the specimen F2-0 showed a linear stress-strain relationship up to failure. The maximum bending stress calculated ranges from 305 to 340 MPa with maximum strain values of 22900 to 26200 microstrains. On the other hand, the stress-strain curve of specimen F2-90 showed a linear response up to around 28000 microstrains and then started to behave non-linearly thereafter with increasing stress until final failure. The nonlinear behaviour could be due to the progressive failure of the matrix and the 90-degree fibres. The specimen in the transverse direction failed between the stress of 118 and 153 MPa and strain levels between 52000 and 67000 microstrains. All the fibre composite skin tested under flexure failed due to fracture of the fibre at the tensile side of the specimen under the loading point as shown in Figure 3.4.

(a) Schematic illustration of flexural test   (b) Actual test set-up
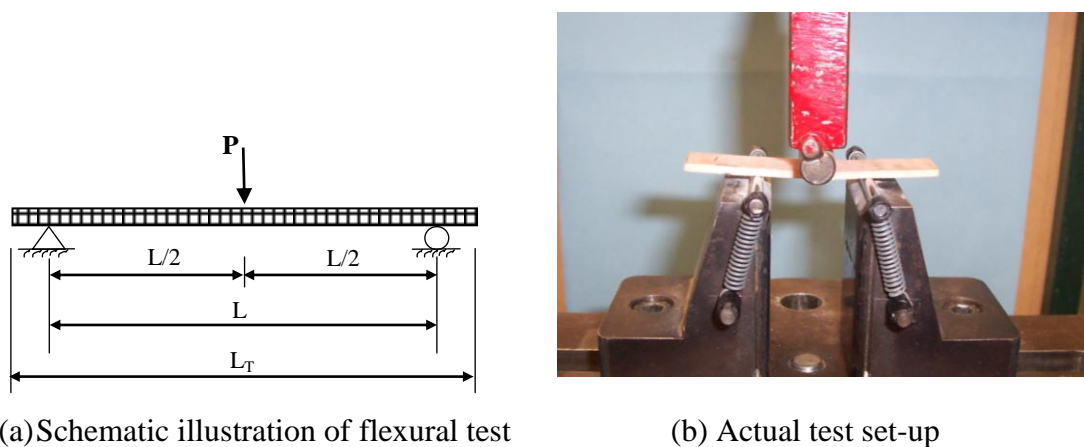
Figure 3.2 Flexural test set-up of fibre composite skins
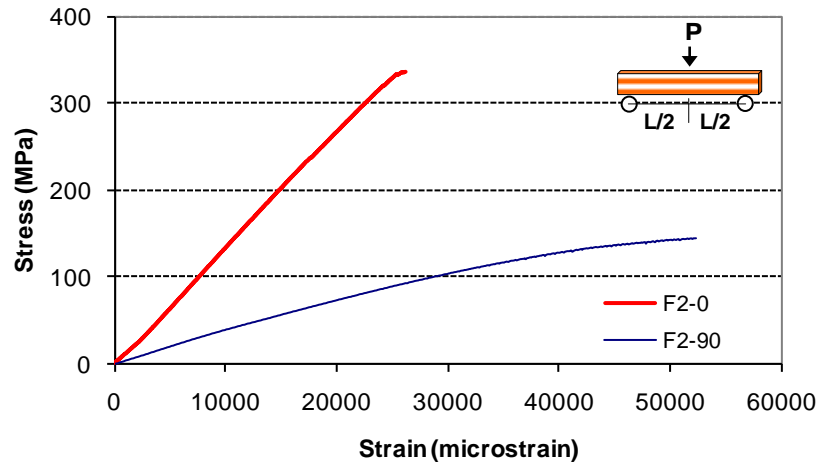
Figure 3.3 Flexural stress-strain relationship for fibre composite skins
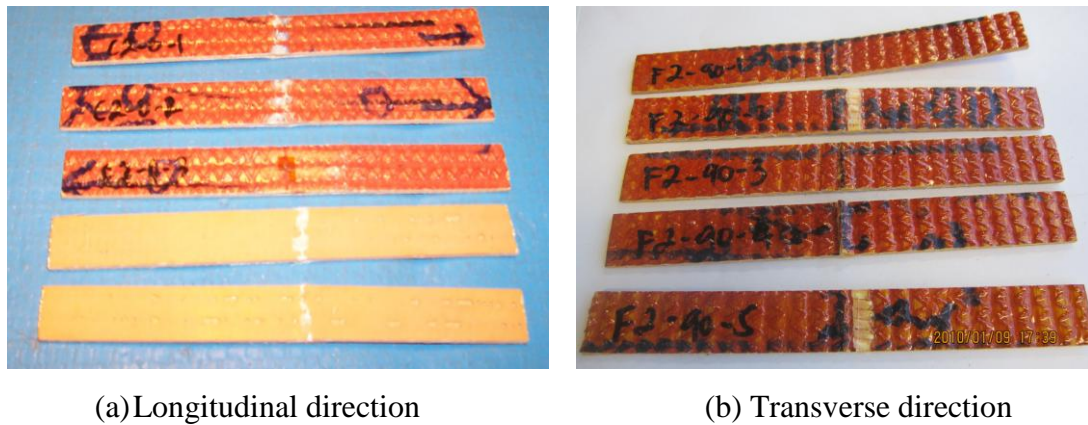
(a) Longitudinal direction   (b) Transverse direction

Figure 3.4 Failure mode of fibre composite skins in flexure

3.3.2 Tensile test

The tensile test of the fibre composite skin was conducted following the ISO 527-1 (1995) standards. Figure 3.5 shows the test set-up and instrumentation for the tensile test of the skin. The specimens were tested in tension using an Avery testing machine (capacity 530 kN) with a loading rate of 1mm/min. The ends of the specimen were carefully clamped onto the testing jaws to prevent slipping at the gripping area and prevent the premature fracture at the grip. All the tensile specimens were instrumented with uniaxial strain gauges to measure the longitudinal strain at any time during the test and up to failure. An extensometer was also provided at the gauge length to measure the longitudinal and transverse deformations for determination of the Poisson's ratio. The extensometer was removed from the specimen when the longitudinal strain of 3000 microstrains was reached to prevent any damage to the test equipment. Data logger was used to record the load and strain

during the test. All specimens were tested up to failure to determine the strength and the failure mode.

The modulus of elasticity, stress-strain behaviour and the failure modes of the tensile specimens were evaluated. The Poisson's ratio was computed as the ratio of the lateral strain to that of the axial strain. The tensile stress was then determined by dividing the applied load with the average cross-sectional area of the specimen. The typical stress-strain diagram of the fibre composite laminates under tensile loading is shown in Figure 3.6. In the figure, T2-0 represents the specimen tested in the longitudinal direction while T2-90 represents the specimen tested in the transverse direction. The modulus of elasticity was calculated from the linear portion of the stress-strain curve between 1000 and 3000 microstrains. The tests have shown that the specimen T2-0 exhibits an almost linear elastic behaviour in tension. However, a slight decrease in stiffness at a strain of about 6000 microstrains (stress of around 90 MPa) was observed which could be due to the formation of tensile cracks in the resin. The maximum tensile stress calculated in the longitudinal direction ranges from 232 to 257 MPa with maximum strain values of 16000 to 18000 microstrains. A similar behaviour was observed in the specimen T2-90. The stress increased linearly with strain but showed a decrease in stiffness at a strain value of about 6000 microstrains (around 70 MPa). Again, this decrease in stiffness could be due to the cracking of the resin matrix. The maximum tensile stress calculated for specimen T2-90 varied from 210 to 219 MPa with strain values around 24000 micro strains.

All of the specimens failed due to tensile failure of the unidirectional fibres within the gauge length with no observed slip or failure in the anchorage zone. In the longitudinal direction, failure was initiated by the rupture of the 0-degree fibres (Figure 3.7a). The tension failure along the longitudinal direction was instantaneous and catastrophic as the specimen failed in an explosive manner. In the transverse direction, cracks in the resin matrix were observed at the initial application of the load. A light "click" sound was then heard indicating the failure of the 90-degree fibres. However, the specimen continued to resist the applied load and failed at a slightly higher strain due to the fracture of the 0-degree fibres (Figure 3.7b).

(a) Schematic illustration of tensile test   (b) Actual test set-up
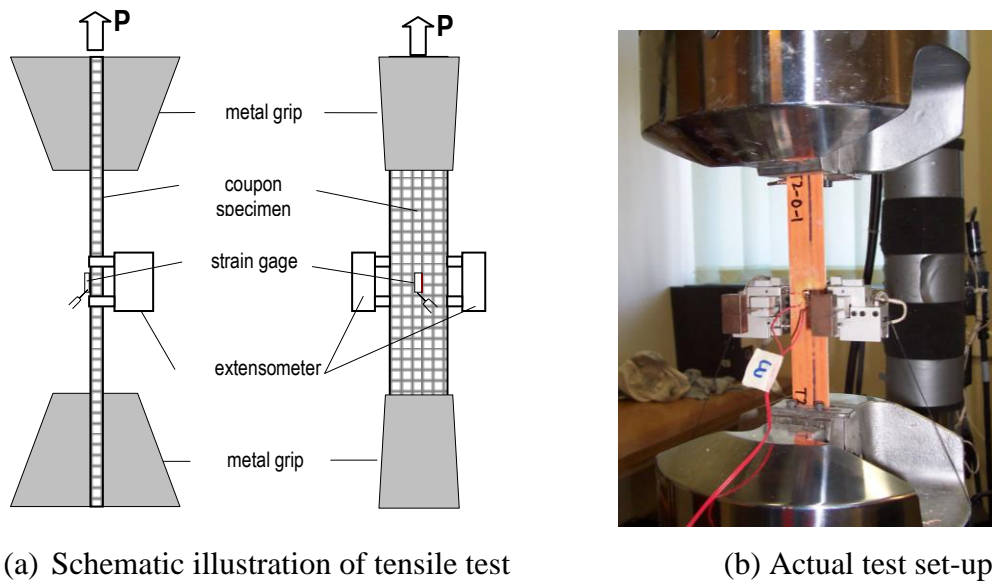
Figure 3.5 Tensile test set-up of fibre composite skins
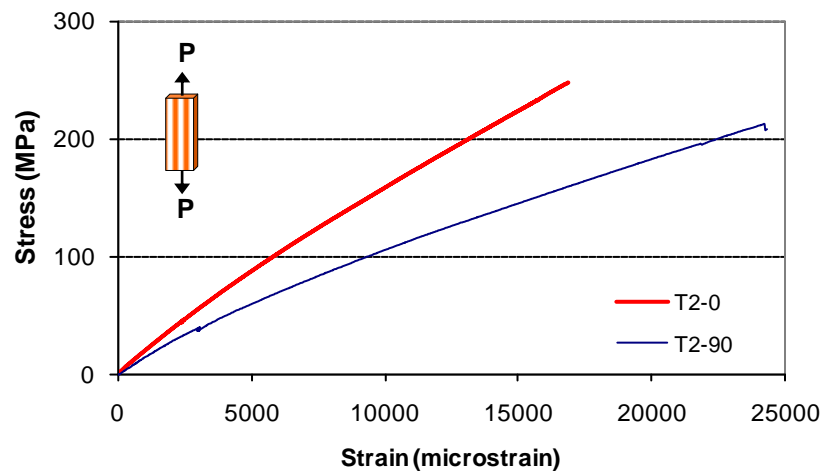
Figure 3.6 Tensile stress-strain relationship for fibre composite skins

(a) Longitudinal direction   (b) Transverse direction
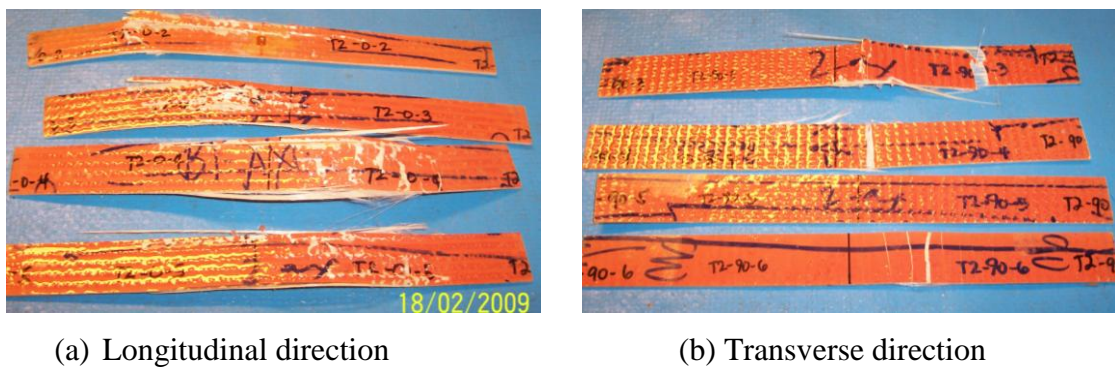
Figure 3.7 Failure mode of fibre composite skins in tension

3.3.3 Compressive test

The compressive test of the skin was carried out following the ISO 14126 (1999) standard. Figure 3.8 shows the test set-up and instrumentation for the compressive test of fibre composite skins. All of the compressive test specimens were instrumented with a single element, foil resistance strain gauges in the gauge section to measure the strain during the test. The strain data were then used to calculate the compressive modulus and determine the strain up to failure of the fibre composite skin under compressive loading. The specimens cut along the longitudinal and transverse directions were loaded at the end in a universal testing machine by the Wyoming Modified Celanese Compression test fixture at the rate of 1 mm/min until failure. The specimen was compressed and the subsequent deformation at various loads was recorded. After each test, the specimen was carefully removed from the test fixture and the failure mode was observed and recorded.

(a) Schematic illustration of compressive test   (b) Actual test set-up
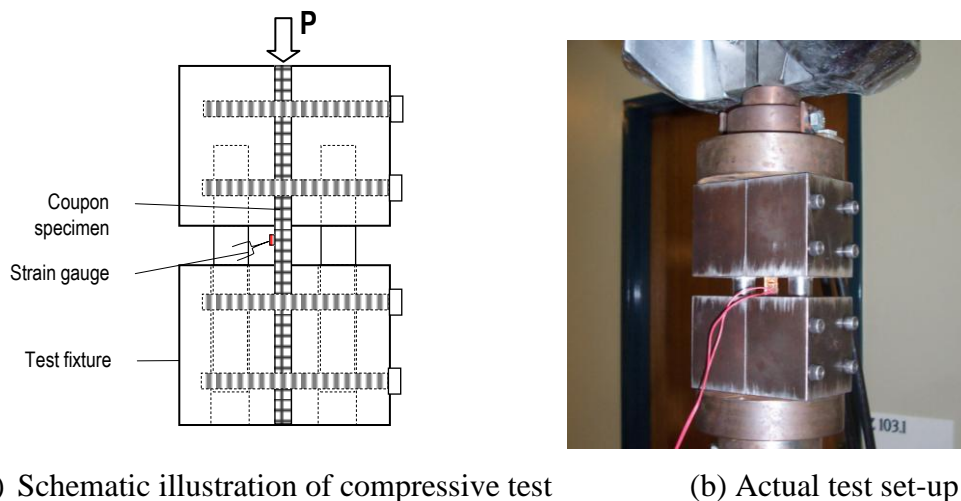
Figure 3.8 Compressive test set-up of fibre composite skins

Figure 3.9 shows the typical stress-strain relationship of the fibre composite skins under compressive loading. In this figure, C2-0 represents the specimen tested in longitudinal direction while C2-90 represents the specimen tested in the transverse direction. The compressive stress was calculated by dividing the applied load with the average cross-sectional area of the specimen while the strain was determined using uniaxial strain gauges attached to the specimen. The compressive modulus was then determined from the linear fit of the stress-strain curve between 1000 and 3000 microstrains. In both the longitudinal and transverse directions, the fibre composite

skin under compressive loading behaved linearly elastic up to failure. In specimen C2-0, the maximum stress calculated ranges from 200 to 226 MPa with strain values from 12000 to 13600 microstrains. On the other hand, the specimen C2-90 failed at a maximum stress of 118 to 132 MPa with a strain of about 11600 microstrains. All of the specimens tested under compression failed by interfibre fracture at the gauge length (Figure 3.10).
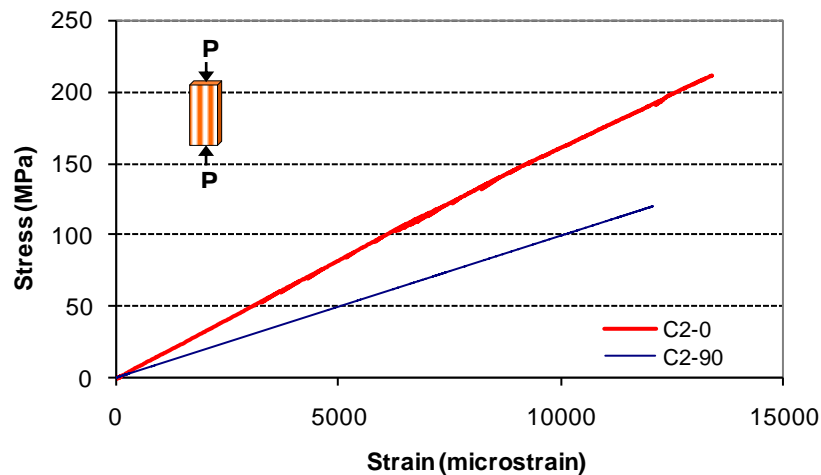
Figure 3.9 Compressive stress-strain relationship for fibre composite skins
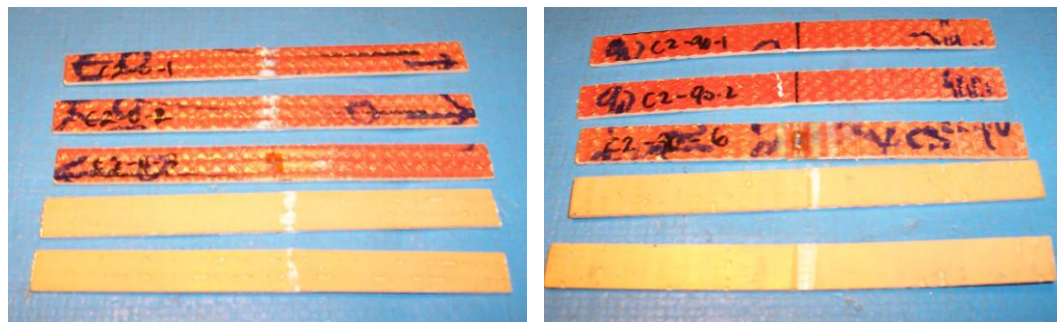
| (a) Longitudinal direction | (b) Transverse direction |

Figure 3.10 Failure mode of fibre composite skin in compression

3.3.4 Shear test

The shear test of the fibre composite skin was conducted following the ASTM D5379/D5379M (1993) standards. Coupon specimens of rectangular beam shape with symmetrically located V-notch at the centre were tested (Figure 3.11). The specimen was loaded on a universal testing machine by a modified Iosipescu shear test fixture at a constant head speed of 1 mm/min. The applied load was measured with a 22 kN load cell and recorded into the data acquisition System 5000. Three of

the five specimens were provided with resistance strain gauges oriented at $\pm 45^{o}$ to the loading axis bonded in the middle of the specimen to determine its shear response during the entire loading. The average shear strain is then determined from the strain gauges using the relation:

$$\gamma_{ave} = \varepsilon_{+45} - \varepsilon_{-45} \tag{3.1}$$

The average shear stress is determined by dividing the applied load by the area of the cross section between the notches while the apparent shear modulus is calculated by dividing the average shear stress by the average shear strain.

$$\tau_{ave} = \frac{P}{A} \tag{3.2}$$

$$G_{ave} = \frac{\tau_{ave}}{\gamma_{ave}} \tag{3.3}$$

Figure 3.12 shows the typical shear stress-strain relationship of the fibre composite skins. In this figure, S2-0 represents the specimen tested in the longitudinal direction while S2-90 represents the specimen tested in the transverse direction. The experimental shear stress-strain curves showed that the fibre composite skins used in this study exhibits a linear behaviour up to a shear strain of 4000 microstrains in the longitudinal direction. A significant reduction in shear stiffness was then observed until failure at an ultimate shear strain of about 30000 microstrains. This reduction in stiffness could be due to the tensile cracking of the matrix. The specimen failed at an average shear strength of 23.2 MPa. On the other hand, the specimen S2-90 failed at an average shear strength of 21.8 MPa and shear strain of around 26000 microstrains. The shear modulus was determined from the initial linear region of the shear stress-strain curve. In general, the fibre composite skins in both the longitudinal and the transverse directions behaved similarly under shear loading. This could be due to the behaviour of the matrix resin dominates during the application of loads. However, the presence of more 0° fibres in the longitudinal direction resulted to the fibre composite skins to fail at slightly higher stress and strain than in the transverse direction. The skin failure is mainly due to shear failure at the notch of the specimen (Figure 3.13).
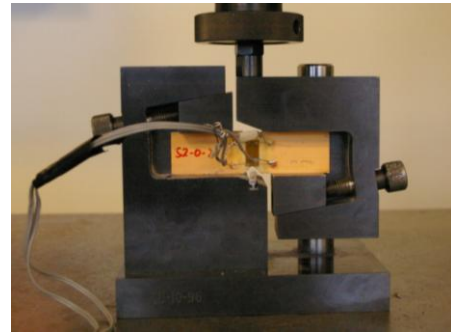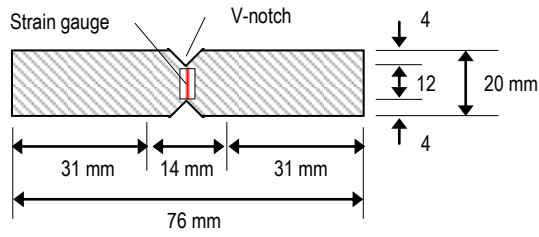
(a) Details of specimen for shear test (b) Actual test set-up

Figure 3.11 Set-up for shear test of fibre composite skins
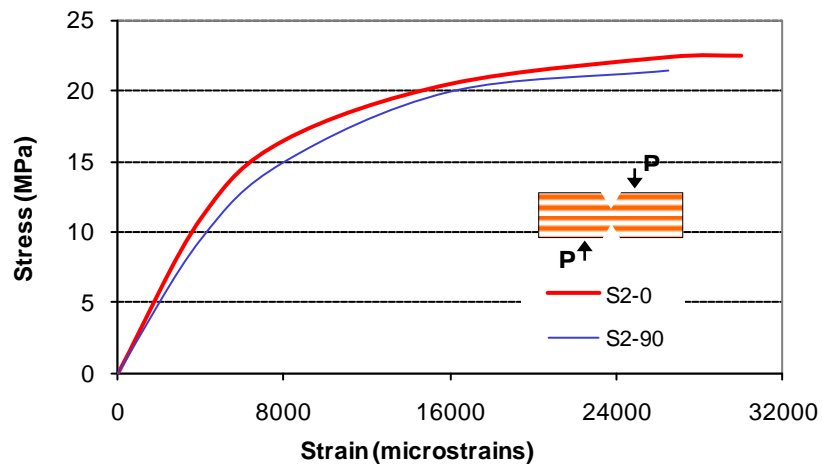
Figure 3.12 Shear stress-strain relationship for fibre composite skins
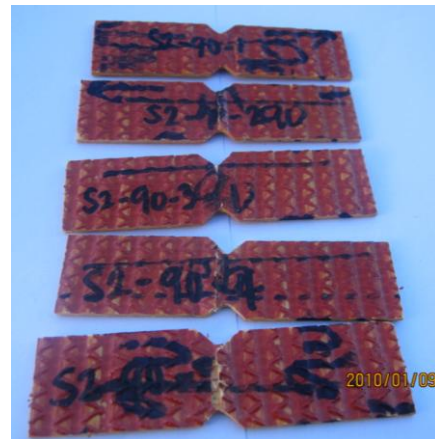
(a) Longitudinal direction (b) Transverse direction

Figure 3.13 Failure mode of fibre composite skin in shear

3.4 Core characterisation

The test specimens for the characterisation of the core material were obtained directly from the composite sandwich panels by sanding off the fibre composite skins on both sides. The mechanical properties of the core were obtained by conducting flexural, shear, flatwise compression and tensile tests. Table 3.2 summarises the details of the specimen for the characterisation of the modified phenolic core.

Table 3.2 Details of specimens for characterisation of the phenolic core

Type of test	Test standard	No. of coupons	Dimensions (mm)		
			length	width	thickness
Flexural	ISO 14125:1998	5	200	50	10
Tensile	ASTM D638-91	5	140	25	12
Compressive	ASTM C365-94	5	50	50	20
Shear	ASTM D5379-93	5	76	20	10
	Asymmetrical beam	5	240	50	10

3.4.1 Flexural test

The flexural test of the phenolic core was conducted following the ISO 14125 (1998) standard. Figure 3.14 shows the test set-up for the flexural test of the core material. Steel plates were provided under the loading point and at the supports to prevent indentation failure. The specimen was simply supported and was tested under 3-point loading with the span set at approximately 16 times the thickness of the core. The load was applied at midspan of the specimen at a constant rate of 1 mm/min using a 10 kN MTS testing machine. The load and midspan deflection were recorded up to failure to determine the strength and elastic properties of the phenolic core material.

The experimental stress-strain relationship of the core material under flexural loading is shown in Figure 3.15. The experimental results showed that the modified phenolic core material behaved almost linearly elastic under flexural loading. However, a slight decrease in the modulus was observed at 6000 microstrains (7.8 MPa) which could be due to the development of tensile microcraking at the bottom of the core. The modified phenolic core failed at a maximum flexural stress between 14.1 and 15.3 MPa with a strain of 12100 to 13100 microstrains. The phenolic core failed in a brittle manner without any sign of cracking. The failure of the phenolic core material is due to flexural failure at the midspan of the specimen (Figure 3.16).
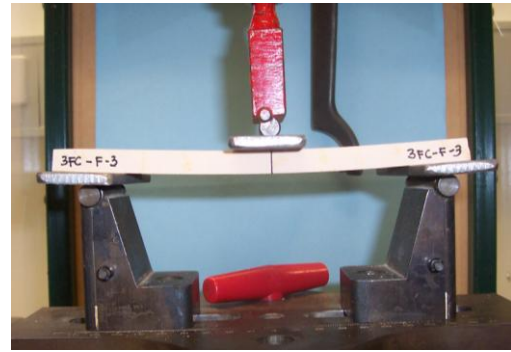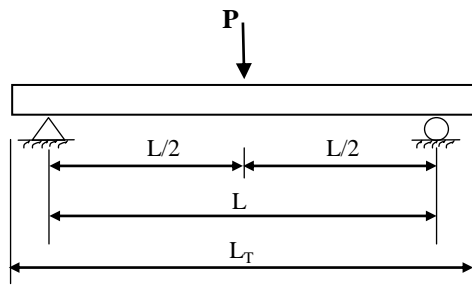
(a) Schematic illustration of flexural test   (b) Actual test set-up

Figure 3.14 Set-up for flexural test of core
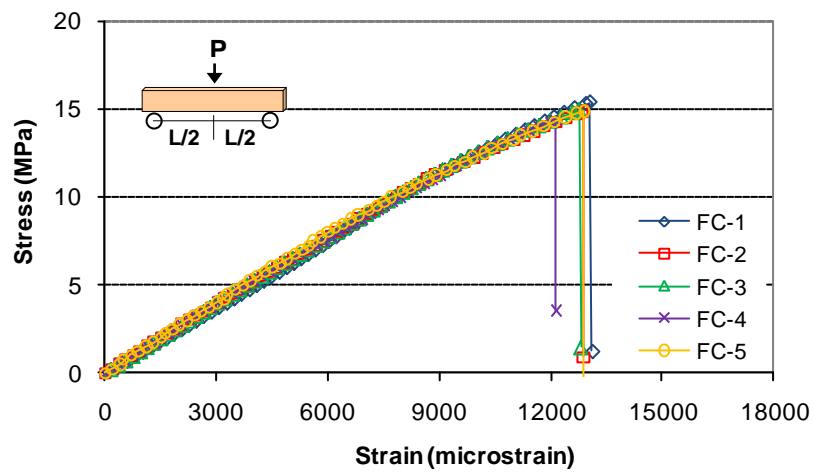
Figure 3.15 Flexural stress-strain relationship at the bottom of the core

Figure 3.16 Failure of the core under flexural test

3.4.2 Dog-bone tensile test

Tensile testing of the core material was performed following ASTM D638 (1991) using the specimens prepared in dog-bone shape. The specimens were prepared by grinding-off the fibre composite skins on the gauge length portion to produce the dog-bone shape while keeping the skins at the specimen ends in order to prevent any damage introduced by the loading fixture. The width of the specimen at the gauge length is reduced to 25 mm and a thickness of 12 mm. The dog-bone tensile specimens were mounted on the 10 kN MTS machine through a fabricated test fixture which held the specimen firmly at the wide ends and pulled until failure. The gauge length is fixed at 40 mm with a crosshead speed set at 1 mm/min. The strain in the specimen during loading was monitored using a uniaxial strain gauge attached on the middle of the gauge length. Figure 3.17 shows the details of the specimen and the actual test set-up for the tensile test.

Figure 3.18 shows the tensile stress and strain of the modified phenolic core material; and a linear behaviour was observed up to failure. The core specimen failed at an average tensile strength of 5.97 MPa and a maximum strain of around 6100 microstrains. It is noteworthy that a decrease in the flexural modulus was observed at this level of strain when the core material was tested under bending. It is therefore concluded that cracking in the core material starts to develop at this level of strain. The specimen failed immediately after the formation of the first tensile crack at the gauge length (Figure 3.19). One of the specimens (TDB-3) failed near the test fixture and was not included in the analysis.
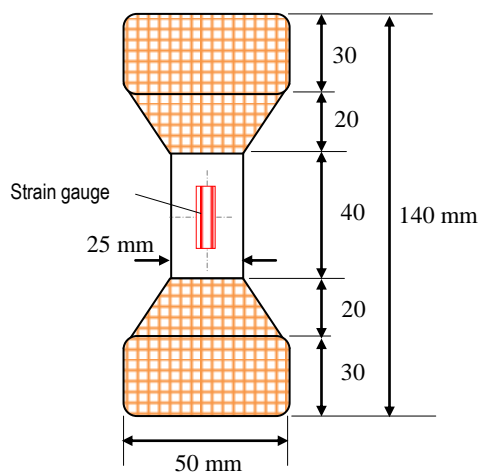
(a) Specimen details for tensile test   (b) Actual test set-up
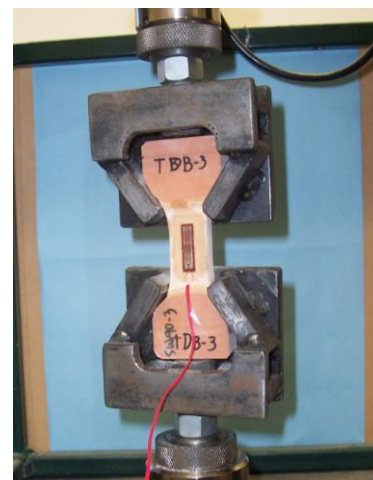
Figure 3.17 Set-up for tensile test of the core
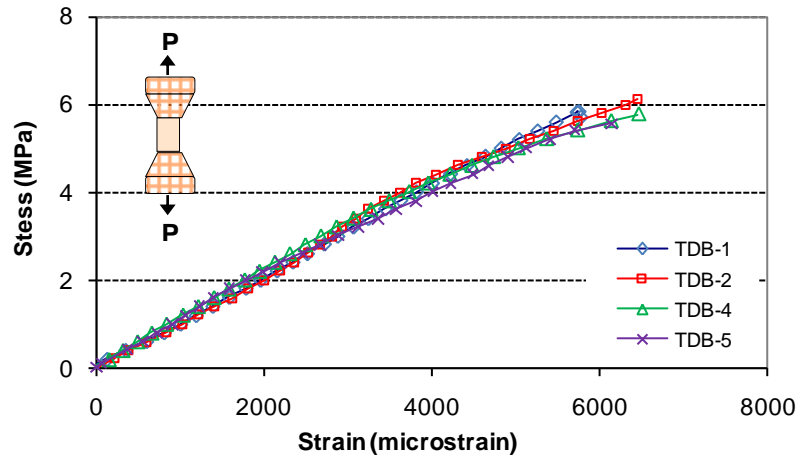
Figure 3.18 Stress-strain relationship of core in tension
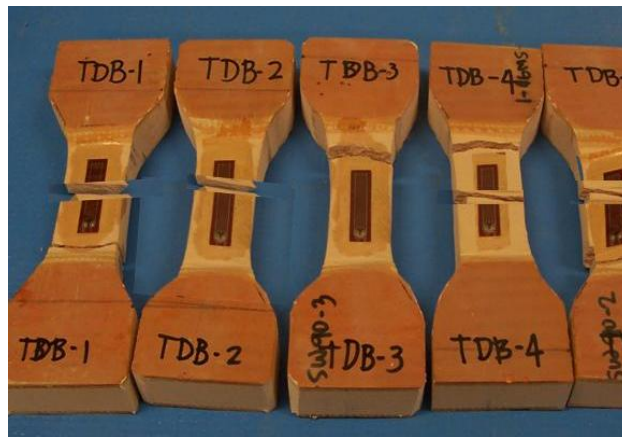
Figure 3.19 Failure mode of the core in tension

3.4.3 Compressive test

One of the main reasons that limit the application of composite sandwich for beams and other similar structures is the low compressive strength of most currently used core materials. Thus, a test was conducted to determine the compressive strength of the modified phenolic core of the composite sandwich structure used in this study. The flatwise compressive test of the core was performed following the ASTM C365 (1994) standards. Figure 3.20 shows the test set-up for the flatwise compressive test of the core material. The test specimens have dimensions of 50 mm x 50 mm with a thickness similar to the actual thickness of the composite sandwich panel. Uniaxial strain gauge was attached to the core surface to determine the strain during testing. The load was applied uniformly on the loading surface of the specimen through a 100 kN MTS machine at a constant cross head speed of 1mm/min. The compressive

strength was calculated by dividing the load by the cross sectional area of the specimen while the strain was determined from the uniaxial strain gauges attached to the phenolic core specimen. The compressive modulus was calculated from the slope of the initial portion of the compressive stress-strain relation curve.

Figure 3.21a shows the typical stress-strain curve obtained from the flatwise compressive test. The graph shows an initial linearly elastic behaviour up to a strain of around 16500 microstrains followed by a plateau up to a strain of around 40000 microstrains. The initial increase in strain could be due to the uneven surface of the fibre composite skin and the plateau to the crushing of the core material. The results showed that the phenolic core has a compressive strength of 21.35 MPa that is comparable to that of normal density concrete. In can also be observed that the strains at maximum stress and at failure were much larger than that of normal concrete with the phenolic core having a compressive modulus of around 1350 MPa. Figure 3.21b shows that the specimens failed by compressive failure of the core.
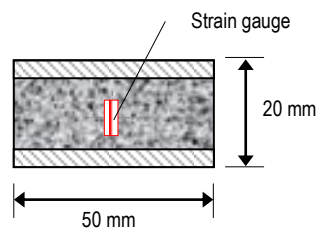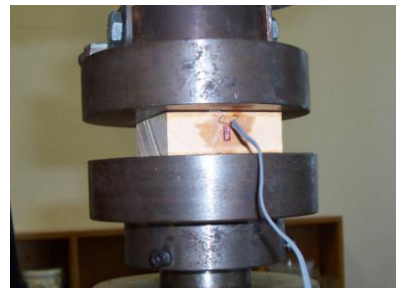
(a) Specimen details   (b) Actual test set-up

Figure 3.20 Set-up for flatwise compressive test of the core
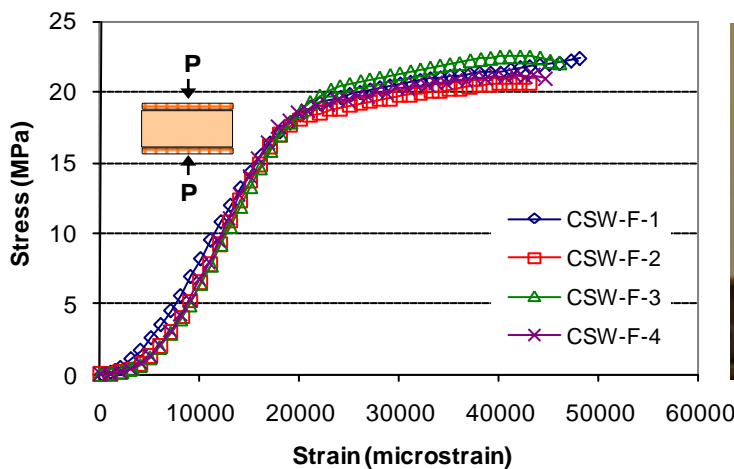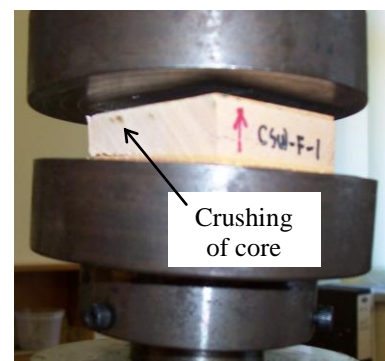
(a) Stress-strain relationship   (b) Failure mode

Figure 3.21 Behaviour of the core under flatwise compression

Another set of specimens was prepared to determine the behaviour of the phenolic core material under compressive loading. The core materials were casted into cylindrical plastic mould with an internal diameter of 50 mm and a height of 100 mm which were then heat-cured at 80°C for 24 hours in an oven. The cylindrical core specimens (Figure 3.22) were tested in compression under 100 kN MTS machine at the loading rate of 1mm/min according to ASTM C39 (2005) standard. All the specimens were weighed and the actual dimensions measured before testing. Strain gauges were attached on the surface of the core material to measure the axial and lateral deformations during loading. A thin rubber padding was provided on top of the core specimen to ensure a uniform load distribution during testing. The compressive strength was calculated by dividing the load recorded with the cross-sectional area of cylindrical core specimens.
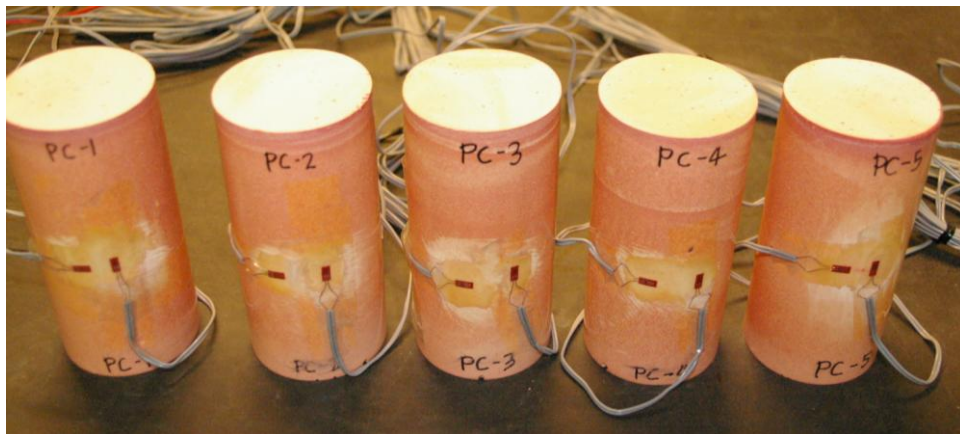
Figure 3.22 Cylindrical phenolic core specimens for compressive test

The stress-strain curve in Figure 3.23a shows that the modified phenolic core material behaves almost linearly under compression at lower level of stress. With the continuous application of load, the core material started to behave nonlinearly up to failure. An abrupt drop in the stress level was observed at a strain between 22000 and 35000 microstrains. The sudden drop in the stress level could be due to the cracks which develop at the top part of the cylindrical core sample (Figure 3.23b). Shortly after the maximum compressive stress of around 23 MPa is reached, the crack width increased and the stress level dropped dramatically. The measured strains in this region indicate the failure mode of the cylindrical specimen. The specimen failed with all the cracks occurring at the top part of the cylinder.

(a) Stress-strain relationship   (b) Failure mode
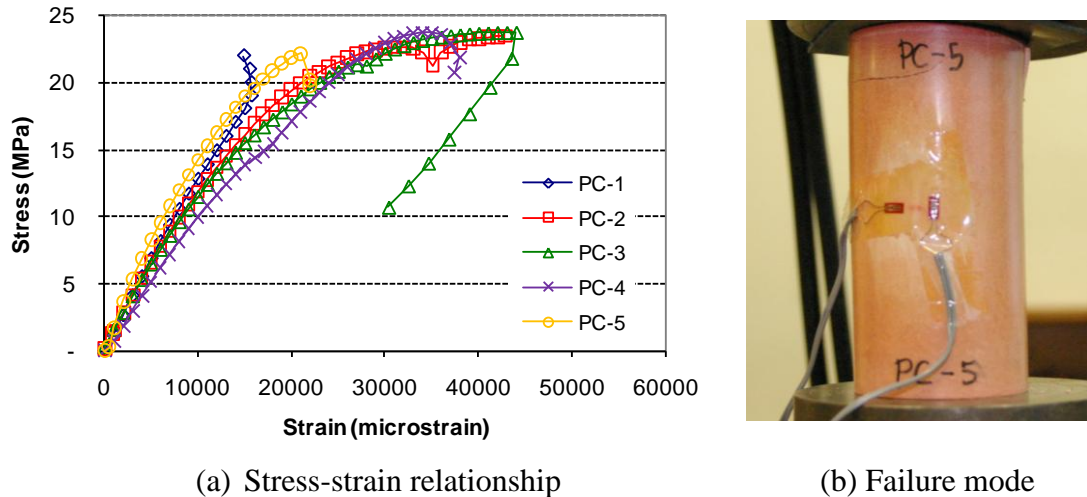
Figure 3.23 Behaviour of the cylindrical core specimens under compression

The results of the two different compressive tests conducted gave the same value of compressive strength and similar stress-strain diagram for the phenolic core material. Due to the relatively low elastic stiffness of the phenolic core, the cell structures of the soft materials are packed together to carry the applied load when the critical stress is reached under compression resulting in almost same compressive strength for the cylindrical and the square cross section shaped specimens. However, the specimens subjected under flatwise compressive test failed at a higher strain than the cylindrical core. The different behaviour can be explained by taking the failure mode of each type of specimen into consideration. The flatwise compression specimen failed mainly by the crushing of the core while the cylindrical specimen failed due to combined cracking and crushing of the core. The increase in the crack width on one side of the cylindrical core further caused the specimen to buckle in the other direction (as shown in Figure 3.23b) resulting to its immediate failure.

3.4.4 Shear test

The shear strength and modulus of the core are important properties which affect the behaviour and failure of sandwich structures. In this study, two types of testing procedure were used to assess the shear strength and the modulus of the modified phenolic core material: the V-notched beam shear test and the asymmetrical beam shear test. The V-notched beam shear test of the core was conducted following the ASTM D5379/ D5379M (1993) standard. Figure 3.24a shows the test set-up for the V-notched beams shear test. Coupon specimens with symmetrically located V-

notches were used as the test specimens. Resistance strain gauges oriented at $\pm45^o$ to the loading axis was bonded at the middle of the specimen to determine its shear response during the entire loading. The specimen was loaded on a 10 kN MTS machine by the Iosipescu shear test fixture at a constant head speed of 1mm/min.

Figure 3.24b shows the test setup and instrumentation for the asymmetrical beam shear for the phenolic core material. The specimen was eccentrically loaded at two trisected points and the supports were applied at the remaining two points. This loading generates a high shear stress at the centre, nearly zero moment, and forces the specimen to fail along a nearly vertical shear crack. The load was applied through a servo-hydraulic universal testing machine with a capacity of 100 kN. Steel plates were provided under the loading points and at the supports to prevent local indentation failure on the core material. Strain gauges were attached on the surface of the specimen along the midline at mid-height to evaluate the shear strain during loading and until final failure. Before each test, the loading pin was set to almost touch the top surface of the specimen. The applied load and strains were obtained using a data logger. All specimens were tested up to failure to determine the shear strength and the mode of failure.

(a) V-notched beam shear   (b) Asymmetrical beam shear
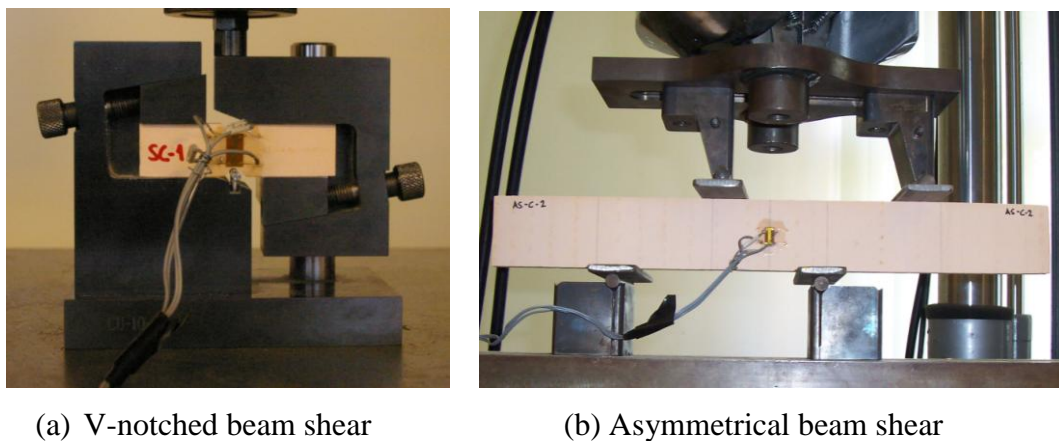
Figure 3.24 Shear test set-up of the core

The stress-strain relationship of the core determined from the V-notched beam shear test is shown in Figure 3.25a. A slight variation in the stress-strain behaviour of the core material was observed especially at the initial application of the load. The variation could be due to the effect of the adhesives used to bond the strain gauges on the small cross sectional area at the centre of the test specimen and the relatively low

shear strength of the core material. However, all of the specimens failed at almost the same amount of applied load. In general, the shear stress increased linearly with strain up to failure. The specimen failed with a maximum shear stress of around 4.25 MPa and a shear strain of around 8200 microstrains. The shear modulus of the core material was then determined from the slope of the shear stress-strain diagram between the strains of 1000 and 3000 microstrains. The core material failed at the notch in a brittle manner with no signs of cracking before failure (Figure 3.25b).

(a) Stress-strain relationship   (b) Failure mode
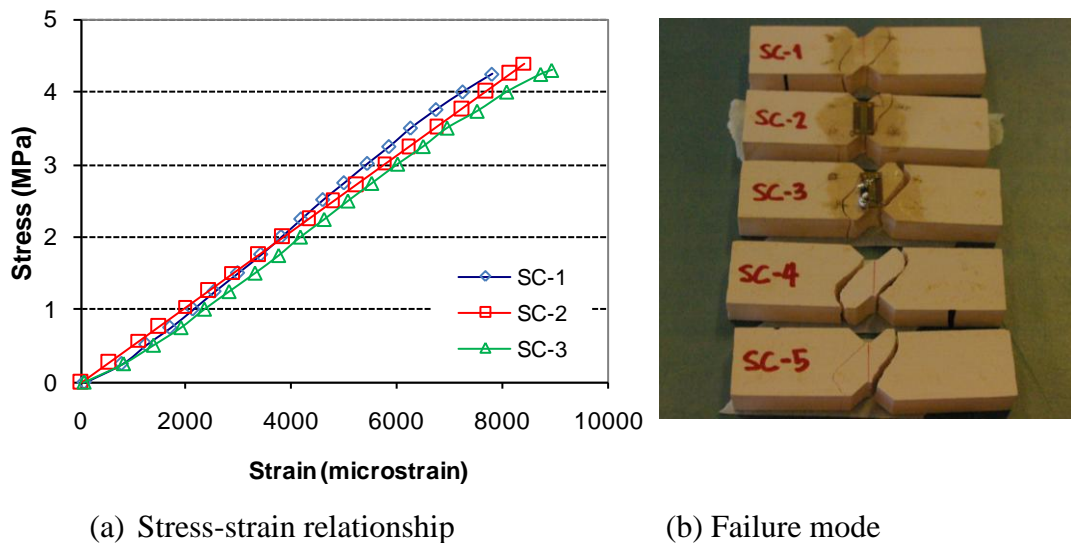
Figure 3.25 Behaviour of the core under V-notched beam shear test

The shear stress-strain relationship of the core material under asymmetrical beam shear test is shown in Figure 3.26a. The core specimen tested under asymmetrical beam shear behaved similar to that of small core specimen. The stress-strain curve shows that the core material behaves linearly elastic up to failure. However, the bigger specimens exhibited slightly higher shear strength. The core material tested under asymmetrical beam shear failed at a maximum shear stress of around 4.54 MPa and a shear strain between 8200 and 8600 microstrains. The shear modulus of the core material was determined from the slope of the shear stress-strain diagram between the strains of 1000 and 3000 microstrains. All of the tested specimens failed in a brittle manner with no signs of cracking before failure. The failure of the core occurred at the location of maximum shear with an almost vertical shear crack as shown in Figure 3.26b.

(a) Stress-strain relationship   (b) Failure mode
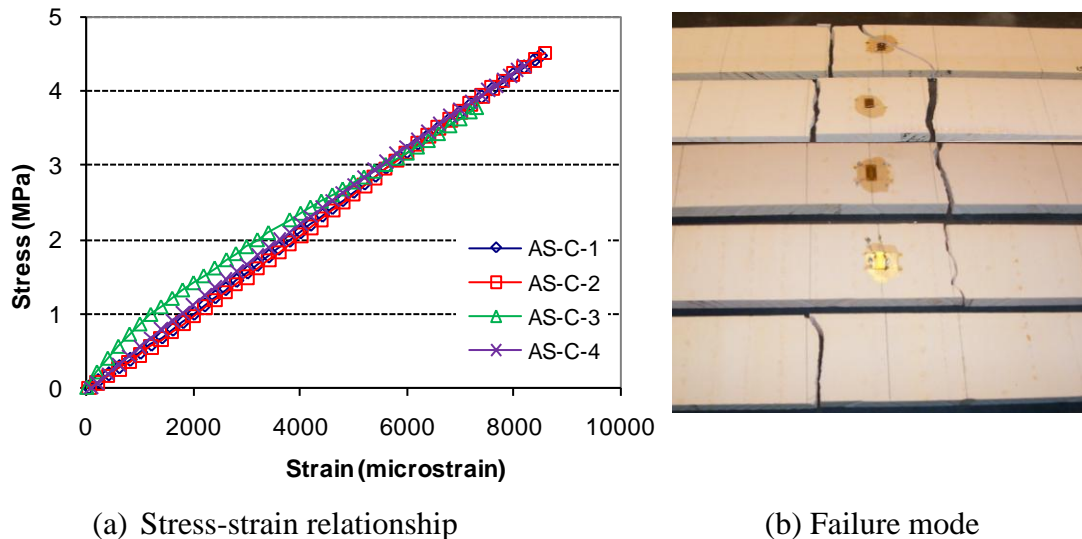
Figure 3.26 Behaviour of the core under asymmetrical beam shear test

3.5 Summary of mechanical properties of the skin and the core material

The average value and the standard deviation for the strength and elastic properties of the fibre composite skin and the phenolic core determined from the different coupon tests are summarised in Tables 3.3 and 3.4. The bi-axial glass fibre laminates has a fibre fraction of 45% by weight and an average density of 1365 kg/m^3 with a standard deviation of 27.10 kg/m^3 while the modified phenolic core material has an average density of 855 kg/m^3 with a standard deviation of 11.57 kg/m^3. In the table, all the elastic properties have been determined by considering the linear approximation in accordance with the ISO and ASTM standards.

Table 3.3 Characteristics of the bi-axial glass fibre laminates

Test	Property	Longitudinal direction		Transverse direction	
		Average	Std Dev	Average	Std Dev
Flexure	Elastic modulus (GPa)	14.28	0.88	3.66	0.24
	Peak stress (MPa)	317.37	27.95	135.05	11.01
	Strain at peak (%)	2.29	0.14	5.26	0.43
Tensile	Elastic modulus (GPa)	15.38	0.63	12.63	0.62
	Peak stress (MPa)	246.80	10.38	216.27	10.26
	Strain at peak (%)	1.61	0.01	2.37	0.09
	Poisson's ratio	0.25	0.01	0.13	0.01
Compression	Elastic modulus (GPa)	16.10	0.57	9.95	0.76
	Peak stress (MPa)	201.75	18.56	124.23	9.12
	Strain at peak (%)	1.24	0.15	1.25	0.06
Shear	Shear modulus (MPa)	2.47	0.11	2,173.92	171.60
	Peak stress (MPa)	23.19	0.69	21.81	0.86
	Strain at peak (%)	3.08	0.11	2.38	0.05

Table 3.4 Characteristics of the phenolic core

Test	Property	Testing Values	
		Average	Std Dev
Flexure	Elastic modulus (GPa)	1.33	0.01
	Peak stress (MPa)	14.32	0.40
	Strain at peak (%)	1.22	0.05
Tensile	Elastic modulus (GPa)	1.03	0.01
	Peak stress (MPa)	5.97	0.28
	Strain at peak (%)	0.61	0.02
Compression	Elastic modulus (GPa)	1.33	0.07
(ASTM C365)	Peak stress (MPa)	21.35	0.98
	Failure strain (%)	4.04	0.14
(ASTM C39)	Elastic modulus (GPa)	1.35	0.01
	Peak stress (MPa)	22.99	1.13
	Failure strain (%)	3.51	0.07
	Poisson's ratio	0.29	0.04
Shear	Shear modulus (GPa)	0.53	0.01
(ASTM D5379)	Peak stress (MPa)	4.25	0.19
	Strain at peak (%)	0.81	0.03
(Asymmetrical beam)	Shear modulus (GPa)	0.52	0.01
	Peak stress (MPa)	4.54	0.03
	Strain at failure (%)	0.82	0.01

3.5.1 Validity of test results

The results from the various tests of coupons were compared to determine if there is a significant difference in the measured values. Based on the results, the variability of the modulus and strength values for all the tested specimens is less than 10%. This result indicates that the reproducibility of the test is quite high which proves that the fabrication of the fibre composite laminates and the phenolic core material is consistent with the actual manufacturing process and the experimental procedures were conducted within acceptable margin of error.

3.5.2 Behaviour of bi-axial (0/90) glass fibre laminates

The results of the coupon tests indicate that the stress-strain relationship of the fibre composite skin of the composite sandwich structure is linear up to failure with an instantaneous and catastrophic failure mode. On the other hand, the coupons cut in the transverse direction showed a linear response at a relatively low amount of strain which then started to behave non-linearly with increasing stress until failure. This nonlinear response could be caused by the matrix softening or the formation of cracks in the matrix between the 90° fibres.

Based on the result of the coupon test, the fibre composite skin has a slightly lower tensile modulus compared to its compressive modulus in the longitudinal direction. The average tensile modulus is around 15400 MPa while the compressive

modulus is around 16100 MPa. This lower tensile modulus could be due to the existence of manufacturing defects such as voids and microcracks. These defects tend to open in tension loading and cause a lower overall initial tensile modulus. This fact was also observed by Haj-Ali and Kilic (2002) on pultruded fibre composite materials, where small cracks and voids present in their specimen continued to grow significantly under tensile loading. In addition, the resin itself is stronger in compression than in tension. Similarly, the slightly higher elastic compressive modulus of the fibre composite skin than the tensile modulus can be influenced by the resin matrix as the primary mode of failure for unidirectional fibres under compressive load is fibre buckling. The matrix prevents the fibres from buckling by providing additional stability to the specimen. In general, however, the fibre composite skin gives a lower compressive strength than tensile strength. Based on the result of the experiment, the fibre composite skin will fail in compression of around 12300 microstrains (stress of around 201 MPa) and around 16100 microstrains (stress of 246 MPa) under tension. These strain and stress values can be used as the critical criteria in a maximum strain and/or stress type failure of the innovative fibre composite sandwich structure.

3.5.3 Behaviour of the phenolic core

The results of the various tests of coupons showed that the modified phenolic core material behaved linearly elastic in flexure, tensile and shear but showed a non-linear elastic behaviour in compression. The core material failed in a brittle manner with no signs of cracking before failure except in compression where the core material exhibited a more ductile deformation and failed due to cracking and crushing of the core. The results also show that the modulus of elasticity of the core under tension is almost similar to the initial compressive modulus. However, the tensile strength of phenolic foam core is only 25% of the compressive strength. More importantly, the results of the experiment showed that the phenolic core material has better mechanical properties compared to balsa wood and other more expensive foam core systems listed by Beckwith (2008). The phenolic core exhibited higher shear modulus and strength as well as higher compression stiffness and strength compared to more traditional polymer foam core materials. This result suggests the great potential of the modified phenolic foam as a core material of a composite sandwich panel for structural applications. The high stiffness and strength in shear and

compression of the phenolic core material will prevent the premature failure of the composite sandwich structure due to wrinkling of the skin. However, the density of the phenolic core is relatively higher than the typical density range of balsa wood and commonly used foam core materials.

The test results showed that the core material failed at an average compressive strength of around 23 MPa. This compressive strength is comparable to that of normal density concrete. In comparison with concrete of the same strength, the strains at maximum stress and at failure were much higher for the modified phenolic core material. The crushing of the concrete usually occurs at a strain of 3000 microstrains compared to at least 30000 microstrains for the modified phenolic core material. The compressive stress-strain curves display significant nonlinearity which indicates that the modified phenolic core material has better capability to absorb energy than concrete. Furthermore, the tensile strength of modified phenolic foam core is almost 25% of its compressive strength compared to only 10% for concrete. The general behaviour of the phenolic core is comparable to that of concrete. It exhibited a high strength and a nonlinear behaviour in compression but showed a weak strength and a linear elastic behaviour in tension. This almost similar behaviour of the modified phenolic core material to concrete suggest that simplified concrete material models could be used in the design and analysis of the composite sandwich structure made up of this core material.

The composite sandwich panel has an overall density of around 990 kg/m^3 while the modified phenolic core has a density of 850 kg/m^3. This shows that unlike other composite sandwich structures where the core contributes only up to 50% of the total weight, the modified phenolic core contributes to almost 85% of the total weight while the top and bottom skins only account for the 15%. The higher density of the phenolic core material improved the compressive strength and rigidity of the composite sandwich structure. It will not crush easily under point loading and could be suitable for use in structural applications. Overall, the density of the structural composite sandwich panel is comparable to that of hardwood red gum timber which weighs 900 kg/m^3 air dried (Bootle, 1983) but still very much less compared to concrete and steel which weigh 2400 kg/m^3 and 7850 kg/m^3, respectively.

3.6 Conclusions

A detailed experimental investigation was conducted using coupon specimens to characterise the mechanical properties of the glass fibre composite skins and the modified phenolic core material of a novel composite sandwich structure. The test of coupons has proven to be invaluable in the determination of the elastic modulus and strength properties of the constituent materials of the composite sandwich structure. The results showed that the glass fibre composite skins behaved linearly elastic up to failure with a tensile strength much higher than its compressive strength. On the other hand, the phenolic core behaved differently in tension and compression. The core material behaved linearly elastic in tension and failed immediately after the formation of the first crack but exhibited a non-linear behaviour in compression. The core exhibited higher strength and modulus in shear and compression compared to traditional core material systems. The better mechanical properties of the phenolic core combined with the high-strength and lightweight fibre composite skins suggests the great potential of the novel composite sandwich panel for structural applications. Given the similarity of the core material to the well-known behaviour of concrete, it is likely that the simplified concrete model will give reasonable prediction of the structural behaviour of the novel composite sandwich structures.

The established mechanical properties of the fibre composite skin and the phenolic core material are used in the analytical investigation and estimation of failure load of the individual fibre composite sandwich structures and beams made by gluing a number of these composite sandwich panels together. The constitutive models of these materials are used in the numerical modelling of the composite sandwich beams behaviour.

In Chapter 4, the flexural behaviour of the novel fibre composite sandwich structures in the flatwise and in the edgewise positions is presented.

Chapter 4

Flexural behaviour of fibre composite sandwich structures in flatwise and in edgewise positions

4.1 Introduction

The many advantages of fibre composite sandwich structure favour its application for civil infrastructure. However, very limited attempt has been made so far to use these materials for structural beam applications although engineers have a wide range of composite sandwich panels. The main reason could be that most of the currently used core materials are not appropriate for this type of structural application. The extensive material characterisation of the skin and core in Chapter 3 of a novel fibre composite sandwich panel has shown that this material has strength and stiffness suitable for structural applications. The satisfactory performance in several building and residential projects and the flexibility of this composite sandwich panel has shown a high possibility in using this material in the development of structural beams. However, before this material can be used in beam application, understanding of the behaviour of the individual sandwich structure and their failure mechanisms are necessary. This chapter will focus on the behaviour of such fibre composite sandwich structure when subjected to flexural loading.

A number of researches have studied the behaviour and failure modes of sandwich structures in flexure (Mouritz and Thomson, 1999; Daniel and Abot, 2000; Dai and Thomas Hahn, 2003; Belouettar et al., 2009; Jen and Chang, 2008; and Reis and Rizkalla, 2008). In these studies, the composite sandwich structures are tested in the flatwise position as it is commonly used as structural panels for roof, floor, walls and bridge decks. In this position, the sandwich structure is loaded normal to the face of the panel. When loaded normal to the face of the panel, the skins located at the top and bottom carry the flexural load and the inner core, the shear. In beams and similar applications, the structural components are used in the edgewise orientation for higher strength and stiffness. These applications are similar to structural plywood loaded in the plane of the panel when utilised as shear webs of composite box beams, I-beams or glue-laminated beams. Clearly, there is an application for composite

sandwich structure in the edgewise position. However, there are currently no available reports on the strength and failure mechanisms of sandwich beams tested in the edgewise position. Hence, the behaviour of the composite sandwich structure under edgewise loading remains to be investigated as it may behave differently because the skins and the core are positioned to carry both flexure and shear.

The flexural behaviour of a structural composite sandwich structure in the flatwise and edgewise positions is discussed in this chapter. A good understanding of the behaviour and failure mechanisms of the individual composite sandwich structure in the two different positions is necessary in order to design a structural beam made from this composite material. The load-deflection behaviour, stress-strain behaviour, failure load and the failure mechanisms of this composite sandwich structure were evaluated under 4-point static bending test. Using simple mechanics formulae, the strength and stiffness of the composite sandwich beams were predicted theoretically using the properties of the skin and core materials established from the coupon tests and were compared with the experimental results. Finite element simulations were also conducted to further verify the behaviour of the composite sandwich beams using the effective mechanical properties of the constituent materials.

4.2 Experimental program

4.2.1 Test specimen

The composite sandwich panels with nominal thicknesses of 18 mm and 20 mm were cut into required specimen dimensions and tested without any treatment or modification. Five replicates for each specimen type were prepared and tested. The details of the specimen are listed in Table 4.1. In the table, B, D, L, and L_T correspond to the width, depth, test span, and total length of the composite sandwich structures, respectively. Specimen 4FSW-I-F represents an 18 mm thick fibre composite sandwich structures tested in the flatwise position under 4-point static bending while specimen 4FSW-I-E represents an 18 mm thick fibre composite sandwich structures tested in the edgewise position. On the other hand, specimens 4FSW-II-F and 4FSW-II-E represents the 20 mm thick composite sandwich structures tested in the flatwise and edgewise positions, respectively.

Table 4.1 Details of composite sandwich specimens for flexural test

Specimen name	B (mm)	D (mm)	L (mm)	L_T (mm)	Orientation of testing
4FSW-I-F	50	18	300	400	Flatwise
4FSW-I-E	18	50	300	400	Edgewise
4FSW-II-F	50	20	400	500	Flatwise
4FSW-II-E	20	50	400	500	Edgewise

4.2.2 Test set-up and procedure

The static flexural test of fibre composite sandwich structures was performed in accordance with the ASTM C393 (2000) standard. For specimen 4FSW-I, the load was applied at the third and at the two-third points of the span (Figure 4.1a) while the load was applied at 0.4 and at 0.6 of the span for specimen 4FSW-II (Figure 4.1b) through a 100 kN servo-hydraulic universal testing machine with a loading rate of 3 mm/min. The test set-up in Figure 4.1b was adopted to increase the shear span to depth ratio of the beam without significantly increasing the length of the specimen and eliminating the possible shear failure. The loading pins and the supports had a diameter of 20 mm. For specimens tested in the edgewise position, steel plates were provided under the loading points to prevent premature failure. Figure 4.2 shows the actual test set-up and instrumentation for the static flexural test of the composite sandwich structures. Uni-axial strain gauges were attached to the top and the bottom surfaces at the midspan of the composite sandwich beams to evaluate the longitudinal strain during loading and until final failure. Before each test, the loading pin was set to almost touch the top surface of the composite sandwich specimen. The applied load, displacement and strains were recorded and obtained using a System5000 data logger. The test was discontinued after the failure in the composite sandwich beams was observed.

(a) 4FSW-I   (b) 4FSW-II
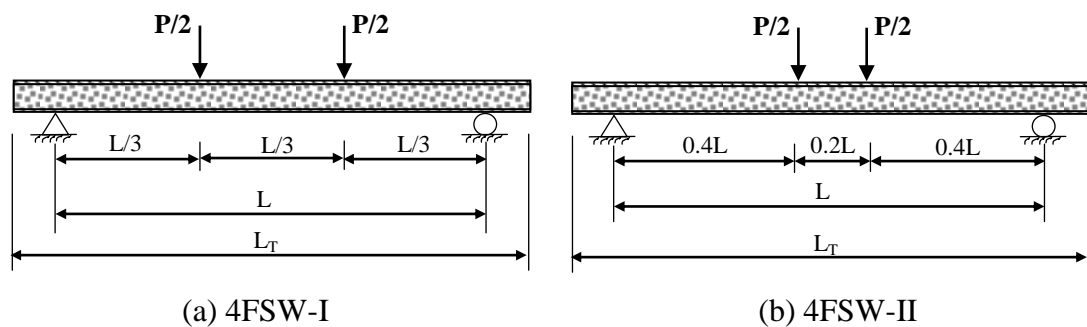
Figure 4.1 Schematic illustration of flexural test of composite sandwich structures
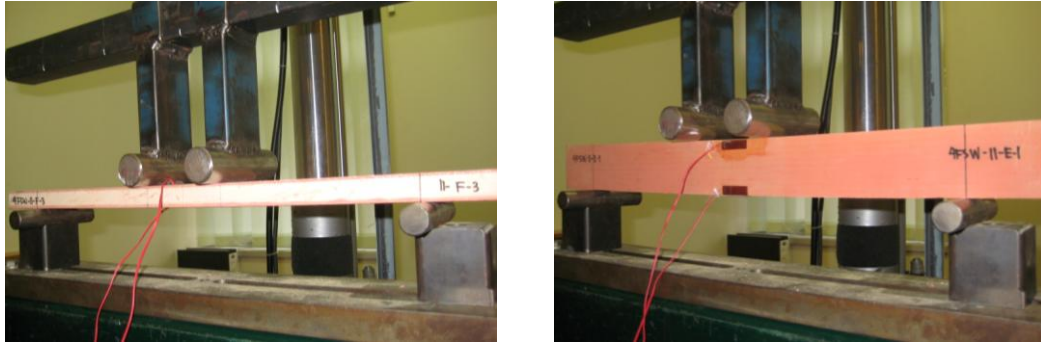
(a) Flatwise   (b) Edgewise

Figure 4.2 Actual test set-up for specimen 4FSW-II

4.3 Experimental results and observations

The experimental results of the 4-point static bending test of the composite sandwich structures are discussed in the following subsections. The load-displacement relationship, load-strain relationship and the failure mode of the composite sandwich structures in the flatwise and in the edgewise positions are discussed in detail.

4.3.1 Load-deflection behaviour

The typical load displacement relationship of the composite sandwich specimens tested in the flatwise and in the edgewise positions is shown in Figures 4.3 and 4.4. Figure 4.3 shows that the load of specimen 4FSW-I-F increased linearly with deflection until a load of 3000 N where a slight decrease in stiffness was observed after. The reduction in stiffness was due to crack initiation in the core material. Furthermore, small load drops were observed before the specimen failed. This could be due to the wrinkling of the compressive skins or the presence of some imperfections on the skins. When the core failed, an abrupt drop in the load was observed and the specimen failed subsequently (point A). The specimen 4FSW-I-F failed at an applied load of around 4650 N with a midspan deflection of 13.7 mm.

The load-deflection behaviour of specimen 4FSW-I-E showed a linear behaviour with a slight reduction in stiffness at a load of around 4500 N. Further reduction in bending stiffness was observed with the appearance of damage. At a load of around 6700 N (point B), a reduction in stiffness was observed due to the initiation of tensile cracks in the core at the constant moment region. At this stage, the strain gauge attached to the tensile side of the specimen broke and could no longer measure the strain. At a maximum applied load of 8150 N (point C), a

significant drop in the load was observed due to the compressive failure of the skin followed by shearing of the core. The load dropped to almost 75% of the maximum applied load (point D). This load drop was caused by a decrease in stiffness resulting from the total failure of the core material which suggests that the core did not contribute to the overall stiffness of the composite sandwich structure. After the load drop, the specimen continued to sustain the load but never exceeded the previous peak load as only the fibre composite skins were carrying the load. The specimen subsequently failed due to the tensile failure of the fibre composite skin.
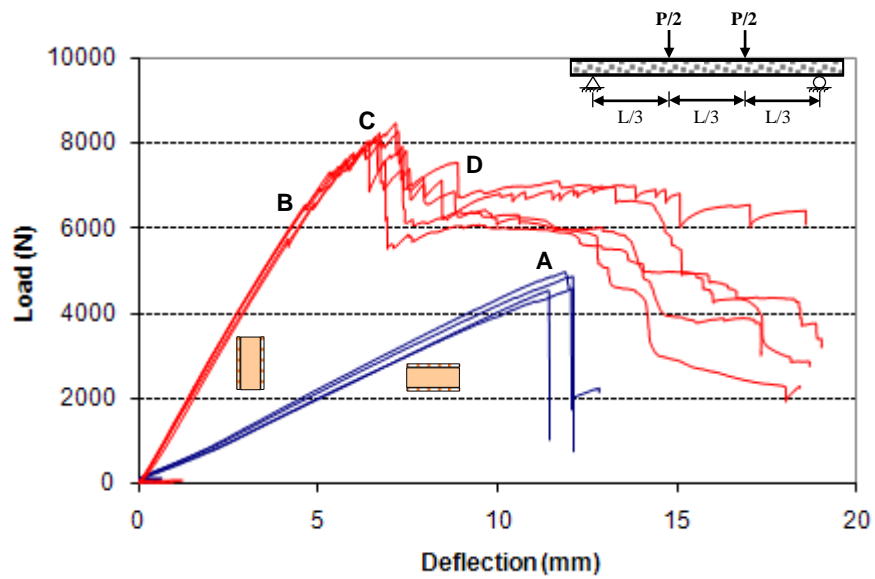
Figure 4.3 Load-midspan deflection relation of specimen 4FSW-I
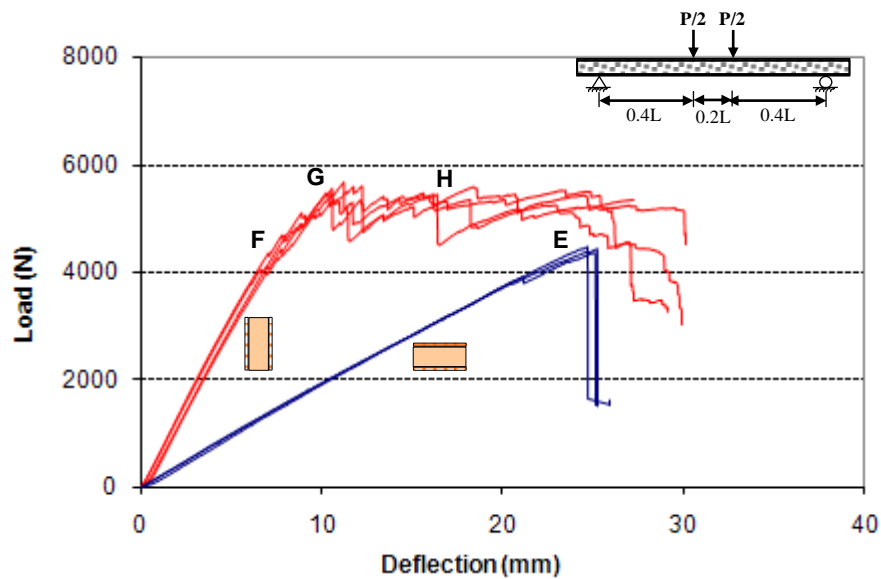
Figure 4.4 Load-midspan deflection relation of specimen 4FSW-II

Figure 4.4 shows the load and midspan deflection relation of specimens 4FSW-II-F and 4FSW-II-E. The specimen 4FSW-II-F failed at an applied load of around 4880 N with a midspan deflection of 25.6 mm (point E). The load of specimen 4FSW-II-E increased linearly with deflection but showed a reduction in stiffness at a load of around 4000 N and a deflection of 6.9 mm (point F) due to the tensile cracking of the core material. The sandwich specimen then continued to carry load until compressive failure of the skin at a load of 5250 N (point G) and a deflection of 10.6 mm. A significant drop in load was observed after compressive failure of the skin but the specimen continued to carry load until tensile failure of the fibre composite skin (point H).

In general, the composite sandwich structures in the flatwise position deflected more than twice the specimens in the edgewise position under the same level of applied load. This is due to the increase in the moment of inertia of the composite sandwich beams in the edgewise position as deflection is inversely proportional to the effective moment of inertia. The specimens in the edgewise position failed at a higher load than that of the flatwise position due to the difference in the failure mode. The presence of the vertical skins of the composite sandwich structures in the edgewise position could explain this behaviour as this prevented the premature failure of the core material and resulted to a pseudo-ductile behaviour.

4.3.2 Stress-strain behaviour of fibre composite skins

Figure 4.5 shows the typical bending stress and bending strain relationship at the top and bottom surfaces of the fibre composite sandwich structures in the flatwise and the edgewise positions. In the figure, the tensile and compressive stresses are the induced bending stresses at the bottommost and topmost skins of the composite sandwich structures, respectively. The tensile and compressive strains on the other hand were determined from the strain gauges attached to the composite sandwich specimens. The tensile stress-strain relation is designated with a (T) while the compressive stress-strain relation is designated with a (C).
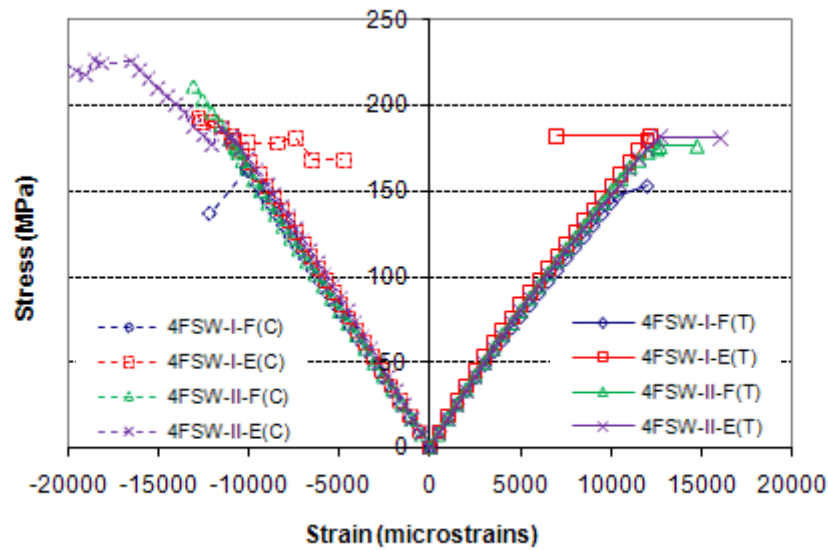
Figure 4.5 Stress-strain behaviour of sandwich structures under 4-point bending

The results suggest that the longitudinal strains (both tension and compression) in the fibre composite skins increased linearly with stress for all the specimens before any failure was observed. There is also evidence that the fibre composite skins behaved slightly stiffer in compression than in tension. A slight decrease in stiffness at a strain of around 6000 micro strains corresponding to a stress of around 95 MPa was observed for all specimens in tension. This slight decrease in stiffness is due to the initiation of core cracking at the tensile side of the specimen. The specimen 4FSW-I-F failed at a stress of around 147 MPa and tensile strain of 10300 micro strains. These stress and strain levels were only 60% of the maximum stress and strain of the fibre composite skins established from the test of coupons (listed in Table 3.3). Thus, it is concluded that the premature failure of specimen 4FSW-I-F occurred due to the combined flexure and shear as this specimen has relatively shorter span. On the other hand, the strain gauge at the tension side of specimen 4FSW-I-E broke at a stress of around 170 MPa and a strain of 12000 microstrains indicating the developments of flexural cracks. It is noteworthy that this value of strain is comparable with the flexural failure strain of the core material established from the test of coupons. However, the fibre composite skins prevented the sudden failure of the composite sandwich structures. Non-linearity in the compression strain was then observed indicating the further development of failure in the composite sandwich structures in the edgewise position. The specimen 4FSW-I-E then failed at

a compressive stress of 198 MPa and a compressive strain of around 12800 microstrains. These stress and strain levels are almost similar to the failure stress and strain of fibre composite skin in compression established from the coupon tests.

A nearly linear stress-strain relationship was observed at the top and the bottom fibre composite skins of specimens 4FSW-II-F and 4FSW-II-E up to failure. Both the specimens reached the maximum compressive stress of 201 MPa and strain of 12400 microstrains. These values represent the stress and strain at which the fibre composite skins failed in compression based from the results of the coupon tests. The specimen 4FSW-II-F failed at a compressive stress of around 213 MPa and strain of 13300 microstrains while the specimen 4FSW-II-E failed at a compressive stress of around 226 MPa and strain of 16500 microstrains. The slightly higher values of failure stress and strain of specimen 4FSW-II-E could be due to the presence of a thicker core which prevented the compression buckling of the fibre composite skins thereby, slightly delaying its failure.

4.3.3 Failure behaviour

Figures 4.6 and 4.7 show the typical failure mode of the composite sandwich structures tested under 4-point static bending. The results of the experiment showed that the specimen 4FSW-I-F failed in a brittle manner due to shear failure of the core under the loading point followed immediately by debonding between the bottom skin and the core at the end of the specimen (Figure 4.6a). The failure of the core appeared to initiate in the vicinity of the applied load, indicating a stress concentration effect. This observed failure could be due to the effect of shear stress as these specimens have relatively shorter span than specimen 4FSW-II. One of the specimens tested failed due to local skin wrinkling. A close observation on the specimen revealed that this failure occurred due to the presence of voids at the top skin (under the loading point) of the composite sandwich specimen.

The core bending stress changes from tensile at the bottom and compression at the top under flexural loading. When the core fails in tension, tensile cracking was observed at the constant moment region in the specimen 4FSW-I-E. However, the vertical skins prevented the crack width from increasing and its eventual failure. The specimens continued to carry load until compressive failure of the fibre composite skins (Figure 4.6b). This mode of failure showed that the skins and the core material

are efficiently utilised as the fracture of the skins is the optimal failure of the fibre composite sandwich structures (He and Hu, 2008).

Flexural cracks in the core were observed at the bottom of the specimen 4FSW-II-F but these cracks did not cause immediate failure. Figure 4.7a shows that the specimen 4FSW-II-F failed due to compressive failure of the fibre composite skin followed by the successive debonding between the compressive skin and the core. This failure behaviour is similar to the observation of Gibson and Ashby (1997) where interface bond collapse occurs on sandwich structure once a pre-existing crack-like failure is present at the interface. There was also no visible failure of the bottom skin under tension. Tensile cracking of the core was also observed in specimen 4FSW-II-E. However, the presence of the non-horizontal skins prevented the crack width from increasing to cause failure. The specimen 4FSW-II-E failed in a ductile failure mode due to the progressive compressive failure of the fibre composite skin followed by tensile failure of the skin (Figure 4.7b).

(a) Flatwise   (b) Edgewise
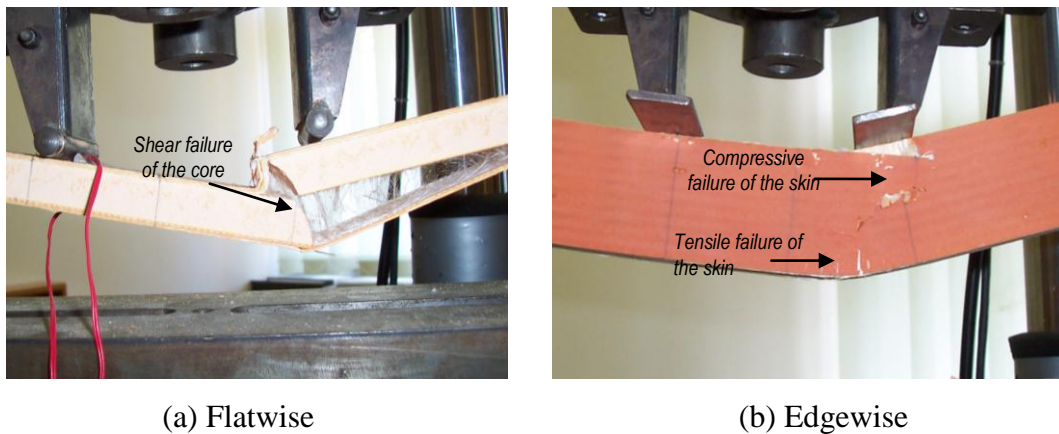
Figure 4.6 Failure mode of specimen 4FSW-I

(a) Flatwise   (b) Edgewise
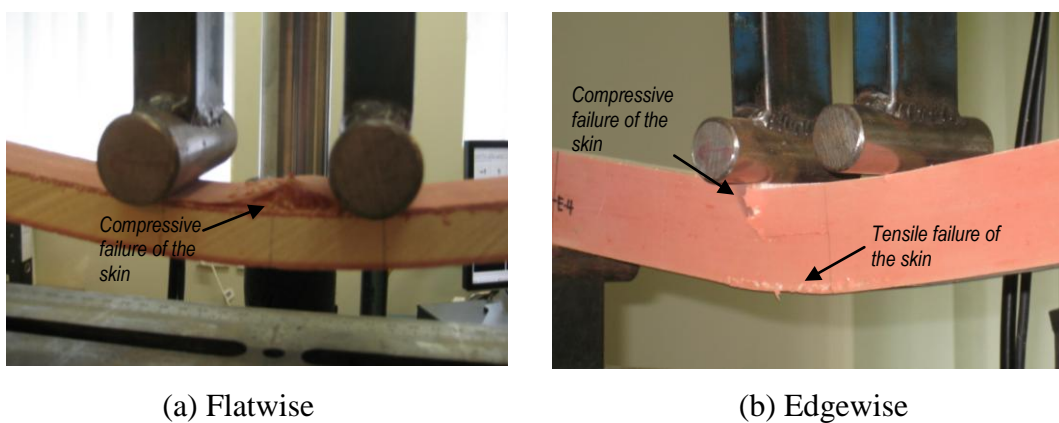
Figure 4.7 Failure mode of specimen 4FSW-II

4.4 Estimation of the failure load and mechanisms of sandwich structures

The load at which the composite sandwich structures will fail under static bending were predicted using the mechanical properties of the fibre composite skin and the core material established from coupon testing. In the estimation of the failure loads, the maximum stresses of the constituent materials are used. In this estimation, it is assumed that the fibre composite skins and the core material behaved linear elastic up to failure. The failure mode of the composite sandwich structures is determined by the geometry, the material properties and the loading configuration. Figure 4.8 shows the different components of the composite sandwich section. In the figure, t_s and t_c are the thicknesses of the skin and the core, respectively and d is the distance between the centre of the skins, $t_c + t_s$.

(a) Flatwise   (b) Edgewise
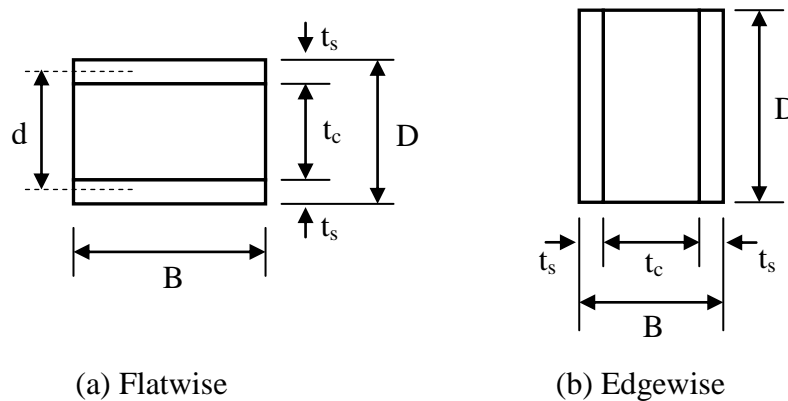
Figure 4.8 Composite sandwich section

Allen (1969) and Gibson (2007) suggested that a simple mechanics of materials formula can be used to calculate the load of the different failure modes when the beam parameters are known, and the lowest of these failure loads would govern the design of the composite sandwich structure. The following are the most common failure mechanisms in composite sandwich structures under bending (Vinsons, 1999; Steeves and Fleck, 2004; Russo and Zuccarello, 2007).

(a) Skin compressive/tensile failure;

(b) Core shear failure; and

(c) Core failure in tension/compression.

4.4.1 Skin failure

Daniel and Abot (2000) concluded that the bending behaviour of composite sandwich structures, whether loaded under three or four-point loading is governed by the skin failure. Compression or tensile failure of the fibre composite skin occurs when the axial stress reaches the maximum strength of the skin material. In the previous chapter, it was found out that the skin has higher tensile strength than compressive strength. Thus, it is expected that the failure of a symmetrical composite sandwich structure will occur due to compressive failure of the top skin. Similarly, Lingard (1993) found out that the failure load of sandwich structures under four-point bending to cause skin wrinkling was about the same load to cause compressive failure of the skin at midspan between the loading points. The peak strength P_{sf} for this failure mode to occur under four point bending can be predicted by:

$$P_{sf} = \frac{2(EI)\sigma_{sc}}{CLE_s D} \tag{4.1}$$

where C is 1/6 for specimen 4FSW-I and 1/5 for specimen 4FSW-II, EI is the flexural stiffness, σ_{sc} and E_s are the maximum compressive strength and the modulus of elasticity of the skin, respectively. The derivations of equation 4.1 are given in Appendix A.1. In the analysis of sandwich structures, it is usually assumed that the core only supports the shear and the skins, flexure (Bekuit et al., 2007). In the novel composite sandwich structure, the contribution of the core and the skin in both flexural and shear stiffness were considered. The flexural stiffness of the sandwich structures was obtained using the sum of the flexural stiffness of the constituent parts, about the centroidal axis of the composite sandwich section. The flexural stiffness, (EI) in the flatwise position is calculated using equation 4.2 and in the edgewise position using equation 4.3.

$$(EI)_{flat} = \frac{Bt_s^3}{6}E_s + \frac{Bt_s d^2}{2}E_s + \frac{Bt_c^3}{12}E_c \tag{4.2}$$

$$(EI)_{edge} = \frac{t_s D^3}{6}E_s + \frac{t_c D^3}{12}E_c \tag{4.3}$$

where E_c is the modulus of elasticity of the core.

4.4.2 Core shear failure

The shear failure occurs when the shear strength of the core is exceeded in the flatwise position (Steeves and Fleck, 2004) while shear failure in the edgewise position occur when the shear strength of the skin is exceeded. The peak core shear strength P_{cs} for composite sandwich structure in the flatwise position is predicted by the equation 4.4 and in the edgewise position using equation 4.5:

$$P_{cs(flat)} = \frac{2\tau_c(EI)}{(E_s t_s d / 2 + E_c t_c^2 / 8)} \tag{4.4}$$

$$P_{cs(edge)} = \frac{4\tau_s D}{3}\left(2t_s + t_c \frac{E_c}{E_s}\right) \tag{4.5}$$

where τ_c and τ_s are the shear strength of the core material and the fibre composite skin, respectively. The basis of equations 4.4 and 4.5 are detailed in Appendix A.2.

The peak strength due to shear failure of composite sandwich structures is estimated using the shear modulus of the skin and the core. This relationship is considered, as the modulus of elasticity of the core is only 1/11 to that of the modulus of elasticity of the skin, however, its shear modulus is almost 1/5 to that of the skin. Consequently, the transformed area of the sandwich structure into an equivalent skin will be more than twice bigger than the transformed area using the ratio of the shear modulus. Thus, this might better predict the shear capacity of the novel composite sandwich structure. The peak strength P_{csG} for composite sandwich structure in the flatwise direction is predicted using equation 4.6 and in the edgewise direction using equation 4.7. In equation 4.6, *(GI)* is calculated similarly as equations 4.2 and 4.3 with the modulus of elasticity of the skin and the core replaced with its corresponding shear modulus.

$$P_{csG(flat)} = \frac{2\tau_c(GI)}{(G_s t_s d / 2 + G_c t_c^2 / 8)} \tag{4.6}$$

$$P_{csG(edge)} = \frac{4\tau_s D}{3}\left(2t_s + t_c \frac{G_c}{G_s}\right) \tag{4.7}$$

where G_s is the shear modulus of the skin and G_c is the shear modulus of the core. The derivations of equations 4.6 and 4.7 are explained in Appendices A.3.

4.4.3 Core failure in tension and compression

The core material will fail if the normal stress in tension and/or compression is exceeded. Since the tensile strength of the modified phenolic core material is less compared to its compressive strength, it is predicted to fail first due to tensile failure. The peak strength P_{cf} in the flatwise and edgewise directions for this failure mode can be predicted by:

$$P_{cf(flat)} = \frac{2(EI)\sigma_{cb}}{CLE_c t_c} \tag{4.8}$$

$$P_{cf(edge)} = \frac{2(EI)\sigma_{cb}}{CLE_c D} \tag{4.9}$$

where σ_{cb} is the maximum bending strength of the core. Derivations of these equations are detailed in Appendix A.1.

4.5 Analytical prediction of the composite sandwich structure behaviour

A more detailed theoretical prediction of the failure load, stress-strain relationship and load-deflection behaviour of the composite sandwich structures under flexural loads and considering the different behaviour of the fibre composite skin and the core material in tension and in compression established from coupon testing was conducted. In this analytical prediction, a simple fibre model analysis was used to estimate the flexural behaviour of composite sandwich structures.

4.5.1 Fibre Model Analysis

The behaviour of fibre composite sandwich structures under flexural loading was predicted using a simple Fibre Model Analysis or FMA (Park and Paulay, 1975). This fundamental design methodology is similar to the conventional steel-reinforced concrete and FRP-reinforced concrete. According to ACI 440R (2007), regardless of the reinforcing material, the design of reinforced concrete is based on the cross-sectional equilibrium, strain compatibility, and the constitutive material behaviour. Using these assumptions, the load and midspan deflection behaviour, load-strain relationship and failure load of composite sandwich structures were determined.

The FMA model was based on the layer-by-layer approach to evaluate the sectional forces corresponding to a given strain distribution at a specific section. Nominal flexural capacity was calculated from the constitutive behaviours of the

fibre composite skin and the core material using strain compatibility and internal force equilibrium principles. Debonding reduces the stiffness of the structure and makes it susceptible to buckling under in-plane compression. This is common for sandwich structures with low compressive strength core material. Due to the high strength of the phenolic core, a perfect bond between the skins and the core, and the strains in the skins and the core were assumed directly proportional to their distance from the neutral axis. These assumptions were based on Bernoulli's hypothesis of strain compatibility: that plane sections remain plane which require perfect bonding between the skins and the core material, and that no slip occurs. Similarly, a perfect bond is assumed between adjacent layers of the fibre composite skins. The stress was computed by multiplying the strain to the modulus of elasticity of the materials. The internal force at each layer was calculated by multiplying the stress to the area of layer and the cross-sectional force equilibrium (in summation of forces, the net tensile force shall be equal to the net compressive force) was applied.

The basic assumptions in FMA are illustrated in Figure 4.9. When the core is still uncracked, all the layers or element i (with thickness, t_i) contribute to the moment capacity of the section as illustrated in Figures 4.9a and 4.9c. However, when the core cracks in the flatwise position, the contribution of the core in tension is neglected (Figure 4.9b). In the edgewise position, only the cracked core section is neglected as the vertical skins keep the core together to carry the load (Figure 4.9d).

The FMA also takes into account the constitutive material behaviour for fibre composite skin and modified phenolic core material as shown in Figure 4.10. The fibre composite skin is modelled as a linear elastic material in both tension and compression with a slightly higher modulus in compression (Figure 4.10a). On the other hand, a linear stress-strain relation is used to model the core material in tension while a simplified bilinear stress-strain behaviour in compression. The bilinear stress-strain behaviour of the core in compression is characterised by a linear elastic up to a limiting strain of 0.016 then a constant stress of 21.35 MPa until the failure strain of 0.035 (Figure 4.10b). In Figure 4.10b, $f_{c(t)}$ and $\varepsilon_{c(t)}$ represent the cracking strength in tension and the corresponding cracking strain of the core material while $f_{c(c)}$ and $\varepsilon_{c(c)}$ are the compressive strength and the corresponding elastic strain. In addition, the average thickness and in-plane shear properties of the constituent materials obtained experimentally (listed in Table 3.3) are used.

(a) Uncracked core (flatwise)

(b) Cracked core (flatwise)

(c) Uncracked core (edgewise)

(d) Cracked core (edgewise)
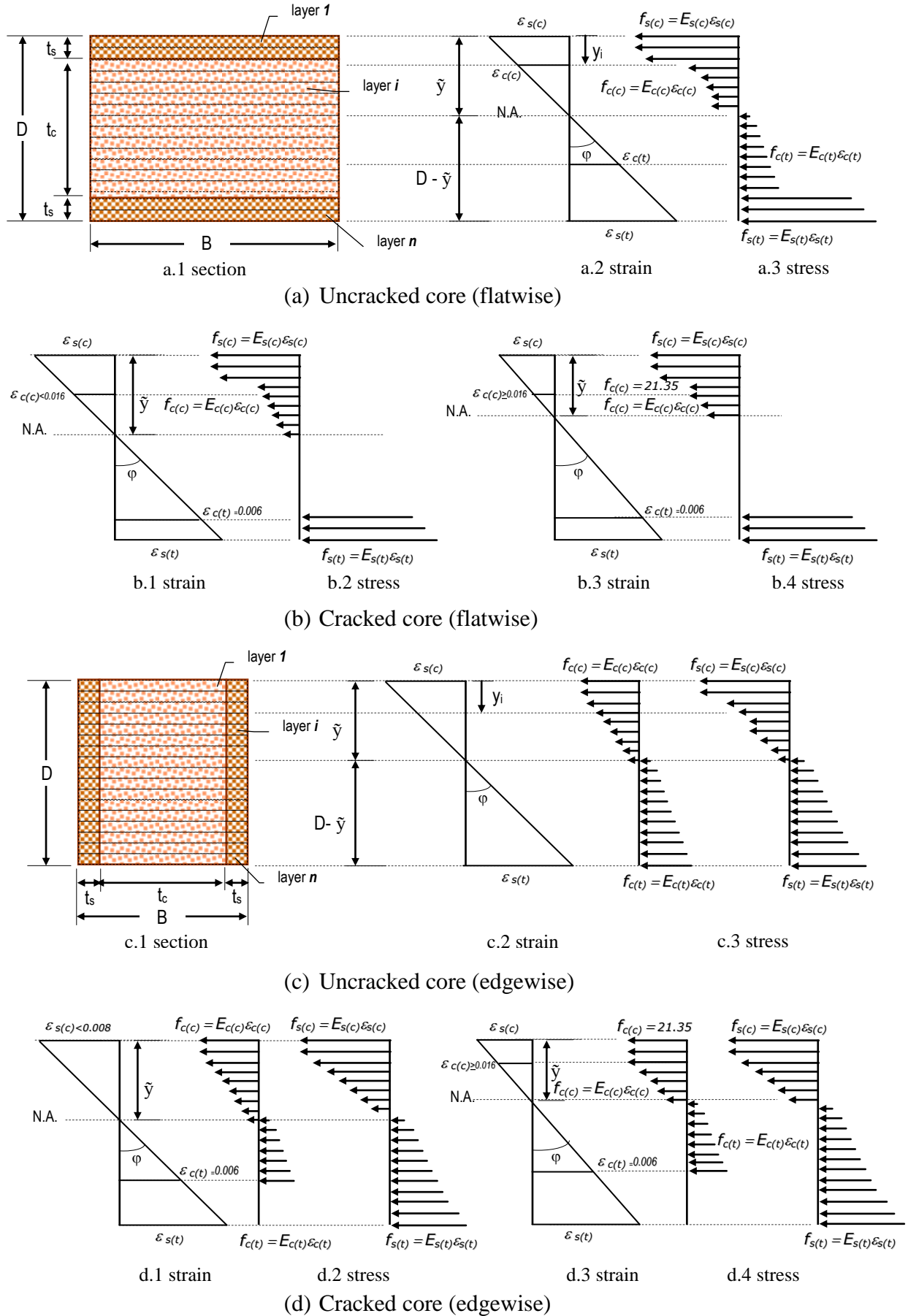
Figure 4.9 Basic assumptions in Fibre Model Analysis

(a) Bi-axial glass fibre composite skin   (b) Modified phenolic core
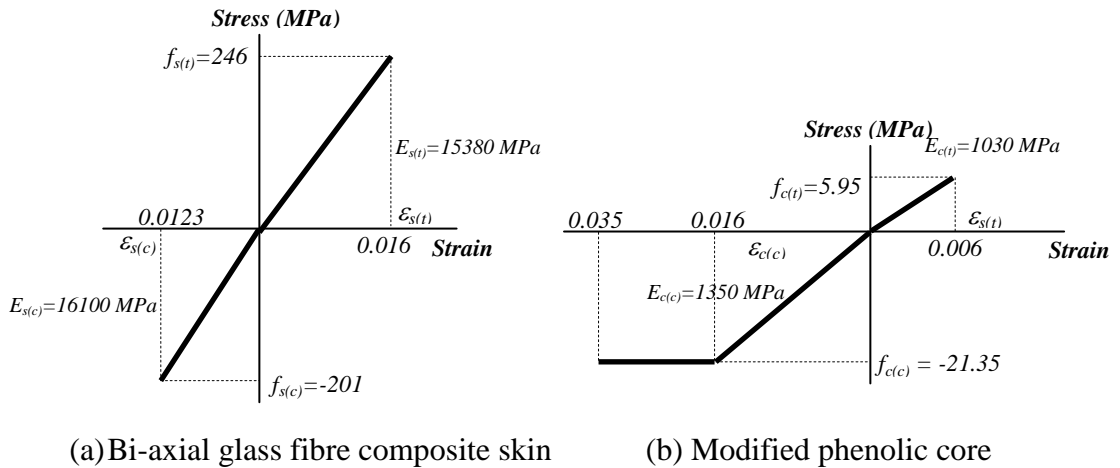
Figure 4.10 Constitutive models for basic materials of the sandwich structures

The initial iteration starts by assuming a compressive strain value at the topmost layer of the fibre composite sandwich structure. For a given top strain, the bottom strain is solved for by iteration until the summation of forces is equal to zero. The corresponding neutral axis depth for these set of top and bottom strains which satisfies the force equilibrium principle is calculated using the relation 4.10. The strain, ε_i at element i is related to the top strain, distance from the top of the element, y_i and the curvature, φ of the composite sandwich section which can be determined using equation 4.11. Based on Figure 4.9, the curvature of the composite sandwich section or the rotation per unit length of the composite sandwich beam can be determined using the relation 4.12. The stresses are then calculated from the strain at each layer multiplied by its corresponding elastic modulus.

$$\bar{y} = \frac{-\varepsilon_{s(c)}D}{(\varepsilon_{s(t)} - \varepsilon_{s(c)})} \tag{4.10}$$

$$\varepsilon_i = \varepsilon_{s(c)} - \varphi y_i \tag{4.11}$$

$$\varphi = \frac{\varepsilon_{s(c)} + \varepsilon_{s(t)}}{D} \tag{4.12}$$

where $\varepsilon_{s(c)}$ is the strain in the extreme fibre composite skin in compression and $\varepsilon_{s(t)}$ is the strain in the extreme fibre in tension. The force equilibrium equations and nominal flexural capacity can be written as:

$$\sum P = \sum_{i=1}^{n} f_{s(c)i} A_{s(c)i} + \sum_{i=1}^{n} f_{c(c)i} A_{c(c)i} + \sum_{i=1}^{n} f_{c(t)i} A_{c(t)i} + \sum_{i=1}^{n} f_{s(t)i} A_{s(t)i} = 0 \qquad (4.13)$$

$$M_n = \sum_{i=1}^{n} f_{s(c)i} A_{s(c)i} y_i + \sum_{i=1}^{n} f_{c(c)i} A_{c(c)i} y_i + \sum_{i=1}^{n} f_{c(t)i} A_{c(t)i} y_i + \sum_{i=1}^{n} f_{s(t)i} A_{s(t)i} y_i \quad (4.14)$$

where n_i is the number of layers that the composite sandwich section was subdivided, $f_{s(c)i}, f_{c(c)i}, f_{c(t)i}$, and $f_{s(t)i}$ are the stresses at each layer of the skin in compression, core in compression, core in tension and skin in tension, respectively while $A_{s(c)i}$, $A_{c(c)i}$, $A_{c(t)i}$, and $A_{s(t)i}$ are the corresponding areas of each layer of the skin in compression, core in compression, core in tension and skin in tension, respectively and M_n is the nominal flexural capacity of the composite sandwich section.

4.5.2 Failure load

The maximum load that the composite sandwich section could carry was determined using the simplified FMA. In the experimental test conducted, it was observed that failure of composite sandwich beams under static bending could be limited into two cases; either compressive or tensile failure of the skin. These two cases were checked to identify the failure mode and determine the maximum load that the composite sandwich section could carry. Compressive failure of the skin occurs when the top strain reaches 12400 microstrains while tensile failure of the skin occurs when the strain at the bottom most skin layer reaches 16100 microstrains. In the calculation of the failure load, the contribution of the core in tension was neglected when the tensile strength of the core is reached in the flatwise position. However, only the cracked core section is neglected for composite sandwich structure in the edgewise position when calculating for the failure load. In the edgewise position, the fibre composite skins at the tensile side act as a bridge for the cracked core, enabling the uncracked core material to still carry the load. In the flatwise position, final failure of the composite sandwich structures was due to compressive failure of the skin while failure in the edgewise position is due to progressive compressive failure and tensile failure of the fibre composite skins.

4.5.3 Flexural stiffness, EI

The flexural stiffness is necessary to evaluate the load-deflection response of the composite sandwich structures. The equivalent flexural stiffness of a sandwich

section is the sum of the flexural stiffness of the different parts in the sandwich structure. However, the simplified equation for the calculation of *EI* in equations 4.2 and 4.3 for symmetrical sandwich section cannot be used directly for the novel composite sandwich structure as the elastic properties of the constituent materials are different in tension and compression. Similarly, both the contribution of the skin and the core were considered in the calculation of *EI*. This is also the case for sandwich structures with carbon/epoxy skins and Divinycell core studied by Gdoutos and Daniel (2008b), wherein the stress-strain behaviour of the skin is different in tension and compression. This consideration is however in contrast with the assumption made by Daniel and Abot (2000) and several other researchers where the core contribution is neglected in the calculation of the flexural stiffness of the sandwich structures.

The relatively higher compressive modulus of the core and skin than tensile modulus suggested that the neutral axis is not lying at the mid-depth of the section even though the composite sandwich structure was fabricated with symmetrical top and bottom skins. Thus, the neutral axis depth should be calculated first to determine the distances of the centre of each layer. As discussed in the earlier section, the neutral axis depth can be calculated from the set of top and bottom strains that satisfies the force equilibrium principle in equation 4.13. Similarly, the neutral axis depth, *c* of the composite sandwich section can be determined by taking the summation of the first moment of the area of each layer multiplied by their corresponding elastic modulus with respect to the outermost skin divided by the summation of the area of each layer multiplied by their corresponding elastic modulus using equation 4.15. The *EI* of the composite sandwich beams in the flatwise and edgewise positions can now be estimated using equations 4.16 and 4.17. Similarly, the shear stiffness *GA* to account for shear deformation can be calculated using equations 4.18 and 4.19. These relationships are used further in the calculation of the *EI* and *GA* of the composite sandwich beams with cracked core material.

$$c = \frac{\sum\limits_{i}^{n} A_i E_i d_i}{\sum\limits_{i}^{n} A_i E_i} \qquad (4.15)$$

$$EI_{flat} = \sum_{i=1}^{n} \left[\left(\frac{Bt_i^3}{12} + Bt_i d_i^2 \right) E_i \right] \tag{4.16}$$

$$EI_{edge} = \sum_{i=1}^{n} \left[\left(\frac{t_s t_i^3}{6} + 2t_s t_i d_i^2 \right) E_s + \left(\frac{t_c t_i^3}{12} + t_c t_i d_i^2 \right) E_c \right] \tag{4.17}$$

$$GA_{flat} = \sum_{i=1}^{n} Bt_i G_i \tag{4.18}$$

$$GA_{edge} = \sum_{i=1}^{n} t_i (2t_s G_s + t_c G_c) \tag{4.19}$$

4.5.4 Load deflection behaviour

The load-deflection behaviour of the composite sandwich structures was obtained using the shear deformation theory proposed by Timoshenko (Bank, 2006). In the Timoshenko beam theory, the total deflection is the sum of the deflections due to bending and shear deformations. The relatively low shear stiffness of the core compared with that of the skin usually results in a significant shear deformation that should be accounted in the total deflection of sandwich structures (Barbero, 1999). Thus, the total deflection of the composite sandwich structures can be written as:

$$\Delta_{total} = \Delta_b + \Delta_s \tag{4.20}$$

$$\Delta_{total} = \int_0^L \frac{M_u M_L}{EI} dx + \int_0^L \frac{V_u V_L}{kGA} \tag{4.21}$$

where Δ_{total}, Δ_b and Δ_s denote the total deflection, deflection due to bending and shear, respectively while M_u and M_L are the bending moments due to unit and actual load, respectively and V_u and V_L are the shear due to unit and actual load, respectively. By solving equation 4.21, the maximum mid-span deflection for a simply supported composite sandwich beam under 4-point bending shown in Figure 4.1 are given by the following:

$$\Delta_{4FSW-I} = \frac{23PL^3}{1296(EI)} + \frac{PL}{6kGA} \tag{4.22}$$

$$\Delta_{4FSW-II} = \frac{59PL^3}{3000(EI)} + \frac{PL}{5kGA} \tag{4.23}$$

where $\Delta_{4FSW\text{-}I}$ is the deflection at midspan for specimen 4FSW-I and $\Delta_{4FSW\text{-}II}$ is the deflection at midspan for specimen 4FSW-II. The derivations of the midspan deflection of sandwich structures are detailed in Appendix A.3. In the prediction of the load-deflection relationship, the effective flexural and shear stiffness are used. A shear correction factor, $k = 1.0$ is assumed in the analysis. As long as the core remains uncracked, the flexural and shear stiffness of the sandwich structures are equal to the sum of the EI and GA of all layers taken about the neutral axis depth of the uncracked section. When tensile strength of the core is reached, cracks are developed resulting to the reduced stiffness of the sandwich structures. Under this condition, the EI and GA were based on the cracked section of the sandwich structures. The EI is equal to the sum of the EI of all the uncracked layers while the skin and core layers under the cracked core were neglected in the calculation of the shear stiffness. Similarly, the assumptions made by Natterer and Hoeft (1987) on the prediction of the load and deflection behaviour of hybrid timber-concrete girders that only a single cross-section over the whole length of the beam is considered.

As mentioned in the previous discussion, the FMA is based on the layer-by-layer approach to evaluate the sectional forces corresponding to a given strain distribution at a specific section. Thus, the number of layers that the cross section was subdivided might have an effect on the accuracy and reliability of the results. Initial evaluation conducted showed that the minimum thickness of each layer should be at least equal to quarter of the thickness of the skin to give a reliable result.

4.6 Finite element modelling of composite sandwich structure behaviour

Numerical simulations were carried out to verify the analytical solutions and to compare with the experimental measurements of the flexural behaviour of the sandwich structures. The finite element (FE) model was also developed to determine if the behaviour and the ultimate capacity of the composite sandwich structures could be predicted using the constitutive material behaviour established from test of coupons. Consequently, simulations of the 4-point static bending test of the sandwich structures using Strand7 finite element program (2005) have been performed in the FCD-XPP-034 computer (CPU-Intel P4). The FEM was carried out simulating the specimen and the loading set-up in the actual experimental conditions to have a reliable result. In the model, the size of the brick elements for skins and core were almost the same which resulted to a considerable number of elements as the skins are

thin. Due to symmetry, only one-fourth of the sandwich structures (with dimensions listed in Table 4.1) was modelled to reduce the computational time. The skin and the core were modelled as 20-node hexahedron (Hexa20) solid/brick elements with aspect ratios between 1.1 and 1.4. The number of brick elements and nodes used to developed the FE model for composite sandwich structures in the flatwise and in edgewise positions is listed in Table 4.2. Similarly, a quarter of the total load is distributed as node forces on top of the loading roller. Figures 4.11 and 4.12 show the numerical model used to simulate the 4-point static bending tests of specimens 4FSW-I and 4FSW-II in the flatwise and in edgewise positions, respectively.

Table 4.2 Summary of the FE model for sandwich structures using brick elements

Specimen	Hexa20 bricks	Nodes	Solution time
4FSW-I-F	12168	55976	3 hours 56 minutes
4FSW-I-E	11270	49633	6 hours 30 minutes
4FSW-II-F	16788	76462	6 hours 40 minutes
4FSW-II-E	15745	75124	8 hours 59 minutes

(a) Flatwise   (b) Edgewise
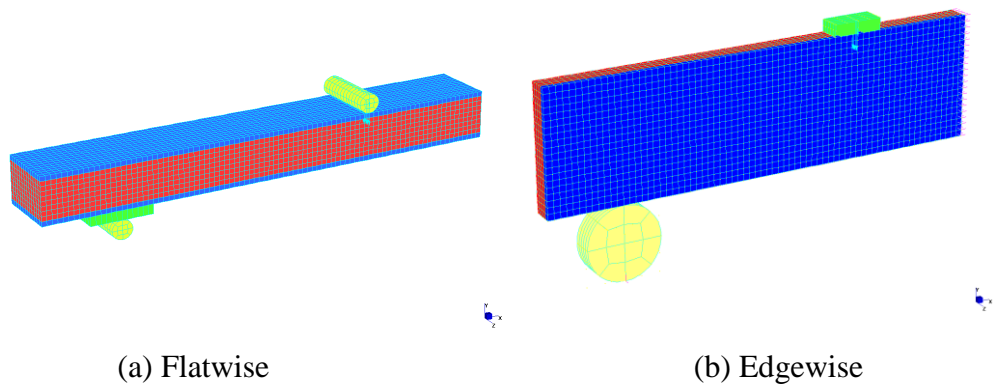
Figure 4.11 FEM model of specimen 4FSW-I

(a) Flatwise   (b) Edgewise
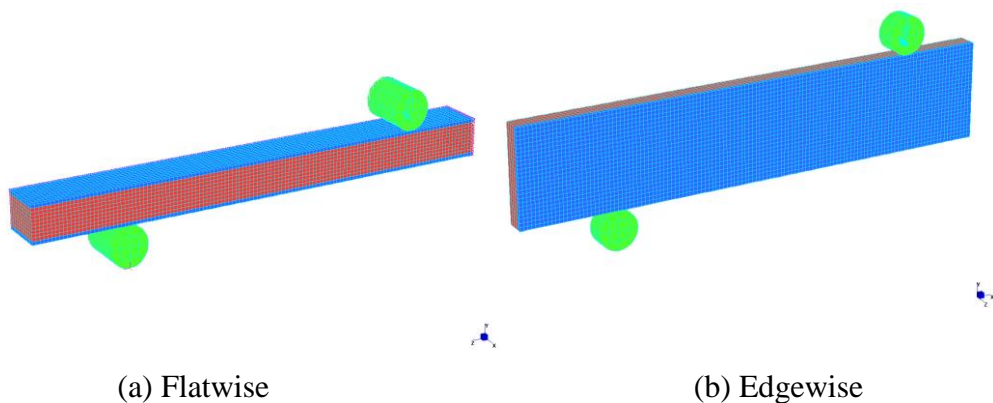
Figure 4.12 FEM model of specimen 4FSW-II

In both models, nonlinear static analyses were conducted considering the behaviour of the constituent materials in Figure 4.10. The fibre composite skin was modelled as linear elastic materials until failure while the core, with linear stress-strain relationship in tension and bi-linear stress-strain relationship in compression. In addition, the skin was assumed to be perfectly bonded to the core, eliminating the debonding failure mode. Analysis was conducted using the nonlinear static solver in Strand7. In Strand7, the nonlinear calculation was performed by automatic load stepping to the total external load and the solution procedure is terminated when the final load level is reached. The failure of the sandwich beam is defined in the FEM model as the strain at which the maximum strength in the elements exceeded either the maximum tensile, compressive or shear strength of the material. After each analysis, the deflection, bending stress-strain relationships at the topmost and bottommost brick elements at the midspan of the composite sandwich beams and the shear stress in the core at each load increment are recorded.

4.7 Predicted results and comparison with experiments

The results of the analytical prediction and numerical simulations of the flexural behaviour of the composite sandwich beams and comparison with the experimental results are discussed in the following sections.

4.7.1 Failure load

The prediction equations in section 4.4 were used to determine the maximum load and the governing failure for the novel composite sandwich structures. For specimen 4FSW-I-F, the dominant failure mode was predicted to be core shear. On the other hand, tensile failure of the core was the predicted dominant failure mode for specimen 4FSW-I-E. The estimated maximum load due to core shear failure and due to compressive failure of the skin was also calculated. For specimen 4FSW-II-F, the failure mode was predicted to be either tensile failure of the core or compressive failure of the skin while the predicted failure mode for specimen 4FSW-II-E was tensile failure of the core. Table 4.3 shows the predicted failure load and the maximum load of the sandwich structures based on experimental investigations.

Table 4.3 Actual and predicted failure load of composite sandwich structures

Specimen name	Failure load based on experiment (N)	Predicted failure load (N)			
		[1]Shear failure of core	[2]Shear failure of core	Compressive failure of the skin	Tensile failure of the core
4FSW-I-F	4657	6441	5792	5927	6212
4FSW-I-E	8150	16387	11815	8024	6738
4FSW-II-F	4554	7128	6380	4406	4316
4FSW-II-E	5589	17063	12678	5403	4453

Note: [1]Calculated using equations 4.4 and 4.5 for flatwise and edgewise positions, respectively.
[2]Calculated using equations 4.6 and 4.7 for flatwise and edgewise positions, respectively.

The specimen 4FSW-I-F failed due to shear failure of the core. However, the predicted failure load for this type of failure using equations 4.4 and 4.6 are 40% and 25% higher respectively than the actual failure load. This shows that using the shear modulus of the skin and the core can better predict the failure load of the composite sandwich structures due to core shear failure. The difference however between the predicted and the actual failure load could be due to the combined effect of the flexural stresses on the sandwich structures resulting in a slightly lower failure load.

The predicted failure load due to the compressive failure of the skin for specimen 4FSW-I-E is nearly equal (1.5% lower) to that of the actual failure load. Tensile cracking of the core was observed at a load equal to the predicted load that the sandwich structure will fail due to tensile failure of the core. Again, the skins prevented the tensile crack from widening and the failure occurred only when the skin failed due to compressive failure.

The predicted load due to tensile failure of the core for specimen 4FSW-II-F is 5% lower. However, the tensile cracks did not cause failure of the beam as the skin at the tension side of the specimen bridged the cracked core together. On the other hand, the predicted load due to compressive failure of the skin is only 3% lower than the actual failure load. This clearly shows that for longer specimens under bending, the failure load of the composite sandwich structure is governed by failure of the fibre composite skins. The difference however on the predicted and the actual failure load could be due to the variation of the specimen dimensions. For specimen 4FSW-II-E, the predicted failure load due to compressive failure of the skin is comparable to the actual failure load. Similar to the specimen 4FSW-I-E, the skins of specimen

4FSW-II-E prevented the tensile failure of the core. The failure of the specimens occurred only when the skin failed due to compressive failure.

The results showed that the failure load of the composite sandwich structures can be predicted well using the mechanical properties of the constituent materials established from coupon testing. Similarly, the results indicated that the failure mode of the composite sandwich structures tested in this study depends largely on the compressive strength of the fibre composite skins.

4.7.2 Longitudinal stress-strain behaviour of fibre composite skins

The longitudinal stress-strain relationship of the fibre composite skins predicted analytically and numerically and the result of the 4-point static bending tests on composite sandwich beams are shown in Figures 4.13 and 4.14. In these figures, the experimental, FEM and the FMA stress-strain relations are designated by Expt, FEM and FMA, respectively while the specimen tested in the flatwise and edgewise positions are represented with F and E, respectively. The experimental results show an almost linear stress-strain relationship in both tension and compression and a good agreement with the predicted stress-strain relation based on the FMA and FEM up to final failure. A higher strain is measured in tension than in compression. This further confirms that the fibre composite skins have a slightly lower modulus in tension than in compression as also observed in the test of coupons.

The strain at the top of the composite sandwich structures matches the strain at the bottom. This showed that there is no debonding between the skins and the core and the assumption of compatibility of strains throughout the depth of the composite sandwich section, and the equilibrium of internal force resultants are valid. As discussed in the previous sections, the specimen 4FSW-I-F failed at 10500 microstrains in tension and around 10000 microstrains in compression which suggest that the strength of the fibre composite skins was not fully utilised. As indicated in Figure 4.13, a decrease in stiffness was observed in specimen 4FSW-I-E at a tensile strain of around 12000 microstrains due to the development of flexural tensile cracking in the core. The specimen 4FSW-I-E then failed at 13000 microstrains in the compressive skin which is comparable with the compressive failure of fibre composite skin listed in Table 3.3. Similar stress-strain behaviour was observed in specimen 4FSW-II-F and specimen 4FSW-II-E as these specimen failed due to compressive failure of the fibre composite skins (Figure 4.14). In all specimens, a

slight decrease in stiffness was observed at a tensile strain of 6000 microstrains due to the initiation of tensile cracking of the core material. Furthermore, the recorded maximum compressive strain of 13000 microstrains is comparable with the failure strain of the fibre composite skin in compression established from coupon testing.

In general, the results showed that both FMA and FEM analysis can predict the stress-strain behaviour of fibre composite sandwich beams. The difference in the FMA and the experimental results in all the tested sandwich beams is less than 5%. The small discrepancy observed could be attributed to the variations in the dimensions of the composite sandwich beam specimens.

(a) Flatwise

(b) Edgewise
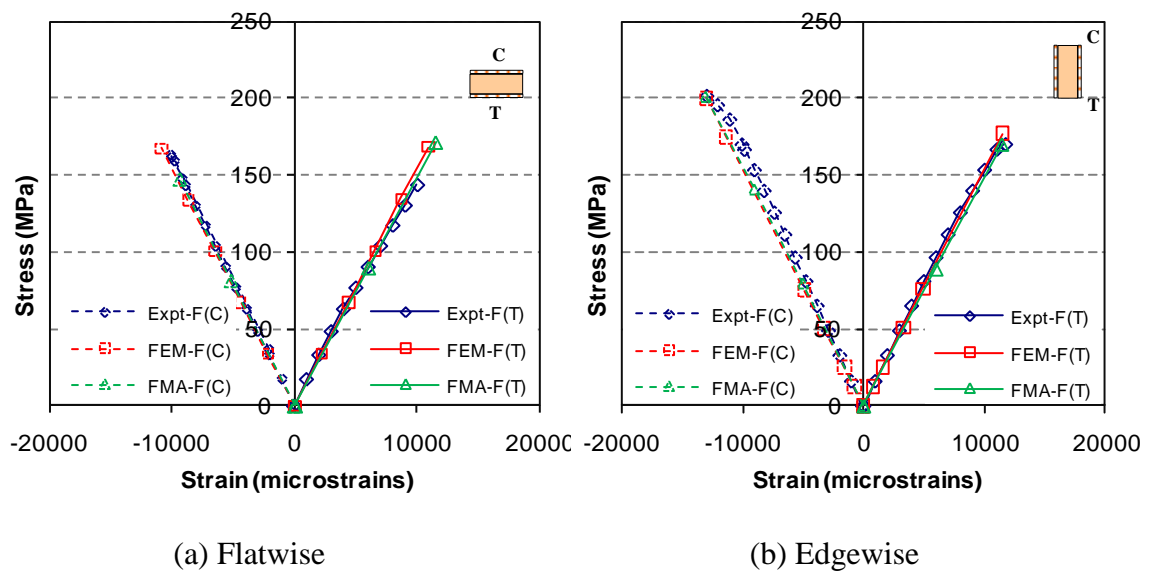
Figure 4.13 Experimental, FEM and FMA stress-strain behaviour of 4FSW-I

(a) Flatwise

(b) Edgewise
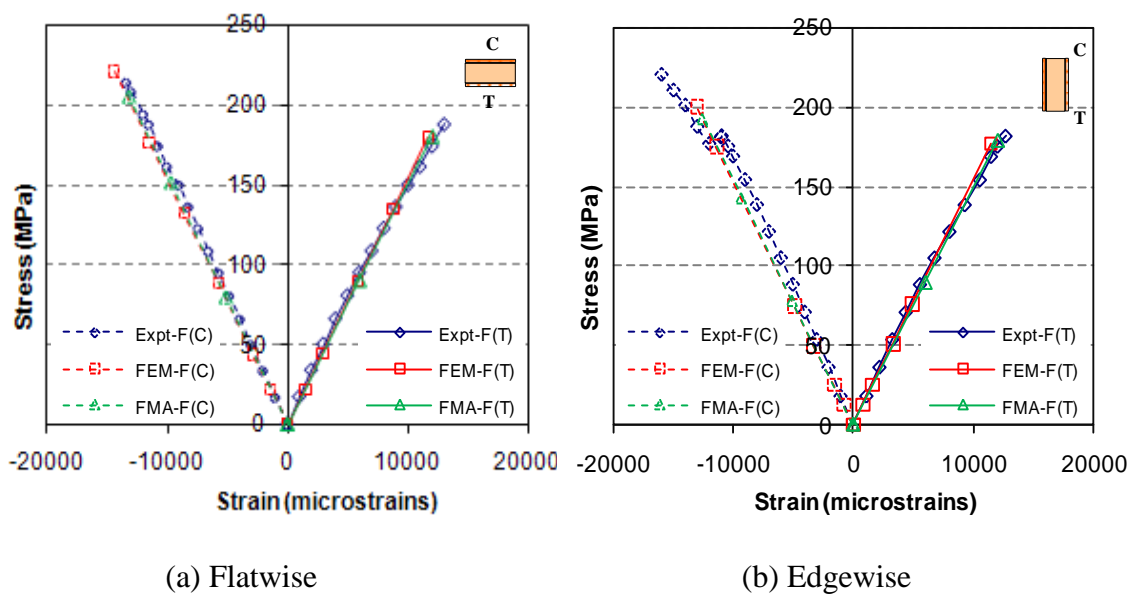
Figure 4.14 Experimental, FEM and FMA stress-strain behaviour of 4FSW-II

4.7.3 Load-deflection relationship of composite sandwich structures

The comparison of the FMA, FEM and experimental load and midspan deflection relation curves for composite sandwich structures tested under 4-point static bending are shown in Figures 4.15 to 4.18. In the calculations, the contribution of the core in the flexural stiffness is considered. This contribution is approximately 10% in the flatwise position and more than 25% in the edgewise position. Using the constitutive material behaviour determined from the coupon tests, the results of the FMA and FEM have provided results in good agreement with the experiment.

Under bending, the predicted load deflection behaviour of the composite sandwich structure using FMA are similar to that of the FEM results. The load increased linearly with deflection then a slight decrease in stiffness was observed due to the initiation of tensile cracking of the core at a strain of 6000 microstrains. The specimen then failed when the compressive strength of the top skin was reached.

Figures 4.15 and 4.16 show that the difference between the predicted and the experimental results is only 2% for composite sandwich structures tested in the flatwise position. However, the difference can go as high as 5% for the specimens in the edgewise position. The reason for this could be due to the behaviour of the skin as it is subjected both to flexural and shear deformation. Similarly, the skins are subjected to both tension and compression unlike in the flatwise position where the fibre composite skins is subjected only to either compressive or tensile forces.

The comparison of the experimental and analytical prediction considering and not considering shear deformation is shown in Figures 4.17 and 4.18. The analytical load-deflection behaviour of the composite sandwich structures in the flatwise and edgewise positions which does not include shear deformation are designated as FMA-F(2) and FMA-E(2), respectively. The shear deflection of specimen 4FSW-I loaded in the flatwise position is around 5% of the total deflection and around 8% when loaded in the edgewise position (Figure 4.17). However, the contribution of shear in the total deflection of the composite sandwich structures decreased for specimen 4FSW-II. This is due to the longer test spans of these specimens. The shear deformation of the composite sandwich specimens in the flatwise position is only 3% and only 5% in the edgewise position (Figure 4.18). The higher shear deflection in the edgewise position is due to the contribution of the vertical skins in the shear rigidity of the composite sandwich structures.
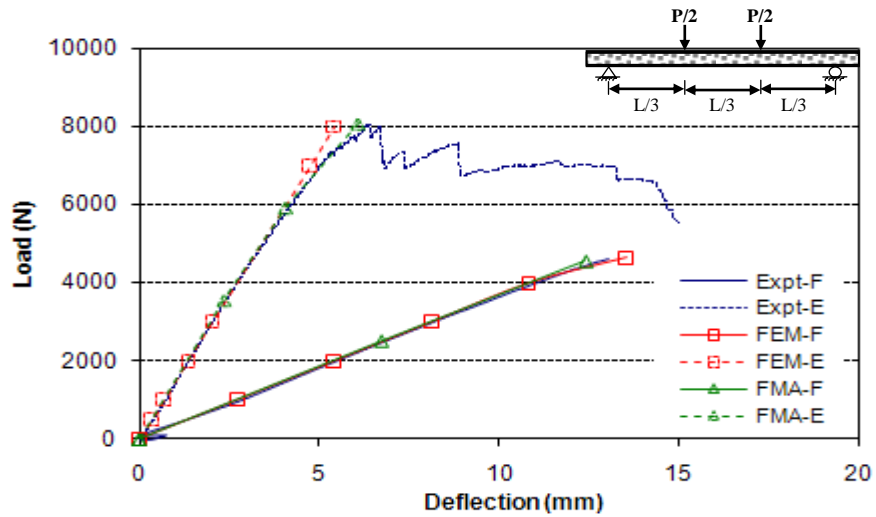
Figure 4.15 Experimental, FEM and FMA load-deflection behaviour of 4FSW-I
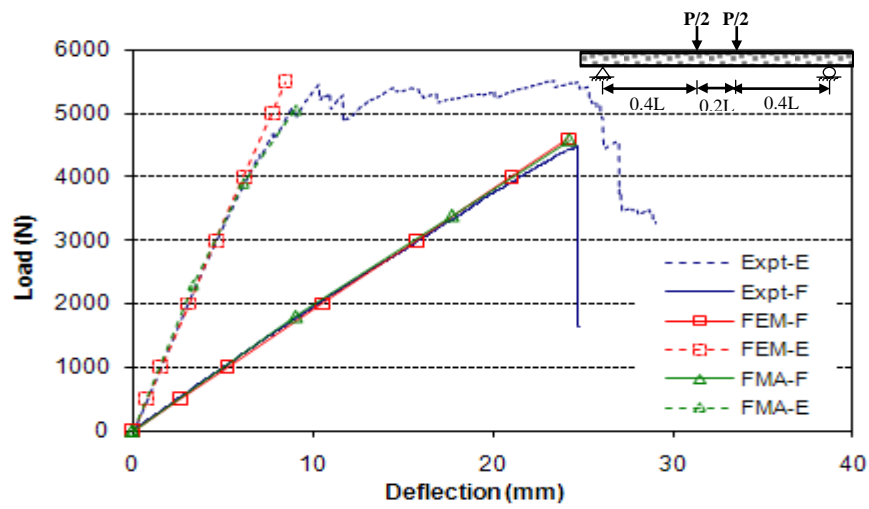
Figure 4.16 Experimental, FEM and FMA load-deflection behaviour of 4FSW-II
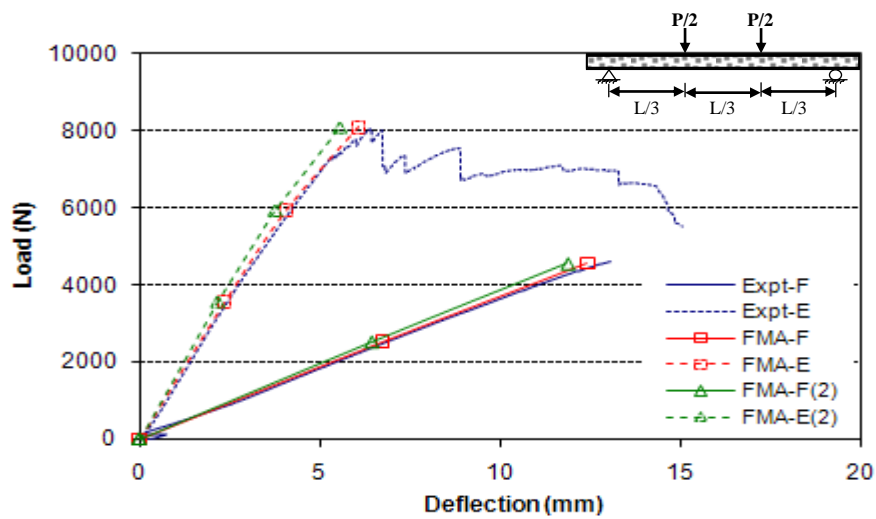
Figure 4.17 Load-deflection of 4FSW-I with and without shear deformation
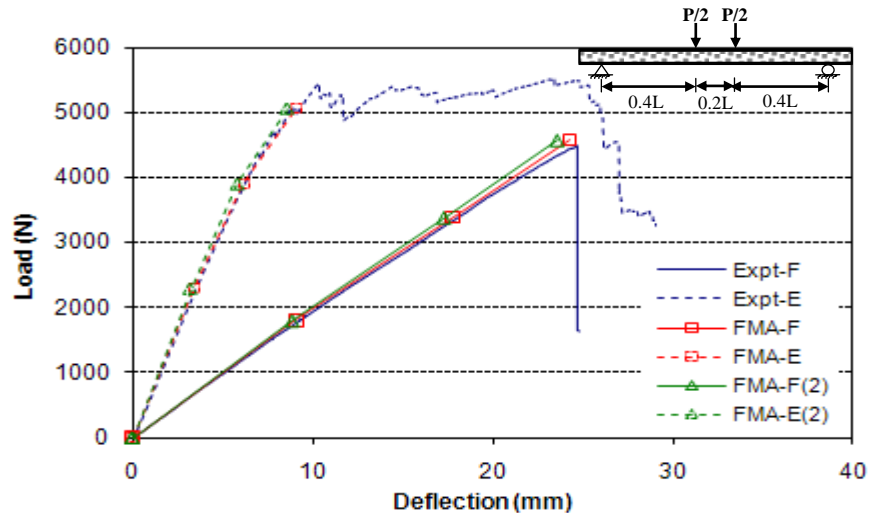
Figure 4.18 Load-deflection of 4FSW-II with and without shear deformation

4.7.4 Failure behaviour

The failure mechanisms of the composite sandwich structures under 4-point static bending based on the numerical simulations are shown in Figures 4.19 and 4.20. The results of the FEM analysis showed a good agreement with the experimental results. Using the maximum stresses where the skin and the core material will fail, the FEM analysis was successful in the prediction of the failure mechanisms of the beams tested in flatwise and in edgewise positions. Based on the FEM model, the shear failure of the core under the loading point of the specimen 4FSW-I tested in the flatwise position (Figure 4.19a) occurred at a load of 4650 N while compressive failure of the skin in the edgewise position (Figure 4.19b) occurred at a load of 8000 N. On the other hand, specimen 4FSW-II will both fail due to compressive failure of the skin at any point between the loading rollers. Compressive failure of the skins occurred at a load of 4500 N for specimens tested in the flatwise position and a load of 5200 N for specimen tested in the edgewise position (Figure 4.20). In all specimens, the failure mechanisms predicted from the FEM simulations are similar to the failure mechanisms observed in the experimental investigation. These results further show that the FEM simulations can better predict the failure load due to shear failure of the core which cannot be predicted by using the simple FMA.

(a) Flatwise   (b) Edgewise
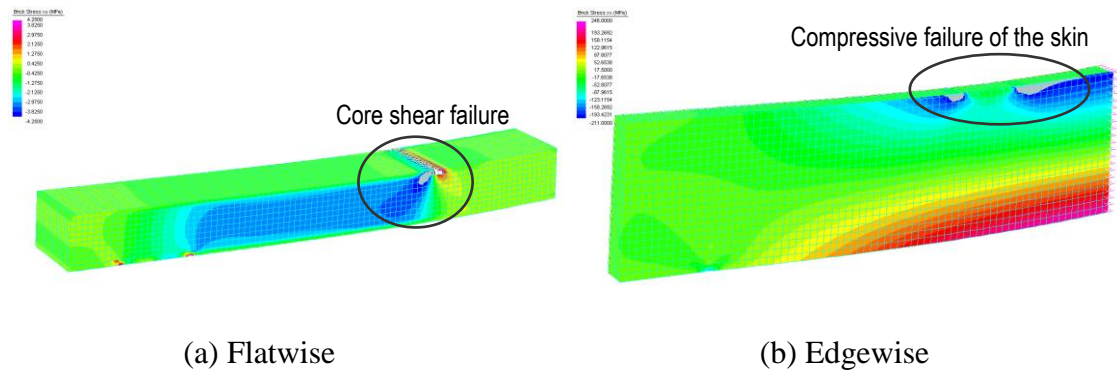
Figure 4.19 Predicted failure of specimen 4FSW-I based on FEM analysis

(a) Flatwise   (b) Edgewise
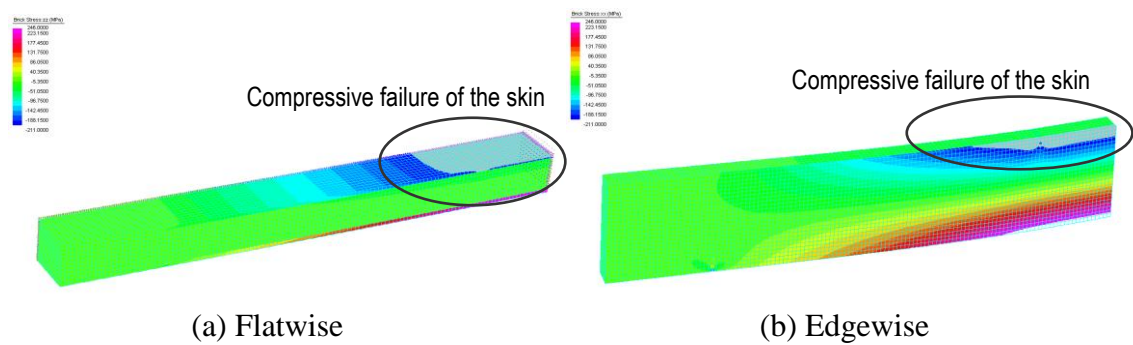
Figure 4.20 Predicted failure of specimen 4FSW-II based on FEM analysis

4.8 Conclusions

The flexural behaviour and failure mechanisms of a novel composite sandwich structure in flatwise and in edgewise positions have been studied experimentally, analytically and numerically. The experimental investigation showed that under flexural loading, the composite sandwich beams in the flatwise position failed with sudden brittle type failure due to combined flexural and shear failure of the core for shorter specimens and compressive failure of the skins followed by debonding between the skin and the core for relatively longer specimens. In the edgewise position, the presence of vertical fibre composite skins increased the ultimate strength of the composite sandwich structures. When tensile cracks of the core occurred, the skins prevented it from widening and prevented the sudden failure of the sandwich structures. In this position, the sandwich structures deflected only half that in the flatwise position under the same level of load due to its higher bending stiffness. More importantly, the composite sandwich structures in the edgewise position failed at a higher load than that of the specimens in the flatwise position.

The contribution of the high strength core material in the flexural and shear stiffness is significant and should be included to determine the overall behaviour of

the composite sandwich structures. Theoretical prediction of failure loads using the mechanical properties of the constituent materials established from the coupon tests was found to be in good agreement with the experimental results. In the simple FMA and FEM simulations, consideration of the bilinear elastic behaviour of the phenolic core material in compression provided a better understanding of the flexural behaviour of fibre composite sandwich structures up to the maximum load. The analytical model agreed very well with the experiments and the FE analyses, giving confidence in the validity of the underlying assumptions.

Finally, the result of this study showed the high potential of this novel composite sandwich structures for laminated beam. An increase in flexural stiffness due to sandwich effect suggest the application of composite sandwich structures in flatwise position in the outermost layers to carry tensile and compressive stresses. Similarly, the higher capacity of the composite sandwich structures in the edgewise position suggest that the strength is significantly improved by the introduction of the vertical fibre composite skins, thus could be used in the inner portion of the laminated beams to carry shear.

In Chapter 5, the behaviour of the novel fibre composite sandwich structures in carrying shear loading is discussed.

Chapter 5

Shear behaviour of fibre composite sandwich structures with high strength core material

5.1 Introduction

The fibre composite sandwich structure made up of glass fibre composite skins and a modified phenolic core material showed excellent flexural behaviour, as detailed in Chapter 4. In the same way, it is of considerable importance to understand fully the shear behaviour of this sandwich construction before it can be used in structural applications. For structural beam application, the shear strength of the core is an important consideration when designing sandwich structures. This chapter discusses the behaviour of this sandwich structure under transverse and in-plane shear loads.

In a number of sandwich structures, the main design criterion is the shear strength of the core material. It has been demonstrated that, under service loads, most sandwich constructions failed due to shear failure of the core (Kampner and Grenestedt, 2007). This brittle nature of the core material causes a sudden collapse after the formation of the first crack. In structural applications, this is more critical as thicker and higher density core is required to transfer the shear between the top and bottom skins compared to other industrial applications (Styles et al., 2007). Hence, a shear failure of the core material will have an adverse effect on the performance of composite sandwich structures and may be the limiting factor in designing such structures. It is essential therefore to eliminate the possibility of this type of failure to be able to efficiently use composite sandwich construction in structural applications.

In this chapter, the shear behaviour of the novel composite sandwich structures with high strength core material is discussed with emphasis on the in-plane shear behaviour. Attempts to improve the performance of the composite sandwich structures by making the fibre composite skins carry some of the shear loads usually carried by the core have been made. In order to achieve this, the composite sandwich structures were tested both in the flatwise and in the edgewise positions. The introduction of the vertical fibre composite skins on both sides of the core material when the sandwich structures is placed in the edgewise position, it is anticipated that

the shear resistance of the sandwich structures will improve as the vertical skins are likely to carry part of the shear load. This concept is similar to shear strengthening of structures with fibre reinforced polymer to meet specific structural requirements (ACI 440R, 2007). FRP laminate or fabric reinforcement are provided parallel to the principal tensile stress at the sides of the web of concrete beams to increase the shear capacity of the concrete members (Bakis et al., 2002; Stonebraker et al., 2008). FRP is now also being bonded on the sides of beam to reinforce wood in shear (Triantafillou, 1997). Using this concept, the fibre composite skins of the composite sandwich structure could provide additional shear strength and control the shear cracks of the core. Utilising the sandwich structure in the edgewise position will reduce the core shear stress and prevent the premature and brittle failure of the core. This concept is anticipated to lead towards the improvement of the performance of the composite sandwich structures while maintaining the simplicity of the production process. The contribution of each component of the composite sandwich structure in carrying the shear should be characterized. Currently, there are no available reports on the investigation on the shear strength and failure mechanisms of composite sandwich structures in the edgewise position which is the main aim of this study.

5.2 Shear test for composite sandwich structures

The accurate knowledge on the mechanical properties of composite sandwich construction is a fundamental requirement for its utilization as a competitive structural material. However, there still exists a problem in describing accurately the true shear behaviour of the composite sandwich material due to lack of accurate test methods. Several test methods, namely, Iosipescu shear test, V-notched rail shear test, picture frame test, and bending test of short beams were developed to determine the shear properties of composite materials. However, most of these tests have several difficulties and limitations in performing a reliable and accurate measurement for composite sandwich structure under shear loading.

The Iosipescu shear test was first developed to measure the shear strength of metal rods (Iosipescu, 1967). In the early 80s, Walrath and Adams (1987) developed a test fixture known as the '*modified Wyoming fixture*', which was included in the ASTM standard D5379-93 (ASTM D5379/D5379M, 1993) and is widely used in composite research laboratories. Although, the Iospescu shear test is appropriate in determining the shear strength and modulus of fibre composite materials, the

relatively small size of the fixture used in this test limits its application for composite sandwich structures. Another test method is the V-notched rail shear test (ASTM D7078, 2005) which incorporates the attractive features of the existing Iosipescu and two-rail shear tests (ASTM D4255/D4255M-01, 2001). This test method has been standardised as ASTM D 7078. Results from this test showed a reduced shear stress concentration near the rails and produces relatively uniform shear stress distributions in the specimen gauge section for a variety of carbon/epoxy laminates. This test method depends on the excellent gripping of the specimen on the test fixture, thus requires a larger gauge section than a standard Iosipescu shear test specimen (Adams et al., 2007). However, it is very difficult to attain adequate gripping with a standard fixture especially for high shear strength composite materials. The picture frame test (shown in Figure 5.1a) on the other hand is regarded as the most accurate test giving the modulus of rigidity for composite panels (Bowles and Vanucci, 1986). This test method however, requires complex specimen preparations and special test fixtures. In the study conducted by Lebrun et al. (2003), the results showed large differences on the shear behaviour of a polypropylene/glass fabric with the standard picture-frame test method due to improper alignment of the fibres with the frame. In this case, tension forces in the fibres are higher such that the recorded load is much larger than the load necessary to shear the specimen.

The most simple test method to determine the shear properties of composites would be the bending tests of short beams (ASTM C393, 2000). The bending test involves three-point bending of short sandwich beam to ensure shear failure of the core. The results of this test, however, might be inaccurate and not give 'pure' shear strength due to the influence of flexural stresses. For direct shear test of the core material, the core or the composite sandwich structure was adhesively bonded to two steel adherents loaded in tension (ISO 1922, 1981). The adherents should be sufficiently stiff to obtain a stress state of nearly pure shear in the core material. Most tests showed that the direct shear test is not applicable for composite sandwich structure with high-density core material. Using this test method, Russo and Zuccarello (2007) observed that the actual rupture of the sandwich panel with high-strength PVC core is caused by the skin-core interface and not shear failure of the core. This result was also observed in the earlier experimental studies conducted for composite sandwich beams with modified phenolic core material. The delamination between the plies of fibres occurred during the test using sandwich specimen while

debonding between the glue line and the core material occurred using only the core material. Thus, Omar (2008) developed a rocket testing procedure to assess the shear properties of low-density and high-density core materials. In this test method, the core material was bonded to FRP pultrusions in a symmetric set-up as shown in Figure 5.1b. The results of his experiment showed that the testing values of the shear modulus of the core material vary by almost 20% with the data provided by their manufacturers. These showed that the current test standards have some limitations and drawbacks for shear characterisation of composite sandwich structures.

(a) Picture frame test (Lebrun et al., 2003)   (b) Rocket testing (Omar, 2008)
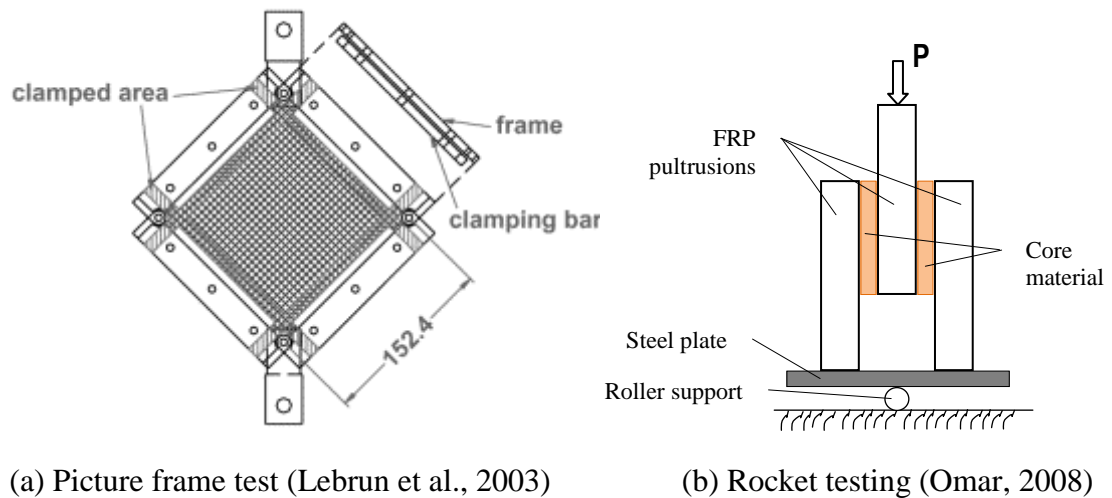
Figure 5.1 Shear test methods for composite sandwich structures

In this chapter, the shear behaviour of both the transverse and in-plane directions of the composite sandwich structures is examined using asymmetrical beam shear test with a view of using this composite material as a shear loading component in a structural laminated beam. In Chapter 3, the accuracy of shear strength of the phenolic core material by this test method has been checked against that obtained by the well-established Iosipescu shear test. The results show that the shear strength and modulus values from the two methods differed only by 2% for the core specimens. The result of the experimental investigation on the in-plane shear behaviour of the novel fibre composite sandwich structure is also presented. Particular emphasis is on the contribution of the vertical skins in the shear capacity and failure mechanisms of the composite sandwich structures under in-plane loading. Finite element simulations were also performed to develop an understanding of the shear behaviour of composite sandwich structures when subjected to load with the possibility of predicting its ultimate capacity and verify this with the experimental
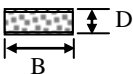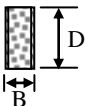
results. A theoretical formula is proposed to calculate the shear strength of the composite sandwich structures using the shear properties of the fibre composite skin and the phenolic core material.

5.3. Experimental program

5.3.1 Test specimen

The specimens for shear testing were cut into required dimensions from the novel fibre composite sandwich panels which has a nominal thickness of 20 mm. Similar specimens were prepared both in the flatwise and in the edgewise positions. In all tests, the span for maximum shear a, is held constant at 80 mm due to the limitation of the test fixture. Five replicates for each specimen type were prepared and tested with only 3 replicates from each type were provided with strain gauge. After a significant number of trials, it was found that a composite sandwich structures with a depth of 50 mm will produce shear failure to occur in the prescribed plane of fracture without any twisting or out-of-plane torsion of the specimen. The test also produced valid results with significant reduced variability. This specimen size is almost 3 times bigger than the Iosipescu shear test specimen. The V-notch is also not provided to the composite sandwich structures to simplify the specimen preparation. The details of the specimen for asymmetrical beam shear test are listed in Table 5.1. In this table, the composite sandwich structures tested in the flatwise position is designated as specimen AS-SW-F while the sandwich structures tested in the edgewise position is designated as specimen AS-SW-E.

Table 5.1 Details of specimens for asymmetrical beam shear test

| Specimen name | Illustration | Dimensions (mm) | | | | Orientation of testing |
		B	D	a	L	
AS-SW-F		50	20	80	240	Flatwise
AS-SW-E		20	50	80	240	Edgewise

5.3.2 Test set-up and procedure

The shear behaviour of composite sandwich structures was determined following the asymmetrical beam shear test. This test setup is a modification of the Iosipescu shear

test for composite materials. In this test method, the specimen was eccentrically loaded at two trisected points and the supports were applied at the remaining two points. This loading configuration generates a high shear stress and a nearly zero bending moment at the centre of the specimen. The schematic diagram of the asymmetrical beam shear test and the simplified shear and bending moment diagrams for this test set-up are shown in Figure 5.2. Initially, the shear capacity of only the core material was determined to serve as a reference on the contribution of the skins in the shear capacity of sandwich structures. Results of this test have already been discussed in Chapter 3.

The actual setup and instrumentation for the asymmetrical beam shear test is shown in Figure 5.3. The load was applied through a 100 kN MTS servo-hydraulic universal testing machine with a loading rate of 1.3 mm/min. A steel spreader beam was used to transfer the single load applied by the loading machine to the specimen asymmetrically. The loading pins and the supports had a diameter of 20 mm. In the edgewise position, 30 mm steel plates were provided under the loading points and at the supports to prevent local indentation failure on the composite sandwich beams. Resistance strain gauges oriented at $\pm 45^{\circ}$ (A2A-06-C-085C-500 type, supplied by Biolab Pty Ltd., Australia) to the loading axis were attached on the surface of the specimen along the middle line at mid-height to evaluate the shear response during the entire loading regime. Before each test, the loading pin was set to almost touch the top surface of the composite sandwich specimen. The applied load and strains were obtained using a System 5000 data logger. All specimens were tested up to failure to determine the shear strength and the mode of failure while being observed for any indications of specimen twisting or out-of-plane torsion.

(a) Asymmetrical beam shear test   (b) Shear and moment diagrams
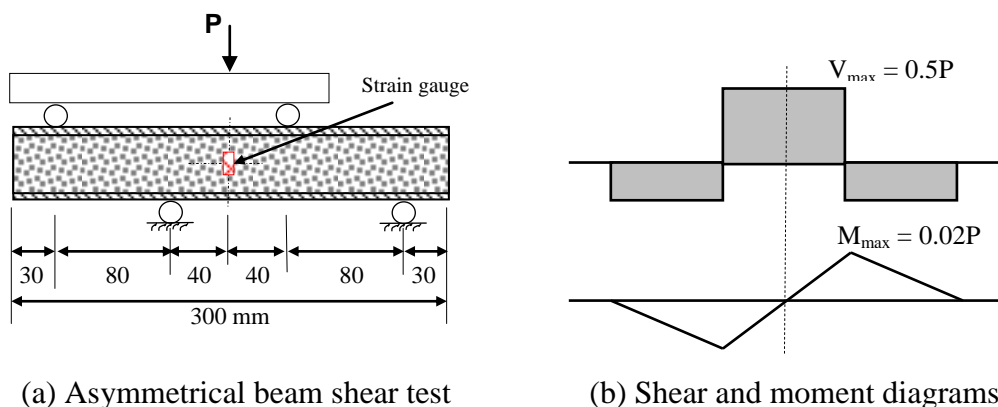
Figure 5.2 Schematic illustration of asymmetrical beam shear test

(a) Specimen AS-SW-F   (b) Specimen AS-SW-E
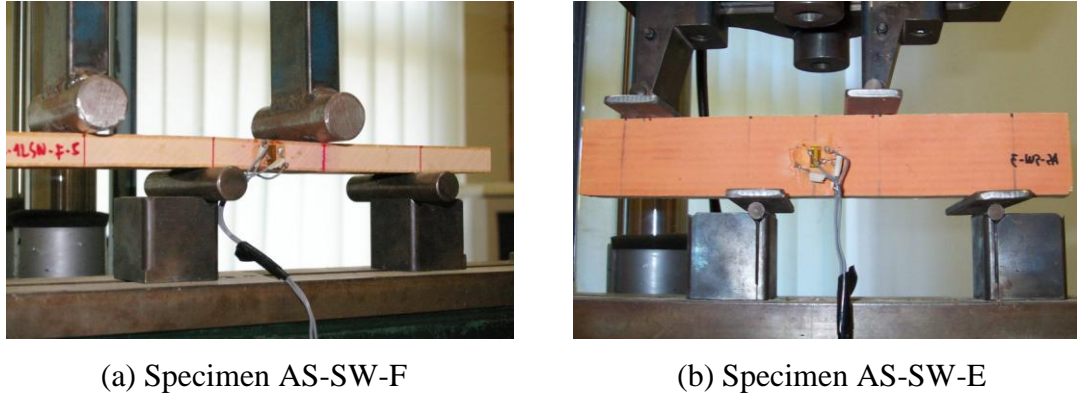
Figure 5.3 Test set-up for sandwich structures under asymmetrical beam shear test

5.4. Experimental results and discussion

In this section, a comparison between the behaviour of the sandwich beams in the flatwise and in the edgewise positions under asymmetrical beam shear test is made.

5.4.1 Failure load

Table 5.2 summarises the load at first shear crack of the core material and the maximum load carried by the composite sandwich structures tested in the flatwise and in the edgewise positions. For specimen AS-SW-F, the load at first crack in the core is also the maximum load as the specimen failed immediately after the formation of the first shear crack in the core material. A comparison of the failure load showed a higher load for specimens tested in the edgewise than in the flatwise position. The magnitude of the maximum load at failure is almost double for specimen AS-SW-E than that of specimen AS-SW-F. Interestingly, the load when the first crack in the core was observed in the edgewise position is significantly higher than the failure load recorded for the flatwise position.

Table 5.2 Failure load of composite sandwich structures under shear

Specimen name	Number of specimens	Load (N)			
		At 1st crack	Std deviation	Failure load	Std deviation
AS-SW-F	5	10523	240	10523	240
AS-SW-E	5	16568	350	17606	290

5.4.2 Load and crosshead displacement behaviour

The load and crosshead displacement behaviour of the composite sandwich structures under asymmetrical beam shear test throughout the loading regime is shown in Figure 5.4. The figure indicated that the applied load on specimen AS-SW-F increase almost linearly with the crosshead displacement of the testing machine. The load then suddenly dropped indicating the failure of the sandwich structures. For specimen AS-SW-E, a linear load-crosshead displacement relation occurred up to approximately 16.5 kN. After this point, a slight drop in the load was observed due to the shear cracking of the core. After which, the load increased again indicating that the skins continued to carry shear loading. Before ultimate failure, there was a significant shear cracks observed in the skins and an increased amount of deflection with a gradual decrease in the load. This apparent stiffening of the specimen AS-SW-E is due to the progressive development of shear cracks in the skins and can also be explained by the nonlinear behaviour of the fibre composite skin in shear.
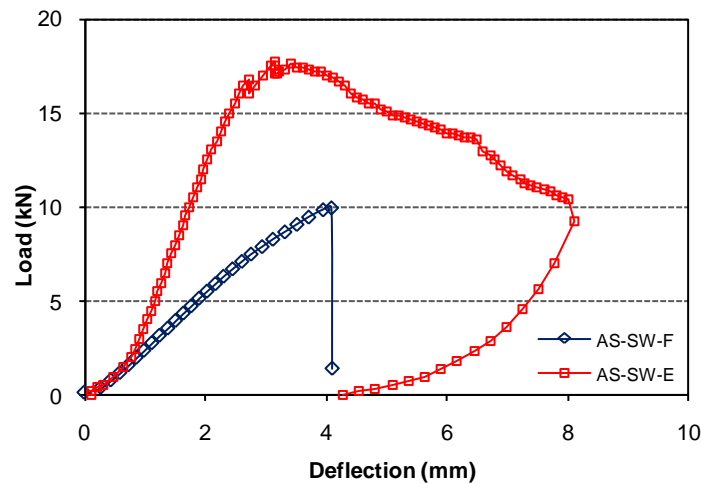
Figure 5.4 Load-crosshead displacement relationship of sandwich structures

5.4.3 Stress-strain behaviour

An initial check was conducted to determine if the asymmetrical beam shear test creates a pure shear for composite sandwich structures at the location of maximum shear. Zhou et al. (1995) suggested that if the shear strain is pure, both tensile and compressive strains should be equal and opposite in sign, which can be checked with the responses of strain gauge attached to the specimen. Thus, the diagonal tensile (+45°) and compressive (-45°) strain gauge measurements were plotted against the applied load during the entire test regime. Figure 5.5 shows the load and shear strain

relationship of the sandwich structures tested in the flatwise and in the edgewise positions. In this figure, the absolute value of the strain measured by the (-45°) strain gauge is calculated to compare directly with that of strain measured by the (+45°) strain gauge to determine if there is a difference between the strain measurements. It can be observed from the figure that both tensile and compressive strain values from the asymmetrical beam shear test for specimens AS-SW-F and AS-SW-E are very close throughout the test, suggesting the presence of a reasonably pure field of shear strain at the mid-depth and midspan of the sandwich specimen. At a higher load, some imbalance between tensile and compressive strains for the sandwich structures tested could be due to the microcracks in the core material which increase the tensile deformation compared with the compressive deformation. These results further confirm that the asymmetrical beam shear test is capable of characterizing the shear behaviour of composite sandwich structure with high strength core material.

(a) Specimen AS-SW-F   (b) Specimen AS-SW-E
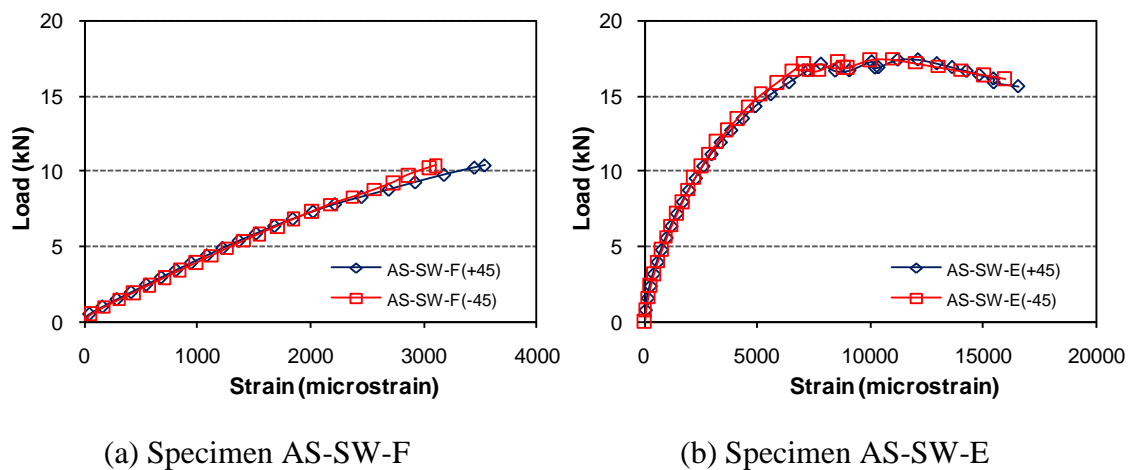
Figure 5.5 Load-diagonal strain of composite sandwich beam

The shear stress-strain relationship of the sandwich beam specimens provided with strain gauge is shown in Figure 5.6. The average shear stress of the composite sandwich structures is calculated by dividing the shear force with the transformed area of the composite sandwich section while the shear strain is determined from the indicated normal strains of the $\pm 45°$ strain gauges attached to the specimen. In the flatwise position, the cross section of the composite sandwich structure was transformed into an equivalent core material while in the edgewise position into an equivalent skin material. This assumption was based on the observed failure mode of composite sandwich structures under asymmetrical beam shear test which is

described in the next section. This approximation makes the contribution of the core and the skin equal because they will have the same properties.

(a) Specimen AS-SW-F　　　　　　　　(b) Specimen AS-SW-E
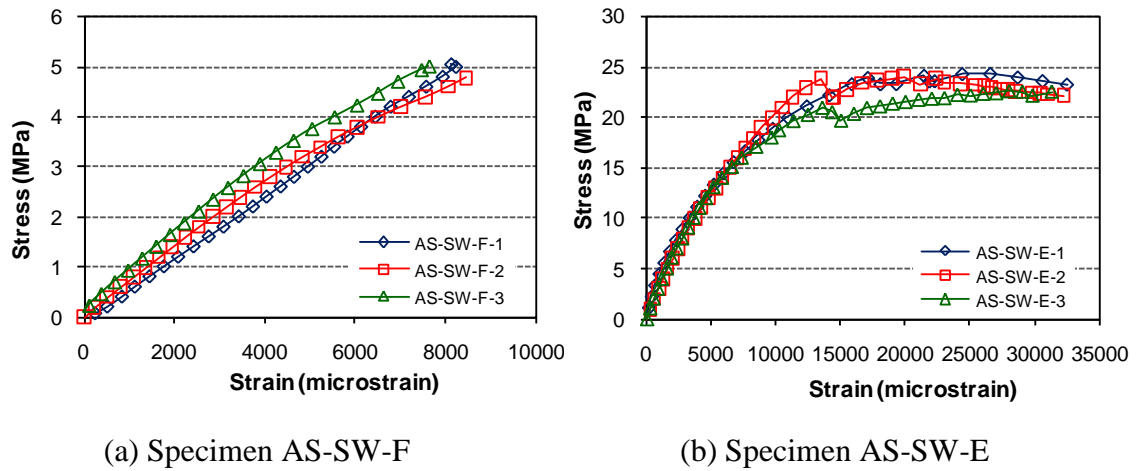
Figure 5.6 Shear stress-strain behavior of composite sandwich beam

The results showed that the sandwich specimens tested in the flatwise position behaved almost linearly with strain up to failure while the in-plane shear behaviour showed non-linearity at higher strain. Notice a consistent reproducibility in response within the test specimens which indicate the asymmetrical beam shear test provide an accurate and reliable shear test data for composite sandwich structures. As illustrated in Figure 5.6a, specimen AS-SW-F failed at a shear strain between 7800 and 8400 microstrains. This level of strain is comparable to the maximum shear strain recorded in the core from the coupon tests. However, the slightly higher shear strength of the sandwich structures at failure compared to the shear strength of the core material is due to the contribution of the fibre composite skins in carrying the shear.

Figure 5.6b shows that the shear behaviour of specimen AS-SW-E is similar to the shear behaviour of the fibre composite skins (shown in Figure 3.12). The shear stress-strain curve shows a linear response at a relatively low amount of strain then started to behave non-linearly with increasing stress until final failure. The non-linearity was amplified after tensile cracking of the core. Similarly, a plateau was observed after reaching the ultimate shear capacity. This is due to the combined shear and compressive failure of the core with the skin still holding the failed core material. The maximum shear stress recorded for composite sandwich structure is around 23 MPa with strains of around 30000 microstrains. It is interesting to note that this value of shear strength is comparable to the maximum shear strength of the

fibre composite skin established from coupon testing. This also showed that the contribution of the fibre composite skin in the shear strength of composite sandwich structures in the edgewise position has a dominant effect. In comparison to the shear stress-strain behaviour of the skins, the composite sandwich structures behaved slightly stiffer compared to the skin alone at a low level of shear stress. This difference in shear stiffness is not significant but could be attributed to the composite action of the core and the skins. These results further suggest that under shear forces, the composite sandwich construction, with two skins and a high strength core material, behaved together as one unit when loaded in-plane. However, this was only possible due to the high strength of the core material which prevented the compressive buckling of the skins, leading to realisation of its full shear strength. Such an interaction made the shear behaviour of the sandwich structures with phenolic core unique as a composite material.

5.4.4 Failure behaviour

Figure 5.7 shows the failure behaviour of fibre composite sandwich structures under asymmetrical beam shear tests. The results of the experiment showed that the composite sandwich structures tested in the flatwise position failed in a brittle manner due to shear failure of the core followed by the successive debonding between the skin and the core (Figure 5.7a). As this specimen has a shear span to depth ratio of 4, the failure behaviour might also have been affected by flexure. The lack of reinforcement through the thickness direction of the core material results in relatively lower shear strength of specimen AS-SW-F compared to the shear strength of specimen AS-SW-E. Consequently, the shear cracks in the core material are more likely to occur in composite sandwich structures tested in the flatwise position. For all tested specimen AS-SW-F, the composite sandwich structures failed after the formation of first shear crack in the core material under the loading point. In this position, a diagonal shear crack of approximately 45° propagates through the core at the location of maximum shear. This failure is brittle and sudden which is accompanied by a loud noise after the appearance of the first crack. This result is encouraging as Soltis and Rammer (1994) suggested that in areas of pure shear, cracks should develop at 45° to the failure plane. This observed failure behaviour further shows that the asymmetrical shear test is effective in inducing shear failure in the composite sandwich beam specimens.

(a) Specimen AS-SW-F   (b) Specimen AS-SW-E
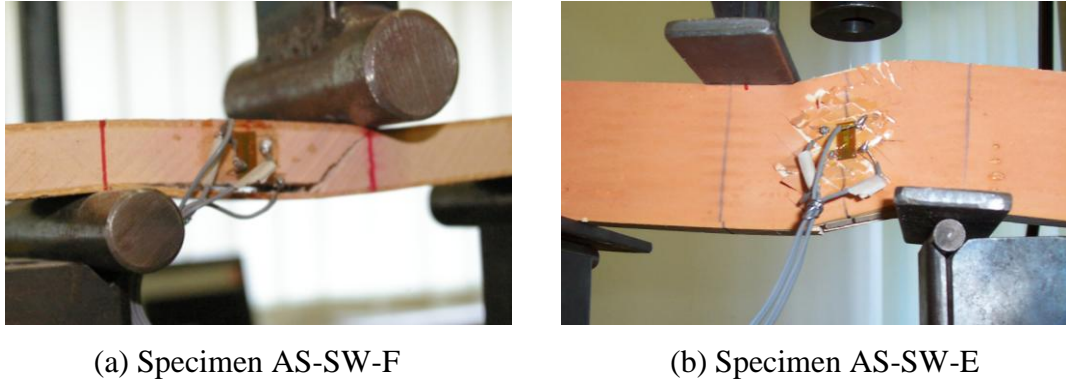
Figure 5.7 Failure of composite sandwich structures in shear

Figure 5.7b shows the failure mode of specimen AS-SW-E. During the test, there was no twisting observed for all specimens in the edgewise position until final failure. In this position, the specimen AS-SW-E showed large strains at failure. The presence of vertical skins inhibits the development of cracks in the core. When the shear crack in the core was observed at a shear stress of around 21.5 MPa (an applied load of around 16 kN), a drop in the shear stiffness was noticed. The presence of the skins on both sides of the core prevented the core crack width from increasing and did not cause failure. The specimen continued to carry load up to a maximum shear stress of 22.5 MPa (applied load of 17.6 kN). Shear cracking of the skin was then subsequently observed. With increasing load, the shear failure became obvious due to the scaling of the resin at the skins. Furthermore, the cracking on the skins were contained within the location of the maximum shear, close to the pure shear region. Based on these observations, it can be concluded that the vertical skins increase the shear capacity of the composite sandwich structures in the edgewise position by preventing the widening of cracks in the core thereby increasing the ultimate load of the specimens. In addition, this observed behaviour in the edgewise position is more likely influenced by the short shear span to depth ratio of the specimen.

Following each test, the failed specimen was carefully removed from the test set-up and examined for any signs of compressive or indentation failure on the loading points and at the supports. Only a minimal bearing and indentation marks were observed on these points which suggest that the 30 mm width steel plates have distributed the applied load very well. Determination of a sufficient plate width that prevented the indentation and compressive failure on composite sandwich structures is discussed in Appendix B.

5.5 Theoretical evaluation of the shear strength

Various theories for predicting the shear strength of structures strengthened with externally bonded fibre reinforced polymer have been reported in many studies. Similarly, the capacity of structural plywood under in-plane loading has already been established. In general, most of the proposed expressions to predict the ultimate load of plywood and structures strengthened for shear with fibre composites were based on the assumption that the total shear capacity is equal to the sum of the shear capacity provided by each material. In this section, some of the available equations were used to calculate the shear strength of composite sandwich structures. Based on the results of the study, an empirical equation is proposed taking into account the basic shear strength and stiffness values of the skins and the phenolic core material.

5.5.1 Composite sandwich beam equations

Most of the available research and literature predict the shear strength of the composite sandwich structures by considering that the shear stress is predominantly carried by the core, as the skins of most sandwich structures are thin (Steeves and Fleck, 2004). While this can be applied directly to composite sandwich structure in the flatwise position, this is not applicable to sandwich structures in the edgewise position. The mechanism of shear resistance is different in the edgewise position as both the skins and the core are supporting shear. Thus, in the calculation of the shear strength of composite sandwich structures, both the contribution of the skin and the core are considered. The shear capacity of the sandwich structures due to failure of the core material is estimated by equation 5.1 while the shear capacity when the sandwich beam fail due to shear failure of the fibre composite skin is estimated by equation 5.2. In the flatwise positions, these equations were also used by using the width, *B* of the sandwich beam instead of the depth, *D*.

$$P_{sw\_c} = \tau_c \left(2t_s + t_c \right) D \tag{5.1}$$

$$P_{sw\_s} = \left(2t_s \tau_s + t_c \tau_c \right) D \tag{5.2}$$

5.5.2 American Plywood Association – The Engineered Wood Association, 1995

The American Plywood Association (1995) recommends procedures and criteria for conducting and evaluating the structural performance of plywood products. They

also suggest methods for the design and fabrication of glued all-plywood beams. In the characterisation of strength when the plywood is loaded in the plane of the panel, it is assumed that the shear stresses are carried by all veneer layers. As all veneer layers are carrying shear, the effective shear area is based on the the sum of the thicknesses of all the veneers multiplied by the depth of the panel. Similarly, they recommended that the effective modulus of rigidity under edgewise shear, G_{sw} for plywood panel could be obtained using equation 5.3 below. This effective modulus is estimated by multiplying the thicknesses of the component material with its corresponding shear modulus divided by the total thickness of the panel. The effective shear modulus is then multiplied with the homogenous cross sectional area of the plywood under in-plane shear and the shear strain observed in the plywood. Because the shear failure of the core material in shear occurred immediately after the incidence of the first crack and at an average strain of 8000 microstrains, this value of strain was chosen as the base strain corresponding to failure of the composite sandwich structures. Using this relation, the shear capacity of the composite sandwich section, P_{sw} could be estimated using equation 5.4.

$$G_{sw} = \frac{1}{B}\left(2t_s G_s + t_c G_c\right) \qquad\qquad (5.3)$$

$$P_{sw} = BDG_{sw}\gamma_{sw} \qquad\qquad (5.4)$$

where B is the total thickness or width of the composite sandwich structures, t_s and t_c are thicknesses of the skin and core, respectively, D is the depth, G_s and G_c are the shear moduli of the skin and core, respectively, and γ_{sw} is the shear strain.

5.5.3 Shear strength of concrete structures with bonded steel and FRP plates

The shear capacity of concrete structures can be increased significantly by attaching steel plates or fibre composites on each side to the web (Ehshani and Saadatmanesh, 1997). The ACI 318 Code (1995) provisions for shear design use the concept that the nominal shear strength of a reinforced concrete (RC) member is taken as the sum of the shear carried by the concrete and web reinforcement. The additional shear force provided by the fibre composites for shear strengthened beams can be computed as the average shear stress multiplied by area the FRP reinforcement covering two sides of the beam (Al-Sulaimani et al., 1994). This straightforward procedure was also used by Papanicolau et al. (2007) to calculate the contribution of textile reinforced

mortar jacket to shear resistance of masonry walls. In another shear strengthening work conducted by Adhikary and Mutsuyoshi (2006), they have experimentally and numerically investigated the effectiveness of web-bonded continuous steel plates for shear strengthening of RC beams having internal stirrups. In the analysis, the ultimate shear strength of RC beams with web-bonded continuous horizontal steel plates is computed by adding the contributions from concrete, internal shear reinforcement and the external steel plates. They have computed the contribution of concrete and the internal shear reinforcement using established formula while they have assumed that the shear contribution of steel plates by using the average shear stresses in steel plates over its depth and thickness. This conventional method of calculating the shear capacity seems to apply to sandwich structures with some modification. The shear capacity of the sandwich section can be determined by multiplying the area of the skin and the core by their corresponding shear strength as shown in equation 5.5. This relation is similar to equation 5.2.

$$P_{sw} = \left(2t_s\tau_s + t_c\tau_c\right)D \tag{5.5}$$

5.5.4 Triantafillou, 1998

Triantafillou (1998) presents a compilation of analytical models for the contribution of fibre composites to the shear capacity of strengthened elements. Among the different models he presented, the analysis of wood members strengthened with fibre composites is very similar to the analysis of shear strength for fibre composite sandwich structures. Triantafillou suggested that the analysis of the shear strength of wood members reinforced with FRP laminates or fabrics is straightforward, following basic principles of mechanics. The contribution of FRP reinforcement in the shear capacity is determined by transforming the FRP into equivalent wood using the ratio of the FRP elastic modulus to wood elastic modulus in the longitudinal direction. Similarly, the failure of the wood reinforced with FRP occurs when the maximum shear stress becomes equal to the shear strength of the wood. Another important assumption in his analysis is that debonding of the FRP prior to wood shear failure should not occur. Using this definition, the shear capacity of the composite sandwich structures when all the materials are transformed into equivalent core can be estimated using equation 5.6 while the shear capacity when all the materials were transformed into an equivalent skin is estimated using equation 5.7.

$$P_{sw\_c} = \tau_c (t_c + 2t_s \frac{E_s}{E_c})D \qquad\qquad (5.6)$$

$$P_{sw\_s} = \tau_s (t_c \frac{E_c}{E_s} + 2t_s)D \qquad\qquad (5.7)$$

where τ_c and τ_s are the shear strength of the core and skin, respectively and E_s and E_c are the modulus of elasticity of the skin and the core respectively.

5.5.5 Kawasaki et al., 2003

Kawasaki et al. (2003) investigated the fundamental shear properties of wood-based sandwich panel of plywood overlaid low-density fibreboard to develop this material as a shear wall. In their study, a "*semi-rigid*" theoretical model to estimate the load capacity of the wood-based sandwich panel based is proposed. In this estimation, the shear strains in the skin γ_s and the core are not the same but are dependent of each other. The wood based sandwich panel would then fail when the shear strain of the core, γ_c was exceeded with γ_s 120% of the γ_c. The results of their research suggested that this approach gave a closer approximation to their experimental results. Using this relation, the capacity of the sandwich structure is estimated as equation 5.8.

$$P_{sw} = (2\gamma_s G_s t_s + \gamma_c G_c t_c)D \qquad\qquad (5.8)$$

5.5.6 Proposed shear strength equation

An empirical equation based on the shear properties of the skin and the phenolic core was proposed to predict the shear strength of the composite sandwich structures after the analysis of the experimental results. Based on this prediction, the shear capacity of the novel composite sandwich structures is not a simple superposition of the shear strength of the core plus the shear strength provided by the skins. In the proposed prediction equation, the shear modulus of the materials, the strain at failure, γ_f and the failure mechanisms are regarded as the main contributor in the overall shear strength of the novel sandwich structures. The basic equation for shear strength, P_f is based on the failure strain multiplied by the corresponding shear modulus and shear area of the fibre composite skin and the core as written in equation 5.9.

$$P_f = \gamma_f (G_s A_s + G_c A_c) \qquad\qquad (5.9)$$

where A_s and A_c are the shear areas of the skin and the core, respectively. In this particular equation, when the shear failure of the composite sandwich structures is governed by the shear failure of the core material, the failure strain of the core is taken as the strain at failure, i.e. $\gamma_f = \gamma_c$. The shear capacity of the composite sandwich section, P_c due to shear failure of the core material can then be written as:

$$P_c = \gamma_c (G_s A_s + G_c A_c) \tag{5.10}$$

$$P_c = \gamma_c G_c (\frac{G_s}{G_c} A_s + A_c) \tag{5.11}$$

$$P_c = \tau_c (\frac{G_s}{G_c} A_s + A_c) \tag{5.12}$$

On the other hand, when the failure is governed by the shear failure of the vertical fibre composite skins, the failure strain of the skin is taken as the failure strain of the sandwich structures, i.e. $\gamma_f = \gamma_s$. In this relation, perfect bonding between the skins and the core is assumed with the full strength of the fibre composite skins realised and the core is contributing to the shear capacity up to final failure of the specimens.

$$P_s = \gamma_s G_s (A_s + \frac{G_c}{G_s} A_c) \tag{5.13}$$

$$P_s = \tau_s (A_s + \frac{G_c}{G_s} A_c) \tag{5.14}$$

Introducing a transformation factor n_G, which is defined as the ratio of the shear modulus of the fibre composite skin to that of the core and considering the individual thicknesses and depth of the constituent materials, equations 5.12 and 5.14 can be written as equations 5.15 and 5.16, respectively.

$$P_c = \tau_c (2t_s n_G + t_c) D \tag{5.15}$$

$$P_s = \tau_s (2t_s + \frac{1}{n_G} t_c) D \tag{5.16}$$

It was observed during the course of the experimental study that the failure of all specimens tested in the flatwise position was a shear failure in the core while in the edgewise position was a shear failure of the vertical skins. Thus, the proposed equations might better predict the shear capacity of the novel sandwich structures.

5.6 Predicted shear strength and comparison with experiments

The maximum applied load under asymmetrical beam shear test of composite sandwich structures was calculated using the existing and the proposed equations for shear strength. Table 5.3 summarises the predicted and the measured failure load of the sandwich specimens under asymmetrical beam shear test. For comparison, the actual and predicted failure load in shear of a 10 mm thick core material (specimen AS-C) was also included to determine the contribution of the skins in the shear strength of the sandwich structures. The maximum load is calculated as twice the shear strength given by equations 5.1 to 5.16. The predicted and the actual capacity of the phenolic core using all the shear equations are nearly equal. This result is expected as the core is an isotropic material. The results suggest that that the average shear strength of the sandwich structures tested in the flatwise position can be predicted accurately when the failure load is calculated based on the shear strength of the core material (equation 5.15). The difference between the predicted and the actual load is only around 5%. In this position, the contribution of skin in carrying the shear is around 15% and the remaining 85% is resisted by the core material.

Table 5.3 Actual and predicted shear strength of composite sandwich structures

Specimen name	Failure load (kN)								
	Actual	5.1	5.2/5.5	5.4	5.6	5.7	5.8	5.15	5.16
AS-C	4.43	4.3	4.3	4.24	4.48	---	4.28	4.31	--
AS-SW-F	10.52	8.6	15.33	22.58	23.61	14.28	14.21	11.16	16.36
AS-SW-E	17.61	8.6	15.33	22.58	23.61	14.28	14.21	11.16	16.36

The predicted in-plane shear strength for composite sandwich structure using equation 5.16 gives an almost 7% lower load than the actual failure load. It can be observed however that this predicted load is comparable to the load when the first shear crack on the specimen was observed. This result clearly shows that the calculation of the maximum shear strength of the composite sandwich structure should be based on the shear strength of the fibre composite skin as the final failure of the composite sandwich structure is due to shear failure of the vertical skins.

The failure load predicted using equations 5.4 and 5.6 gives a higher load than the actual failure load of composite sandwich beams tested in the edgewise position. It is because in this equation, the materials were converted into an equivalent skin

material using the ratio of the elastic modulus. This resulted in an area provided by the core of only 25% while the skins to almost 75%. Using the ratio of the shear moduli resulted in a 55% contribution from the core and only 45% from the skin. On the other hand, the shear strength and modulus increased significantly if compared to core material alone. The increase in shear strength of the composite sandwich structure can be in the ratio of the shear strength of the skin to that of the core material. In the edgewise position, the contribution of the vertical skins in carrying the shear is almost 60% while the core carries the remaining 40% of the load.

The results of the experimental investigations further show that the shear strength of the composite sandwich structure with high strength core material can be predicted reasonably using the mechanical properties of the constituent materials. The results also indicated that the failure mode of the composite sandwich structures in the flatwise position is governed by the shear strength of the core while in the edgewise position largely depends on the shear strength of the fibre composite skins.

5.7 Finite element modelling of the shear behaviour of sandwich structures

Finite element (FE) simulations were carried out to have a detailed understanding of the behaviour of sandwich beams under asymmetrical beam shear test loaded in the transverse and in-plane directions. The results of the numerical simulation and comparison with the experimental results are presented in this section.

5.7.1 FEM of composite sandwich structures

Numerical analyses of the shear behaviour of composite sandwich structures were carried out using the Strand7 finite element software in the FCD-XPP-034 computer (CPU-Intel P4). The numerical simulation was conducted to analyse the stress and strain fields in the test section of sandwich specimens tested in the flatwise and in the edgewise positions. The nominal dimensions of the specimen used in the experimental work and simulating the actual loading conditions were used in the FE model to ensure that the result is comparable to that of the experimental results. The FE models of the composite sandwich beams under asymmetrical beam shear test are shown in Figures 5.8 and 5.9. Due to symmetry along the width of the specimen, only one-half of the composite sandwich structures was modelled using Hexa20 brick elements. The details of the FE model for composite sandwich structures under asymmetrical shear test and the computational time are listed in Table 5.4.

In the FE model, the skin and the core were modelled as linear elastic materials with mechanical properties listed in Tables 3.3 and 3.4. Analysis was conducted using the linear static solver in Strand7 with a number of load cases (of increments of 1 kN). In each load case, the shear stress and strain on the brick elements at the region of maximum shear were checked to see if it exceeds the maximum allowable shear stress and strain limits of the skin and the core material.

Table 5.4 Summary of the FE model for composite sandwich structures

Specimen	Hexa20 bricks	Nodes	CPU time (secs)
AS-SW-F	13380	62942	1858.3
AS-SW-E	15528	72103	2073.6
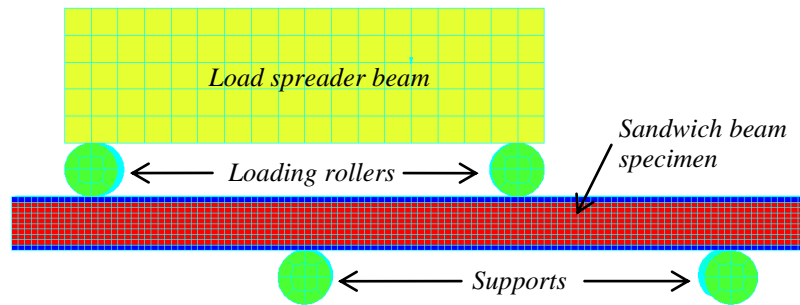
Figure 5.8 FE model of specimen AS-SW-F
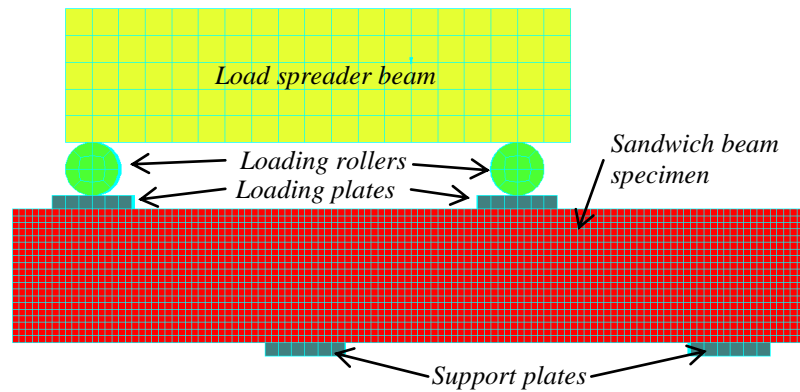
Figure 5.9 FE model of specimen AS-SW-E

5.7.2 Failure load

Using the maximum stress where the skin and the core materials will fail in shear, the FEM analysis has reasonably predicted of the failure load of the composite sandwich structures under asymmetrical beam shear test. In the analysis, the

specimen in the flatwise position is assumed to fail when the shear stress in the core reaches 4.5 MPa while the specimen in the edgewise position will fail when the shear stress in the skin is 23 MPa. The results of the FEM showed that the shear failure of the core of flatwise specimen occurred between 10 and 10.5 kN while the shear cracking of the core for specimen loaded in-plane occurred between 14.5 and 15 kN and shear failure of the skins occurred between 16.5 and 17 kN. In both directions, failure of the sandwich structures occurred at the region of maximum shear.

5.7.3 Stress-strain relationship

The shear stress-strain relationship in the central region of the composite sandwich structures predicted using FEM and the results of the asymmetrical beam shear test are shown in Figure 5.10. In this figure, the shear stress-strain behaviour based on FEM when loaded in the transverse (flatwise) and in-plane (edgewise) directions are designated by FEM (F) and FEM (E), respectively. In both composite sandwich structures, a good agreement between the predicted values using FEM and the experimental results was observed only at the initial linear portion of the stress-strain curve as only the linear analysis was considered in the FE simulations. A more detailed numerical analysis that takes into account the non-linear behaviour of the skin should be conducted to obtain a better prediction for the shear behaviour. This complex numerical simulation is beyond the scope of this study. However, the FE simulations showed that it can reasonably predict the load that the composite sandwich structures will fail in shear.

(a) AS-SW-F   (b) AS-SW-E
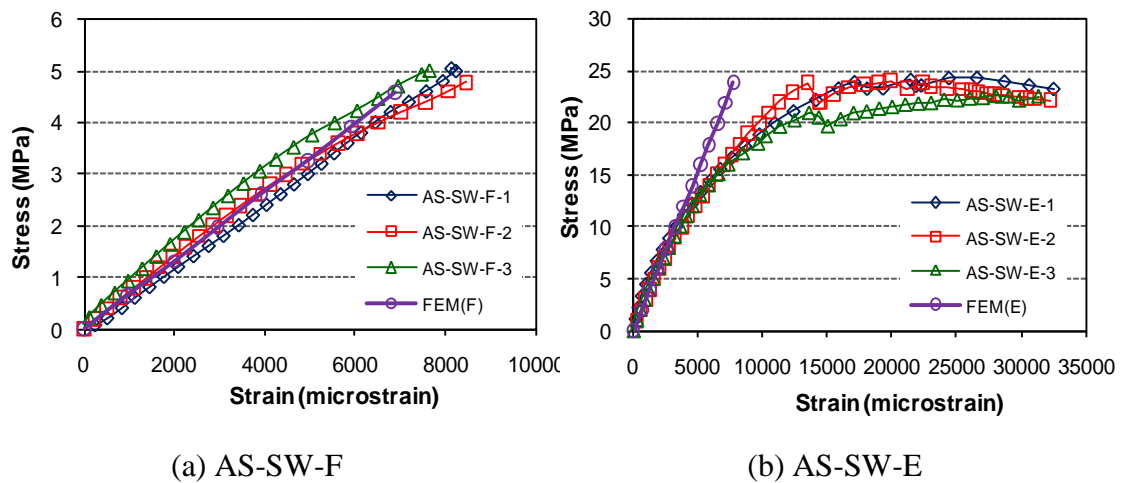
Figure 5.10 FEM and experimental shear stress-strain behaviour of AS-SW

5.7.4 Failure behaviour

The failure mechanisms of the composite sandwich structures under asymmetrical beam shear test based on the FEM are shown in Figure 5.11. In this figure, the contour of shear strain of the composite sandwich structures at the location of the maximum shear is shown. In both specimens AS-SW-F and AS-SW-E, the failure mechanisms predicted from the FEM simulations are similar to the failure mechanisms observed in the tests (as shown in Figure 5.7). At a load between 10 and 10.5 kN, the shear stress and strain on the core of the specimen in the flatwise position reached the maximum stress and strain limits as established from the coupon test. This level of load is similar to the actual failure load of the composite sandwich structures in the flatwise position. In the edgewise position, the shear failure in the core reaches the topmost and bottommost core layers at a load between 14.5 and 15 kN. At this level of applied load, a decrease in shear stiffness in the sandwich beam was observed during the experimental investigation which indicated the shear failure of the core material. At a load between 16.5 and 17 kN, the maximum shear stress of the fibre composite skins was reached at this level of load, indicating the failure of the sandwich beam tested in the edgewise position. These results further shows that using the material properties determined from the coupon tests, the numerical models have provided results in good agreement with the experiment. The FEM simulations also verify that there is no localised compressive and indentation failure in sandwich beams even without steel plate for load applied in the transverse direction while providing a 30 mm plate width minimises the stress concentration of sandwich beams on the loading points and at the supports when the sandwich beam is tested in the edgewise position. As can be seen from Figure 5.11b, only slight signs of stress concentration occurred at the edges of the support plates.

(a) AS-SW-F   (b) AS-SW-E
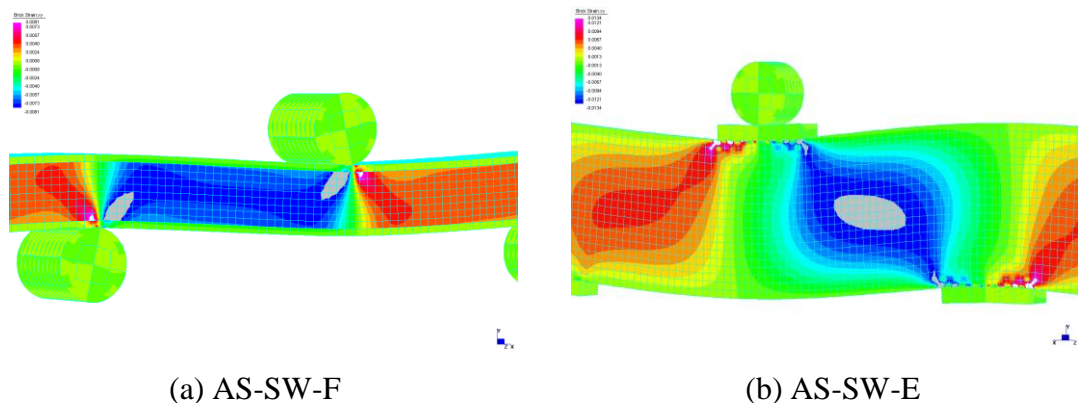
Figure 5.11 Predicted failure of sandwich specimens based on FEM

5.8 Conclusions

In this chapter, the shear behaviour of a sandwich structure made up of glass fibre composite skins and phenolic core was determined using asymmetrical beam shear test. The result of the experimental investigation showed that the shear behaviour of the composite sandwich structures loaded in-plane is significantly influenced by the skins while the behaviour of the sandwich structures when loaded in the transverse direction is governed by the core material. The presence of the vertical skins adds to the overall strength of the specimen tested in the edgewise position by preventing the widening of the crack in the core and delayed the shear failure until all the fibres crossing the cracked core failed. In this position, the skins carries almost 60% of the applied load compared in the flatwise position where the skin carries only 20%.

Based on the results of the study, the asymmetrical beam shear test is recommended as a test method for determining the shear properties of composite sandwich structures with high strength core material. This test method is effective in inducing shear failure in the composite sandwich structures and gives a good estimation of the shear strength. However, a much larger experimental study would be needed in order to establish the validity of this test procedure.

The theoretical prediction equations to estimate shear strength of the composite sandwich structures showed a good agreement with the experimental results. Using the shear moduli of the constituent materials and taking into account the observed failure mechanisms of the novel composite sandwich structures gives a good estimation of the shear strength. Similarly, the FEM simulations of the shear behaviour of composite sandwich structures showed a good agreement with the experimental results at the linear elastic region. The predicted shear strength and failure mechanisms of the composite sandwich structures are comparable with the actual results of the asymmetrical beam shear test.

The results of this investigation showed that significant improvement on the shear strength can be attained when the composite sandwich panels are positioned edgewise. The increase in strength with the introduction of the vertical skins suggests the high potential of its utilization as a shear loading component in a structural beam.

This chapter showed the high potential of the novel sandwich structure for glue-laminated beam. The behaviour of a number of these fibre composite sandwich structures bonded together to pave the way in the development of structural components from this composite material is investigated and discussed in Chapter 6.

Chapter 6

Behaviour of glue-laminated fibre composite sandwich beams

6.1 Introduction

The flexibility of composite sandwich construction allows novel structural developments from this material. Composite sandwich panels can be formed to carry loads that cannot be carried by individual sandwich structure. Composite sandwich structures can also be designed to a desired stiffness and strength with no additional weight to suit various structural applications. After evaluating the favourable characteristics of the individual sandwich structures in flexure and shear as detailed in Chapters 4 and 5 respectively, an innovative beam concept made completely from this sandwich structure has been developed to increase the use of sandwich construction in civil engineering applications. As these fibre composite sandwich panels are produced in limited thicknesses, a structural beam can be manufactured by gluing several sandwich panels together either in the flatwise or edgewise positions. This chapter presents the results of the experimental and numerical investigations into the behaviour of the glue-laminated composite sandwich beams.

The concept of gluing smaller structural elements to produce a single large, structural member to support a greater load has been used many years in the construction industry. In timber engineering, several layers of suitably selected smaller pieces of lumber are horizontally or vertically laminated (either by nailing or gluing) to produce structural glue-laminated timber (Boughton and Crews, 1998; Moody et al., 1999). Leichti et al. (1990) also suggested that bonding together lumber and plywood into beams provide a high degree of structural efficiency. Consequently, several bridge decks have been constructed by nailing together timber placed in the edgewise position (Johnson, 2002). In the field of composite materials, Lopez-Anido and Xu (2002) developed a structural system based on the concept of sandwich construction with strong and stiff fibre composite skins bonded to an inner glulam panel. The glulam panels were fabricated with bonded eastern hemlock laminations. Wagners CFT Manufacturing in Toowoomba, Australia has been

producing bridge girders, boardwalks and road bridges using adhesively bonded pultruded fibreglass sections (Kemp, 2008). The behaviour of several bridge girder profiles produced by longitudinally or transversely bonding fibre composite modular box members was studied by Kwak et al. (2009). Similarly, most currently available commercial fibre composite decks are constructed using assemblies of adhesively bonded pultruded shapes (Bakis et al., 2002). These studies show that the concept of gluing a number of composite sandwich panels to form a structural beam is highly practical. However, before this system can be used effectively for civil infrastructure, an investigation on the behaviour of this beam concept is necessary and a simple prediction equation of its failure behaviour should be established.

In the design of glue-laminated beams, the high-quality materials are typically provided at the outer laminations for higher strength and stiffness (Hernandez et al., 1997). Similarly, Rammer (1996) suggested that the strength of the glue-laminated beams is governed by the weakest lamination within the beam section. Failure of the glue-laminated beam can happen just after the strength of the weakest lamination is exceeded. During flexural loading, it has been demonstrated that most sandwich construction failed due to shear failure of the core material (Kampner and Grenestedt, 2007). The brittle nature of the core causes a sudden collapse of the sandwich structure and could become the limiting factor in designing such structures. In structural design of reinforced concrete, shear is accounted for by providing shear reinforcement such as stirrups in beams and dowels in slabs (Mirsayah and Banthia, 2002). In the context of fibre composite sandwich structures, there have been some attempts to increase the shear strength of composite sandwich construction. Although a number of these developments have lead to the improvements in shear behaviour of sandwich structures, these entail complex and costly process.

The overall objective of this study is to evaluate through experimental and analytical investigations the mechanical behaviour of glue-laminated fibre composite sandwich beams in bending and shear. The effects of the number and the orientation of sandwich laminations on the strength, stiffness and failure behaviour of glue-laminated composite sandwich beams are discussed. Simplified calculation method to describe the approximate behaviour and the governing failure mechanisms of the glue-laminated composite sandwich beams is also presented. Numerical analyses are also conducted to verify the experimental and analytical results.

6.2 Experimental program

The 4-point static bending and the asymmetrical beam shear tests of the glue-laminated composite sandwich beams are discussed in this section.

6.2.1 Test specimen and preparation

Figure 6.1 shows the preparation of the glue-laminated composite sandwich beams. A number of composite sandwich panels were assembled and glued together in 2, 3 and 4 layers using Techniglue-HP R5 structural epoxy resin supplied by ATL Composites. The glued sandwich panels were then clamped for 24 hours to initially cure the epoxy and were removed from clamping to post-cure at 90°C for 8 hours to attain good bonding between the sandwich laminations (Figure 6.1a). After curing, the glue-laminated sandwich panels were cut to the required specimen width (Figure 6.1b). The glued sandwich beams with 3 and 4 laminations were prepared with similar width and depth to eliminate the geometrical effects. The descriptions of the test specimens are listed in Table 6.1. In this table, the *B* and *D* represent the width and depth of the glued sandwich beam, respectively while the L_f and L_v denote the test spans in flexure and shear, respectively.

The last four configurations shown in Table 6.1 were prepared by wrapping the sandwich beam specimen with one layer of 750 g/m^2 tri-axial glass fibre composite (0/+45/-45). The fibre wraps were provided through hand lay-up process in two different stages covering the top and bottom surfaces with one layer of tri-axial glass fibres and the sides with 2 layers of fibres. Hyrex 201 epoxy resin (Rogers, 2004) was used to impregnate and bond the fibre wraps. The effect of glass fibre wraps on the strength and stiffness of glued sandwich beams are discussed in Appendix C.
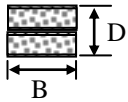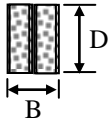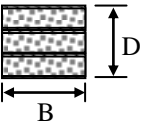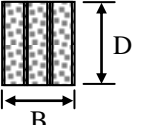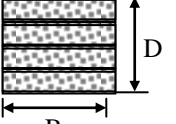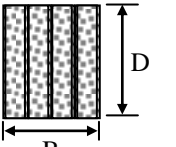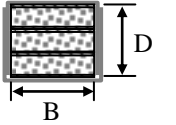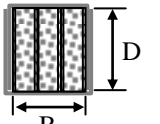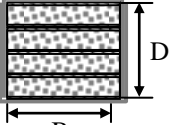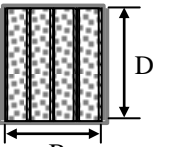
(a) Clamping of glued sandwich panels   (b) Cutting of sandwich beams

Figure 6.1 Preparation of glue-laminated composite sandwich beams

Table 6.1 Description of test specimens for glue-laminated sandwich beams

Specimen	Illustration	Number of specimens	D, mm	B, mm	L_f, mm	L_v, mm	Orientation of testing
2LSW-F		2	40	50	400	240	Flatwise
2LSW-E		2	50	40	400	240	Edgewise
3LSW-F		2	60	60	1200	240	Flatwise
3LSW-E		2	60	60	1200	240	Edgewise
4LSW-F		2	80	80	1200	240	Flatwise
4LSW-E		2	80	80	1200	240	Edgewise
3LSW-WF		1	60	60	1200	--	Flatwise
3LSW-WE		1	60	60	1200	--	Edgewise
4LSW-WF		1	80	80	1200	--	Flatwise
4LSW-WE		1	80	80	1200	--	Edgewise

6.2.2 Test set-up and procedure

Figure 6.2 illustrates the test set-up for flexural and shear tests of glue-laminated composite sandwich beams. The 4-point static bending test on composite sandwich beams (Figure 6.2a) was performed in accordance with the ASTM C393 (2000) standard while the shear test was performed using an asymmetrical beam shear (Figure 6.2b). Strain gauges were attached to the specimen in both tests to evaluate the strain during the entire loading regime. All of the specimens were tested up to failure to determine the strength and failure mechanisms. The applied load, displacement and strains were recorded and obtained using a data logger.

(a) Flexural test   (b) Asymmetrical beam shear test
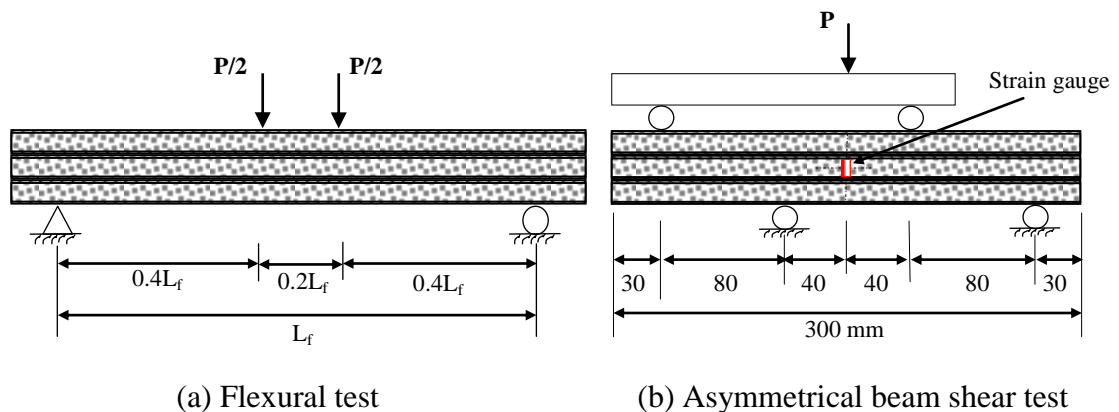
Figure 6.2 Test set-up for glue-laminated sandwich beams

6.3 Flexural behaviour of glue-laminated sandwich beams

The behaviour and failure mechanisms of the glue-laminated composite sandwich beams in flexure are reported in this section. The effects of the number and the orientation of composite sandwich laminations on the strength, stiffness and failure mechanisms of the glue-laminated sandwich beams are also discussed.

6.3.1 Experimental results and observation

6.3.1.1 Failure load

Table 6.2 summarises the failure load of the glue-laminated sandwich beams under 4-point static bending test. The experiment provided consistent results as a variation of less than 5% was recorded for the failure load of all the tested specimens. For beams with the same number of sandwich laminations, a higher failure load was observed in specimens tested in the edgewise position than in the flatwise position. This could be due to the different orientation of the fibre composite skins within the

specimen which affected the failure behaviour of the glued sandwich beams. For comparison, the failure load of the single sandwich structures is included in the list.

Table 6.2 Failure load of composite sandwich beams under flexural test

Specimen	Flatwise (N)		Edgewise (N)	
	Peak load	Std. deviation	Peak load	Std. deviation
1LSW	4554	52	5560	58
2LSW	9472	392	13772	67
3LSW	9318	194	11247	165
4LSW	20869	448	26086	399

6.3.1.2 Load-deflection behaviour of glued composite sandwich beams

The load and midspan deflection behaviour of glue-laminated composite sandwich beams under 4-point static bending is shown in Figures 6.3 and 6.4. In Figure 6.3, the behaviour of the individual composite sandwich beams is also included for comparison. The figure shows that the deflection of specimen 1LSW-F increased almost linearly with load up to final failure. The load of specimen 1LSW-E increased linearly with deflection but showed a reduction in stiffness when tensile cracking of the core occurred. The specimen then continued to carry the load but before the final failure, there was an increase in deflection of the beam even without an increase in the applied load due to progressive failure of the vertical skins. The load of specimen 2LSW-F increased linearly with deflection until a load of 6000 N and a deflection of 7 mm. After this load, a non-linear response was observed until failure. When the tensile cracks occurred in specimen 2LSW-E at an applied load of 11000 N, a slight drop in the load was observed. After compressive failure of the skins, the beams were still able to carry load but showed a large deflection until failure.

Similar load deflection behaviour was observed in specimens with 3 and 4 laminations (Figure 6.4). The load deflection curves for specimen 3LSW-F and 4LSW-F are almost linear until the development of flexural tensile cracks in the core material. A decrease in stiffness was then observed until failure of the specimen. A decrease in stiffness was also observed in specimen 3LSW-E and 4LSW-E when tensile cracks of the core developed. As the loading continues, there is a gradual decrease in the bending stiffness due to progressive failure of the fibre composite

skins. Specimen 3LSW-E and 4LSW-E continued to carry load even after compressive failure of the outer fibre composite skins. The specimen then behaved non-linearly with a reduced stiffness up to failure.

In both composite sandwich beams with 3 and 4 laminations, the specimens in the flatwise position behaved slightly stiffer than specimens in the edgewise position. However, the glue-laminated sandwich beams in the edgewise position failed at a higher load than the beams in the flatwise position. The load-deflection curve also indicated that the sandwich beams tested in the flatwise position failed in a brittle manner while the sandwich beams in the edgewise beams failed progressively.
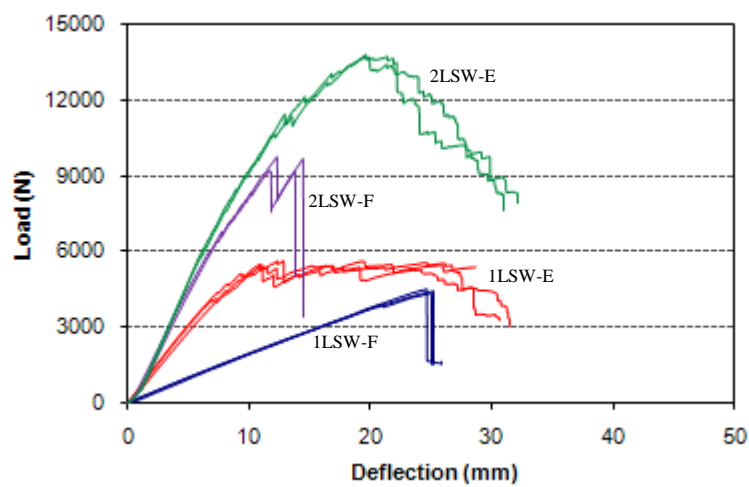
Figure 6.3 Load and midspan deflection relationship of specimen 1LSW and 2LSW
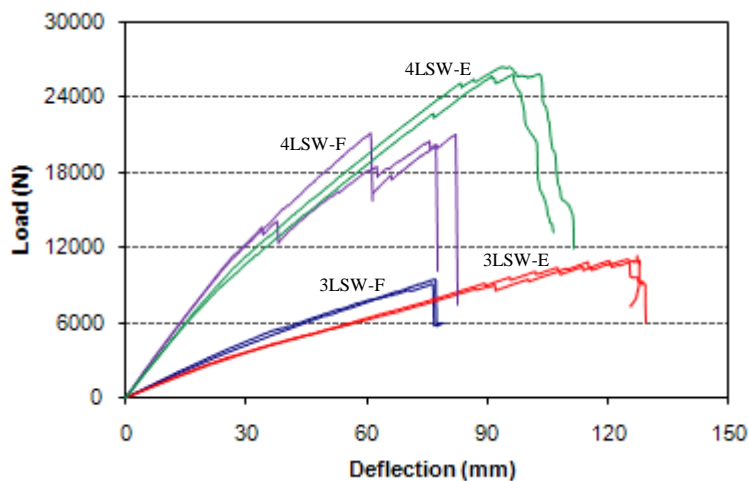
Figure 6.4 Load and midspan deflection relationship of specimen 3LSW and 4LSW

6.3.1.3 Failure behaviour of composite sandwich beams

Figure 6.5 shows the different failure modes of the glue-laminated sandwich beams are shown in Figure 6.5. Flexural tensile cracks of the core were observed at the bottom layers of specimen 2LSW-F but the skin on the tensile face of the beam bridged the cracked core together to prevent failure. The specimen 2LSW-F failed due to shear failure of the core with some skin wrinkling under one of the loading points followed immediately by debonding between the core and the skin as shown in Figure 6.5a. Tensile cracks of the core were also observed in specimen 2LSW-E. The presence of the vertical skins prevented the premature failure and made the sandwich beams to fail due to the progressive compressive failure of the skin followed by tensile failure of the skin as shown in Figure 6.5b.
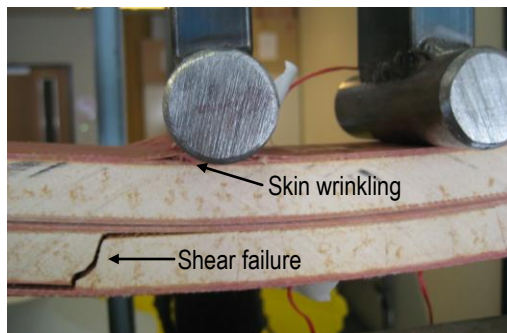
(a) Specimen 2LSW-F
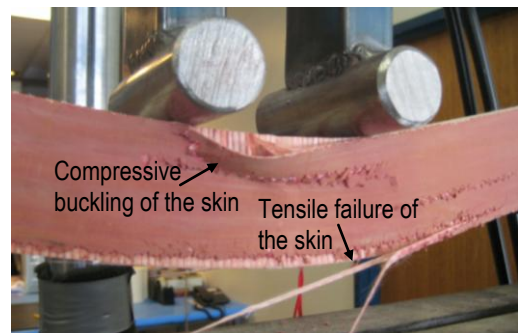
(b) Specimen 2LSW-E
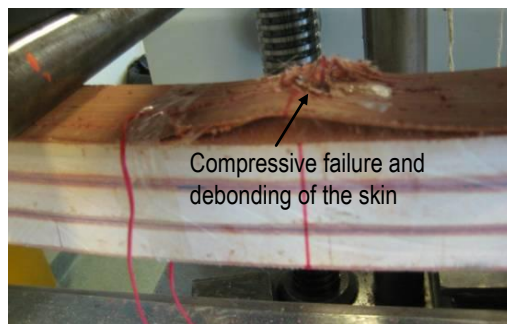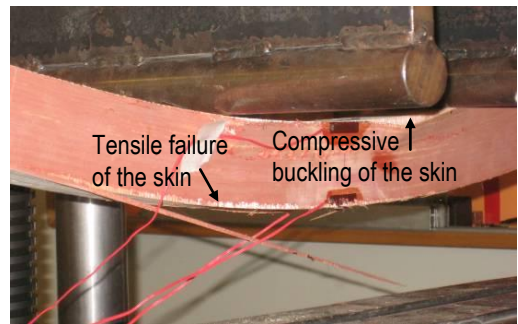
(c) Specimen 3LSW-F

(d) Specimen 3LSW-E
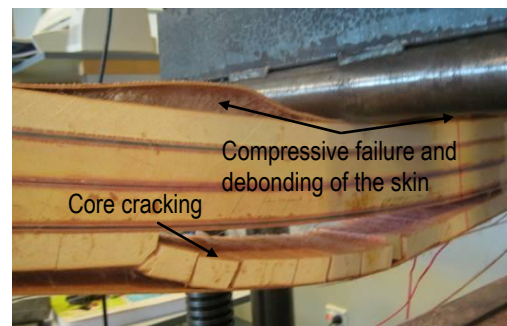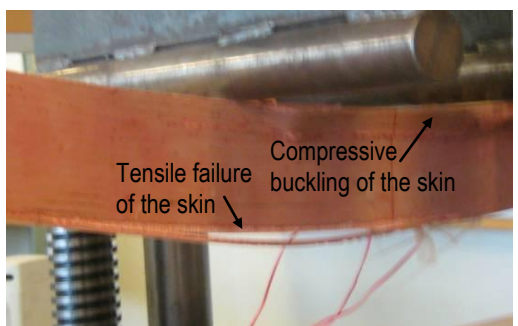
(e) Specimen 4LSW-F

(f) Specimen 4LSW-E

Figure 6.5 Failure of glue-laminated sandwich beams in flexure

Flexural cracks were observed on the core of the bottom most sandwich layers for flatwise specimens with 3 and 4 laminations. The cracks originated at the top of the tensile skin and progressed with the application of load. When the depth of the flexural cracks on the core reached the level of the next skin, the crack width increased and a significant drop in the load was observed. The presence of the skins however prevented the immediate extension of the cracking of the core to the core of the next sandwich laminations. With increasing load, flexural cracks also developed on the core of the upper sandwich laminations. The glued sandwich beams in the flatwise position failed due to the compressive buckling of the skins followed by the debonding between the bottom skin and the core as shown in Figures 6.5c and 6.5e.

Tensile cracks of the core were observed in the edgewise specimens at the early application of load. As more cracks developed on the core, the stiffness of the specimen decreased, and subsequently increasing the deflection. The continuous application of load caused the outermost compressive skins to delaminate from the core and cause the cracks to propagate horizontally at the region of constant moment. Splitting of the tensile fibre composite skins were then observed. This failure resulted to a decrease in lateral stability and eventually caused compression buckling of the detached skins. Final failure of the glued sandwich beams in the edgewise position was due to tensile failure of the skins followed immediately by simultaneous compressive failure of the skins and the crushing of the core (Figures 6.5d and 6.5f).

6.3.1.4 Displacement and longitudinal strain relationship

The displacement and longitudinal strain relationship of specimens 3LSW and 4LSW are shown in Figure 6.6. In this figure, the longitudinal tensile and compressive strains are designated with *(T)* and *(C)*, respectively. The results showed that the strains in both tension and compression increased linearly with displacement at the early stage of load application. However, a stiffer displacement-strain relation curve can be noted for specimen 3LSW-F than 3LSW-E but became almost similar for specimen 4LSW. In all the tested specimens, a higher longitudinal strain is measured in the tension than in compression. This further confirms that the fibre composite skins have a slightly lower modulus in tension than in compression as also observed in the test of coupons.

(a) Specimen 3LSW   (b) Specimen 4LSW
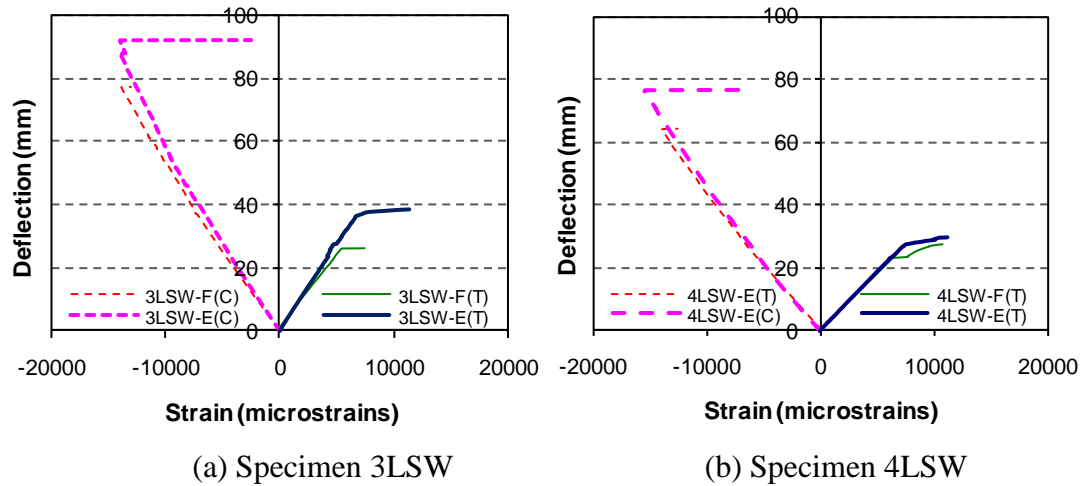
Figure 6.6 Displacement and strain relationship of specimens 3LSW and 4LSW

At a longitudinal tensile strain of around 6000 microstrains, the strain gauge at the tension side of the specimen broke, indicating the development of cracks in the core material. This level of strain is comparable with the failure strain of the phenolic core material in tension established from the test of coupons (see Table 3.4). Non-linearity in the longitudinal compressive strain was then observed indicating the further development of cracks in the core material. The strain gauge on top of the specimen broke at a compressive strain of around 12400 microstrains which indicated the compressive failure of the topmost fibre composite skins. The value of longitudinal strain represents the strain at which the fibre composite skins failed in compression as determined from the coupon tests. In this level of strain, the specimen tested in the flatwise position failed instantly while the specimen in the edgewise position continued to carry load and failed at a higher load than expected. Thus, the maximum level of strain at which the sandwich beam tested in the edgewise position failed was not captured by the strain gauges attached to the specimen. The final failure of the edgewise specimen occurred only when the core crushed in compression followed by buckling of the inner fibre composite skins. However, for all specimens, the complete load-deflection curve was recorded, allowing the measurement of the maximum applied load and deflection.

6.3.2 Effect of number of sandwich laminations on bending stiffness

The flexural stiffness, *EI* of the glue-laminated composite sandwich beams was calculated using the elastic properties of the fibre composite skin and the core material listed in Tables 3.3 and 3.4, respectively and the simple sandwich beam theory. The calculations were made assuming that no interlayer slips occurred and the laminated sandwich beams acted as a solid section with perfect bonding. This is reasonable as experimental investigations showed no debonding failure on the gluelines, hence full composite action is developed on the glue-laminated sandwich beams. The contribution of the epoxy adhesives on the flexural stiffness is also neglected. The flexural stiffness of the glued sandwich beams in the flatwise and in the edgewise positions was estimated using equations 6.1 and 6.2, respectively.

$$EI_{flat} = \sum_{i=1}^{n} \left[\left(\frac{Bt_s^3}{12} + Bt_s d_s^2 \right) E_s + \left(\frac{Bt_c^3}{12} + Bt_c d_c^2 \right) E_c \right] \qquad (6.1)$$

$$EI_{edge} = \frac{nD^3}{6} \left(t_s E_s + \frac{t_c}{2} E_c \right) \qquad (6.2)$$

where t_s and t_c are the thickness of the skin and core, respectively, d_s and d_c are the distances from the centre of the skins and the core to the neutral axis of the section, respectively, E_s and E_c are the moduli of elasticity of the skin and core, respectively, and *n* is the number of sandwich laminations in the glued sandwich beams.

Equation 6.3 was obtained based on the deflection formula of a uniform, static sandwich structures with loading configuration shown in Figure 6.2a using the classical beam theory. The effective bending stiffness, *(EI)eff* which considers the combined effect of bending and shear deformations was determined from the results of the experiment. Using the initial linear elastic portion of the load-midspan deflection curve (Figures 6.3 and 6.4), the *(EI)eff* was calculated using the relation:

$$(EI)_{eff} = \frac{59}{3,000} L^3 \left[\frac{\Delta P}{\Delta v} \right] \qquad (6.3)$$

where *(ΔP/Δv)* is the slope of the load-deflection curve. The apparent bending modulus of elasticity, E_{app} was then computed by dividing *(EI)eff* by the second moment of area of the homogenised cross-section of the glued sandwich beams. The predicted *EI*, calculated stiffness, E_{app}, maximum load, P_{max} and bending moment, M_{max} of the sandwich beams obtained from the experiment are reported in Table 6.3.

Table 6.3 Predicted *EI*, calculated stiffness, E_{app} and failure load

Specimen	*EI* ($x10^6$), Nmm^2	*EI$_{eff}$* ($x10^6$), Nmm^2	E_{app}, N/mm^2	P_{max}, N	M_{max}, N-m
1LSW-F	256	247	8073	4554	364
1LSW-E	844	819	3957	5589	447
2LSW-F	1287	1207	4188	9472	758
2LSW-E	1411	1373	3723	13788	1103
3LSW-F	4753	4851	4253	9318	2236
3LSW-E	4107	4270	3969	11247	2699
4LSW-F	13997	14811	4047	20869	5008
4LSW-E	12581	13196	3988	26086	6260

The results show that for individual composite sandwich beams in the flatwise position, shear deformation has no significant effect on the bending stiffness as the difference between the predicted and the calculated stiffness is only 3%. On the other hand, the *(EI)$_{eff}$* for the 2 sandwich beams bonded together is 3-7% lower than the predicted values. This suggests that shear deformation could have contributed to the total deformation of the sandwich beam in the edgewise position due to the decreased span to depth ratio. For longer beams with 3 and 4 laminations, the *(EI)$_{eff}$* is slightly higher than the predicted *EI*. The difference between the predicted and *(EI)$_{eff}$* is higher in specimens with 4 laminations as these beams have lower span to depth ratio than the specimens with 3 laminations. In general, both *EI* and *(EI)$_{eff}$* in the flatwise is higher than that in the edgewise position for specimens with 3 and 4 laminations.

Figure 6.7 shows the relationship between the apparent bending modulus of the glue-laminated composite sandwich beams and the number of laminations. The results showed that the E_{app} of the glue-laminated composite sandwich beams in the flatwise position decreases with increasing number of laminations. This decrease in E_{app} when the composite sandwich beams were glue laminated in the flatwise position is expected as the fibre composite skins near the neutral axis of the section did not contribute as much stiffness as the outermost skins. For both 3 and 4 laminations, the bending stiffness in the flatwise position is 7% higher than in the edgewise position. Moreover, the E_{app} of the individual composite sandwich beams in the edgewise position is almost equal to that of the glued composite sandwich beams. This clearly shows that the modulus of elasticity in the edgewise position is

not affected by the number of laminations as the shear stresses induced by the flexure are not carried across the glue lines. Most importantly, the results showed that the E_{app} of the composite sandwich beams in the flatwise and edgewise positions converges with increasing laminations. This information suggested that in the construction of beams with higher depth of the same width, it is better to glue together composite sandwich structures in the edgewise position as these beams will result to higher strength with the same stiffness but with fewer but longer gluelines.
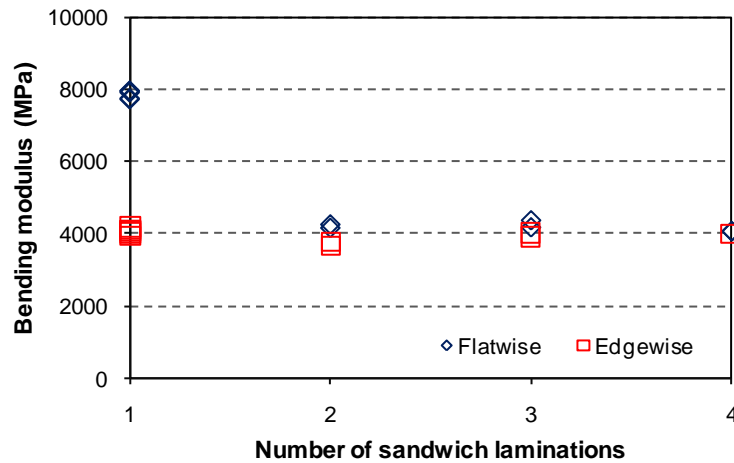
Figure 6.7 Apparent bending modulus of glue-laminated sandwich beams

6.3.3 Effect of number of sandwich laminations on bending strength

The relative performance of the glue-laminated composite sandwich beams tested in the flatwise and edgewise positions was determined by calculating the apparent bending strength based on the results of the experimental investigation. Similar assumptions that no interlayer slips occurred and the glue-laminated sandwich beams acted as a solid section with perfect bonding were made. The maximum bending strength on the outermost skin layer, $\sigma_{b,exp}$ was determined from the maximum load measured in the experiment, P_{max} and was calculated using equation 6.4.

$$\sigma_{b,\exp} = \frac{P_{\max} L_f D}{10(EI)_{eff}} E_s \qquad (6.4)$$

Figure 6.8 shows the maximum bending strength of the glued sandwich beams for the different number of laminations. The results of the analysis showed that for individual composite sandwich beams, the bending strength of specimens in the flatwise position is similar to that of the specimens in the edgewise position. In these

sandwich beams, the specimens failed due to compressive failure of the skins at a stress of around 200 MPa. It is noteworthy that this stress value represents the level at which the skins failed in compression as determined from the coupon test. In the glue-laminated sandwich beams tested in the flatwise position, there was no difference on the bending strength observed for the different number of laminations. Thus, it can be concluded that the bending strength of glue-laminated sandwich beam in the flatwise position is not affected by the presence of gluelines. This result further suggests that the bending strength of the glue-laminated sandwich beams in the flatwise position depends largely on the compressive properties of the skins.
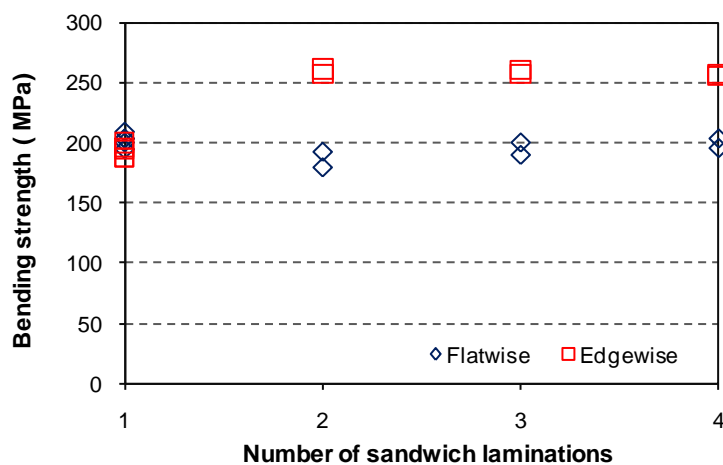
Figure 6.8 Bending strength of glue-laminated sandwich beams

Gluing the composite sandwich beams together in the edgewise position resulted to an increase of at least 25% in bending strength. The results also showed that the bending strength of sandwich beams in the edgewise position increases with increasing number of laminations. The bending strength of glue-laminated sandwich beam specimens is higher than individual laminations. In the edgewise position, the vertical skins prevented the widening of the tensile cracks in the core. The structural epoxy adhesives have also provided some reinforcing effects which increased the buckling resistance of the bonded vertical skins, delaying its failure thereby increasing its strength. This shows that the glue lines acted as a load-distributing element and hold the glued sandwich beams together. This load sharing mechanisms led to the increased performance of the glue-laminated composite sandwich beams in the edgewise position. Similar to engineered timber products, the strength-reducing characteristics of glue-laminated sandwich beams are dispersed within the sandwich

laminations and have much less of an effect on strength properties in contrast with the individual sandwich beams. Thus, relatively high strength properties were obtained for glue-laminated beams than for individual composite sandwich beams.

6.3.4 Effect of beam orientation on failure behaviour

Most of the glue-laminated sandwich beams tested in the flatwise position failed in a brittle manner due to compressive failure of the topmost fibre composite skin followed immediately by debonding between the skin and the core. The compressive failure of the skin caused a total collapse of the sandwich beams as the remaining materials are incapable of absorbing the released energy. This failure behaviour suggests that the flexural strength of the glued sandwich beams tested in the flatwise position depends largely on the compressive properties of the fibre composite skin.

In the edgewise position, the failure behaviour of the sandwich beams suggests that in this position the specimens will fail in a ductile manner due to progressive failure of the skin. Even after compressive failure of the skin at the outermost sandwich laminations, the beams continued to carry load until failure as the load was shed to the inner bonded sandwich laminations. The observed failure behaviour indicates that in multiple sandwich beams bonded together in the edgewise position, the defect in individual beams is compensated by the stronger, adjacent sandwich beams. This failure behaviour is significant as one of the most common concerns in designing fibre composite structures is its brittle failure behaviour. The staggering and progressive failure of the fibre composite sandwich beams when utilised in the edgewise position could provide early identification that the design load has been exceeded and an adequate warning of impending failure of the structure.

The results of the experimental investigation showed neither delamination nor slipping occurred on the glue lines for both the flatwise and the edgewise sandwich beams. This suggests that the structural epoxy adhesives used in this study has provided a highly efficient glue joint between the composite sandwich laminations and the full capacity of the glue-laminated composite sandwich beams was attained. This is expected as the bond strength provided by the Techniglue-HP R5 structural epoxy resin as determined by a lap shear test (Appendix D) is more than the shear strength of the core material. Thus, the glued sandwich beams will fail first by shear failure of the core material before any debonding failure occurs in the glue lines.

6.4. Shear behaviour of glue-laminated sandwich beams

The behaviour of the glued sandwich beams under asymmetrical beam shear test when loaded in the flatwise and edgewise positions are discussed in this section.

6.4.1 Experimental results and observations

6.4.1.1 Failure load

Table 6.4 summarises the load at first shear crack of the core and the maximum shear load carried by the glued sandwich beams. For specimens tested in the flatwise position, the load at first crack also corresponds to the maximum load as the beam failed immediately after the formation of the first shear crack in the core. As expected, the shear capacity of the glued beams increases with increasing number of laminations. The specimens with the same number of laminations and tested in the edgewise position failed at a higher load than in the flatwise position. Similarly, the load when the first shear crack in the core was observed in the edgewise specimen is significantly higher than the failure load recorded for the flatwise specimens.

Table 6.4 Failure load of sandwich beams under asymmetrical beam shear test

Specimen	Flatwise (N)		Edgewise (N)			
	Peak load	Std. deviation	Load at 1st crack	Std. deviation	Peak load	Std. deviation
AS-1LSW	10523	240	16568	350	17606	288
AS-2LSW	19717	212	33170	733	40347	2293
AS-3LSW	37446	362	57790	468	78350	1725
AS-4LSW	70622	1756	99328	346	138360	4682

6.4.1.2 Load and crosshead displacement behaviour

Figure 6.9 shows the load and the displacement of the crosshead during the entire test regime for the glue-laminated sandwich beams with 2, 3 and 4 sandwich laminations. As indicated in the figure, the failure in the beams is represented with a load drop in the load-crosshead displacement relation curve. For specimens with flatwise laminations, the load increased linearly with the displacement of the crosshead until final failure. A sudden load drop was observed which indicated the final failure of the beam. In the edgewise position, the load increased linearly with the crosshead displacement until the first load drop was observed. This load drop is due to the

initiation of shear cracks in the core. After which, a non-linear load and crosshead displacement relation was observed due to the progressive shear failure of the skins. After the maximum load is reached, a decrease in the capacity of the specimen AS-2LSW was observed with increasing displacement of the crosshead. For specimens AS-3LSW and AS-4LSW, a plateau was observed when the maximum load is reached followed by an immediate drop in the load indicating the final failure.
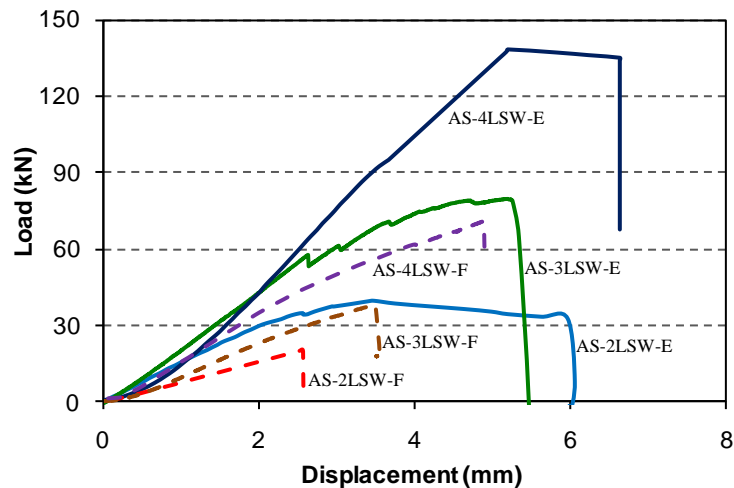
Figure 6.9 Load and crosshead displacement relation of sandwich beams

6.4.1.3 Load-strain behaviour

Figure 6.10 shows the applied load and the indicated normal strains of the $\pm 45^o$ strain gauges attached to the glued sandwich beams tested under asymmetrical beam shear. Figures 6.10a, 6.10c and 6.10e show that the recorded $\pm 45^o$ strains on the specimens tested in the flatwise position increased linearly with the applied load up to failure. In the edgewise position, gluing the sandwich beams together resulted to an almost linear load and strain behaviour up to the initial shear cracking of the core. A non-linearity on the load-strain curve and a decrease in stiffness were then observed after this load up to failure. For specimens with 2 and 3 laminations, the glue-laminated sandwich beams continued to carry load even after the initial shear failure of the skins was observed (Figures 6.10b and 6.10d). The failure in shear of the outermost skins (where the strain gage is attached) also resulted to a decrease in shear strain recorded in the specimens. For sandwich beams with 4 laminations, a decreasing load was recorded when the shear failure of the outermost skins occurred (Figure 6.10f). This shows that for glued sandwich beams with higher laminations, the specimens will immediately fail when shear failure of the skins is observed. Unlike

in single sandwich beams where the strain gauges captured the non-linear behaviour up to failure, the failure of the outermost skins of the glued beams resulted to the immediate failure of the strain gauges, thus the failure strain was not measured.

(a) Specimen AS-2LSW-F

(b) Specimen AS-2LSW-E

(c) Specimen AS-3LSW-F

(d) Specimen AS-3LSW-E

(e) Specimen AS-4LSW-F

(f) Specimen AS-4LSW-E
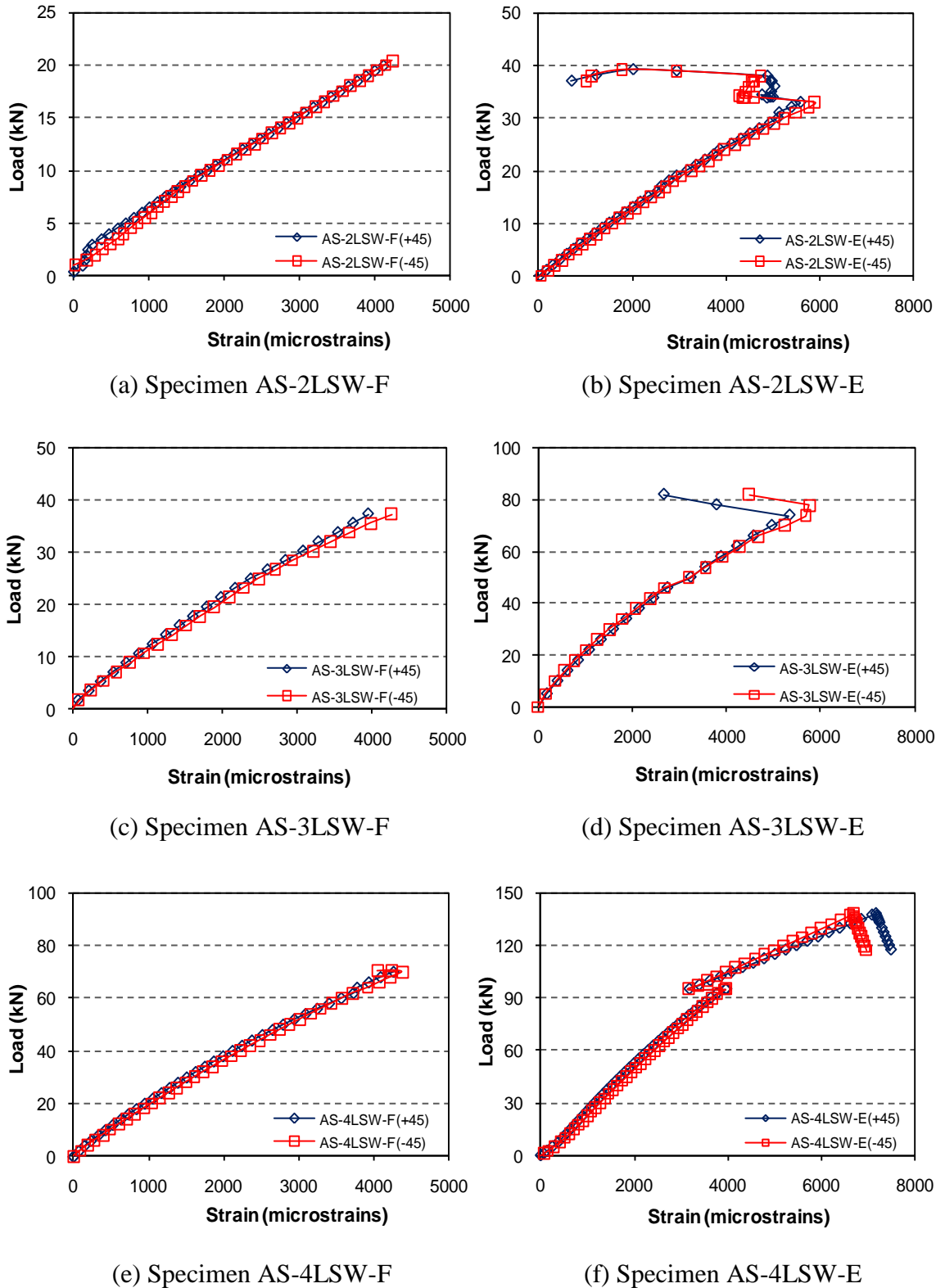
Figure 6.10 Load and $\pm45^{o}$ strain relationship of glued sandwich beams

6.4.1.4 Failure behaviour

Figure 6.11 shows the failure behaviour of the glue-laminated composite sandwich beams under asymmetrical beam shear test. The experimental results show that the glued sandwich beams in the flatwise position failed after the formation of the first shear crack in the core at the location of the maximum shear (Figures 6.11a and 6.11c). This failure is brittle and sudden which is accompanied by a loud noise.

The initial failure of the glued sandwich beams in the edgewise position is the shear cracking of the core as indicated by the load drop in the load and crosshead displacement relation curve. The vertical skins however inhibit the further development of shear cracks in the core. The specimens then continued to carry the load before shear cracking of the skin was observed. With increasing load, the shear failure became more evident due to the scaling of the resin at the outermost skins (Figures 6.11b and 6.11d). This failure behaviour showed a more progressive failure than the beams in the flatwise position. However, compared to individual sandwich structures, the glued sandwich beams exhibited a more brittle failure behaviour with increasing laminations. This could be due to the joining effect of the adhesives which strengthen the bonded skins together thereby increasing its shear stiffness.
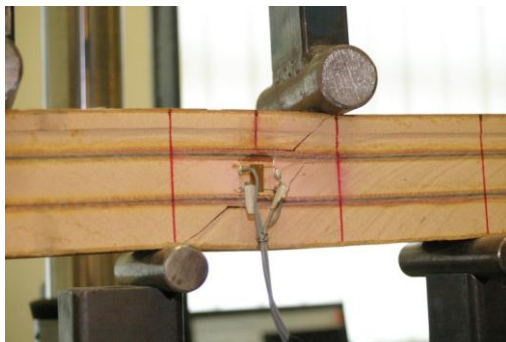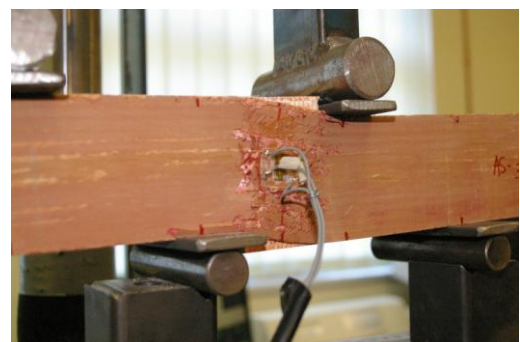
(a) Specimen AS-3LSW-F	(b) Specimen AS-3LSW-E
(c) Specimen AS-4LSW-F	(d) Specimen AS-4LSW-E
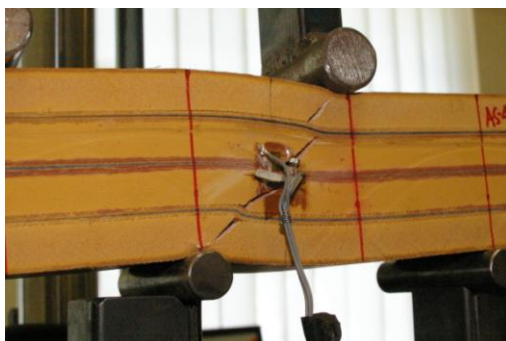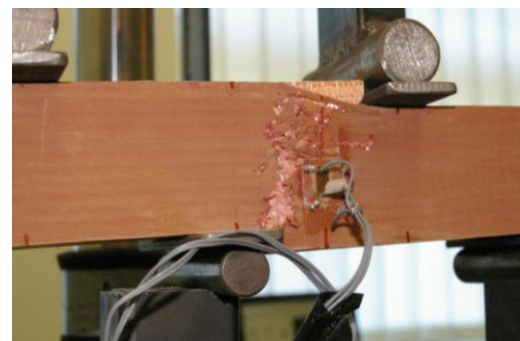
Figure 6.11 Failure of glue-laminated sandwich beams in shear

6.4.2 Effect of number and orientation of sandwich laminations on shear strength

The apparent shear strength of the glue-laminated sandwich beams was determined by dividing the shear force on the maximum shear region with the area of the homogenised beam section assuming an elastic response. Assumption that the glue-laminated beams acted as a solid section with perfect bonding was also made. Figure 6.12 shows the shear strength of the glue-laminated beams with different number of sandwich laminations. The results indicate a slightly higher variation in shear strength in the sandwich beam specimens tested in the edgewise position than in the flatwise position. The larger difference in the shear strength of sandwich beams tested in the edgewise position is due to the complex shear behaviour of the fibre composite skin while the shear behaviour of the core material is more predictable.
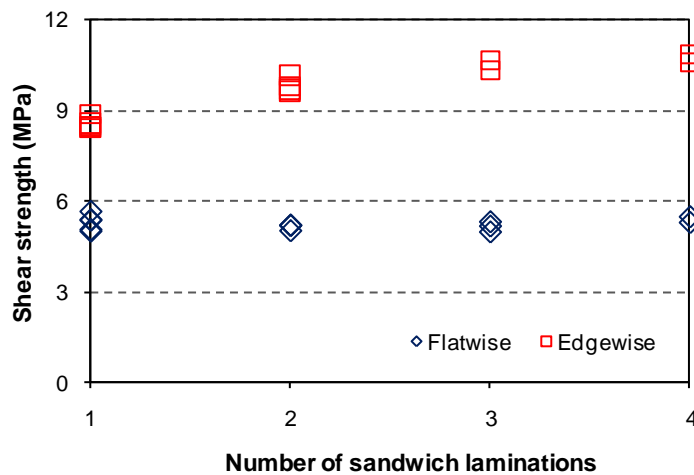
Figure 6.12 Shear strength of glue-laminated sandwich beams

The number of sandwich laminations has no significant effect on the shear strength of the glued sandwich beams in the flatwise position. In this position, the shear strength of glued beams is almost constant or slightly decreases with increasing sandwich laminations. The calculated shear strength of the beams in the flatwise position is between 4.8 and 5.5 MPa. This shear strength is comparable to the shear strength of the phenolic core material suggesting that the shear strength of the glue-laminated beams in the flatwise position is governed by the shear strength of the core material regardless of how many laminations are there in a beam section. The slightly higher shear strength of the sandwich beams at failure compared to the shear strength of the phenolic core material as determined by the coupon test could be due to the contribution of the mid-layer fibre composite skins in carrying the shear.

In the edgewise position, increasing the number of sandwich laminations resulted in an increasing shear strength for the glue-laminated beams. This can be attributed to the presence of structural epoxy which bonded together the skins and acted as a load distributing element to the individual sandwich beams. This resulted in a thicker and a more stable skin section due to the laminate restraining effect which increased its shear stiffness and strength. Test results showed that the shear strength of sandwich beams in the edgewise position increased by at least 20% when glued together compared to a single sandwich beam. The edgewise specimen has a shear strength of almost 9 MPa for single sandwich beam but increased to around 11 MPa when sandwich beams were bonded together. The shear strength of the glue-laminated sandwich beams in the edgewise position is almost double than that of the sandwich beams in the flatwise position with higher sandwich laminations.

The higher shear strength of the glued sandwich beams in the edgewise position is due to the presence of the vertical skins which impeded the propagation and growth of shear cracks of the core. Furthermore, the increase in the failure strength of the glued sandwich beams in the edgewise position can be attributed to the presence of structural epoxy which increased the shear stiffness of the skins due to the laminate restraining effect. Thus, an improvement in the shear behaviour can be made by orienting the composite sandwich beams in the edgewise position.

6.4.3 Effect of sandwich beam orientation on failure behaviour

The failure of the glue-laminated sandwich beams tested in the flatwise and in the edgewise positions occurred along the intended shear plane. As expected, shear failure of flatwise specimens was sudden and catastrophic. In this position, the glued sandwich beams failed due to shear failure of the core. The sandwich beam lost its capacity to carry load instantly without any residual load-carrying capacity beyond the peak load, which was observed in the edgewise specimens. The results showed that the glued sandwich beams tested in the edgewise position failed progressively as indicated by the load-displacement and load-strain relation curves. The applied load increased steadily until an initial shear crack in the core developed and a slight reduction in load was observed. The presence of vertical skins impeded the shear cracking propagation and growth in the core to cause failure. On continued loading, this load reduction was recovered and exceeded. Subsequently, additional load drops caused by progressive shear failure of the remaining skins occurred until final failure.

6.4.4 Effect of shear span- to-depth ratio (a/D) on shear strength

The limitation of the test fixture to set the shear span lesser than 80 mm for sandwich beams with lower depth resulted in a varying shear span-to-depth ratio (*a/D*) for the tested specimens. It is well established that the failure mode of rectangular reinforced concrete beams without shear reinforcement is strongly dependent on the *a/D* (ACI-ASCE 426, 1973). For a concrete beam with *a/D* ≥ 6, failure usually occurs in bending but for *a/D* < 6, the beam usually fails in shear (Ng and Soudki, 2010). Due to the relatively low elastic modulus of fibre composites, concrete members reinforced with fibre composite materials experience reduced shear strength compared to the shear strength of those reinforced with the same amount of steel reinforcements (ACI 440R, 2007). El-Sayed et al. (2006) found that a concrete beam reinforced with fibre composites and with *a/D* < 6.5 usually fails in shear. In composite sandwich structure, Dai and Thomas Hahn (2003) indicated that shorter sandwich beams exhibited higher shear strength than beams with longer span. Similarly, Yamane et al. (2000) and Yoshihara and Furushima (2003) pointed out that the shear strength of structural timber tends to increase by decreasing *a/D*. They suggested that the maximum shear stress of timber can be evaluated when the short beam test of the asymmetric four-point loading method is conducted for *a/D* ratio near the range of 4. In this study, the *a/D* ratio of not more than 4 was examined.

The shear strength of the composite sandwich beams with different *a/D* ratios is shown in Figure 6.13. The *a/D* ratio of beams in the flatwise position ranges from 1 to 4 while the *a/D* ratio of beams in the edgewise position ranges only from 1 to 1.7. In all the *a/D* ratios, the composite sandwich beams failed in shear at the region of maximum shear. As indicated in the figure, there is no significant difference in the shear strength of sandwich beams tested in the flatwise position regardless of the *a/D* ratio. This can be explained by the brittle behaviour of the core wherein the shear failure occurred after the formation of the first shear crack. On the other hand, the shear strength of composite sandwich beams in the edgewise position trends to decrease as the *a/D* ratio increases. Noticeably, the glued sandwich beams with 2 laminations has relatively higher shear strength than individual sandwich beams even though they have the same *a/D* ratio. This could be due to the wider section of the glued composite sandwich beams. In general, the shear strength of the sandwich beams in the edgewise position is significantly higher than the sandwich beams in the flatwise position for the same *a/D* ratio. This result again showed that a more stable

and stronger section can be attained by gluing the composite sandwich beams in the edgewise position. Furthermore, the results indicated that for *a/D* ratio of 1 to 4, the shear strength of the composite sandwich beams can be stably obtained.
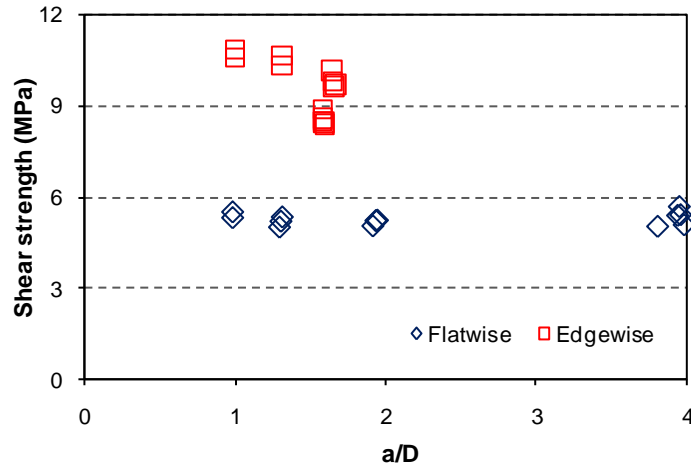
Figure 6.13 Shear strength of sandwich beams with different a/D ratio

6.5 Evaluation of glue-laminated composite sandwich beam behaviour

Theoretical evaluation of the flexural behaviour of the glue-laminated composite sandwich beams was conducted. The shear equations presented in Chapter 5 were extended to calculate the shear strength of the glued sandwich beams. Numerical simulations were also performed to verify the analytical and experimental results.

6.5.1 Fibre Model Analysis

The behaviour of glue-laminated fibre composite sandwich beams in flexure was predicted using a simple Fibre Model Analysis (FMA) presented in Chapter 4. In the analysis of the flexural behaviour of glued sandwich beams, the contribution of the core and the skin in both flexural and shear stiffness were considered. The constitute model for the phenolic core material in Figure 4.10b is used in the FMA while a modified constitutive models for the fibre composite skins for sandwich beams tested in the edgewise position is illustrated in Figure 6.14. In the estimation of the failure load, the maximum stress and strain of the skins and the core listed in Tables 3.3 and 3.4 are used. For sandwich beams tested in the flatwise position, the specimen will fail when the compressive strength of the topmost fibre composite skin is reached. For glue-laminated composite sandwich beams tested in the edgewise position, the failure of the inner (and bonded) fibre composite skin in compression occurs only

when the core material started to behave non-linearly in compression (at a strain of around 16000 microstrains) though the outermost skins failed at a level of maximum strain (12400 microstrains) established from the test of coupons. This assumption seems to more adequately represent the mechanical behaviour of glued sandwich beams in the edgewise position which was verified in the experimental investigation.
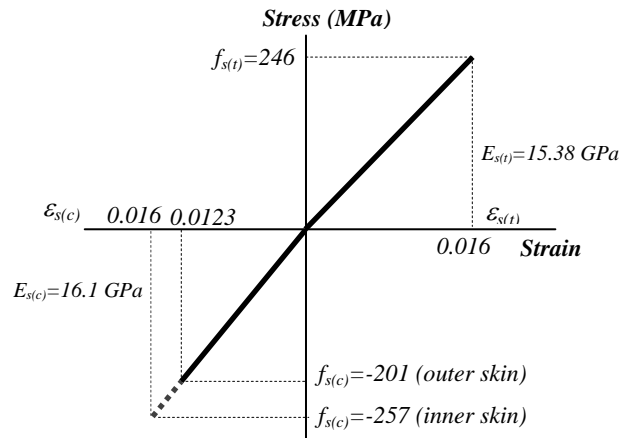
Figure 6.14 Modified constitutive models for bi-axial glass fibre composite skin

An analysis method to allow the cracking of the core material, commonly used in reinforced concrete (RC) analysis was incorporated in the FMA as cracking of the core material has some influence on the overall stiffness and performance of the glue-laminated composite sandwich beams. In the analysis of the flexural behaviour using FMA, cracking of the core will occur when the limiting strain in tension determined from the coupon test is reached. This approach infers that a crack initiates first at the bottom of the sandwich beam specimen. Once the crack in the core has formed, the bottom fibre composite skin becomes the principal tensile load-carrying element at that location. As with RC beams, analysis can be simplified by disregarding any tensile contribution of the cracked core material to the strength and stiffness of the beam. By ignoring the cracked core material, the neutral axis shifts up the beam section, and the overall stiffness of the beam is reduced. From the point where cracking of the core occurs until failure, the uncracked section stiffness of the glue-laminated sandwich beam changed to the cracked section stiffness. Using these assumptions, the mid-span load-deflection response of glue-laminated sandwich beams was calculated and compared to the experimental and numerical results.

6.5.2 Approach to estimate shear strength

The failure mode of all the glue-laminated sandwich beams tested in the flatwise position was a shear failure in the core while the beams in the edgewise position was a shear failure of the vertical skins. These failure behaviours are similar to the observed failure mode of individual sandwich structures as presented in the Chapter 5. Thus, the shear resistance of the glued sandwich beams was estimated using the theoretical prediction equations in Section 5.5.6. The shear capacity of the glued beams in the flatwise, P_{F_G} and in the edgewise position, P_{E_G} are estimated using equations 6.6 and 6.7, respectively. The failure load in the flatwise beams is calculated based on the maximum shear strength of the core while the failure in the edgewise beams is assumed when the shear strength of the skins is reached.

$$P_{F\_G} = n\tau_c \left(t_c + 2t_s \frac{G_s}{G_c} \right) B \qquad (6.6)$$

$$P_{E\_G} = n\tau_s \left(t_c \frac{G_c}{G_s} + 2t_s \right) D \qquad (6.7)$$

6.5.3 Finite element modelling and verification of sandwich beam behaviour

Finite element (FE) analyses were performed to determine the responses of the glue-laminated composite sandwich beams in flexure and in shear. The actual geometry of the model is created with the nominal dimensions of the composite sandwich beams using Hexa20 brick elements to replicate the actual geometry of the specimens. The details of the FE model to simulate the behaviour of the glue-laminated beams in the flatwise and edgewise positions in flexure and shear is presented in Appendix E.

The numerical simulation of the behaviour under static bending and asymmetrical beam shear tests of the glued sandwich beams was conducted using the nonlinear and linear static solvers, respectively using Strand7 finite element software in the FCD-XPP-034 computer (CPU-Intel P4). After each analysis, the failure load, midspan deflection, bending stress-strain relationship, and shear stress-strain response of the glued sandwich beams were determined.

6.6 Predicted results and comparison with experiments

The results of the analytical prediction and numerical simulations on the behaviour of glue-laminated composite sandwich beams and the comparison with the results of the experimental investigation are discussed in this section.

6.6.1 Predicted behaviour in flexure

6.6.1.1 Failure load and mechanisms

Table 6.5 summarises the predicted load at first crack of the core and failure load of the glue-laminated sandwich beams based on FMA and FEM simulations and the actual loads at first core crack and at failure based on experimental investigations.

Table 6.5 Actual and predicted failure load of glued sandwich beams in flexure

Specimen	Load at first core crack (N)			Failure load (N)		
	Actual	FMA	FEM	Actual	FMA	FEM
2LSW-F	4387	4833	4800	9472	10915	9200
2LSW-E	4782	4539	4500	13772	12712	13200
3LSW-F	4188	4027	4100	9318	8940	9200
3LSW-E	3553	3424	3500	11247	10525	10600
4LSW-F	9186	8967	9100	20869	19710	19800
4LSW-E	8869	8242	8200	26086	24208	24400

Using the maximum strain of 6000 microstrains when the core cracks in tension, the FMA and the FEM simulations were successful in the prediction of the load at first crack of the composite sandwich beams tested in flatwise and in edgewise positions. The difference between the predicted and the actual load is only 3 to 10%. The slightly higher load measured at the first cracking of the core compared to the results of the analysis could be associated with the physical constraints of the experiment or could be due to the variation of the composite sandwich beam dimensions. In terms of ultimate load at failure, the predicted failure load of the specimen tested in the flatwise position is almost equal to that of the actual failure load. The predicted failure load due to the compressive failure of the skin (at a maximum strain of 12400 microstrains at the topmost skin) is nearly equal to that of the actual failure load, except for specimen 2LSW-F which failed due to the combined effect of flexure and shear. However, this failure load due to combined

flexure and shear was reasonably predicted in the FEM simulation. In general, the difference between the predicted and the actual load for glue-laminated sandwich beams in the flatwise position is only 4-5%. On the other hand, the predicted failure load of the glued sandwich beams tested in the edgewise position using the modified constitutive behaviour of the bonded fibre composite skin is almost 8% lower than the actual. The higher actual load than the predicted values could be due to the gluing of the sandwich beams together which resulted to a more stable and stronger section. In general, the results of the FMA and FEM analyses gave a conservative but reasonable value for the failure load of the glued composite sandwich beams.

6.6.1.2 Load-deflection behaviour

The comparison of the experimental and analytical load-deflection behaviour of the glue-laminated composite sandwich beams are shown in Figures 6.15a to 6.15f. In these figures, the predicted load-deflection behaviour of glue-laminated sandwich beam using FMA and FEM simulations and the results of the experimental investigation are designated with FMA, FEM and Expt, respectively. The figures show that the predicted load-deflection relation based on a simple FMA and FEM simulations is in good agreement with the experimental results especially before cracking in the core material. In all the specimens tested, the load increases with deflection until cracks in the core at a strain of around 6000 microstrains developed. A decrease in stiffness was observed after this load which was represented by a small kink in the load-deflection relation curve.

A slight disparity between the predicted load-deflection behaviour and the result of the experimental results was observed after cracking of the core. This difference in the load-deflection behaviour after cracking of the core could be due to the initiation of delamination between the skin and the core which further reduces the stiffness of the beam. This complex behaviour could not be predicted using the proposed simplified analysis and even with the FEM simulations. Nonetheless, the difference in the predicted and experimental results is only 4% for beams tested in the flatwise position but can go as high as 8% for the beams in the edgewise position. The reason for this could be due to the behaviour of the vertical fibre composite skin as it is subjected both to flexural and shear deformation. Similarly, the fibre composite skins are subjected both to tension and compression unlike in the flatwise position wherein the skins is subjected only to either compressive or tensile forces.
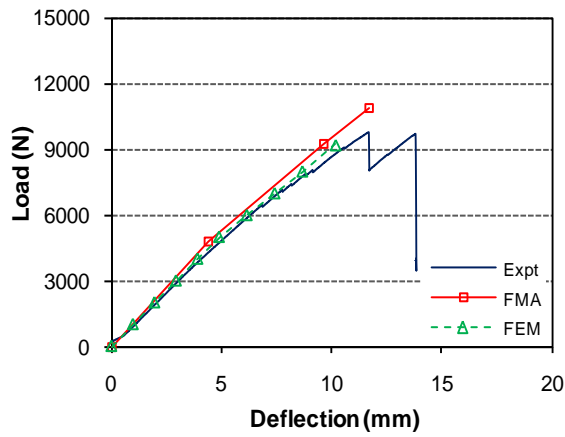
(a) Specimen 2LSW-F
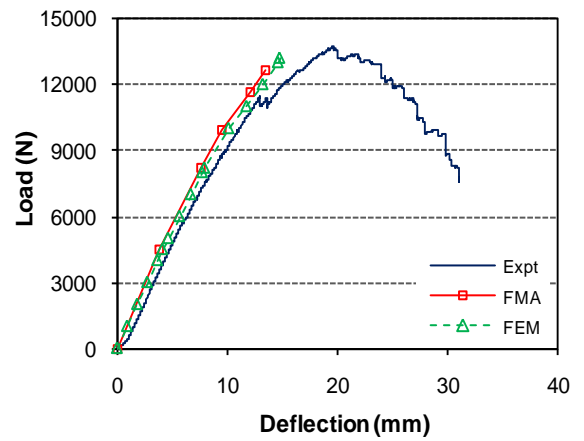
(b) Specimen 2LSW-E
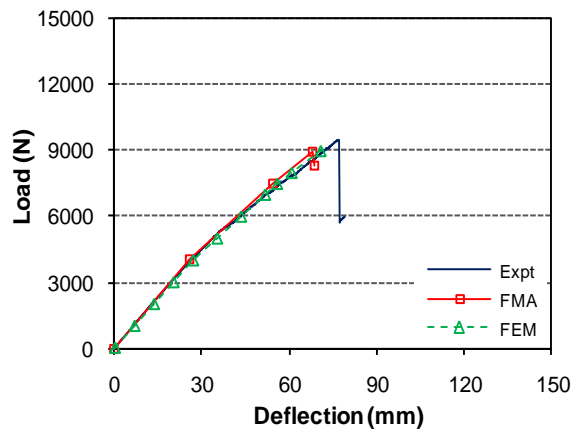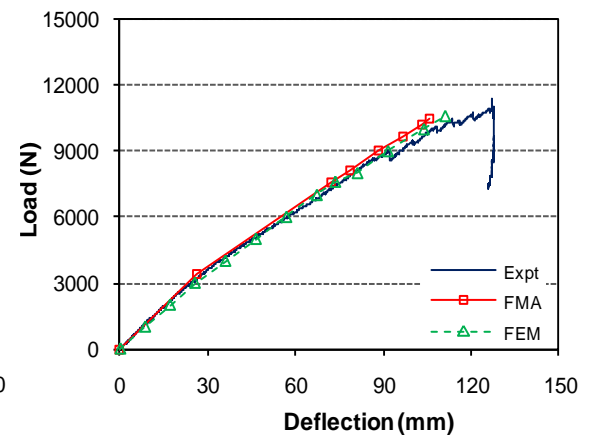
(c) Specimen 3LSW-F

(d) Specimen 3LSW-E
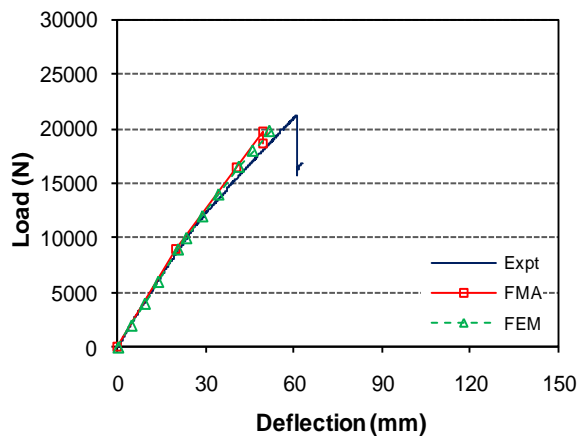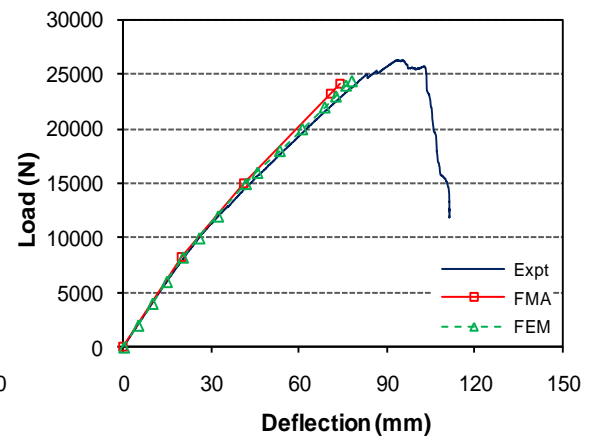
(e) Specimen 4LSW-F

(f) Specimen 4LSW-E

Figure 6.15 Load and midspan displacement relationship of glue-laminated beams

6.6.1.3 Load and longitudinal strain relationship

The comparison of the predicted load and longitudinal strain relationship determined using FMA and the experimental result is shown in Figures 6.16 and 6.17. In these figures, the experimental and the FMA load-strain relation are designated by Expt and FMA, respectively while the longitudinal tensile strain is designated with (T) and the longitudinal compressive strain with (C). The experimental results showed an almost linear load-strain relationship and a good agreement with the predicted load-strain relationship based on FMA. The results verified that the strains in both tension and compression increased linearly with load at the early stage of load application. The result also verified that longitudinal strain at the top of the composite sandwiches matches the strain at the bottom. This showed that there is no debonding between the skins and the core and the assumption of compatibility of strains throughout the depth of the composite sandwich section, and the equilibrium of internal force resultants are valid. In general, the results showed that a simplified FMA can reasonably predict the load-strain behaviour of composite sandwich beams. The difference in the FMA and experimental results is less than 5%. The small discrepancy observed could be attributed to the variations in the dimensions of the glue-laminated composite sandwich beam specimens.
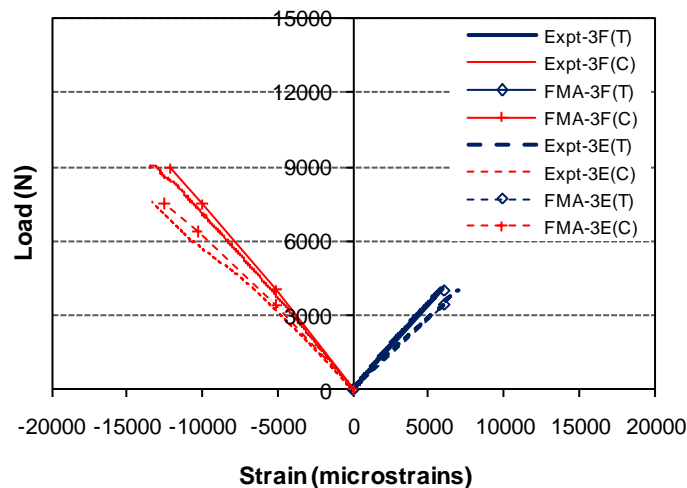
Figure 6.16 Load and longitudinal strain relationship of specimen 3LSW
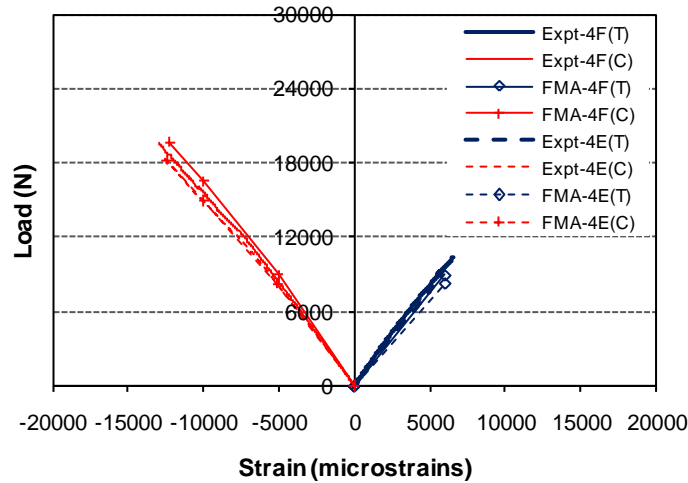
Figure 6.17 Load and longitudinal strain relationship of specimen 4LSW

6.6.1.4 Failure behaviour

Figures 6.18a to 6.18f shows the predicted failure behaviour of glued sandwich beam under 4-point static bending test. Using the maximum strains where the skin and the core material will fail, the FEM analysis was successful in the prediction of the failure mechanisms of the glue-laminated composite sandwich beams. Based on the FEM model, the sandwich beams tested in the edgewise position will fail due to compressive failure of the topmost skins at the region of maximum bending moment except for specimen 2LSW-F where shear failure of the core occur under the loading point at a load of 9000 N. On the other hand, the glue-laminated composite sandwich beams failed due to simultaneous compressive and tensile failure of the inner and bonded fibre composite skin at any point between the loading rollers. In all of the specimens, the failure mechanisms predicted from the FEM simulations are similar to the failure mechanisms observed in the experimental investigation.

(a) Specimen 2LSW-F   (b) Specimen 2LSW-E

(c) Specimen 3LSW-F

(d) Specimen 3LSW-E

(e) Specimen 4LSW-F
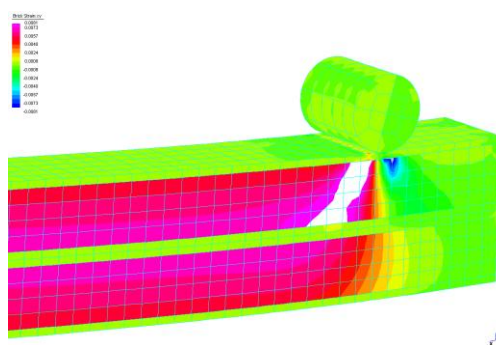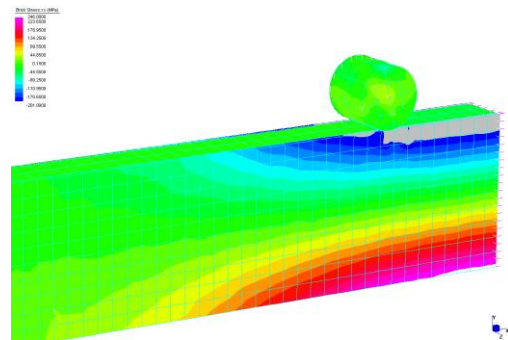
(f) Specimen 4LSW-E
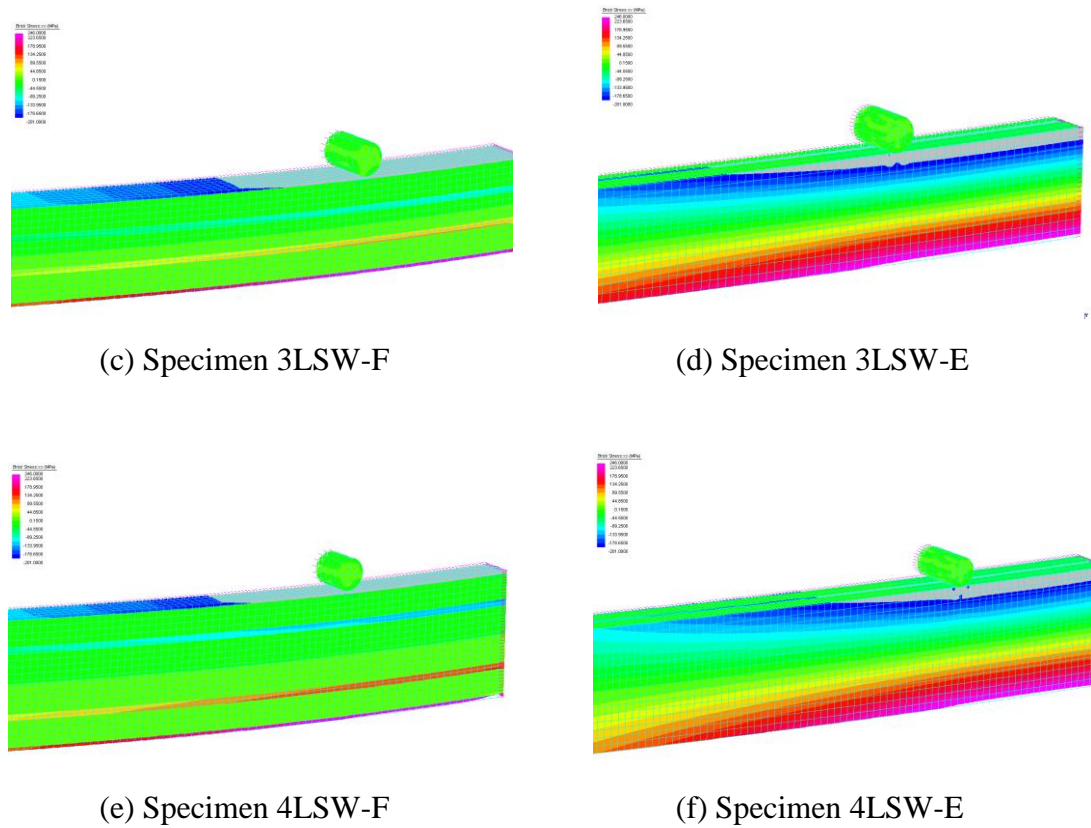
Figure 6.18 Predicted failure behaviour in flexure of glued sandwich beams

6.6.2 Predicted behaviour in shear

6.6.2.1 Failure load

Table 6.6 summarises the actual failure load based on the experimental investigations and the predicted failure load in shear of the glue-laminated composite sandwich beams using equations 6.6 and 6.7 and based on the FEM simulations.

Table 6.6 Actual and predicted failure load of glue-laminated beams in shear

Specimen	Failure load (N)		
	Actual	Predicted	FEM
AS-2LSW-F	19717	22816	23000
AS-3LSW-F	37446	41502	42000
AS-4LSW-F	70622	75260	75000
AS-2LSW-E	40347	31404	31500
AS-3LSW-E	78350	59165	61000
AS-4LSW-E	138360	103866	105000

In the flatwise position, the predicted failure load gives only 6-14% higher than the actual failure load. This suggest that the shear strength of the beams tested in the flatwise position can be reasonably predicted considering the shear strength of the core. In the edgewise position, the predicted failure load gives a 7% lower load than the actual for individual laminations but an almost 25% lower load than the actual failure load for glued sandwich beams. However, this predicted load is comparable to the load when the first shear crack on the core was observed (Table 6.4). A closer predicted failure load to the actual can be obtained using equation 6.7 if the 20% increase in shear strength of the glued sandwich beams in the edgewise position observed in the experimental investigation would be accounted in the theoretical prediction. This suggests that the shear strength of the glued beams in the edgewise position could be predicted accurately when the strength of the skin is considered.

Using the maximum shear stress of the skin and the core, the FEM simulations was successful in the estimation of the failure load of the glue-laminated composite sandwich beams under asymmetrical beam shear test. Also, the failure load determined from the numerical simulation is almost the same with the predicted failure load using equations 6.6 and 6.7 for glued composite sandwich beams in the flatwise and the edgewise positions, respectively.

6.6.2.2 Shear stress-strain behaviour

The shear stress-strain relationship of the glue-laminated sandwich beams tested in the flatwise and in the edgewise positions are shown in Figures 6.19 and 6.20, respectively. The results showed that the predicted shear stress and strain relationship using the FEM analysis showed a good agreement with the experiment. As illustrated in Figure 6.19, the glue-laminated sandwich beam tested in the flatwise positions failed at a shear strain of around 8000 microstrains. This strain level is similar to the failure strain where the phenolic core material fails in shear. The glue-laminated sandwich beam failed at shear strength slightly higher than that of the core material due to the contribution of the fibre composite skin. In the edgewise position, gluing the sandwich beams together resulted to an almost linear shear stress-strain behaviour until failure (Figure 6.20). In comparison to the experimental results, the sandwich beams in the edgewise position failed at a slightly lower level of shear strength and strains. This could be due to the reinforcing effect of the epoxy adhesive to the bonded vertical skins which was not accounted in the FEM simulations.
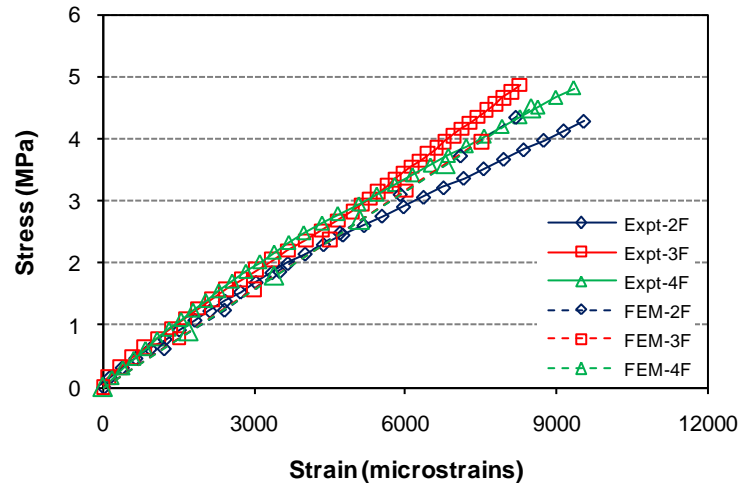
Figure 6.19 Shear stress and strain relationship of flatwise beams
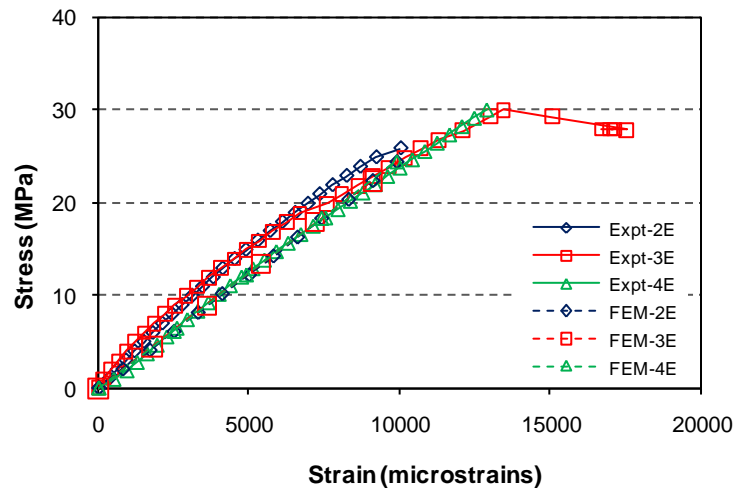
Figure 6.20 Shear stress and strain relationship of edgewise beams

6.6.2.3 Failure behaviour

Figures 6.21a to 6.21f shows the failure behaviour of glued sandwich beams under asymmetrical beam shear test based on the FEM simulation. The predicted failure mechanisms using the FEM showed good agreement with the failure behaviour observed in the experiment. In all of the specimens tested, the shear failure of the glued sandwich beams occurred in the region of maximum shear. In the flatwise position, the glue-laminated beams failed due to shear failure of the core on the topmost and the bottom most sandwich laminations which progressed to the core of the inner laminations with the continuous application of load. In comparison with the actual failure behaviour, the shear failure of the core for glued sandwich beams in the flatwise position occurred simultaneously in all sandwich laminations after the appearance of the first shear crack and not progressively. This could be due to the

large energy released when shear failure of the core material occurred which caused the total collapse of the sandwich beam. This complex failure behaviour in shear of the glue-laminated sandwich beams in the flatwise position could not be modelled in Strand7 but the load when a shear failure occurs can be predicted reasonably.

In edgewise glued sandwich beams, the predicted failure mode is shear failure of the skins. In the FEM simulation, the maximum shear stress and strain of the core is exceeded at a load comparable to the applied load when the first shear crack of the core was observed experimentally. However, this was not considered as the failure load of the beam in the edgewise position. The final failure of the glue-laminated sandwich beam in the edgewise position is due to shear failure of the vertical skin.

(a) Specimen 2LSW-F (b) Specimen 2LSW-E

(c) Specimen 3LSW-F (d) Specimen 3LSW-E

(e) Specimen 4LSW-F (f) Specimen 4LSW-E
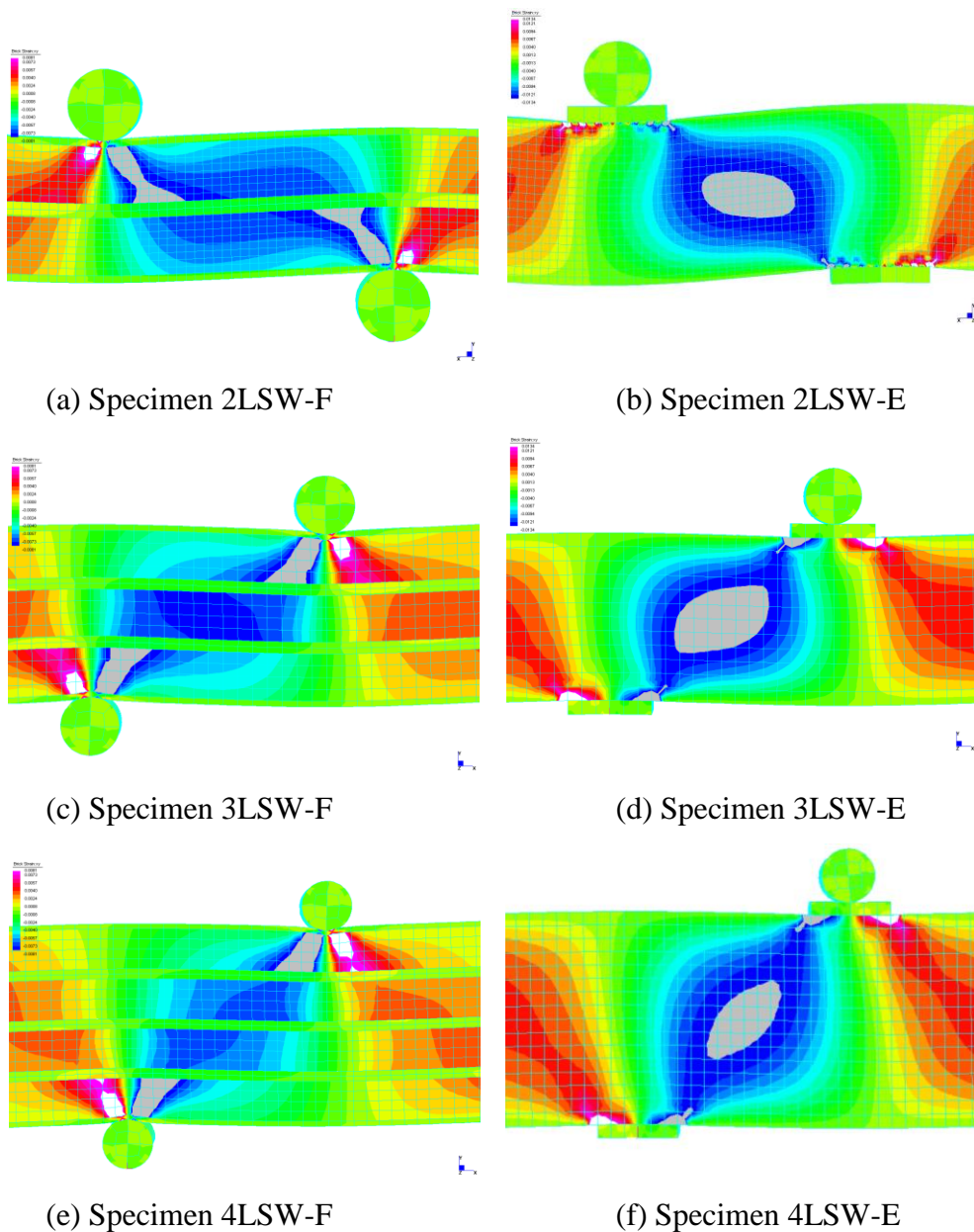
Figure 6.21 Predicted failure behaviour in shear of glued sandwich beams

6.7 Conclusions

The behaviour of glue-laminated composite sandwich beams in the flatwise and the edgewise positions was determined through experimental, analytical and numerical investigations with a view of using this material for structural applications. The results showed that gluing the composite sandwich beams together resulted in a stronger and more stable section than individual sandwich beams alone.

The flexural behaviour of the glue-laminated sandwich beams in the flatwise position is governed by the compressive properties of the skin. In this position, there was no increase in the bending strength and a decrease in stiffness was observed with increasing number of sandwich laminations. The flatwise sandwich beams failed by the compressive failure of the skin followed by the debonding between the skin and the core, thus resulting to brittle failure. Using the same amount of material, the glue-laminated sandwich beams in the edgewise position could offer up to 25% increase in flexural strength compared to beams in flatwise position but with a slightly lower bending stiffness. The presence of vertical skins in the edgewise position increases the bending strength and resulted to a more progressive failure behaviour. The final failure of the beams in the edgewise position is due to simultaneous compressive failure of the inner skins, crushing of the core and tensile failure of the skins. Furthermore, the overall effect of one-layer of tri-axial glass fibre wraps on the flexural behaviour of the glue-laminated sandwich beams cannot be justified with the additional cost of fibres and preparation. Even with fibre wraps, the failure initiation of the glued sandwich beams is almost the same as that for specimens without wraps.

The number of sandwich laminations has no significant effect on the shear strength of the glue-laminated sandwich beams tested in the flatwise position. In this position, the shear strength is almost constant regardless of how many laminations are there in a beam section as the failure is governed by the shear strength of the core. In the edgewise position, the glue-laminated sandwich beams achieved over 200% shear strength than beams in the flatwise position. The higher shear strength of the glue-laminated sandwich beams in the edgewise position can be attributed to the vertical skins which also resulted in a progressive failure of the beams.

Theoretical prediction and numerical simulations of the flexural behaviour of the glue-laminated composite sandwich beams considering the constitutive behaviour of skin and core and the behaviour of the individual sandwich structures were found to be in good agreement with the experimental results. At the same time, the

prediction equation for shear strength gives reasonable results on the failure load of glue-laminated sandwich beam in the flatwise position but gives a lower predicted load than the actual in the edgewise position. A closer predicted load to the actual failure load can be obtained if the percentage increase in shear strength in gluing the composite sandwich beam in the edgewise position would be accounted for.

The results of the study point towards the high feasibility of using glue-laminated sandwich construction for structural beam in the civil engineering infrastructure. A case study on the suitability of this composite sandwich beam for a replacement timber turnout railway sleeper is discussed in Chapters 7 and 8.

Chapter 7

Analysis of a typical turnout sleeper system for critical design parameters

7.1 Introduction

A comprehensive literature review in Chapter 2 suggested that the advantages of hardwood timber can be simulated using fibre composite materials with the added advantages. The extensive investigation on the behaviour of a novel composite sandwich panel and glue-laminated sandwich beams in Chapters 3 to 6 suggests that these materials have the strength and stiffness for structural applications. This chapter explores the practical application of this composite sandwich structure in replacement timber turnout sleeper. In this specific application, fibre composites could be a more competitive material as it has been increasingly difficult to get larger, longer and good quality hardwood timber for turnout sleepers. As the design of structures using fibre composites has been driven by the stiffness requirement rather than strength (Gangarao et al., 2007), a parametric investigation was conducted to ascertain the optimum stiffness of fibre composite sleeper suitable for turnout application. Such an investigation is very important to arrive at the best possible sleeper that will satisfy both strength and serviceability requirements.

There is currently no widely recognised standard on composite sleepers and the standard for existing sleeper materials is being used to design the fibre composite railway sleepers (Lampo et al., 2003). In a railway turnout, sleepers have a particular loading condition due to the track irregularities and the changes in train speed. Accordingly, a higher load is carried by turnout sleepers than the mainline sleepers which complicate its design and analysis. These forces are expected to be more detrimental when using sandwich structures for railway sleepers as it causes shear cracking through the core (Galletti et al., 2008). In actual conditions, Kaewunruen and Remennikov (2009) found out that the railway sleeper failed in either shear-flexure failure modes or only in shear failure type under a train loading. Similarly, the AS 1085.14 (2003) suggested that the design of railway sleepers should be based on the flexural requirements and shall provide adequate shear resistance. It is

Behaviour of fibre composite sandwich structures: *A case study on railway sleeper application*

important therefore to understand more intensely how the turnout sleepers respond to these forces to efficiently design a fibre composite sleeper alternative.

Several researchers have analysed the railway track as a beam on an elastic foundation and their results showed a very good agreement between the theoretical and experimental results (Hetenyi, 1976). Kohoutek (1991) analysed the railway sleeper as a longitudinal beam resting on an elastic foundation which is loaded by a pair of equivalent static load representing the train. In such a model, the contribution of the rail and the adjacent sleepers is represented by a distribution factor which is applied to the wheel load to determine the equivalent static load (Jeffs and Tew, 1991). This distribution factor is based on the type of rail gauge and the spacing of the sleepers. A 2-D beam model which further accounts for variation of subgrade within the length of an individual sleeper was developed by Kohoutek and Campbell (1989). This model, which statically analyses the sleeper on elastic foundation, has the possibility to investigate different lengths, different ballast moduli or different parts of the sleepers with different sectional properties. The investigation conducted by Shahin (2008) concluded that a 3-dimensional finite element analysis rather than 2-dimensional simulation is a more accurate method to investigate the behaviour of ballasted railway foundation, but the higher number of elements using this method greatly increased the computational effort.

Shokreih and Rahmat (2007) investigated the effects of Young's modulus on the response of sleepers as there are many materials being used for railway sleepers. In their work, sleepers were modelled as beams on elastic foundation with constant foundation modulus. The results showed that when the modulus of the beam is higher than that of the foundation, changing Young's modulus of the beam has little effects on the response of the sleepers. Similarly, Shahu et al. (1999) indicated that sleeper support modulus can change dramatically with track construction and this variation can have greater influence on the behaviour of railway sleepers. Further investigation conducted by Ticoalu (2008) showed that using higher support modulus will create smaller rail seat bending moment on the turnout sleepers. These studies have shown that the analysis of beams on elastic foundation has been employed extensively and has been found to be appropriate for analysing railway structures. The results of these studies have also indicated that the bending rigidity of the sleeper and the support modulus directly influence the behaviour of railway sleepers. However, the finite element analyses of the abovementioned studies are implemented

AC Manalo

using only a single sleeper. The presence of at least two sets of continuous rails which connects the sleepers makes the inclusion of the entire turnout essential in the analysis. For this reason, the behaviour of turnout sleepers should be determined for a group of sleepers instead of a single sleeper, as the contribution of the neighbouring sleepers should be taken into account due to the joining effects of the rails.

In this study, a simple and rational structural model which considers the rail, sleeper, ballast, and subgrade in a railway turnout system is developed. The model also considers the effect of the adjacent sleepers on the behaviour of turnout sleepers through the rails secured to the sleepers. Subsequently, the response of the sleepers due to wheel load of a train passing in a railway turnout is investigated. The influence of changes in the support and in the elastic moduli on the performance of fibre composite sleepers were analysed in detail. Furthermore, the effect on the behaviour of timber turnout sleepers when one of the railway sleepers is replaced with a fibre composite sleeper to simulate the spot replacement maintenance strategy is investigated. The result of this parametric investigation could lead to an optimised section for an alternative fibre composite sleeper in a railway turnout.

7.2 Theoretical model for railway turnout

A railway turnout consists of a number of sleepers and rails acting together. Thus, the AS 1085.14 (2003) suggests that the turnout sleepers can be analysed by a more complex grillage model. However, there has been no reported study on the use of such a model to analyse a railway turnout in literature. The commonly available literature on grillage system is in the analysis of slabs, foundations and complex bridge structures. Tan et al. (1998) introduced the grillage analysis method for vehicle-bridge interactions to study the dynamic effects of a moving vehicle on bridge structures. The bridge structure is modelled as a grillage assembly consisting of several longitudinal girder members and transverse beam elements. The results of their analyses showed that the grillage beam simulation represented the response of the whole bridge structure under moving loads with satisfactory accuracy. In another study, Eamon and Nowak (2004) combined the grillage model of the bridge deck with solid elements to analyse the resisting effect of the secondary elements such as diaphragms, barriers and sidewalks on the load carrying capacity of the bridge structural system. The ultimate capacity predictions based on the simplified grillage model were found to be within 3-6% of the more detailed finite element models but

with significantly reduced solution time. Furthermore, Fujikubo (2005) used a sandwich-grillage model to analyse the hydroelastic response of very large floating structures. In his model, the top and bottom deck plates of floating structures are modelled by rectangular membrane elements, while the bulkheads are modelled by beam elements. The results of his analyses showed that his model is effective for the stress analysis of detailed structures or for the progressive collapse analysis of global structures. More recently, Al-Saidy et al. (2008) investigated the effect of damaged steel girder on the overall behaviour of short span composite bridge system using the grillage method of analysis. The results of their analyses showed that the grillage model using STAAD III structural analysis software provided very comparable results with a more accurate three-dimensional finite element analysis.

The abovementioned studies showed that the grillage beam system has been used extensively by several researchers to analyse complex structures because of its simplicity. A similar model was developed in this study using Strand7 finite element software package (Strand7, 2005) to investigate the effect of various parameters on the behaviour of railway turnout sleepers. The railway turnout track is modelled as a grillage beam system consisting of simple beams and beams on an elastic foundation.

7.3 Railway turnout geometry

A standard 1 in 16 right-hand turnout geometry consistent with the existing Australian railway using 60 kg/m rail is investigated. Similarly, a narrow gauge (1067 mm) rail line commonly used in Queensland, Australia is considered (RTSA, 2008). Distance between rail centres is taken as 1137 mm and the spacing of sleepers is 600 mm on centres. Sleeper dimensions were set at 230 mm x 150 mm in consideration of the replacement of deteriorating turnout timber sleepers (ARTC, 2007b). The typical range of sleeper support modulus, U_s is taken as approximately 10 to 40 MPa (Jeffs and Tew, 1991; Tew, 1991; AS 1085.14, 2003). Various types of empirical expressions that have been developed for the calculation of dynamic load factor were presented in Jeffs and Tew (1991). In this study, a combined vertical design load factor, j (including quasi-static and dynamic) as large as 2.5 is used as recommended by AS1085.14 (2003) to account for the dynamic affects of travel speed combined with track and wheel irregularities. Such factor could come from, for example, wheel flats or other defects on the wheel tread, rail joints, and switch crossing (frog) passages. The recommendation from the Australian Standards

AS2758.7 (1996) for the maximum contact pressure at the sleeper-ballast interface for high-quality, abrasion resistant ballast of 750 kPa was adopted. Table 7.1 details the components of the track structure and Figure 7.1 shows the schematic diagram for a turnout sleeper. After consulting with railway industry partners, a loading configuration shown in Figure 7.2 was adopted. In this figure, R_1 represents the rail seat load at the middle wheel set while R_2 corresponds to the front and the rear wheel sets. This loading pattern simulates an axle load of 25 tonnes for a typical heavy axle load common in most Australian railway lines. These 3 sets of wheel load are moved though the turnout tracks to determine the location of the most critical sleepers.

Table 7.1 Details of the components of the track structure

Component	Description
Rail section	60 kg/m
Rail gage (G)	1067 mm
Distance between rail centres (g)	1137 mm
Sleeper spacing	600 mm
Axle load	25 tonnes
Combined vertical load factor (j)	2.5
Modulus of elasticity of sleepers ($E_{sleeper}$)	1 – 10 GPa
Sleeper support modulus (U_s)	10 - 40 MPa
Allowable ballast pressure	750 kPa
Stiffness of rails	200 GPa
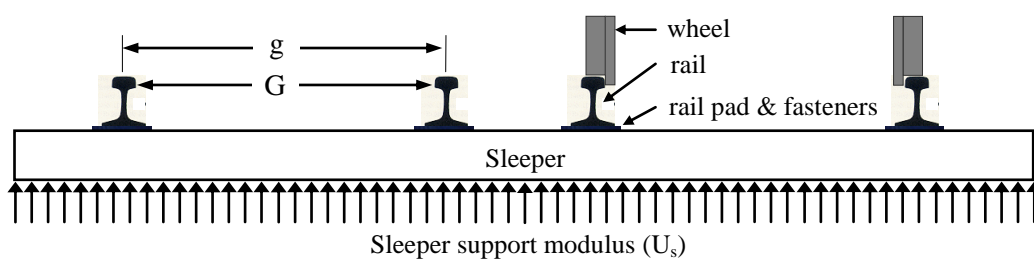
Figure 7.1 Schematic diagram of railway turnout sleeper
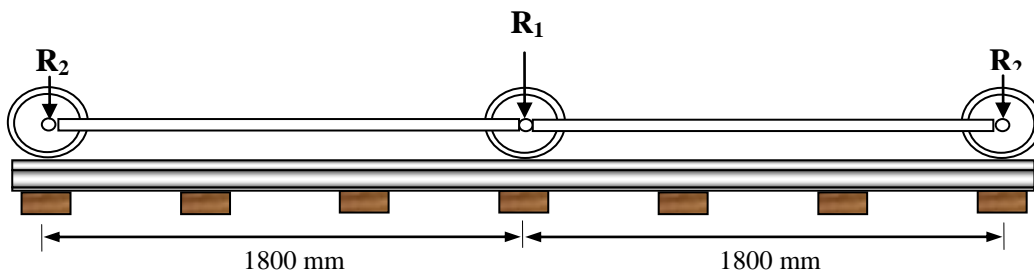
Figure 7.2 Axle load configuration

7.4 Finite element model of the railway turnout

A simplified three dimensional grillage model consisting of longitudinal and transverse beam elements has been developed to analyse the behaviour of railway turnout structure. The model consists of the rails, sleeper plates, sleepers, ballast, and subgrade. The finite element (FE) model considers the rails as long beams continuously supported by equally spaced sleepers. The model consists of a total of 107 sleepers including 10 transition sleepers before the switch and after the longest sleeper in the turnout as shown in Figure 7.3. The transition sleepers are provided to ensure that the wheel load is sufficiently distributed over several sleepers when the train enters and leaves the turnout. Sadeghi (2001) suggested that the effects of wheel loads are negligible for sleepers located more than 5 m or 10 sleepers away from the load points, i.e. sleeper number 1 has almost zero bending moment, shear and deflection when the wheel load is directly over sleeper number 11. The sleepers are laid perpendicular to the through tracks with increasing lengths from the switch until two standard length sleepers could be placed under the through and divergent tracks. The overall length of the modelled track is 61.8 m with sleeper lengths varying from 2.30 m to 4.1 m and the sleeper ends having lengths of 0.58 m.

Strand7 finite element program (2005) is used to model the railway turnout system. The rails and the sleepers are modelled as a grillage beam system with the sleepers resting on an elastic foundation (Figure 7.4). The guard and check rails are omitted to further simplify the modelling procedure. The turnout model is assumed to be in a flat terrain and the effect of irregularities on the track and wheels and the dynamic effects are assumed to be represented by the dynamic load factor. The beams are subdivided into reasonable number of elements to achieve a better accuracy of the results but still within reasonable analysis time. A total of 1339 Beam2 elements and 1046 nodes were used in the turnout model. The model uses one beam element for the rail per sleeper bay and (n_r+1) beam elements for the sleeper, where n_r is the number of rails supported by the sleepers. As the exact cross-section of the 60 kg/m rail (AS 1085.1, 2002) cannot be defined in Strand7 using only 2D beam element, an approximate steel I-section with an almost equivalent moment and torsional inertia shown in Figure 7.5 was used for the rail. Table 7.2 lists the section properties of the 60 kg/m steel rail. The assigned cross-section to the switch blades is similar to that of the standard rails. The sleepers were considered as isotropic beams with a homogenous cross section.
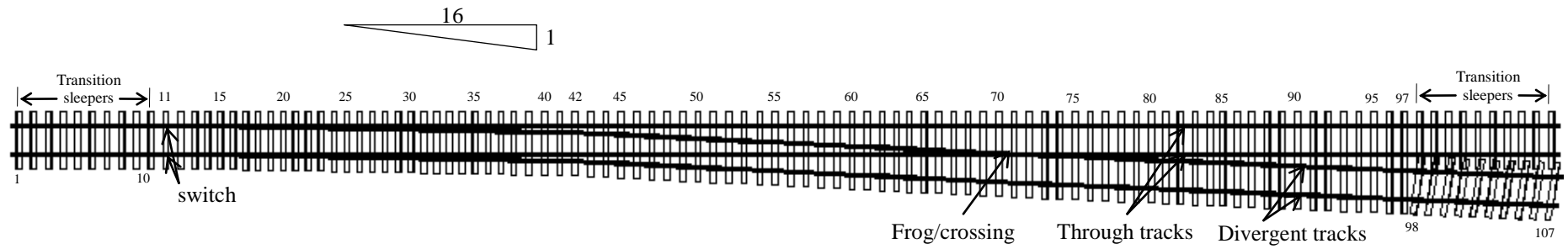
Figure 7.3 Geometry of a 1:16 standard right-hand railway turnout
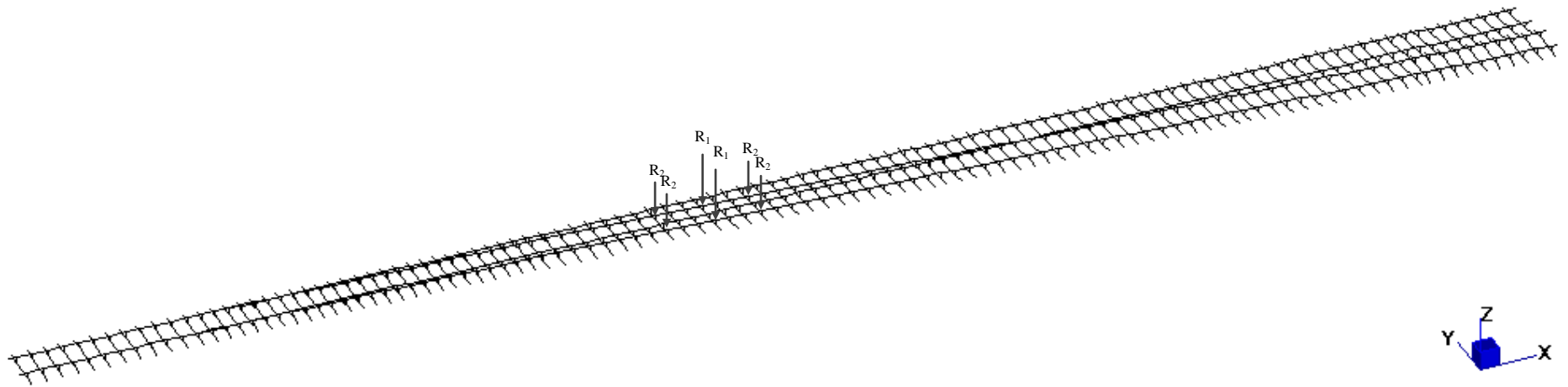
Figure 7.4 The grillage beam model for 1:16 standard right-hand railway turnout

<div align="center">(a)Exact (AS 1085.1, 2003)   (b) Approximate</div>
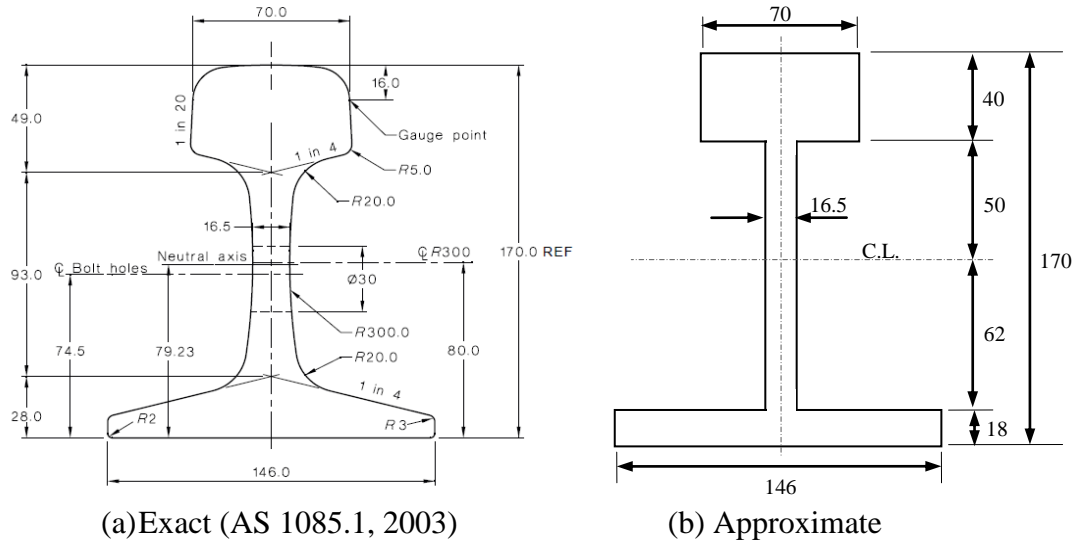
Figure 7.5 Geometrical section of the 60 kg/m steel rail (all units in mm)

Table 7.2 Section properties of the 60 kg/m steel rail

Component	Exact	Approximate
Total area, mm^2	7.7 x 10^3	7.3 x 10^3
Second moment of inertia ($I_{x\text{-}x}$), mm^4	29.3 x 10^6	29.4 x 10^6
Second moment of inertia ($I_{y\text{-}y}$), mm^4	4.9 x 10^6	5.8 x 10^6
Section modulus head, mm^3	322.4 x 10^3	325.9 x 10^3
Section modulus foot, mm^3	369.3 x 10^3	368.7 x 10^3

In the model, the centroids of the rail and sleepers are offset with a distance equal to the sum of half their depths as shown in Figure 7.6a. The beam elements were used to connect the rail and the sleepers, which were placed at the level of their respective centroids (Figure 7.6b). These beam elements representing the rail pads are modelled with an axial stiffness of 310 x 10^6 N/mm in compression which is equivalent to that of the 19 mm thick double shoulder level base rolled-steel sleeper plate used for 146 mm rail base (AS1085.3, 2002) and an axial stiffness of 130 x 10^3 N/mm in tension or equivalent to the static vertical stiffness of timber screw spikes (Thompson and Verheij, 1997). Only the equivalent static wheel load acting on the vertical direction is considered with no lateral and longitudinal loads. The 3 sets of wheel load shown in Figure 7.2 were applied directly to the rails. The support provided by the ballast and subgrade is modelled as an elastic foundation with a combined effective support modulus using Winkler foundation model in Strand7

(Tong, 1969). Dahlberg (2001) suggested that this model is acceptable for static loading of railway track on soft support, like tracks with timber sleepers. The element formulation for beam in elastic foundation is based on thin beam theory where transverse shear deformation is ignored. This model also assumed that the reaction of the foundation is linearly proportional to the deflection of the beam.
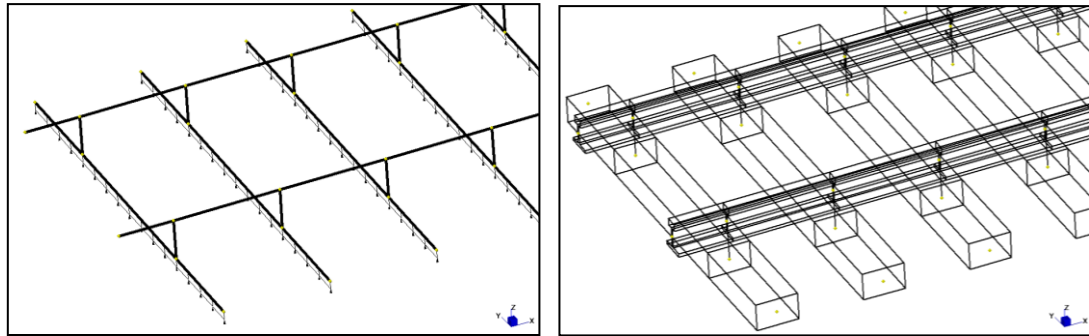
(a) Grillage beam model   (b) Sleeper plate as beam

Figure 7.6 Details of the railway turnout sleeper model

7.5 Parametric study

A parametric study was conducted to determine the behaviour of fibre composite sleepers in a railway turnout with varying modulus of elasticity resting on materials with different sleeper support modulus. The axle load configuration in Figure 7.3 was placed from sleepers 1 to 107 simulating the passing of the train to determine the location of the most critical sleeper and the magnitude of the maximum bending moments, shear forces and vertical deflection on the sleepers.

7.5.1 Equivalent quasi-static wheel load

The AS 1085.14 (2003) states that the distribution of axle loads on the turnout could be determined using the same method used for standard sleepers. Similarly, a number of analytical models developed around the world represents the vehicle by a single bogie with two symmetrical wheel masses (Steffens and Murray, 2005). The magnitude of this equivalent quasi-static force transmitted through the wheel load of a train is calculated following AS1085.14 (2003) and the impact force caused by the train passing through the turnout is considered by the vertical design load factor.

In the AS1085.14, the axle load or vertical load P is a significant factor in the calculation of the design load for sleeper design. In this study, 25 tonnes axle load is

used. The magnitude of the equivalent design static wheel load, Q (in kN) carried by each rail is computed as:

$$Q = (P/2) \; x \; 9.81 \qquad\qquad\qquad (7.1)$$

Rail seat load, R is calculated as a function of design static wheel load, combined vertical design load factor (j) and axle load distribution factor (DF) which corresponds to rail section and sleeper spacing. This gives:

$$R = jQ(DF) \qquad\qquad\qquad (7.2)$$

A combined vertical design load factor, j (including quasi-static and dynamic) of 2.5 is used as recommended by AS1085.14 (2003) and applied to rail seat load, R_1 while a vertical load factor of 1.5 is applied in the front and the rear seat loads, R_2. In the calculation of rail seat load for the FE model of the railway turnout, a DF of 1 is applied as the axle load is distributed to the sleepers through the continuous rails. This has resulted in a wheel load of around 310 kN for R_1 and 185 kN for R_2 which are used as input to and in the development of the FE model. It is important to note that the load of 310 kN is comparable to the highest impact force observed by Leong (2007) in the actual railhead from passing train wheels with 26 to 28 tonne axle loads. This wheel load was moved along the turnout to investigate the influence of wheel load and to determine the location of the most critical sleepers.

7.5.2 Sleeper support modulus, U_s

Sleepers have an important role of conveying the load from rails to the ballast (Shokrieh and Rahmat, 2007). The ballast then transmits the load to the subgrade and elastically absorbs the deformations induced by the sleepers. The modulus of the ballast and the subgrade supporting the sleepers can change dramatically with track construction and this variation can have greater influence on the behaviour of railway sleepers. Shahu et al. (1999) indicated that deflections of the rails were most influenced by the sleeper support modulus, U_s. Similarly, the U_s has significant influence on the load distribution and sleeper deflection (Cox, 1995). However, it is very difficult to determine the quality of the U_s as it requires a thorough investigation of the trackbed comprising a full assessment of the ballast, sub-ballast and formation condition (Brough et al., 2003). In railway design, it is usually assumed that the ballast, subballast and subgrade are represented by a single element with equivalent

ballast/subgrade stiffness (Steffens and Murray, 2005). According to Jeffs and Tew (1991) and AS 1085.14 (2003), the typical value of U_s lies in the range 10 MPa to 40 MPa. To evaluate the effect of the different U_s, the behaviour of sleepers in a railway turnout was examined under four types of ballast/subgrade stiffness.

The turnout sleepers were modeled as beams on elastic foundation which supports the sleepers continuously along its length. The support modulus was varied from 10 to 40 MPa, with increments of 10 MPa. In the Strand7 model, the U_s was applied as a beam support attribute and the stiffness of the elastic support was set as compression only. This type of support enables the sleepers to effectively rest on a support when the sleepers is pushed onto the support but free to move (the support is removed) when the beam is pulled away from the support. In order to determine the behavior of turnout sleepers, the U_s is assumed uniform throughout the model and adjusted stepwise for all the investigated elastic moduli of sleepers.

7.5.3 Modulus of elasticity of the sleeper, $E_{sleeper}$

The bending stiffness of the sleepers $E_{sleeper}$ can significantly influence the response of the railway track (Grassie and Cox, 1984). For the same cross section of sleeper, the bending stiffness varies according to the type of material used which has different moduli of elasticity. When a fibre composite railway sleeper is used as a replacement sleeper, it is important that this sleeper has similar strength and stiffness characteristics as the existing timber sleepers to avoid uneven distribution of loading forces. However, targeting a higher bending stiffness for a fibre composite sleeper requires significant amount of fibres which could be very expensive as it requires more fibres. Thus, a minimum stiffness that would not significantly affect the behaviour of railway turnout sleepers could result in an optimum design for fibre composite alternatives. Therefore, different sleeper elastic moduli, $E_{sleeper}$ supporting the railway track were investigated. Only the lower range of the modulus of elasticity (1 to 10 GPa) were considered with the objective of developing a fibre composite railway sleeper to replace timber sleepers. This range of $E_{sleeper}$ is reasonable as most of the currently developed fibre composite sleepers are produced with stiffness of not more than 8 GPa (Aravinthan et al., 2010). Similarly, Ticoalu (2008) suggested that the behavior of railway sleeper with stiffness of around 10 GPa did not vary significantly for subgrade modulus values of 20 to 40 MPa.

7.5.4 Spot replacement of timber sleeper

The interest in replacing timber sleepers in the existing railway track with other materials has been stimulated by the increased scarcity of quality timber (Van Erp et al., 2005). Currently, several railway infrastructure industries are replacing only the deteriorated sleepers in the railway track (spot replacement) to reduce the cost of maintenance. This maintenance practice leads to a situation where in the existing timber sleeper track, the replacement sleeper will be of different material and possibly different performance characteristics in service. In a study conducted by Birks et al. (1989), they found out that when steel sleepers are used to replace a deteriorated timber sleeper, the steel sleepers was taking a much reduced load compared with the adjacent timber sleepers. Higher deflections were also recorded for the steel sleeper showing a lower support being supplied to the railway track at the steel sleeper installations. They suggested however, that similar rail seat loads and deflections can be achieved by steel sleeper to the adjacent timber sleepers through careful installation procedures and by properly packed ballast. In another study, Kohoutek (1991) found a variation between the performance of concrete and timber sleepers. He concluded that this variation is caused by the different materials of sleepers mixed in the track. Similarly, the differing height of the timber sleeper to that of the concrete resulted in the load not spread evenly among the sleepers. When a fibre composite railway sleeper is used as a replacement sleeper, it is important that this sleeper closely matches the dimensions and the overall stiffness of the existing timber sleepers to minimize the uneven distribution of forces.

In the numerical simulation, the effect in the behaviour of turnout timber sleepers when the most critical sleeper is replaced with a lower $E_{sleeper}$ is investigated. Only the load case where the wheel load produces the highest positive bending moment, shear and deflection in the turnout sleepers was considered. In the spot replacement analysis, four higher values of $E_{sleeper}$ for existing timber turnout sleepers in the Australian railway lines with the U_s kept constant at 20 kPa were investigated. In the numerical simulation, this $E_{sleeper}$ is kept constant throughout the railway turnout even though in actual, the sleepers in a section of a track are a mixture of sleepers of various ages and with different $E_{sleeper}$.

A summary of the design parameters is listed in Table 7.3. In the table, the *All FRP sleepers* represents the numerical model where all the sleepers in the railway turnout system have the same $E_{sleeper}$ while the *Spot replacement* represents the

simulation where only the most critical sleeper in the railway turnout system is replaced with a low $E_{sleeper}$.

Table 7.3 Design parameters for turnout sleeper system

Description	$E_{sleeper}$ (GPa)	U_s (MPa)
All FRP sleepers	1 - 10	10 - 40
Spot replacement	10, 15, 20 and 25	20

7.6 Results of the parametric study

The behavior of railway turnout sleepers with different combinations of $E_{sleeper}$ and U_s are presented here. The influence of train route and the effects of the steel distance blocks at crossing on the behavior of turnout sleepers are discussed in Appendix F.

7.6.1 Behavior of sleepers with different elastic moduli

The effects of the $E_{sleeper}$ on the behavior of *All FRP sleepers* are summarized in Table 7.4. In the table, +BM and -BM represent the maximum positive and negative bending moment, respectively while +V, and -V represent the maximum positive and negative shear in the sleepers. Only the behavior of sleepers on U_s of 10 and 40 MPa are presented to illustrate the effect of the different $E_{sleeper}$ on the bending moment, shear forces and vertical deflection in sleepers. The details of the negative bending moment and shear in sleepers are presented in Appendix F.3.

Table 7.4 Behaviour of sleepers with different $E_{sleeper}$ and U_s

U_s (MPa)	10				40			
Types of sleeper	Transition		Turnout		Transition		Turnout	
$E_{sleeper}$ (GPa)	*1*	*10*	*1*	*10*	*1*	*10*	*1*	*10*
+BM (kN-m)	9.1	12.4	10.6	18.6	7.6	12.1	9.4	16.1
-BM (kN-m)	3.9	2.5	4.7	5.7	2.7	4.4	3.1	7.5
+V (kN)	55.4	56.5	155.1	155.0	53.3	59.6	152.8	157.6
-V (kN)	54.1	54.8	94.3	129.8	53.1	59.3	93.9	130.4
Deflection (mm)	11.6	9.1	12.9	9.9	4.5	2.9	5.1	3.3

7.6.1.1 Bending moments in sleepers

A plot of the maximum positive bending moments in sleepers due to sets of symmetrical wheel load of a train placed onto rails in the diverging route of the turnout is shown in Figures 7.7 and 7.8. In these figures, the elastic modulus of sleepers is designated as *E* while the bending moment is designated as *BM*. The results of the FE simulations show that the maximum bending moment occurred under the rail seat region for both the transition and the turnout sleepers. The results also show that the positive bending moment increases as the wheel load passes through the switch but decreases before passing through the frog (crossing of the train). The lower bending moment at the frog could be due to the high stiffness of the rail at this section which increases its load-distributing effect.

Figure 7.7 shows that the maximum positive bending moment at the transition sleepers increases with increasing $E_{sleeper}$ at $U_s = 10$ MPa. When the wheel load enters the switch, there is an increase in the magnitude of the positive bending moment in the turnout sleepers. For all $E_{sleeper}$, the maximum positive bending moment occurred in sleeper 42 when the wheel load is passing between the switch and the frog. This result suggests that the maximum bending moment in a railway turnout could occur in sleepers located after the switch and before the frog. At $U_s = 40$ MPa, the magnitude of positive bending moment in sleepers is lower compared to that of $U_s = 10$ MPa (Figure 7.8). An increase in the positive bending moment was again observed in the turnout sleepers when the wheel load enters the switch.

It is important to note that in all the simulations conducted, the maximum bending stress in the rails did not exceed 215 MPa. This bending stress is within the acceptance stress levels of 250 MPa or 0.6 times the proof stress of the rail material as recommended by AS1085.1 (2002).
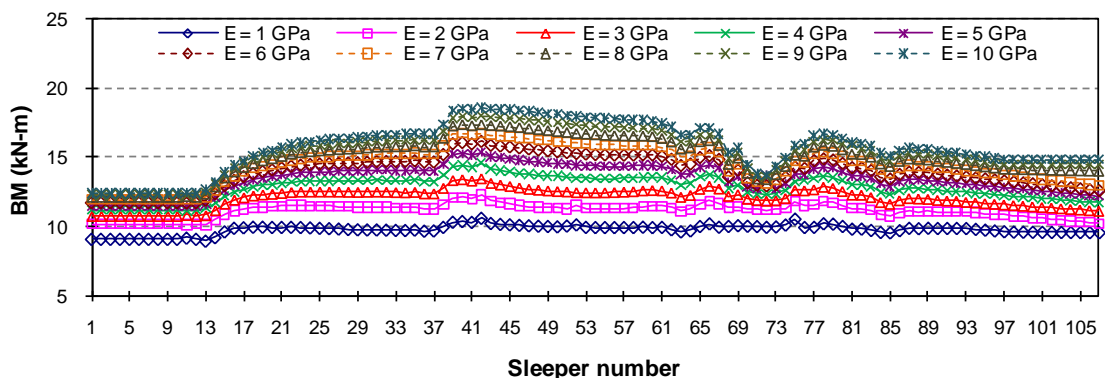
Figure 7.7 Positive bending moment on turnout railway sleepers when $U_s = 10$ MPa
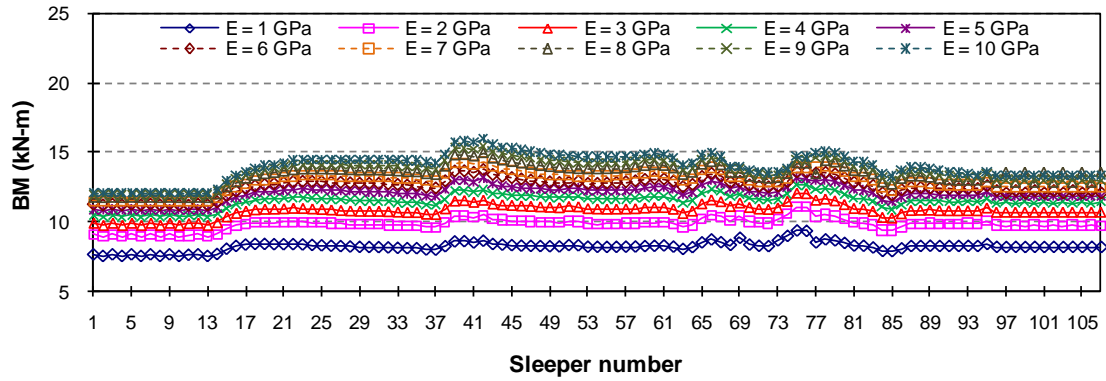
Figure 7.8 Positive bending moment on turnout railway sleepers when $U_s = 40$ MPa

7.6.1.2 Shear forces in sleepers

The shear forces are critical for beams subjected to concentrated loads. In a railway turnout, the change in direction of a passing train causes the maximum shear to occur at the sleepers. Figures 7.9 and 7.10 show the results of the FEM analyses on the maximum positive shear forces incurred by sleepers due to a passing train for all $E_{sleeper}$ considered with support moduli of 10 and 40 MPa, respectively.
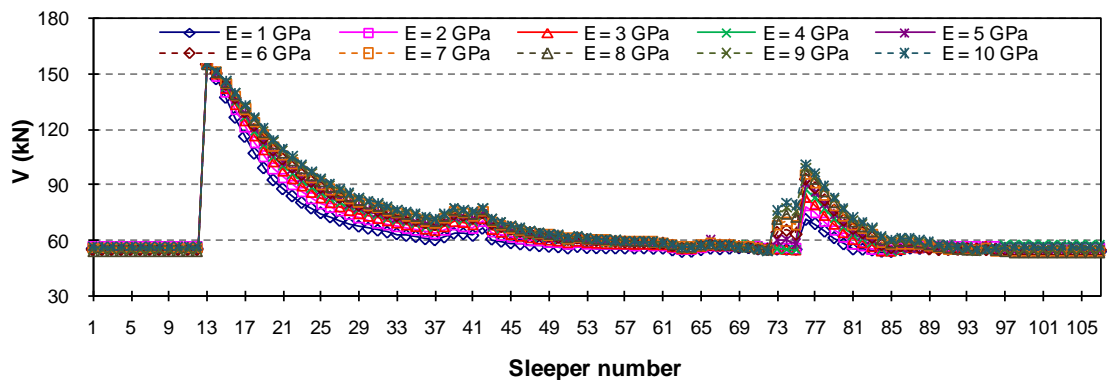
Figure 7.9 Maximum positive shear on turnout sleepers when $U_s = 10$ MPa
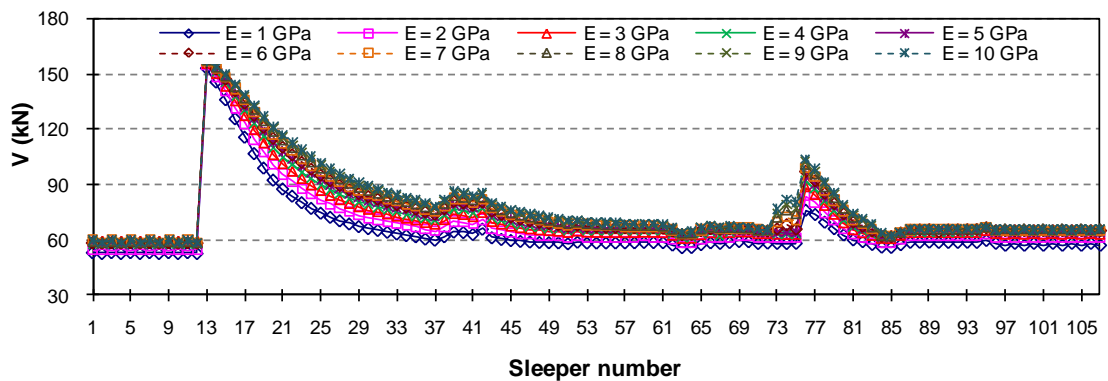
Figure 7.10 Maximum positive shear on turnout sleepers when $U_s = 40$ MPa

The numerical simulation showed that the maximum positive shear force occurred under the rail seat of the transition sleepers at both $U_s = 10$ MPa and 40 MPa. Figures 7.9 and 7.10 indicate that the maximum positive shear force in the transition sleepers does not vary significantly for all $E_{sleeper}$. When the wheel load enters the switch, there is a significant increase in the positive shear force in the turnout sleepers. This increase is because of the flange opening in the switch rails starts in this location. The highest positive shear force occurred when the wheel load, R_1 is seating on sleeper 13. The magnitude of the maximum shear force decreases as the wheel load travels between the switch and the frog. However, an increase in the maximum shear force was again recorded in sleeper 76 just after the wheel load passed through the frog. It is important to note that the highest positive shear force in sleepers 13 and 76 occurs in the region between the through and divergent tracks. The magnitude of this shear force is up to 2.5 times higher than the transition sleepers. This high magnitude of shear force at the switch and the frog can be attributed at the flangeway opening which causes high shear forces in the sleepers. In this location, the train wheel has to "jump" on the flangeway opening which subjected the sleepers to the high, concentrated wheel forces. After the wheel load has passed through the sleeper at the frog, the magnitude of the positive shear force decreases as it enters through the divergent tracks. This high shear force occurs at the sleeper region between the through and divergent tracks.

7.6.1.3 Vertical deflection of sleepers

Figures 7.11 and 7.12 present the maximum vertical deflection or settlement into the ballast of sleepers for each load position for all the different $E_{sleeper}$ investigated when $U_s = 10$ MPa and 40 MPa, respectively. The FEM results show that the maximum settlements of the sleepers occurred under the rail seats when the wheel load, R_1 is placed directly over the sleeper. The results also show that the sleepers with lower modulus of elasticity will settle more than the sleepers with higher $E_{sleeper}$. However, the difference in the magnitude of vertical deflection of sleepers decreases with increasing $E_{sleeper}$. As seen from the figures, there is no significant difference in the vertical deflection of sleepers when modulus of elasticity is between 4 and 10 GPa.

Figure 7.11 shows that the highest vertical deflection observed in the transition and turnout sleepers for *All FRP sleeper* when $U_s = 10$ MPa. As the wheel load enters the switch, the vertical deflection of the sleepers decreases slightly but increases

again after passing the switch. The vertical settlement of the sleeper increases before the wheel load reaches the transition sleepers at the divergent tracks. Similar deflection behaviour of sleepers was observed when $U_s = 40$ MPa (Figure 7.12). Settlement of the sleeper into the ballast decreases with increasing $E_{sleeper}$.
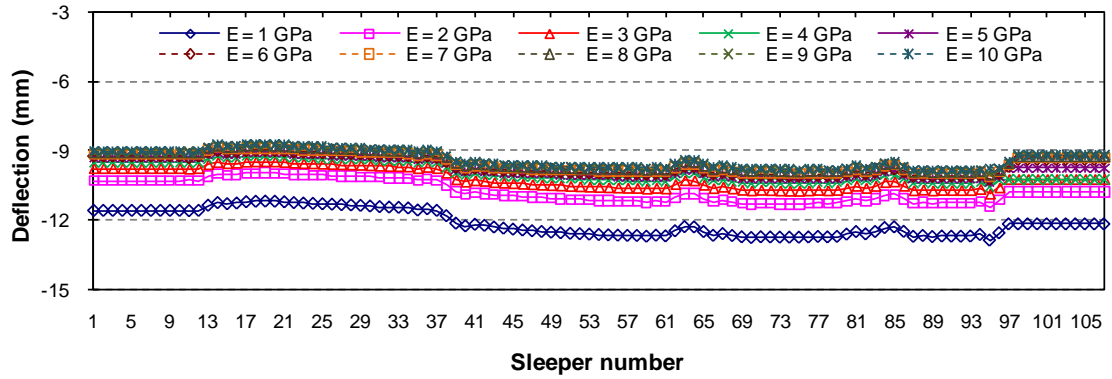
Figure 7.11 Maximum deflection of turnout sleepers when $U_s = 10$ MPa
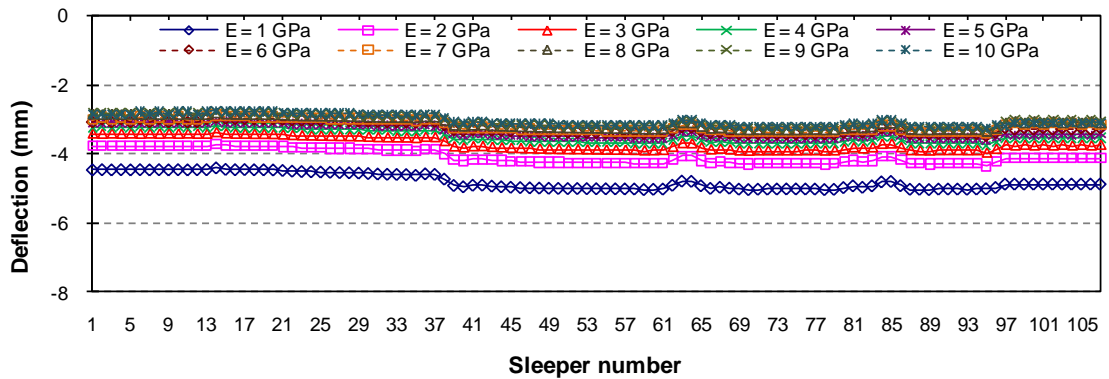
Figure 7.12 Maximum deflection of turnout sleepers when $U_s = 40$ MPa

The highest vertical settlement into the ballast of the transition sleeper occurs under the railseat. The magnitude of the vertical settlement of sleeper decreases as the wheel load enters the switch but increases again after the switch. In general, an increasing deflection was observed as the length of the sleeper increases with low deflection in the sleepers between the switch and the frog. The lower settlement of sleepers in this location could be due to the presence of a rail between the rail seats which acted as a support to lessen the settlement of the sleepers. After the frog, the vertical settlement increased again as the sleepers behaved more like a cantilever beam with the rails on the through tracks acting as supports. Figures 7.13 and 7.14 show the scaled up deflected shape of a turnout sleeper (sleeper 97) when the wheel load is placed after the frog and before the longest sleeper. As can be seen from the

figures, the maximum vertical deflection in sleeper occurred under the rail seat. The results of the FEM analysis also show that the settlement of the sleepers into the ballast is slightly higher under the outer rail seat than under the inner rail seat after the wheel load has passed the frog. This is due to asymmetric loading on longer sleepers when the wheel load is passing through the divergent tracks while the other sleeper end tends to lift due to the elastic foundation. However, this upward deflection on the other end of the sleeper is restricted by the continuous rails on the through or main tracks. For $E_{sleeper} = 1$ GPa, the sleeper ends where the wheel load is placed deflected to its maximum while the other end deflected very minimally as the stiff rails in the main tracks are preventing the more flexible sleepers (Figure 7.13). For $E_{sleeper} = 10$ GPa, the maximum deflection is again observed in the sleeper ends where the wheel load is placed (Figure 7.14). Due to the higher stiffness of the sleepers, the rails could not totally prevent the other sleeper end to deflect upward. Similarly, the combination of the rails and the higher stiffer sleepers resulted to a lesser deflection for $E_{sleeper} = 10$ GPa compared to that of $E_{sleeper} = 1$ GPa.
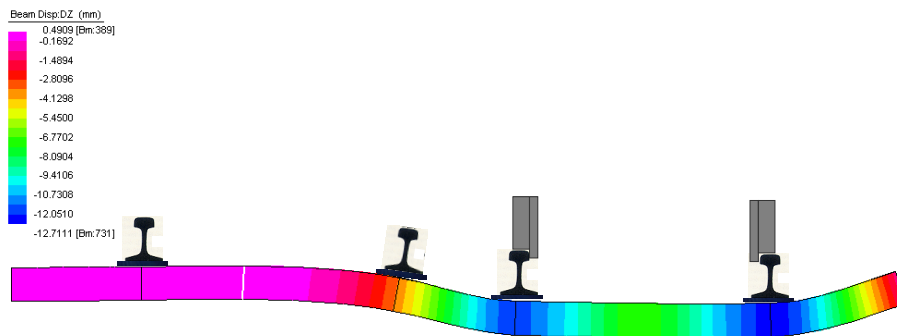
Figure 7.13 Deflection of turnout sleepers when $E_{sleeper} = 1$ GPa and $U_s = 10$ MPa
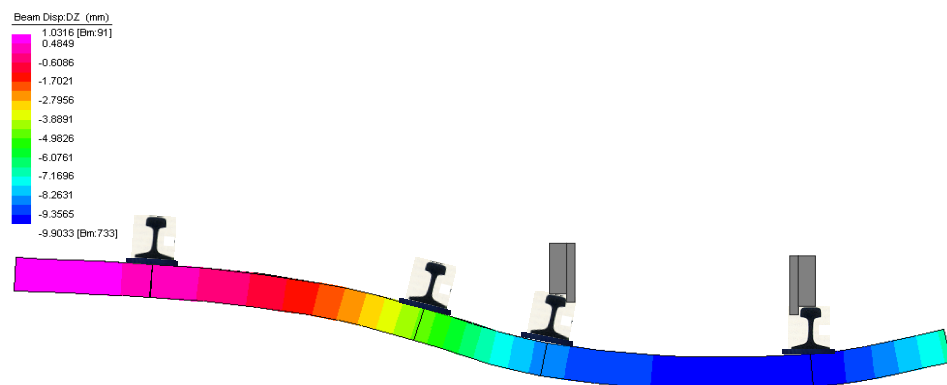
Figure 7.14 Deflection of turnout sleepers when $E_{sleeper} = 10$ GPa and $U_s = 10$ MPa

7.6.2 Behavior of sleeper with different support moduli

The results obtained from the FEM analyses on the behaviour of sleepers on various U_s are presented here. Sleepers with $E_{sleeper}$ of 1 and 10 GPa resting on elastic foundation with U_s of 10 to 40 MPa were modelled to determine the bending moment, shear forces and vertical deflection of sleepers in a turnout. The negative bending moment and shear in sleepers for different U_s are presented in Appendix F.4.

7.6.2.1 Bending moments in sleepers

Figures 7.15 and 7.16 show the maximum positive bending moments in sleepers with $E_{sleeper} = 1$ GPa and 10 GPa resting on different U_s, respectively. The results show that the effect of U_s on the sleeper's positive bending moments is marginal for lower $E_{sleeper}$ but considerable at higher $E_{sleeper}$. At transition and turnout sleepers, the maximum bending moment decreases with increasing U_s. The difference however may not be significant for $E_{sleeper} = 1$ GPa but increases for $E_{sleeper} = 10$ GPa.
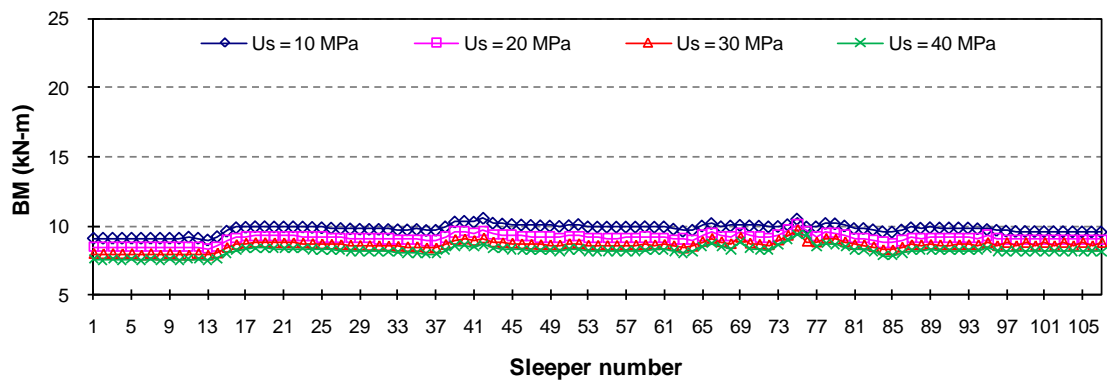
Figure 7.15 Maximum positive bending moment of sleeper when $E_{sleeper} = 1$ GPa
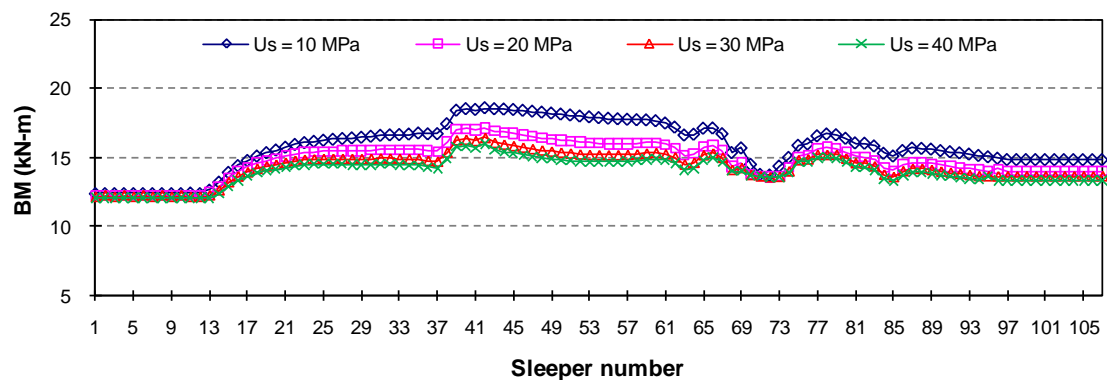
Figure 7.16 Maximum positive bending moment of sleeper when $E_{sleeper} = 10$ GPa

Figure 7.15 shows that the maximum positive bending moment at the transition and turnout sleepers for all U_s when $E_{sleeper} = 1$ GPa. The magnitude of the positive bending moment increases when the wheel load enters the turnout. When $E_{sleeper} = 10$ GPa, the positive bending moment in the transition sleepers is around 12.1 kN-m for all the investigated U_s as shown in Figure 7.16. The positive bending moments again increases when the wheel load enters the turnout. Similarly, a higher bending moment was observed in lower U_s than in higher U_s. The highest positive bending moment in turnout sleepers occurred at sleeper 42 for all the investigated U_s.

The numerical analyses show that the maximum bending moment when $E_{sleeper} = 1$ GPa is not greatly different from each other for all investigated U_s but has a noticeable difference when $E_{sleeper} = 10$ GPa. Moreover, it can be seen that the bending moments in the longer turnout sleepers are more sensitive to the changes in the U_s than the shorter transition sleepers. This finding is similar to that of Namura et al. (2004) where they indicated that the sleeper length has a great influence on its bending moments. The results further indicated that as the sleeper support becomes stiffer there is an increase in the magnitude of the maximum bending moment in the sleepers. Obviously, increasing the value of U_s leads to an increase in the rigidity of the foundation. As a result, the wheel load is distributed only to a fewer sleepers increasing the bending moment experienced by sleeper directly under the load.

7.6.2.2 Shear forces on sleepers

The relationship of the maximum shear force in sleepers on different U_s due to the applied wheel load on the railway turnout is shown in Figures 7.17 to 7.18. The results show that there is only a slight increase in the shear force with increasing U_s.

Figure 7.17 shows that the maximum positive shear force occurred under the rail seat of the transition sleepers for all the investigated U_s when $E_{sleeper} = 1$ GPa. When the wheel load enters the switch, there is a significant increase in the magnitude of positive shear force on the turnout sleepers. The highest positive shear force occurred when the wheel load is seating on sleeper 13 and has a magnitude of around 155 kN. This magnitude of shear force is almost 2.5 times higher than the transition sleepers. The shear force rapidly decreases as the wheel load travels between the switch and the frog. An increase in the maximum shear force was again recorded in sleeper 76 with a magnitude around 71 kN. After the wheel load has passed sleeper 76, the positive shear force in sleeper decreases. The FEM results

showed similar magnitude of shear force acting in sleepers when $E_{sleeper} = 10$ MPa (Figure 7.18). A significant increase in the magnitude of positive shear force was observed when the wheel load travels from the transition to turnout sleepers. The maximum positive shear force in the turnout sleepers ccurred when the wheel load, R_1 is seating on sleeper 13. A high shear force was again recorded in sleeper 76 with a magnitude around 101 kN. After the wheel load has passed this sleeper, the magnitude of the positive shear force decreases.
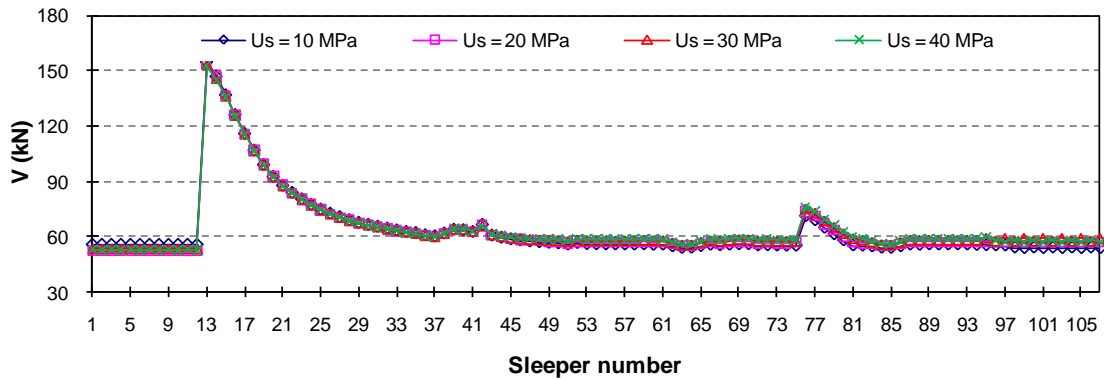
Figure 7.17 Maximum positive shear on sleeper when $E_{sleeper} = 1$ GPa
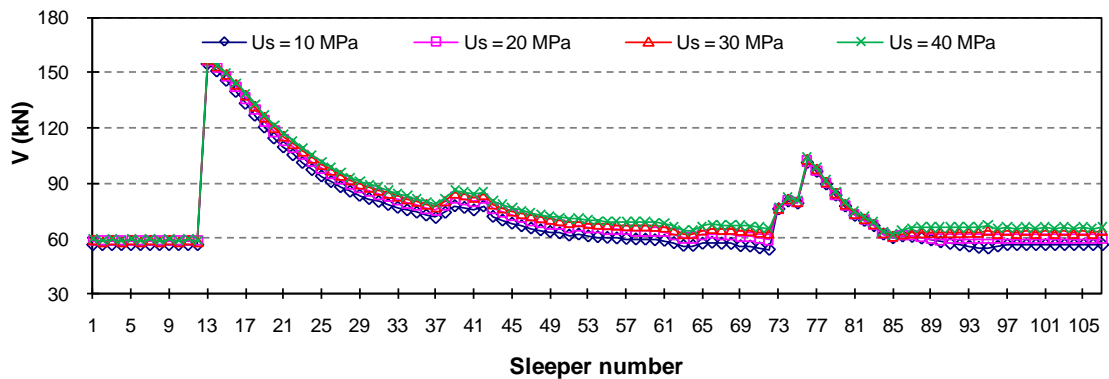
Figure 7.18 Maximum positive shear on sleeper when $E_{sleeper} = 10$ GPa

7.6.2.3 Vertical deflection of sleepers

Figures 7.19 and 7.20 present the vertical deflection of sleepers for all U_s considered when $E_{sleeper} = 1$ GPa and 10 GPa, respectively. It can be seen clearly from the figures that the vertical deflection of sleepers decreases as the support modulus increases. The lower settlement of sleepers between the switch and the frog is due to the presence of rails between the rail seats which prevented the settlement of the sleepers. For both $E_{sleeper} = 1$ GPa and 10 GPa, there is a considerable vertical deflection of sleepers resting on $U_s = 10$ MPa but decrease significantly for $U_s = 20$ MPa or higher.
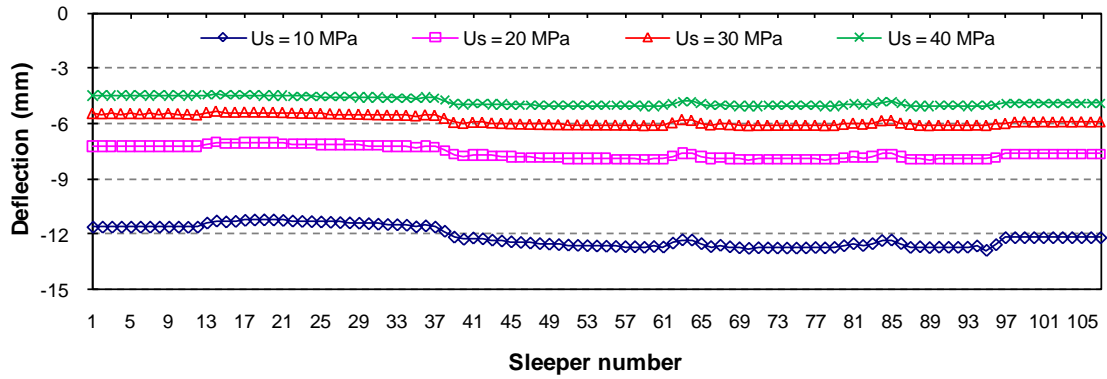
Figure 7.19 Maximum deflection of sleeper when $E_{sleeper} = 1$ GPa
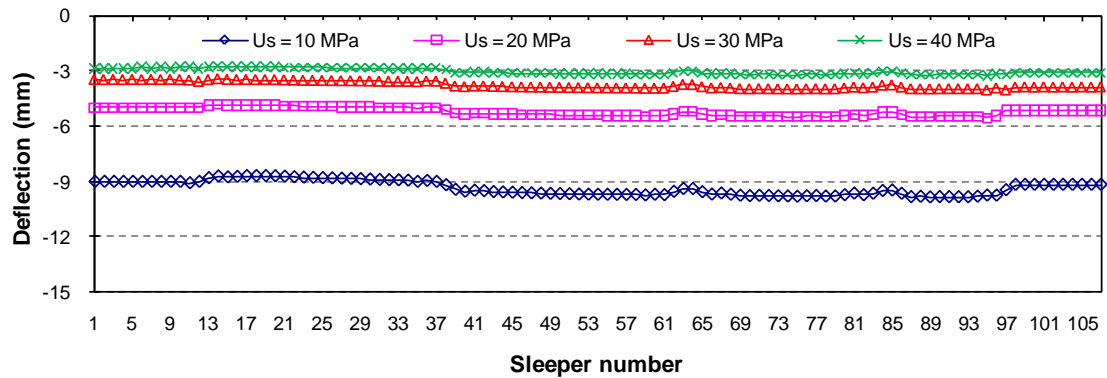
Figure 7.20 Maximum deflection of sleeper when $E_{sleeper} = 10$ GPa

7.6.3 Behavior of turnout sleepers with a spot replacement sleeper

The behaviour of the turnout sleepers when one of the sleepers in a turnout is replaced with a sleeper of low $E_{sleeper}$ is presented here. In the numerical simulation, the most critical sleepers, sleepers 42 and 68 were assigned with a low $E_{sleeper}$ while keeping the elastic modulus of the other sleepers the same to determine the maximum bending, shear and deflection in the railway turnout sleepers. In the analysis of results, the 10 sleepers before and after sleepers 42 and 68 were included.

The distribution of maximum bending moment, shear and vertical deflection among the sleepers in the railway turnout are shown in Figures 7.21 to 7.23, respectively. In these figures, *All_4*, *All_10*, *All_15*, *All_20*, and *All_25* represent the railway track supported by turnout sleepers with the same value of $E_{sleeper}$. On the other hand, the railway track with the most critical sleeper replaced by a fibre composite sleeper with an $E_{sleeper} = 4$ GPa are designated as *4_10*, *4_15*, *4_20*, and *4_25*. The railway turnout supported by $E_{sleeper} = 10$ GPa with the most critical sleeper replaced by a very flexible or a damaged sleeper (elastic modulus of only 1 MPa) is included for comparison and is designated as *0_10*.
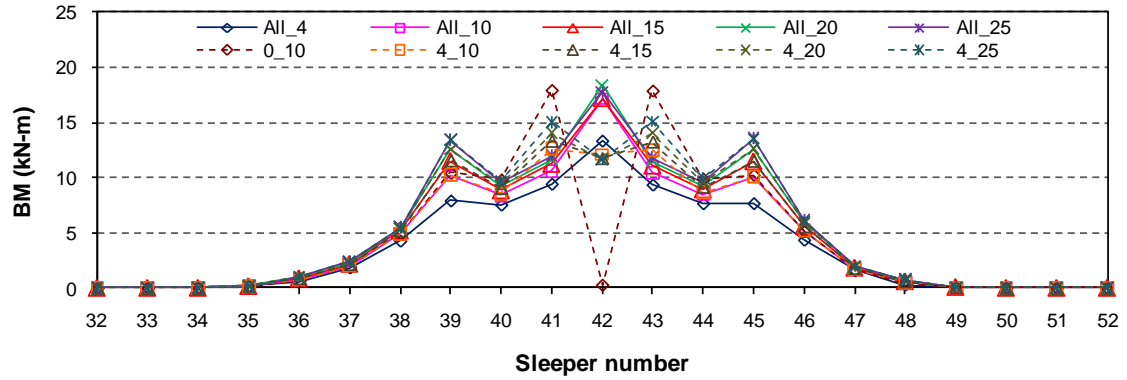
Figure 7.21 Maximum bending moment in sleepers 32 to 52
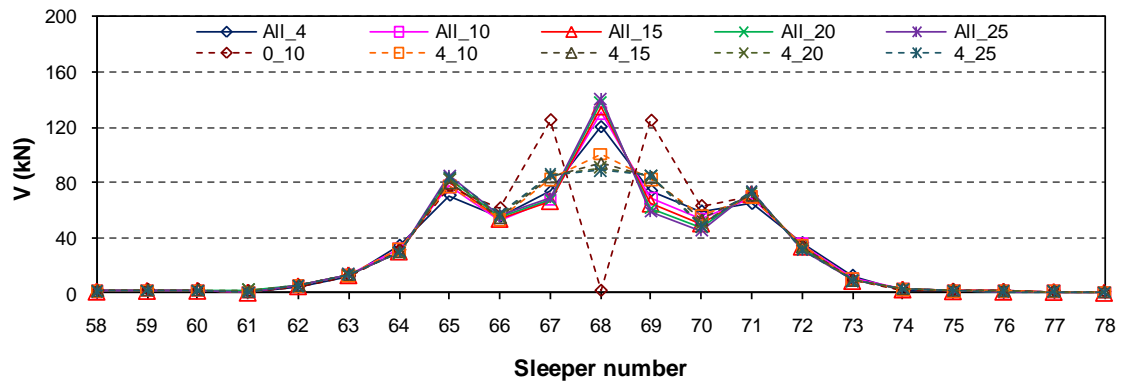
Figure 7.22 Maximum shear in sleepers 58 to 78
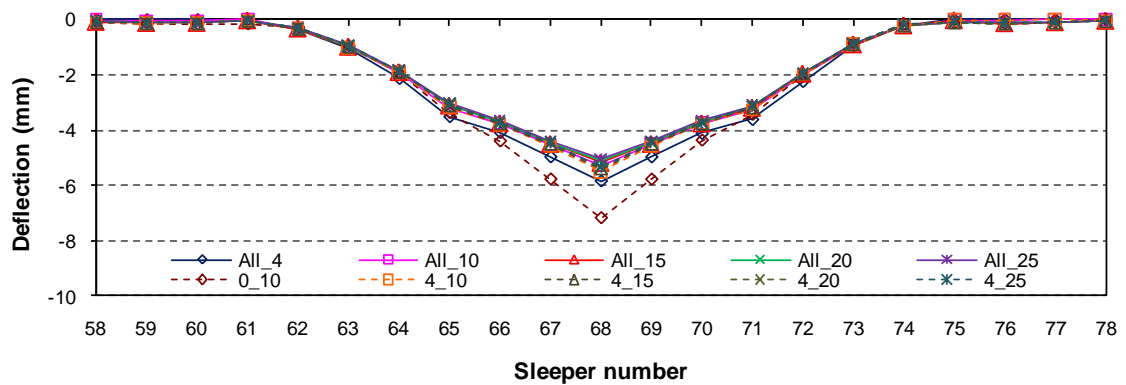
Figure 7.23 Maximum vertical deflection in sleepers 58 to 78

As can be seen from the figures, the behaviour of turnout sleepers with the same $E_{sleeper}$ is almost the same. This is similar to results of the investigation by Ticoalu (2008) wherein she found no significant difference in the maximum bending moment, shear and vertical deflection for turnout sleepers with $E_{sleeper}$ of 10 GPa or higher and are resting on a subgrade of 20 to 40 MPa. However, it can be seen from the figures that replacing sleepers 42 and 68 with an $E_{sleeper} = 4$ GPa has a large influence on the behaviour of the group of turnout sleepers. In Figure 7.21, the results show that the sleeper directly under the rail seat load R_1 has the highest

bending moment. In a railway turnout supported by sleepers with the same $E_{sleeper}$ (*All_10*, *All_15*, *All_20* and *All_25*), the magnitude of bending moment in sleeper 42 is around 18 kN-m while in its adjacent sleepers is around 12 kN-m. Similarly, the magnitude of the bending moment in sleeper 42 for turnout with $E_{sleeper}$ of 10 to 25 GPa is only 20% higher to the bending moment experienced in *All_4*.

Replacing sleeper 42 with an elastic modulus of 4 GPa leads to a lowering overall stiffness of the railway track and therefore a reduction in the bending moment starts to occur in the sleeper just below the load. A reduction in the magnitude of bending moment of almost 30% was observed for sleeper 42 compared to a railway turnout not mixed with a lower $E_{sleeper}$ even though R_1 is directly over this particular sleeper. This reduction in the bending moment in sleeper 42 is however distributed to the neighbouring sleepers as seen by the increase in the bending moment of sleepers 41 and 43. For all the investigated $E_{sleeper}$ value, there is no significant difference in the bending moment in the spot replacement sleeper but the increase in the bending moment in the adjacent sleepers can go as high as 20% for higher $E_{sleeper}$. On the average, the bending moment in the adjacent sleepers is 22% higher than that of sleeper 42. This result shows that a fibre composites sleeper is more effective than steel for a spot replacement sleeper. Birks et al. (1989) indicated that a steel sleeper situated immediately below the load source carries an almost 38% lower bending moment compared to the adjacent timber railway sleepers.

The increase in the bending moment in the adjacent sleepers in *4_10*, *4_15*, *4_20*, and *4_25* is significantly less compared to that of the adjacent sleepers when the spot replacement sleeper has a very low elastic modulus value ($E_{sleeper}$ = 1 MPa). Similarly, the increase in the bending moment in the adjacent sleepers in *0_10* compared to the railway turnout not mixed with a low stiffness sleeper is around 45%. This is almost similar to the observations by Zhang et al. (2008) when they examined the response of a railway track with unsupported sleepers. In their numerical investigation, they represented the unsupported sleeper with a zero value for $E_{sleeper}$. Their results showed that the calculated bending moment in the neighbouring sleepers when the train passes over an unsupported sleeper is almost 40% higher compared with under normal condition. Furthermore, the maximum bending moment in the sleepers 41 and 43 for *0_10* is slightly higher than that of sleeper 42 in the normal railway track. This should not be the case especially when the sleeper is designed based on the maximum bending moment acting on the

sleepers for a track with a constant $E_{sleeper}$. This increased bending moment taken by the adjacent sleepers might result in its early in-service failure. Interestingly, the bending moment experience by the spot replacement sleeper is higher than the bending moment in *All_4* suggesting a better distribution of load among the sleepers. Thus, it can be said that the fibre composite sleepers can be used not only for spot replacement but also in the total replacement of timber sleepers in a railway turnout.

Figure 7.22 shows that sleeper 68 has the highest shear force when R_1 is directly over this sleeper. For a railway turnout without a spot replacement sleeper, the magnitude of shear force in sleeper 68 is at 140 kN, which is almost 50% higher than that of the shear force in the adjacent sleepers. Considering the load is directly over sleeper 68, the shear force at the sleepers 67 and 69 are almost same. When sleeper 68 is replaced with $E_{sleeper} = 4$ GPa, the shear force in sleeper 68 decreases to 95 kN while in the adjacent sleepers increases to 85 kN. This represents an over 30% decrease in shear force in the spot replacement sleeper but only a 20% in shear force in the adjacent sleepers with the shear force among sleepers 67 to 69 differ by only 10%. A slight increase in shear force was also observed in the neighbouring sleepers. In the evaluation of Kohoutek (1991) between the performance of a railway track with mixed timber and concrete sleepers, he found out that the distribution is 30% to timber and 35% to the adjacent concrete sleepers when the load is over the timber sleeper but over 60% for concrete sleeper when the load is directly over the concrete sleeper. This result again showed that a fibre composite sleeper distributes the load better to the adjacent sleepers than a concrete sleeper.

In Figure 7.23, the results show that replacing sleeper 68 with an $E_{sleeper} = 4$ GPa did not significantly change the maximum deflection in the turnout sleepers compared to that of a railway turnout with all the sleepers having the same elastic modulus. The magnitude of vertical deflection in sleeper 68 is well under 6 mm for all the considered $E_{sleeper}$. On the other hand, replacing sleeper 68 with a very low elastic modulus would result to an almost 35% increase in the deflection of the adjacent sleepers. This is almost similar to the results obtained by Lundqvist and Dahlberg (2005) wherein they found out that the vertical displacement of sleepers adjacent to an unsupported sleeper increase by 40%. In the earlier studies by Birks et al. (1989), they have observed a deflection of 9 mm for the inserted steel sleeper compared to only 5 mm for timber when not mixed with a steel sleeper. These results

further show that a fibre composites sleeper is a more effective spot replacement sleeper for timber sleepers in a railway turnout system than concrete and steel.

7.7 Discussion

The effects of the different $E_{sleeper}$ and varying U_s on the behaviour of sleepers in a railway turnout are discussed in this section. An evaluation was also conducted to determine if the behaviour of sleepers using the practical range of values for various track parameters satisfies the technical requirements for railway turnout application.

7.7.1 Effect of elastic and support moduli on bending moment

In the range of the studied $E_{sleeper}$ and U_s, the highest bending moments in sleepers took place when a train is passing through a turnout. The highest positive moment occurred when R_1 is directly on sleeper 42 while the maximum negative bending moment occurred when R_1 is on sleeper 52. Figure 7.24 shows that the maximum positive bending moment occurred under the rail seat region where the axle is placed while the negative bending moment occurred between them (Figure 7.25).

The relationship between the maximum bending moments in turnout sleepers and the $E_{sleeper}$ for the different U_s is shown in Figure 7.26. The magnitude of the positive and the negative bending moments increases with increasing $E_{sleeper}$ but decreases with increasing U_s. The results show that the increase in $E_{sleeper}$ from 1 GPa to 10 GPa has resulted in almost 75% increase in the bending moment, whilst a change in U_s from 10 MPa to 40 MPa reduces the bending moment by 15%. Furthermore, the influence by the changes in the U_s is less in low than in high $E_{sleeper}$. The higher bending moment on sleepers with high $E_{sleeper}$ is due to the greater stiffness of the railway track resulting in a fewer sleepers sharing the load. Compared to transition sleepers, the increase in the bending moment in the turnout sleepers is around 20% for low $E_{sleeper}$ but is in the order of 40-55% for high $E_{sleeper}$. Another area of interest is the redistribution of the load throughout the sleeper system due to the increasing U_s as shown by a decreasing difference in the bending moment in sleepers. This is more obvious when $E_{sleeper}$ is 4 GPa or higher wherein there is no significant difference in sleeper's bending moment for high U_s. Similar result was obtained for spot replacement sleeper wherein the distribution of bending moment among the group of sleepers is similar for $E_{sleeper}$ of 4 GPa or higher. On the basis of

the simulations performed, the fibre composite sleeper should resist minimum positive and negative bending moments of 18.6 kN-m and 7.5 kN-m, respectively.
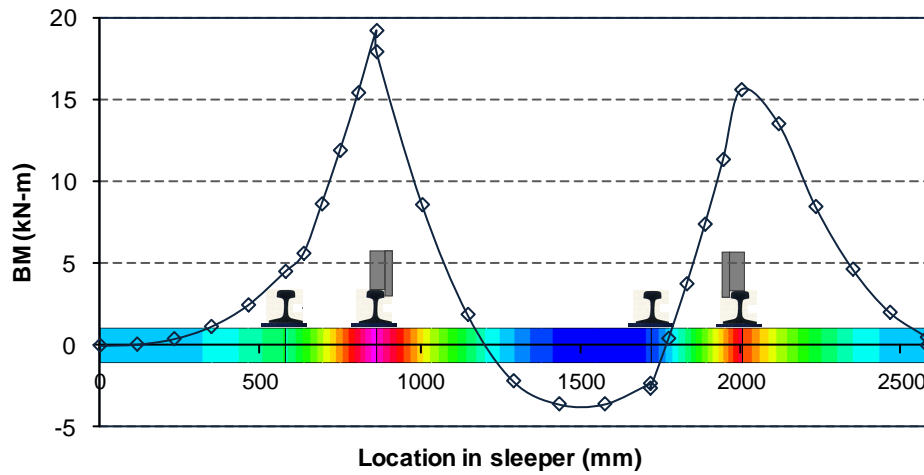
Figure 7.24 Bending moment in sleeper 42
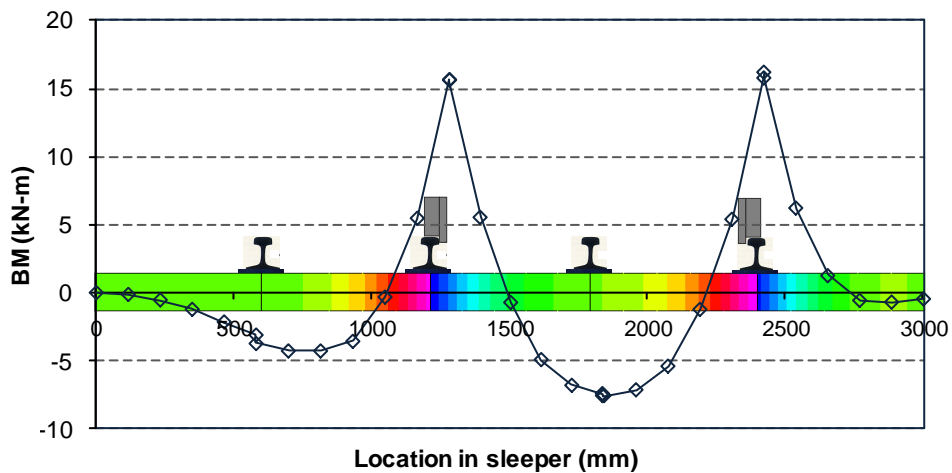
Figure 7.25 Bending moment in sleeper 52
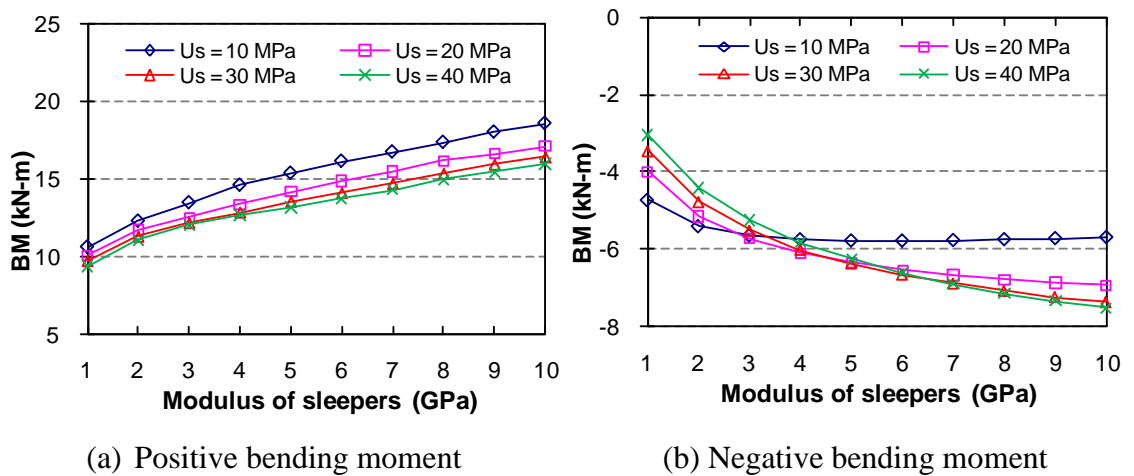
(a) Positive bending moment   (b) Negative bending moment

Figure 7.26 Maximum bending moments on railway turnout sleepers

7.7.2 Effect of elastic and support moduli on shear force

Figure 7.27 shows the maximum positive and negative shear forces in railway turnout sleepers with different $E_{sleeper}$ and U_s. In Figure 7.27a, the positive shear force in the turnout sleepers increases with increasing $E_{sleeper}$ but became almost constant when $E_{sleeper}$ is higher than 4 GPa for all the U_s considered except when $U_s = 10$ MPa wherein a decrease in shear force was observed for $E_{sleeper}$ higher than 3 GPa. On the other hand, Figure 7.27b shows that the magnitude of the maximum negative shear force increases with increasing $E_{sleeper}$. The maximum negative shear force in sleepers occurs near the frog where the steel distance blocks are provided. The higher stiffness of the rail at this location compared to the support modulus resulted in a very small difference in the shear force induced in the sleeper.

(a) Positive shear   (b) Negative shear
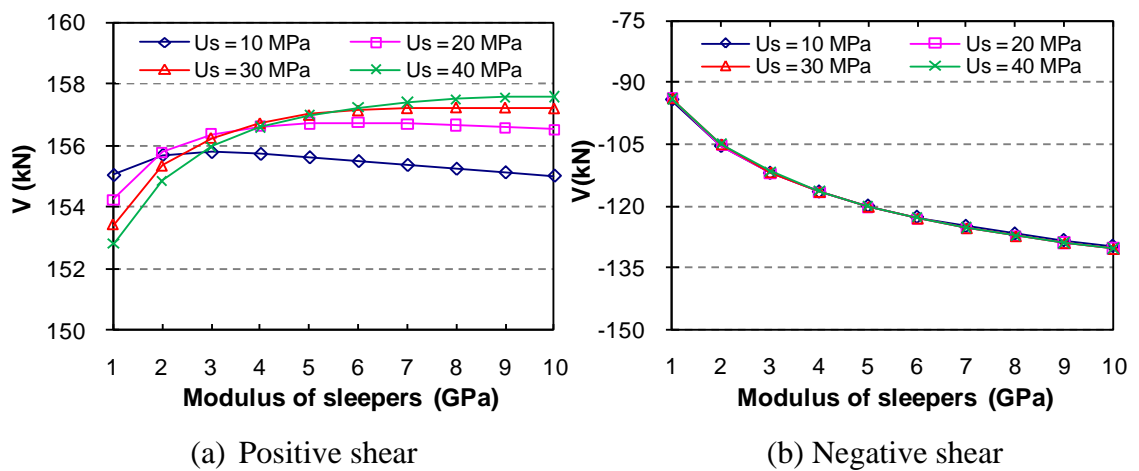
Figure 7.27 Maximum shear forces on railway turnout sleepers

In general, there is no significant difference in the value of highest shear force in the different $E_{sleeper}$ and U_s considered. The increase in $E_{sleeper}$ from 1 GPa to 10 GPa has resulted in only 3% increase in the positive shear force and the increase in U_s from 10 MPa to 40 MPa resulted in only 1.6% increase. On the other hand, the increase in $E_{sleeper}$ from 1 to 10 GPa has increased the magnitude of the negative shear force by almost 40%. The high magnitude of the shear force for higher $E_{sleeper}$ than lower $E_{sleeper}$ on higher U_s is due to the stiffer track modulus which results in the load distributed only to a fewer sleepers, thus a higher force carried by the sleeper directly under the load. Noticeably, the highest shear force occurred on turnout sleeper located just after the switch and the crossing as shown in Figures 7.28 and 7.29, respectively. In this location, shear gets very high in sleeper as the rails are close together. When the wheel load is placed on the diverging track, a lot of the load

on one rail is carried by the adjacent rail. The magnitude of this shear force is almost 2.5 times higher than that of the transition sleepers. This further confirms that the shear force is critical in sleepers when the train changes direction in a turnout. More importantly, the results suggest that the sleepers for turnout application should be designed with a higher shear capacity than the mainline sleepers. The railway turnout sleeper should carry a minimum shear force of 158 kN. The result of the numerical simulation also provided information on the location of the maximum bending moments and shear forces along the sleeper lengths. This information is very helpful in determining where the bulk of the fibre composite materials should be placed in a railway turnout sleeper section for a more cost effective design.
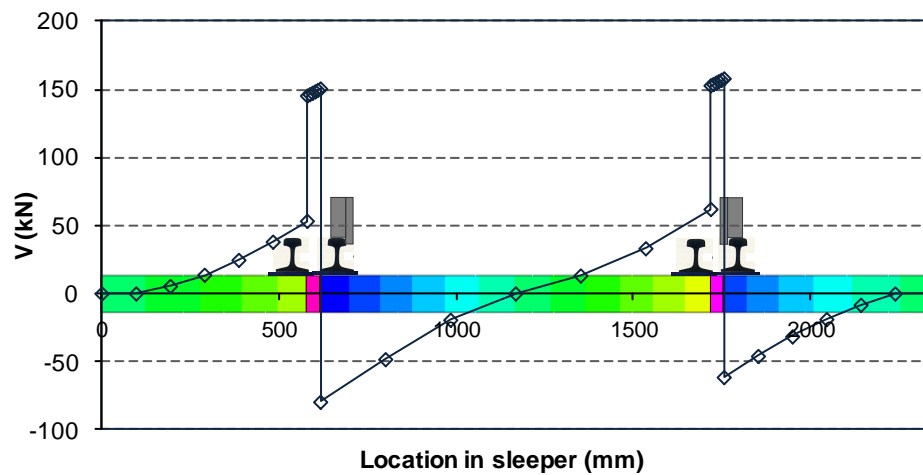
Figure 7.28 Shear force envelope in sleeper at the switch
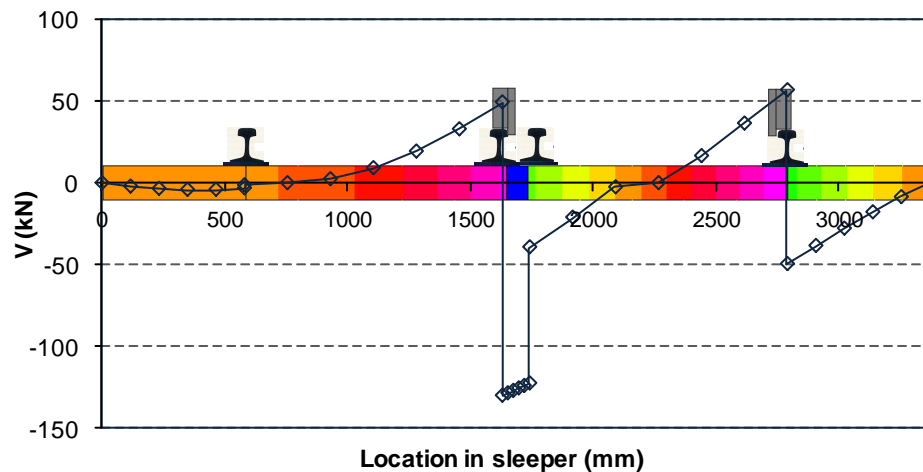
Figure 7.29 Shear force envelope in sleeper at the crossing

7.7.3 Effect of elastic and support moduli on deflection and ballast pressure

Figure 7.30 shows the maximum vertical deflection and the ballast/sleeper pressure of railway turnout sleepers with different $E_{sleeper}$ and U_s. In Figure 7.30b, the contact

pressure between sleeper and ballast is calculated by multiplying the sleeper support modulus and the deflection divided by the width of the sleeper with the compressive stresses that the sleepers exert on the ballast bed considered evenly distributed.

(a) Vertical deflection   (b) Sleeper/ballast pressure
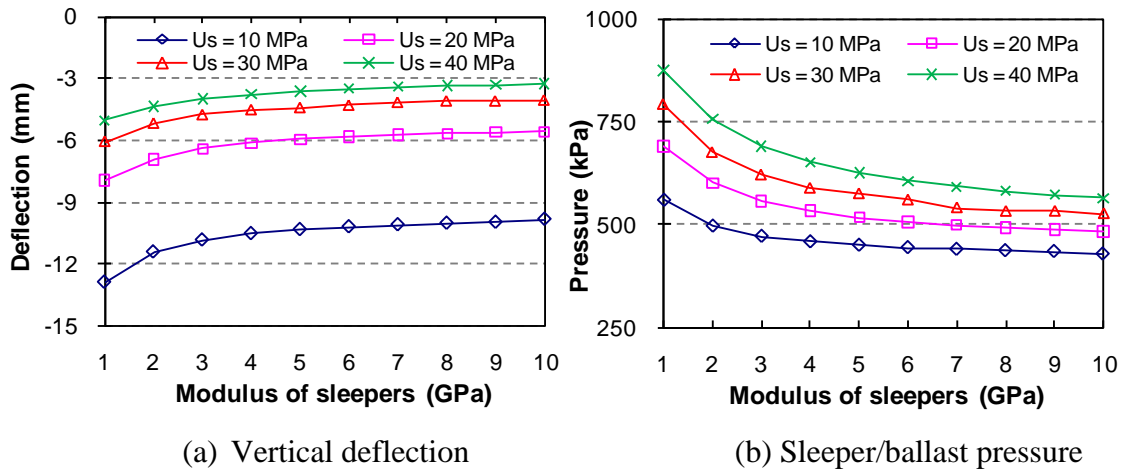
Figure 7.30 Vertical deflection and sleeper/ballast pressure

The analyses show that the U_s has a significant influence on the vertical deflection and the sleeper/ballast pressure. It is clearly observed that the vertical displacement of sleeper decreases with increasing $E_{sleeper}$ and U_s. The lower the U_s, the more likely the sleeper will deflect and settle into the ballast while a more uniform settlement occurs at higher U_s. This also means that sleepers with higher $E_{sleeper}$ provided more stability in railway tracks. On the other hand, the change of the U_s from 10 to 40 MPa increases the pressure between the sleeper and the ballast. This is because the higher U_s tries to isolate the individual sleepers in the turnout resulting in a higher load carried by the sleeper directly under the load. Thus, it can be concluded that a better distribution of the wheels load on the group of sleepers can be attained for lower $E_{sleeper}$ but this will result in higher sleeper deflection.

Figure 7.30a shows that the increase in the modulus of elasticity of the sleepers from 1 to 10 GPa resulted in a decrease in the vertical deflection of the sleepers by 23-36% for the different support moduli considered. However, the results also suggest that varying the $E_{sleeper}$ from 4 GPa to 10 GPa does not make a major difference in deflection particularly for higher U_s. Similarly, the increase in U_s from 10 to 40 MPa decrease the vertical deflection of the sleepers by at least 60%. In Figure 7.30b, it can be seen that increasing the $E_{sleeper}$ from 1 to 10 GPa results in 23-36% decrease in the sleeper ballast pressure. On the other hand, the increase in support modulus from 10 MPa to 40 MPa resulted in an increase in the

sleeper/ballast pressure by as much as 35%. The same magnitude of increase in the sleeper/ballast pressure was observed by Shahu et al. (2008) in their laboratory model test railway track when the sleeper support modulus increased from 10 MPa to 50 MPa. This suggests that the grillage beam analogy to model the entire turnout system is reasonable to use as they are producing meaningful results.

The sleeper deflection under the rail is the main criterion in a railway track analysis (Zakeri and Sadeghi, 2007). For railway tracks in Australia, the maximum static deflection in a railway structure on ballasted track should be around 6.35 mm to give requisite combination for flexibility and stiffness (Jeffs and Tew, 1991). The results indicated that except for a U_s of 10 MPa and railway sleepers with a $E_{sleeper}$ of lower than 4 GPa, the calculated vertical deflection in all the combinations used is within the recommended value. An elastic modulus value of 4 GPa is also needed for a spot replacement sleeper for the timber sleeper railway turnout track to not exceed the maximum allowable vertical deflection. This result further suggests that a fibre composite turnout sleeper at 60 kg/m rail and 600 mm spacing should be supported by a foundation with a U_s of at least 20 MPa or a subgrade of at least good subsoil (gravel). Furthermore, the recommended maximum allowable contact pressure between the sleeper and the ballast of 750 kPa can only be satisfied using a turnout railway sleeper with an $E_{sleeper}$ of at least 3 GPa.

7.8 Conclusions

A simplified three dimensional grillage beam model was used to investigate the behaviour of turnout sleepers with different elastic and support moduli. Turnout sleepers with modulus of elasticity from 1 to 10 GPa for all fibre composites and 10, 15, 20 and 25 GPa for spot replacement on support modulus of 10 to 40 MPa were considered. The results of the numerical simulation suggest that the grillage beam analogy to model the entire turnout system is reasonable as they are producing results comparable to that of other researchers. In all the scenarios investigated, the behaviour of sleepers in railway turnout is most critical between the switch and the frog. The highest bending moment, shear and deflection are produced in this region. Compared to that of the transition sleepers, the magnitude of the bending moment and shear force in turnout sleepers is almost 180% and 250% higher, respectively.

The analyses showed that the changes in the modulus of elasticity and the ballast/subgrade stiffness have a significant influence on the behaviour of turnout

sleepers. The bending moment in turnout sleeper is less affected by the changes in support modulus but affected significantly by changes in the modulus of elasticity. Increasing the support modulus from 10 to 40 MPa resulted in only 15% reduction in the bending moment while the increase in sleeper stiffness from 1 GPa to 10 GPa has resulted in almost 75% increase in the bending moment. The results also indicated that shear force in sleepers is not sensitive both to the changes of the modulus of elasticity and sleeper support modulus. Similarly, sleeper with lower modulus in elasticity and support modulus tend to undergo greater settlement into the ballast.

The results of the FEM analyses provided a basis for an optimum design of fibre composite turnout sleeper alternative. The results suggest that there is no significant difference in the behaviour of sleepers with elastic modulus of 4 to 10 GPa. On the basis of the simulations performed, the fibre composite turnout sleeper should be designed to carry minimum positive and negative bending moments of 19 kN-m and 8 kN-m, respectively and a shear force of 158 kN. Most importantly, it was found that a target modulus of elasticity for the development of a fibre composite sleeper alternative can be as low as 4 GPa provided that the support modulus is at least 20 MPa at 600 mm spacing from the consideration of sleeper/ballast pressure and the requirement for stable track for a maximum total vertical deflection. A spot replacement timber sleeper with this elastic modulus value is also more effective than steel and concrete. Furthermore, the numerical investigation provided information on the location and magnitude of maximum bending moment and shear along the turnout sleeper length which could be very useful in the design and manufacturing of a more cost-effective turnout sleeper.

The critical design values obtained from the extensive numerical simulations are used in the design of full-scale turnout sleepers with different configurations, which is discussed in the next chapter.

Chapter 8

Behaviour of full-scale fibre composite turnout sleepers

8.1 Introduction

Research and development has now focused on fibre composites as this material can be made to have similar usability and design characteristics to hardwood timber with the added advantages. Successful applications of some fibre composite sleepers in actual railways demonstrate the practicality of this technology for mainline sleepers. Nevertheless, much is yet to be learned about the structural performance of these composite materials especially for railway turnout application. In fact, several early developments were not completely successful due to some mechanical property limitations of most composite railway sleepers (Lampo et al., 2003). The extensive work completed on the behaviour of the individual and glue-laminated novel composite sandwich structures suggested that these materials have the strength and stiffness suitable for structural applications. Chapter 7 has also demonstrated that this beam concept can be applied in railway turnout sleeper where only an optimum stiffness is required as this structure is continuously supported by the ballast.

Composite beam has the advantage of allowing the designer to specify different material properties for different parts of the beam cross-section (Lopez-Anido and Xu, 2002). While the properties of the constituent materials of a composite sandwich panels are important key factors in designing laminated structures, the properties of interest in this chapter are the structural performance of the full-scale glue-laminated sandwich beams. Gupta and Siller (2005a, 2005b) suggested that test of small scale specimens is not most of the time representative of the full-scale behaviour of structures. Consequently, Wang et al. (2003) correlated the flexural properties of the large scale laminated veneer lumber (LVL) and of corresponding small specimens through flatwise and edgewise static bending test. They found out that the structural performance of the full scale LVL specimens can be predicted well from the strength and stiffness of small specimens. In contrast, Kamala et al. (1999) and Burdurlu et al. (2007) found out that the bending strength

and stiffness of glue laminated timber is higher than those of corresponding solid timber. Similarly, de Souza et al. (2010) suggested that using the mechanical properties of individual timber components for predicting the structural behaviour of laminated timber structure was not always efficient. In case of fibre composite sandwich structure, the distinct mechanical properties of the skin and the core materials, may considerably affect the overall behaviour of the structure made from these materials, thus it is important to determine the behaviour of full-sized specimens and determine their correlation with the results of the small scale testing.

The evaluation of the ultimate strength and the overall behaviour of full-scale glue-laminated sandwich beams is crucial to its safe and efficient use for railway turnout sleeper application, as well as to its broader use in civil construction. Lampo et al. (2003) suggested that the full-scale testing should be conducted to determine if the fibre composite railway sleeper meets the minimum structural performance specification. Furthermore, Kassa and Nielsen (2008) indicated that a detailed understanding of the structural behaviour of a more durable sleeper material is required to come up with an economical solution for track maintenance. This chapter provides details of the extensive experimental and analytical investigations done which aim to the further understanding of the design and performance issues associated with the eventual application of the glue-laminated sandwich beam for railway turnout sleeper. An evaluation of the suitability of these structural beams for a typical timber railway turnout sleeper is presented in this chapter.

8.2   Development of a full-scale glue-laminated sandwich beams

There have been some developments in the sandwich structure used in the production of full-scale glue-laminated sandwich beam specimens. In Chapters 4 to 6, the investigated composite sandwich panel has a nominal thickness of 20 mm with fibre composite skins of around 1.8 mm thick while the new sandwich panel in Chapter 8 is only 18 mm thick with 3 mm thick top and bottom skins. Thus, the behaviour of the new sandwich structure was verified to have a reasonable estimation of the failure load and prediction of the behaviour of the full-scale glue-laminated fibre composite sandwich beams. The mechanical behaviour of the new generation composite sandwich structures was determined and reported in Appendix G.

8.2.1 The innovative sandwich beam concept

Figure 8.1 shows the different section configurations of the full-scale fibre composite turnout railway sleepers that were considered in this study. Figure 8.1a, 8.1b and 8.1c show a beam section with the composite sandwich panels glued together in the flatwise position, a section with sandwich panels glued together in the edgewise position, and a section with combined sandwich laminations in both flatwise and edgewise positions, respectively. The sections were made by gluing the composite sandwich panels together in different orientations to form the structural beam. These beams were analysed and their structural performance was determined.
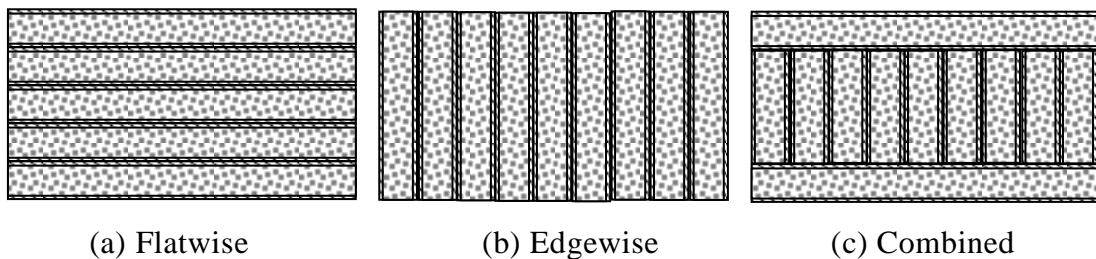
(a) Flatwise	(b) Edgewise	(c) Combined

Figure 8.1 Cross-sections of the full-scale composite sandwich beams

8.2.2 Preparation of full-size sleeper specimens

The full-scale sandwich beam specimens were fabricated by gluing a number of 18 mm thick sandwich panels together as shown in Figure 8.2. The sandwich beams were fabricated with a uniform cross section for turnout sleeper applications as per required by AS 3818.2 (2004). The specimens with flatwise laminations was produced by gluing together 8 sandwich panels while the specimens with edgewise laminations with 13 sandwich panels. The topmost and bottom most laminations in a beam with combined laminations are oriented in the flatwise position to resist bending forces while the middle portion is oriented in the edgewise position to carry shear. After applying the epoxy adhesives and stacking into the required number of laminations, pressure is applied to the assembled specimens using the clamping beds. After post-curing, the adhesive that has squeezed out between the sandwich laminations were removed and planed to smooth out any irregularities between the edges of the specimen. Figure 8.3 shows the actual full-size fibre composite turnout sleeper specimens. Another set of full-scale sandwich beams with fibre wraps was prepared. These specimens have the same configurations as Figure 8.1 but with one layer of 750 g/m^2 tri-axial glass fibre composite (0/+45/-45) wraps.

| (a) Gluing and clamping | (b) Wrapping |

Figure 8.2 Preparation of full-scale glue-laminated composite sandwich beams

Figure 8.3 Full-scale glue-laminated composite sandwich beams

8.2.3 Test specimens

The full-scale composite sandwich beams were produced with nominal dimensions of 150 mm depth and 230 mm width. The specimen tested in flexure has a total length of 2400 mm while the specimen tested under asymmetrical beam shear is 600 mm long. Tables 8.1 and 8.2 list the description of the test specimens in flexure and shear, respectively. In the specimen designation, 4F and AS correspond to specimens tested under static 4-point bending and asymmetrical beam shear, respectively, TS for turnout sandwich, and F, E, and C represent the orientation of the laminations while the W corresponds for the full-scale sandwich beams with fibre wraps.

Table 8.1 Details of full-scale beam specimens for flexural test

Specimen name	Orientation of lamination	Wrapping
4F-TS-F	Flatwise	without wrapping
4F-TS-E	Edgewise	without wrapping
4F-TS-C	Combination	without wrapping
4F-TS-WF	Flatwise	with wrapping
4F-TS-WE	Edgewise	with wrapping
4F-TS-WC	Combination	with wrapping

Table 8.2 Details of full-scale beam specimens for shear test

Specimen name	Orientation of lamination	Wrapping
AS-TS-F	Flatwise	without wrapping
AS-TS-E	Edgewise	without wrapping
AS-TS-C	Combination	without wrapping
AS-TS-WF	Flatwise	with wrapping
AS-TS-WE	Edgewise	with wrapping
AS-TS-WC	Combination	with wrapping

8.3 Full-scale test of fibre composite turnout sleepers

8.3.1 Flexural test

Static four-point bending test were conducted on the full-size fibre composite sandwich beams to determine their flexural strength and stiffness. Figure 8.4 shows the set-up and instrumentation for static bending test. The specimens were simply supported and the load was applied through a spreader beam using a 2000 kN capacity hydraulic jack at a rate of approximately 5 mm/min. The vertical displacement was measured at midspan by using a wire type LVDT (string pot) and uni-axial strain gauges were attached to the top and bottom most surfaces of the specimen to evaluate the strain during loading and until final failure. All specimens were tested beyond peak load to determine the strength and failure mechanisms. The applied load, displacement and strains were recorded using a data logger.
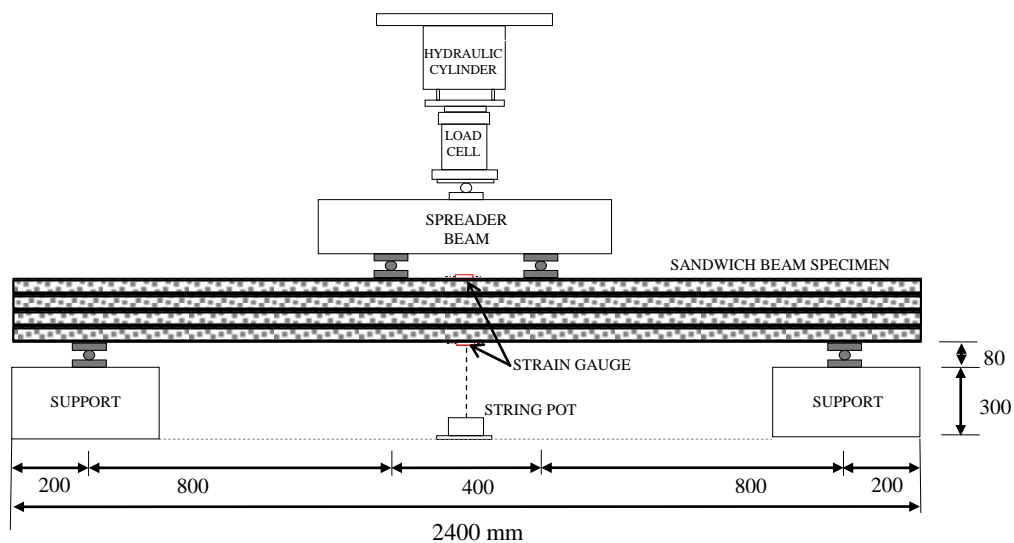
Figure 8.4 Schematic illustration for flexural test of sandwich beams (units in mm)

8.3.2 Shear test

The shear test was performed using an asymmetrical beam shear test following the set-up in Figure 8.5. In all tests, the span for maximum shear is held constant at 150 mm, which is equal to the depth of the full-scale sandwich beams. Resistance strain gauges oriented at $\pm 45^{o}$ to the loading axis were attached to the specimen to evaluate the shear response during the entire loading regime. All the specimens were tested up to failure to determine the shear strength and to observe the mode of failure.
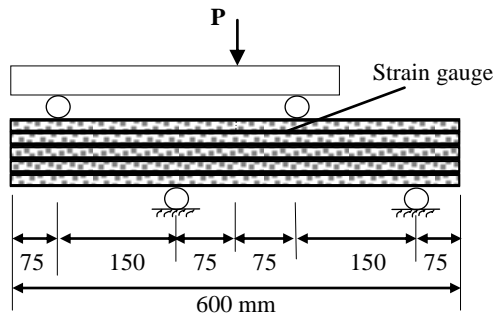
Figure 8.5 Schematic illustration for shear test of sandwich beams (units in mm)

8.4   Experimental results and observations

The results of the experimental investigations on the flexural and shear behaviour of the full-scale sandwich beams are presented here. The strength and failure modes of the beams with different orientation of sandwich laminations are also reported.

8.4.1 Failure load in flexure and shear

Table 8.3 summarises the failure load of the full-scale glue-laminated sandwich beams under 4-point static bending and asymmetrical beam shear tests. The table includes the level at which the first drop in the load was noted as this represents the initiation of failure in the sandwich beam specimens. For all of the specimens tested under asymmetrical beam shear, the first drop in the load corresponds to the maximum load that the sandwich beams could carry. A similar behaviour was observed for specimen 4F-TS-E where the specimen failed immediately after the maximum load was attained.

Table 8.3 Failure load of full-scale composite sandwich beams

Specimen name	Without wrapping (kN)		With wrapping (kN)	
	1st drop	Peak load	1st drop	Peak load
4F-TS-F	162	198	199	204
4F-TS-E	225	225	230	230
4F-TS-C	144	188	184	204
AS-TS-F	512	512	569	569
AS-TS-E	1,314	1,314	1,463	1,463
AS-TS-C	1,121	1,121	1,227	1,227

The results show that the peak load where the specimens 4F-TS-F and 4F-TS-C failed in flexure are the same with the initiation of failure in the specimens with fibre composite wraps. The observed failure behaviour is discussed in detail in the succeeding sections. Based on the result of the experimental investigation, the full-scale specimen with sandwich laminations in the edgewise position has the highest failure load in both flexure and shear among the beam configurations considered. As a general trend, the addition of fibre composite wraps resulted to a higher failure load than the specimens without.

8.4.2 Flexural behaviour of full-scale composite turnout sleepers

8.4.2.1 Load-displacement behaviour

The load and midspan deflection behaviour of the full-scale glue-laminated fibre composite sandwich beams is shown in Figure 8.6. The figure shows that all of the specimens exhibited similar flexural behaviour at the linear portion of the load-deflection curve. The load of all the specimens increased almost linearly with deflection with a slight reduction in stiffness when tensile cracking of the core material occurred. The specimens then continued to carry the load until final failure.

At the compressive failure of the skin, a substantial load reduction was noted in the specimens 4F-TS-F and 4F-TS-C. However, the specimens were able to sustain the increased loading until debonding failure between the topmost compressive skin and the core was observed. For specimen 4F-TS-F, the compressive failure of the topmost skin occurred when the load increased to 162 kN and a deflection of 92 mm resulting to a drop in the load to 152 kN. However, the specimen continued to carry the load and failed at an applied load of 198 kN and a deflection of 137 mm. For

specimen 4F-TS-C, the load increased up to 144 kN and a deflection of 80 mm when the compressive failure of the topmost skin occurred. The specimen then continued to carry the load and failed at an applied load of 188 kN and a deflection of 134 mm. On the other hand, the specimen 4F-TS-E exhibited a two-staged load-deflection behaviour. A slight reduction in stiffness was observed after cracking of the core at a load of around 125 kN and a deflection of 60 mm. The beam then remained elastic with a constant stiffness and failed at an applied load of 225 kN and a midspan deflection of 132 mm due to the simultaneous compressive failure of the skin and crushing of the core material with some tensile splitting of the skins.
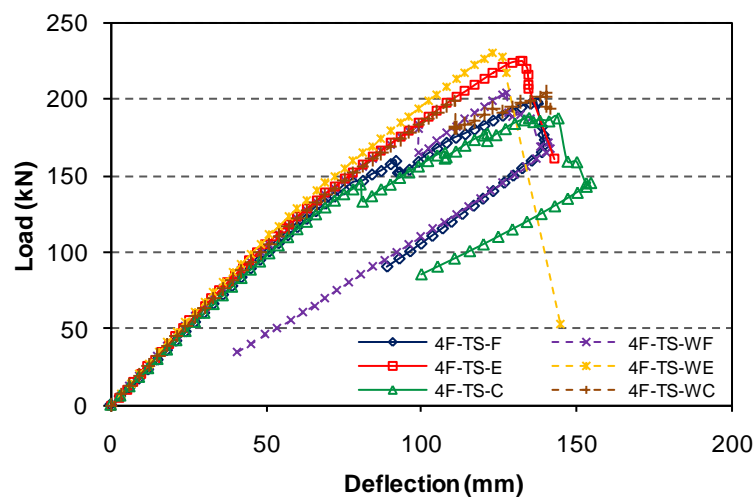
Figure 8.6 Load and midspan deflection relationship of full-scale sandwich beams

The specimens with fibre composite wrap exhibited a slightly higher stiffness and failure load for all the sandwich beam sections considered. The load of specimen 4F-TS-WF, reached to 184 kN and a deflection of 98 mm when a drop in the load was observed but continued to carry the load and ultimately failed at a load of 204 kN and a midspan deflection of 127 mm. The specimen 4F-TS-WC with combined laminations carried a load of 199 kN and deflected by 110 mm at midspan. The load then dropped to 181 kN but increased again until the specimen failed at a load of 204 kN and a deflection of 140 mm. The specimen 4F-TS-WE failed at an applied load of 230 kN and a deflection of 123 mm.

8.4.2.2 Displacement and longitudinal strain relationship

The midspan displacement and longitudinal strain relationship of the full-scale sandwich beams is shown in Figure 8.7. Only the displacement and the longitudinal

strain at the topmost and bottommost skin layers of the specimens without fibre composite wrap are shown for comparison. The experimental results showed that the bending stiffness of all full-scale sandwich beams is almost the same as the shape of the displacement-strain relation curve. It can also be observed from the figure that the displacement-strain relation increases linearly for all the specimens tested for tensile strain less than 12400 microstrains and the relation becomes non-linear thereafter. This level of strain is similar to that of the failure strain in flexure of the core material established from coupon tests, thus it is expected that flexural tensile cracks at the core material will develop at this level of strain, the strain gauge directly bonded to the tension side of the core material in specimen 4F-TS-E broke. On the other hand, the flexural cracking of the core material resulted in a non-linearity at the tensile and compressive strains for specimens 4F-TS-F and 4F-TS-C. In these specimens, the strain gauge on top of the sandwich beam broke at a strain of over 15000 to 17000 microstrains indicating the compressive failure of the topmost fibre composite skins. These failure strains are similar to the failure strains observed for individual sandwich structures. However, the maximum strain at which the specimen failed was not captured by the strain gauges attached to the sandwich beams especially for specimen 4F-TS-E. In lieu of this, the complete load-deflection curve was recorded for all the specimens, allowing the determination of the failure load, maximum deflection and failure strains.
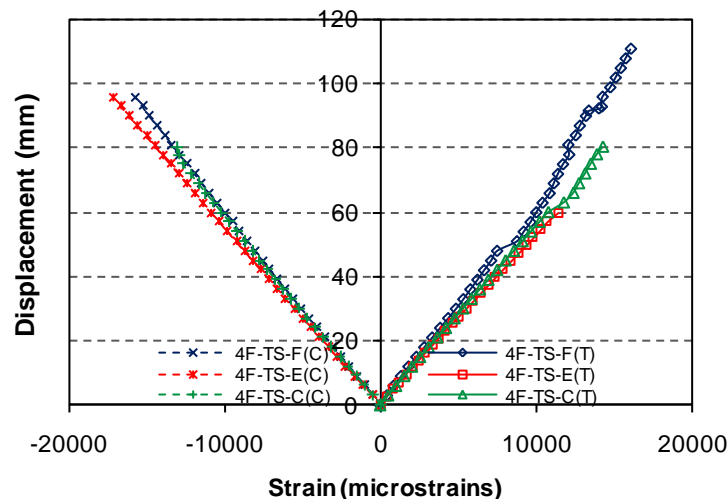
Figure 8.7 Displacement and strain relationship of full-scale sandwich beams

8.4.2.3 Failure behaviour in flexure

Figures 8.8 to 8.10 show the failure behaviour of the full-scale glue-laminated beams under the static 4-point bending test. Flexural cracks were observed in the core material of the bottommost sandwich laminations in specimen 4F-TS-F but this did not lead to failure. The increasing load caused the propagation of the cracks to the core of the next sandwich layers indicating continual stress redistribution among the sandwich laminations. The specimen then failed by compressive failure of the topmost fibre composite skin (Figure 8.8a). However, the failed fibre composite skin was restrained by the two loading plates which made the beam continue to carry the load. It was concluded that if this did not happen, the specimen could have failed after the initial compressive failure of the topmost skin. The final failure of the specimen is due to the debonding of the fibre composite skins near the loading plates outside the constant moment region (Figure 8.8b).

In specimen 4F-TS-E, tensile cracks of the phenolic core were observed at a load of 100 kN. The vertical fibre composite skins prevented the tensile cracks in the core from widening to cause failure however, compressive failure on the outermost fibre composite skins was then observed at the constant moment region. The continuous application of the load caused the fibre composite skin to debond from the core material and made the detached skins to buckle. Simultaneously, tensile cracks in the core and the skin in the bottom tension zone of the sandwich beams developed. The final failure of the sandwich beams with edgewise laminations occurred with a combined failure mode that involves the buckling and debonding of the compressive skin in the outermost laminations and the crushing of the core material, leading to the total collapse of the beam (Figure 8.9).

A similar failure behaviour was observed between specimens 4F-TS-C and 4F-TS-F. The sandwich laminations in the topmost and the bottom most layers of these two beam sections carry the flexural load. At the lower level of applied load, flexural cracks were developed in the core material of the bottom most sandwich laminations followed by the compressive failure of the topmost fibre composite skin (Figure 8.10a). In contrast to specimen 4F-TS-F wherein the flexural cracks in the core material propagated to the core of the next sandwich layer, crack extension was not possible in a section with combined sandwich laminations due to vertical skins of the edgewise sandwich laminations. This has resulted to the concentration of the flexural cracks occurring at the bottom most sandwich laminations leading to a high

flexural stress in the topmost and bottom most skin layers. The debonding of the top and bottom flatwise sandwich laminations between the inner edgewise sandwich laminations was also observed at the final failure (Figure 8.10b). This debonding failure was attributed to the high compressive stresses at the topmost layers which resulted in the buckling of the flatwise sandwich laminations.
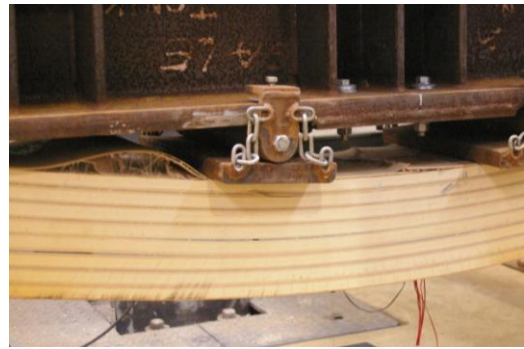
(a) Compressive failure of top skin   (b) Debonding of top skin

Figure 8.8 Failure of specimen 4F-TS-F

Figure 8.9 Failure of specimen 4F-TS-E

(a) Compressive failure of top skin   (b) Buckling of sandwich layers

Figure 8.10 Failure of specimen 4F-TS-C

The specimen with fibre wraps showed similar failure behaviour to the unwrapped ones in all the investigated section configurations. The failure behaviour of the beams with fibre wraps are shown in Figures 8.11 to 8.12. The failure of all the specimens was initiated at the compressive part at the location of maximum bending moment. The fibre wraps increased the capacity of the beam by delaying the failure of the topmost fibre composite skin. After the compressive failure of the skin, progressive failure of the fibre wraps immediately followed (Figure 8.11a). There are several points of debonding failure observed between the fibre wraps and the specimen at the compressive side which was followed by the splitting of the fibre wraps in tension (Figures 8.11b and 8.12b). The final failure of specimens 4F-TS-WF and 4F-TS-WC are the debonding failure of the topmost skin and tensile failure of the bottommost skin. The compressive skin at the outermost sandwich laminations of specimen 4F-TS-WF exhibited local buckling leading to the debonding failure. The splitting of the tensile fibres was also observed at the bottom portion of the beam however, the final failure of this specimen was due to the simultaneous compressive failure of the skins and the crushing of the core (Figure 8.12a).
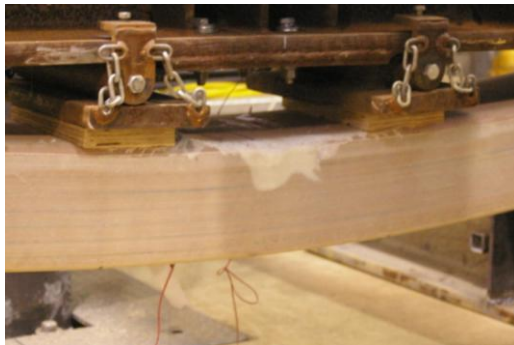
| (a) Compressive failure of skin | (b) Tensile failure of bottom skin |

Figure 8.11 Failure of specimen 4F-TS-WF

| (a) Specimen 4F-TS-WE | (b) Specimen 4F-TS-WC |

Figure 8.12 Failure of specimens 4F-TS-WE and WC

8.4.3 Shear behaviour of full-scale composite turnout sleepers

The behaviour of the full-scale glue-laminated sandwich beams under asymmetrical beam shear test is discussed in this section.

8.4.3.1 Load and crosshead displacement behaviour

Figure 8.13 shows the load and crosshead displacement behaviour of the full-scale glue-laminated sandwich beams under asymmetrical beam shear test. The figure shows the initiation and the final failure in the sandwich beam specimens as represented by the load drop in the load-crosshead displacement relation curve. For specimens AS-TS-F and AS-TS-WF, the load increased linearly with the displacement of the crosshead until final failure. A sudden drop in the applied load was observed which indicated the final failure of the specimens. For specimens AS-TS-F and AS-TS-C, the load increased linearly with the crosshead displacement but became non-linear at higher load. This non-linear behaviour is due to the initiation of shear failure in the vertical skins and the phenolic core going into nonlinear region in compression with some indentation failure under the loading point and at the support at the location of maximum shear. For specimens AS-TS-WF and AS-TS-WC, a more linear relation between the load and crosshead displacement was observed than their corresponding sandwich beam specimens without fibre composite wraps. An abrupt drop in the load was observed after the maximum load was reached indicating the final failure of the sandwich beam specimens. In specimens AS-TS-E and AS-TS-WE, a rapid reduction in resistance was observed after obtaining the peak load, which is characteristic of a shear failure.
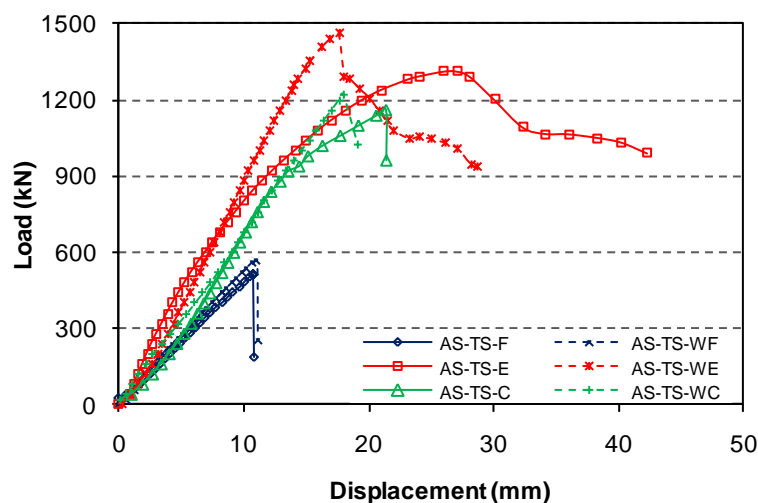
Figure 8.13 Load and crosshead displacement relation of full-scale sandwich beams

In general, a slightly stiffer load and crosshead displacement relation curve was observed in the specimens with fibre composite wraps than those without. The behaviour of all the specimens with fibre wraps is almost linear up to the peak load and failed at a higher load than their sandwich beam counterpart without fibre wraps.

8.4.3.2 Load and shear strain behaviour

Figure 8.14 shows the load and shear strain relation curve for the full-scale glue-laminated sandwich beams. The shear strain is determined from the indicated normal strains of the $\pm 45^{\circ}$ strain gauges attached to the specimen. The results showed that the load in sandwich beam with flatwise lamination increased almost linearly with strain up to failure. The specimen AS-TS-F failed at a shear strain of around 8000 microstrains, a level of strain is similar to the failure strain at which the phenolic core material fails in shear. Similarly, the load and shear strain relation curve of specimens AS-TS-E and AS-TS-C are linear at the initial application of the load but showed non-linearity at higher strains. The additional fibres provided by the wrap cause a slight increase in the shear stiffness of the specimens and resulted in a higher load. In general, all the specimens failed almost immediately when shear failure in the specimens was observed as indicated by the immediate failure of the strain gauges attached.
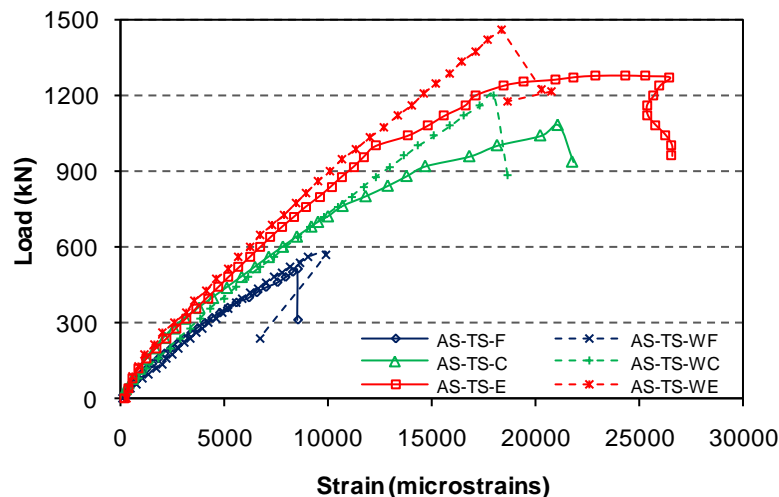
Figure 8.14 Load and shear strain behaviour of full-scale sandwich beams

8.4.3.3 Failure behaviour in shear

Figures 8.15 to 8.17 show the failure of full-scale sandwich beam specimens under asymmetrical beam shear test. The three section configurations showed different

failure behaviours. The failure is typically initiated at the maximum shear region between the inner support and the loading points. The failure was defined by the development of visible crack with the associated decrease in the measured load. The specimen AS-TS-F showed very brittle failure behaviour. It failed abruptly due to shear failure of the core (Figure 8.15a) which in most cases is accompanied by a loud noise with a distinct drop in the applied load and without warning. In contrast, specimens AS-TS-E and AS-TS-C failed more gradually as seen on the load-crosshead displacement curve. The failure of the individual laminations in these specimens was both audible and visible and the shear failure of the skins caused a slight drop in the applied load. This kind of failure behaviour is progressive, which is preferred in structural beam applications. The specimen AS-TS-E failed due to shear failure of the fibre composite skins and the core with some delamination failure between the individual sandwich laminations (Figure 8.16a).

In specimen AS-TS-C, shear failure of the outermost skins in the inner laminations (in the edgewise position) was observed. The continuous application of the load caused the debonding at final failure. The debonding occurred simultaneously in both the top and bottom sandwich laminations (Figure 8.17a). This debonding failure can be attributed to the difference in the shear rigidity of the sandwich beams in different orientations. It can be concluded that the failure was precipitated by the shear failure of the structural adhesive. This is expected as the shear strength of vertical fibre composite skins is higher than the shear strength of the epoxy adhesives. The shear strength of structural epoxy is around 20 MPa (Appendix D) while the shear strength of fibre composite skins is around 28 MPa. Although the specimen showed higher shear strength than the specimen with flatwise laminations, this case illustrates the importance of quality of bonding on the shear strength of glue-laminated sandwich structures.

It is more difficult to detect shear cracks and follow their paths within the specimen with fibre composite wraps compared to the specimens without wraps. Some indentation in the reaction and loading points at the location of maximum shear were observed, however, all of the specimens ultimately failed dominantly in shear. The failure behaviours of specimens with fibre composite wraps are very similar to the specimen without as shown in Figures 8.15b, 16b and 17b. However, the addition of fibre wrap resulted to a failure occurring at a slightly higher load than their unwrapped sandwich beam counterparts.

(a) Without wrapping	(b) With wrapping

Figure 8.15 Failure of specimen 4F-TS-F

(a) Without wrapping	(b) With wrapping

Figure 8.16 Failure of specimen 4F-TS-E
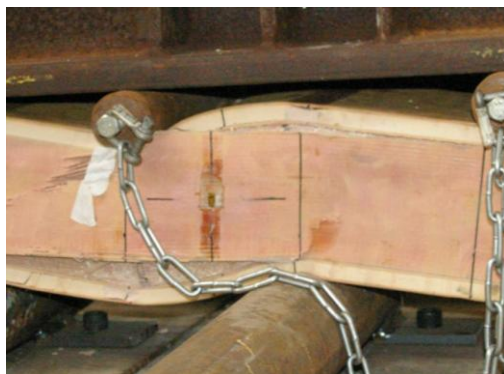
(a) Without wrapping	(b) With wrapping

Figure 8.17 Failure of specimen 4F-TS-C

8.5 Discussions

The effects of the 3 different section configurations on the flexural and the shear behaviours of the full-scale glue-laminated composite sandwich beams are discussed. The effect of fibre wraps on the behaviour of the sandwich beams is also considered.

8.5.1 Effect of the orientation of sandwich laminations on flexural behaviour

The effect of the orientation of sandwich laminations on the flexural behaviour of the glued sandwich beams was evaluated. The effective bending stiffness, $(EI)_{eff}$ was determined from the linear elastic portion of the load-midspan deflection curve in Figure 8.6 and was calculated using the relation given in equation 6.3. This was then divided by the moment of inertia of the beam to determine the effective modulus of elasticity E_{eff}. In the calculation of $(EI)_{eff}$ and E_{eff}, the glued sandwich beam is assumed as a solid homogenous section with perfect bonding. The EI_{eff}, E_{eff} and the maximum bending moment M_{max} are reported in Table 8.4.

Table 8.4 EI_{eff}, E_{eff} and M_{max} of full-scale composite sandwich beams

Specimen	EI_{eff} $(x10^9)$,Nmm^2	E_{app}, kN/mm^2	M_{max}, kN-m
4F-TS-F	322	5.01	79.55
4F-TS-E	340	5.19	90.05
4F-TS-C	326	5.05	75.26
4F-TS-WF	336	5.03	81.62
4F-TS-WE	352	5.20	92.16
4F-TS-WC	338	5.07	81.85

The table shows there is an insignificant difference in the bending stiffness of the full-scale sandwich beams with different section configurations. This is similar to the findings of Burdurlu et al. (2007) and de Souza et al. (2009) wherein they found no differences between the modulus of elasticity values of a laminated veneer lumber (LVL) with different ply organisation when loaded perpendicular (flatwise) and parallel (edgewise) to the glue lines but a slightly higher bending strength in the edgewise position. This result also confirms the earlier findings in Chapter 6 where the stiffness of glue-laminated beams with flatwise and with edgewise sandwich laminations converge with increasing number of sandwich laminations. Furthermore, the vertical fibre composite skins in the specimens with edgewise sandwich

laminations prevented the formation of tensile cracks in the core resulting to an almost constant stiffness of the beam until final failure. An overall reduction in stiffness was observed when flexural cracking of the core occurred in specimens 4F-TS-F and 4F-TS-C. This result suggests that the specimen with edgewise sandwich laminations offers a more constant stiffness throughout the whole loading regime among the different sandwich configurations investigated.

The effects of sandwich orientation on the failure load appear more remarkable in the experimental investigation. The specimen 4F-TS-E failed with the highest bending moment among the different sections investigated. The high failure load of specimens with edgewise sandwich lamination is due to the presence of the vertical skins which increases the loading capacity of the beams. On the average, the specimens with edgewise sandwich laminations is 20% stronger than that of specimens with flatwise and with combined sandwich laminations.

The failure behaviour of all the specimens depends largely on the compressive strength of the skins. In specimens 4F-TS-F and 4F-TS-C, the flatwise sandwich laminations at the topmost and bottommost layers were subjected to the highest bending stresses. Since the fibre composite skin has lower compressive strength than tensile strength, the topmost sandwich layer became the weakest link among the sandwich laminations which eventually controls the overall system strength. The specimen with edgewise sandwich laminations is the most reasonable beam configuration amongst the investigated sandwich beams when stiffness and maximum load are taken into account. This section configuration is also the easiest to manufacture especially if a certain dimension needs to be followed like in spot replacement where the depth of the beams should match the depth of existing turnout timber sleepers.

8.5.2 Effect of the orientation of sandwich laminations on shear behaviour

Bendsten and Porter (1978) observed the effect of orientation on the shear strength of dimensional lumber with the shear strength in the edgewise position significantly stronger than in the flatwise position. Using the five point bending test to evaluate the mechanical properties of LVL, Bradtmuller et al. (1998) concluded that it is inherently more difficult to induce shear failure in joist oriented (edgewise) LVL than in plank oriented (flatwise) LVL. These observations also emerged in the experimental investigation which confirmed that the orientation of sandwich

laminations has a predominant effect on the shear behaviour of glue-laminated sandwich beams. The shear strength of specimens AS-TS-E and AS-TS-C is more than doubled than that of specimen AS-TS-F (see Table 8.2) under asymmetrical beam shear test. This is due to the contribution of the vertical fibre composite skins of the sandwich laminations oriented in the edgewise position in carrying the shear. The effectiveness of vertical skins to carry shear has already proven effective in increasing the shear capacity of structures when Triantafillou (1997) externally bonded CFRP laminates to structural timber members in the critical shear zones. One of the requirements in producing fibre composite sleepers is that, it should not split or crack in any way requiring replacement of the sleeper (Lampo et al., 2003). This clearly shows that the glue-laminated composite sandwich beams with edgewise laminations are very promising from a shear strength point of view.

8.5.3 Effect of fibre composite wraps on structural behaviour

Several studies have shown that structural members fully wrapped with fibre composites showed a significant improvement in structural performance. Issa and Kmeid (2005) indicated that the behaviour of glulam wood beams covered with CFRP is totally different from the uncovered ones. The 1% increase in area due to the additional fibres has changed the failure mode and increased the capacity of the beams by 56%. However, it is important to note that the strength and stiffness of carbon fibres are significantly higher than the glass fibres. Ticoalu (2008) found out that wrapping the glue-laminated LVL and carbon fibre laminate with glass fibres contributed to the strength and to some extent to the stiffness of the beams. The 7.5% increase in area resulted to a 25% increase in strength but only 2.6% in stiffness. According to Gezer and Aydemir (2010), the increase in bending stiffness of most structures wrapped with fibre composites is due significantly to the change of dimensions of the specimen while the increase in strength can be attributed to the local bridging effects and some confining action of the fibre composite wraps.

In glue-laminated sandwich beams, it was found that the fibre wraps has minimal effect on the bending stiffness and strength but has a more pronounced effect on the shear strength. The slope of the load-deflection curve in Figure 8.6 shows slightly stiffer beams for specimens with fibre wraps than specimens without. However, there were insignificant differences on the elastic modulus between the beams with and without wraps due to the amount of the fibre wraps is small.

Figure 8.18 shows the effect of fibre wrap on the bending and shear strengths of sandwich beams. In this figure, F, E and C correspond to the sandwich beam orientation in flatwise, edgewise and combination, respectively. The final failure load in bending is approximately equal for all specimens with and without wraps except for beams with combined laminations which exhibited an almost 7% higher strength for specimen with wrap than their unwrapped counterpart (Figure 8.18a). Wrapping the beams with one-layer of glass fibres resulted in an increase in bending strength of 20% and 40% for beams with flatwise and combined laminations respectively, but with no significant increase in specimens with edgewise laminations. The bridging effect exerted by the fibre wraps inhibits the compressive buckling of the topmost skin, and consequently resulted in a higher load than specimens without wrap. This showed that the fibre wraps acted similar to the loading rollers during testing which prevented the compressive failure of the skin to propagate but could not prevent the debonding failure of the skins. Furthermore, the fibre wraps could not prevent the compressive failure and crushing of the core of the beams with edgewise laminations resulting in a similar failure load for both specimens with and without wrap.

The sandwich beams with fibre wraps showed higher failure load than the specimens without wraps under asymmetrical beam shear. The two additional layers of glass fibre laminate on both vertical sides of the beams have resulted in an increase of almost 10% in shear strength in all the tested specimens (Figure 8.18b). However, the failure of all the specimens tested with and without fibre wraps are almost the same. It is concluded that the fibre wraps only increases the shear strength of the beams due to the additional fibres but did not affect its failure behaviour.

(a) Bending strength   (b) Shear strength
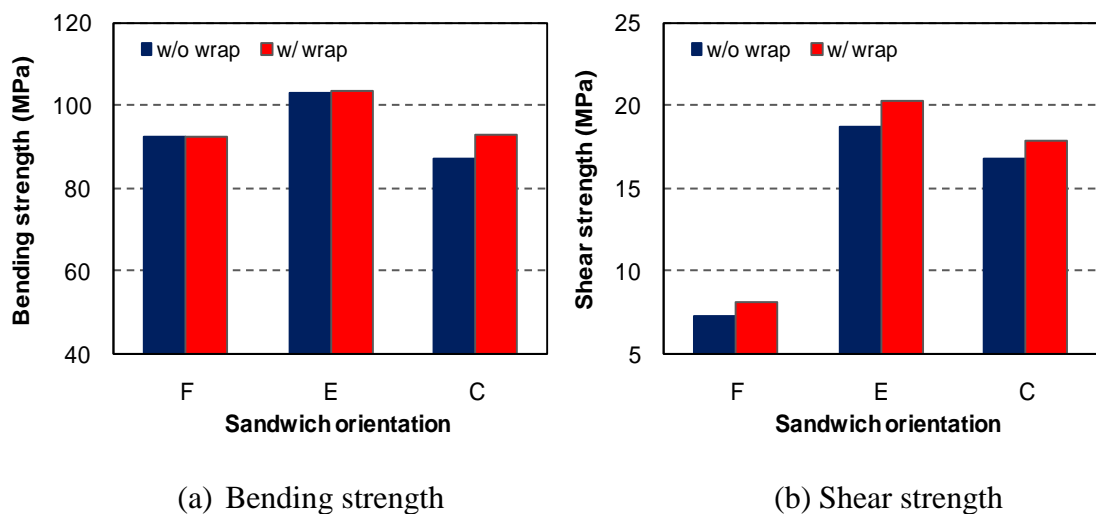
Figure 8.18 The effects of fibre wraps on sandwich beam behaviour

8.5.4 Properties of full-scale sandwich beams in comparison with structural timber

The performance of the full-scale fibre composite sleepers was assessed by comparing their performance with that of timber sleepers and the commercially available fibre composite sleepers in Table 2.3. The effective structural properties of the glue-laminated composite sandwich beams determined experimentally are listed in Table 8.5. The mechanical properties of the turnout sleeper section made up of glue-laminated composite sandwich structures are higher than the minimum performance requirements for fibre composite sleepers recommended by the AREMA (2003b). Moreover, the new fibre composite section has properties far better than the commercially available fibre composite sleepers, except for one with higher strength and stiffness. Furthermore, the low mechanical properties of most of the currently available fibre composite sleepers indicate that they are not suitable for turnout application. This further justifies the need to develop a more cost effective fibre composite railway turnout sleeper with an approved structural performance.

Table 8.5 Structural properties of the glue-laminated sandwich beams

Property	Flatwise	Edgewise	Combination	Timber
Elastic modulus (GPa)	5.01	5.19	5.05	7 – 26
Bending strength (MPa)	75.48	103.19	66.76	64 – 160
Shear strength (MPa)	7.32	18.74	16.82	2 – 7

The strength and stiffness properties of the glue-laminated sandwich beams were also compared to the design properties of the structural timber listed in Australian Standards AS 1720.1 (1998) and the timber grade and performance requirements for timber sleepers in accordance with AS 3818 Parts 1 and 2 (1998). Comparing the investigated sandwich beam configurations with the established properties of existing timber turnout railway sleepers, all the sandwich beams were within the strength grade of the hardwood timber sleepers. The comparison showed that the strength properties of the glue-laminated sandwich beams with flatwise and with combined laminations are similar or higher than that of the stress-grade F22 structural timber while the strength properties of the sandwich beams in the edgewise position are comparable to that of the stress-grade F34 structural timber. This satisfies the minimum requirement of using only stress-grades F17 or higher for special sleepers in a railway turnout as specified by AS 3818 (1998). However, the

elastic modulus of all the sandwich beam concepts is lower than that of the lowest stress grade or F4 structural timber. In Chapter 7, it was found out that only a minimum elastic modulus of 4 GPa is needed for the allowable vertical deflection and ballast/sleeper pressure. Thus, all beam concepts satisfy the minimum elastic modulus requirement of an alternative sleeper for railway turnout application.

The evaluation of the behaviour of the full-scale fibre composite sandwich beams was performed to determine their suitability for replacement timber railway sleepers. The entire structure or portion of the structure is required to meet specific structural performance objectives which are evaluated based on established performance criteria and on an appropriate factor of safety or a structural reliability index. Table 8.6 summarises the design parameters and safety factors for composite turnout sleepers. Considering a standard size of timber turnout sleepers of 150 mm x 230 mm, these loadings will create bending and shear stresses of 22.03 MPa and 4.6 MPa, respectively. Bank (2006) suggested that for designing structural FRP beams, the safety factors for allowable stress design should be applied. Therefore only the beams with edgewise and with combined sandwich laminations could satisfy these performance criteria for railway turnout sleeper application if these safety factors as performance indices for fibre composite sandwich beams are considered. These results suggest that the sandwich beam section can be further optimised for the final design and in the production of prototypes to put this technology in practice.

Table 8.6 Critical design parameters and safety factors for turnout sleepers

Description	Design values	Safety factor (Bank, 2006)
Stiffness	4 GPa	1
Bending	19 kN-m	2.5
Shear	158 kN	3

8.6   Evaluation of the fibre composite turnout sleeper behaviour

Theoretical evaluation and numerical modelling of the flexural and shear behaviour of the full-scale sandwich beams were conducted in parallel to the experimental investigation. In the theoretical and numerical simulations, the mechanical properties and the observed behaviour of the individual new composite sandwich structures were considered.

8.6.1 Fibre Model Analysis

The theoretical failure load and the flexural behaviour of the full-scale glued-laminated composite sandwich beams were predicted using the simplified FMA in Section 6.5.1. In the FMA, the constitutive behaviour of the core in Figure 4.10b and the glass fibre composite skin in Figure 6.14 were used in the analysis. However, the modulus of elasticity of the fibre composite was adjusted to 12.82 GPa as explained in Appendix G.1. Under static bending, the maximum strain and stress criteria are used to predict the failure of the glue-laminated sandwich beams. It is assumed that the compressive failure of the skin occurs when the topmost strain reaches 15600 microstrains while the tensile failure occurs at 18700 microstrains. These correspond to the compressive and tensile stresses of 200 MPa and 240 MPa, respectively which are similar to the failure stresses for the previously tested sandwich structures. The contribution of the core in tension in flatwise beams was neglected when the core cracks while only the cracked core section is neglected for edgewise beams.

8.6.2 Theoretical prediction of shear strength

The prediction equation for shear strength based on the shear properties of the skin and the core materials proposed in Section 6.5.2 was adopted in the estimation of failure load of the full-scale composite sandwich beams under asymmetrical beam shear test. The failure load in shear was calculated using equation 6.6 for specimen with sandwich laminations in the flatwise position while the failure load in shear of the composite sandwich beam with edgewise laminations was calculated using equation 6.7. The possible interaction of sandwich laminations in the flatwise position was not accounted for while it was factored for sandwich laminations in the edgewise position. As found out in Chapter 6, a predicted load closer to the actual failure load can be obtained if the percentage increase in gluing the sandwich beams in the edgewise position is accounted for. In ASTM D 245 (2006), it is suggested that a "*multiple member system*" factor of 1.15 can be applied to design stresses for beams with two or more parallel members provided that an effective connection between each of the individual elements exists. These two equations were combined to calculate the failure load of the sandwich beam with combined laminations. In this beam, the shear strength of the top and bottom flatwise laminations was calculated using equation 6.6 and added to the shear strength provided by the edgewise laminations in the inner portion of the beam which was calculated using equation 6.7.

8.6.3 Finite element modelling and verification

The numerical modelling of the flexural and shear behaviour of the full-scale composite sandwich beams was performed using Strand7 finite element software in the FCD-XPP-034 computer (CPU-Intel P4). The details and assumption of the FE simulation for full-scale composite sandwich beams are presented in Appendix E.2.

8.7 Predicted results and comparison with experiments

The results of the analytical prediction and numerical simulations on the flexural and shear behaviour of full-scale glue-laminated sandwich beams are presented in this section. Only the behaviour of specimens without wrap is considered and correlated with the experimental results.

8.7.1 Failure load of full-scale beams

Table 8.7 summarises the actual and the predicted failure loads under 4-point static bending and asymmetrical beam shear tests of the full-scale glued sandwich beams. The load where compressive failure of the skins was observed in the experimental investigations was considered to be the failure load of the sandwich beams.

Table 8.7 Comparison of actual and predicted failure load of full-scale beams

Specimen	Failure load (kN)		
	Actual	Predicted	FEM
4F-TS-F	162	162	160
4F-TS-E	225	208	210
4F-TS-C	144	167	160
AS-TS-F	512	487	490
AS-TS-E	1,314	1,291	1300
AS-TS-C	1,121	1,098	1100

The compressive failure of the skin for specimen 4F-TS-F occurred at a load of 162 kN. This is very similar to the failure load predicted using the simple FMA and FEM simulations. On the other hand, the predicted failure load of specimen 4F-TS-E using the modified constitutive behaviour of the bonded skins is almost 8% lower than the actual. The higher actual load than the predicted values could be due to the gluing together of the composite sandwich beams which resulted to a more stable and

stronger section. This can also be due to the variation of the estimated values of the mechanical properties of the new composite sandwich panel. In specimen 4F-TS-C, the results of the FMA and FEM analyses gave a predicted load 16% higher than the actual failure load. The high discrepancy between the predicted and the actual load could be due to the complex behaviour of the beam with combined sandwich laminations which could not be accounted for in the simplified FMA and the FEM simulation. In general, the two simplified method of analyses gave a reasonable value for the failure load of the full-scale glue-laminated composite sandwich beams.

The results suggest that the shear strength of the full-scale sandwich specimens can be predicted reasonably based on the shear properties of the constituent materials. The difference between the predicted and the actual load for all specimens is only between 2 and 5%. Furthermore, a factor of slightly over 1.2 appeared to be more appropriate to account for the increase in shear strength of composite sandwich beams bonded together in the edgewise position.

The FEM simulations were successful in the estimation of the failure load of the full-scale composite sandwich beams under asymmetrical beam shear test. The predicted failure load of all glued sandwich beam specimens is only 2-4% lower than the actual failure load. This shows that the estimated shear strength for all sections investigated is conservative and the assumptions used in the analysis are valid..

8.7.2 Predicted behaviour in flexure

8.7.2.1 Load-deflection behaviour

Figures 8.19 to 8.21 show a series of load–deflection curves comparing the experimental with the predicted measurements from the FMA and FEM simulations. The figures show that the predicted load-deflection relations are in good agreement with the experimental results for all sandwich beams especially before any failure was observed in the specimens. The load increases with deflection until cracks in the core developed and resulted in a slight decrease in the bending stiffness which was represented by a small kink in the load-deflection curve.

The predicted load-deflection behaviour of specimen 4F-TS-F agreed very well with the experimental results. As shown in Figure 8.19, the difference in the predicted and the experimental load-deflection curve is only 2-3%. This discrepancy in the load-deflection behaviour slightly increases before compressive failure of the skin was observed. This could be due to the initiation of debonding between the skin

and the core which reduces the stiffness of the beam. This complex behaviour could not be predicted using the proposed simplified analysis and even with the FEM simulations. Furthermore, the simplified analysis and the finite element model are unable to predict the load-deflection response after compressive failure of the topmost skin as both analyses considered this as the final failure of the specimen.

Figures 8.20 and 8.21 show that the difference between the predicted and the actual load-deflection behaviour for specimens 4F-TS-E and 4F-TS-C can go as high as 5%. The high difference in the behaviour of beams with edgewise laminations has been explained in Chapter 4 where it was observed that the vertical skin is subjected to both tension and compression. The difference was more noticeable at higher applied load due to the initiation of failure in the actual beams. In general, there is good agreement between the experimental and the predicted results in terms of values and trend, with the FMA and FEM being slightly higher than the actual.
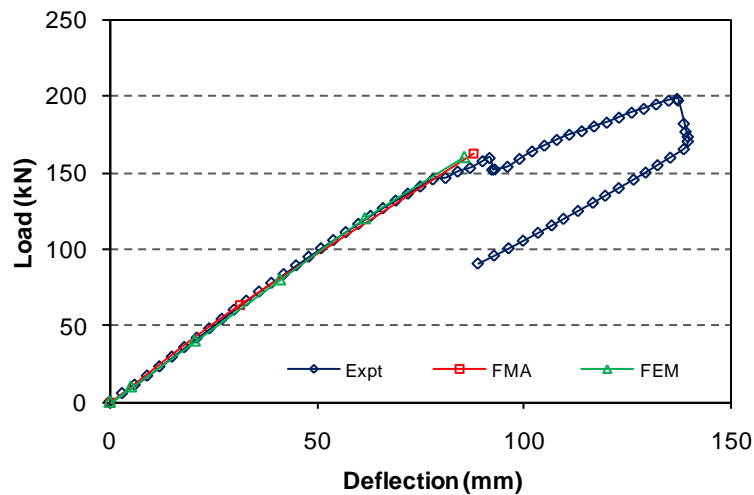
Figure 8.19 Load and midspan displacement relationship of specimen 4F-TS-F
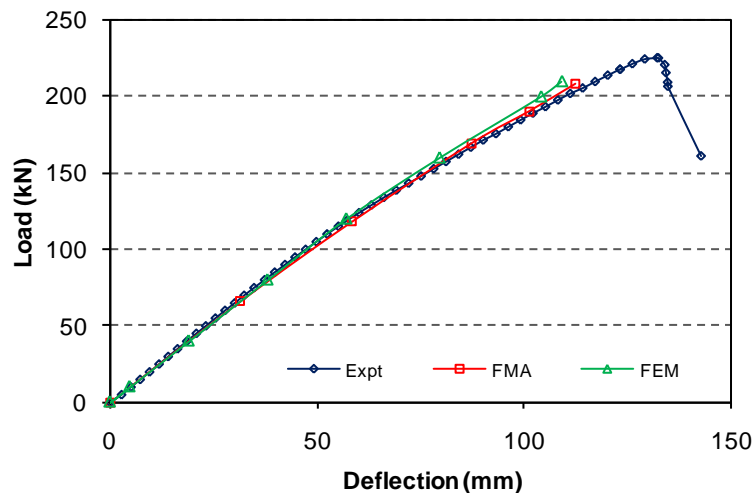
Figure 8.20 Load and midspan displacement relationship of specimen 4F-TS-E
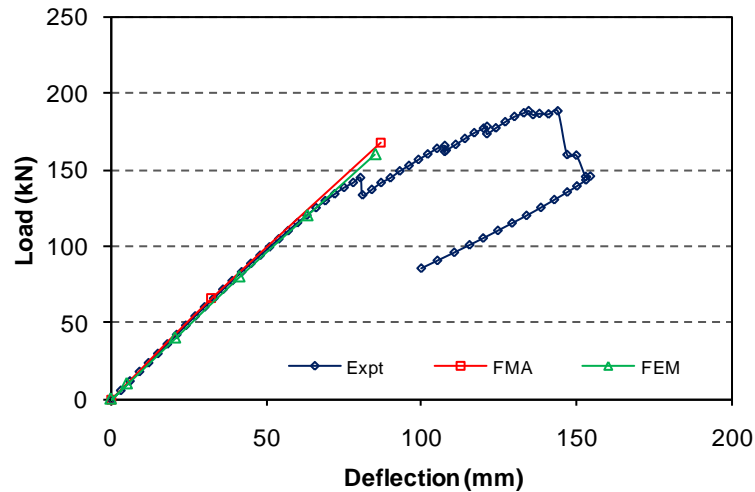
Figure 8.21 Load and midspan displacement relationship of specimen 4F-TS-C

8.7.2.2 Load and longitudinal strain relationship

The comparison of the predicted load and longitudinal strain relationship determined using FMA, FEM and based on the experimental results of specimens 4F-TS-F, 4F-TS-E and 4F-TS-C are shown in Figures 8.22 to 8.24, respectively. The different figures show that the predicted and the actual bending strains in the topmost and bottommost skins are matching well at all levels of applied load and up to failure of the strain gauges. At a tensile strain of around 12000 microstrains, the strain gauge at the tension side of the specimen broke indicating the development of flexural cracks in the core. Non-linearity in the tensile and compressive strains was then observed indicating the further development of cracks in the sandwich beams. Furthermore, a significant drop in the load at a compressive strain of around 15000 microstrains indicates the compressive failure of specimens 4F-TS-F and 4F-TS-C (Figures 8.22 and 8.24). This failure strain is similar to the failure strain of constituent materials established from the test of coupons and to the observed behaviour in individual sandwich beams. On the other hand, the maximum predicted longitudinal strains for specimen 4F-TS-F could not be compared to the results of the experimental investigation as the strain gauges attached to the specimen broke before the final failure (Figure 8.23). The results still showed that the simplified FMA and FEM can predict the load-strain behaviour of the full-scale glue-laminated sandwich beams with a small discrepancy from the experimental results. The discrepancies between the predicted and the actual behaviour can be attributed to the variation in the dimension of the specimens and the estimated value of mechanical properties of the new composite sandwich panel.
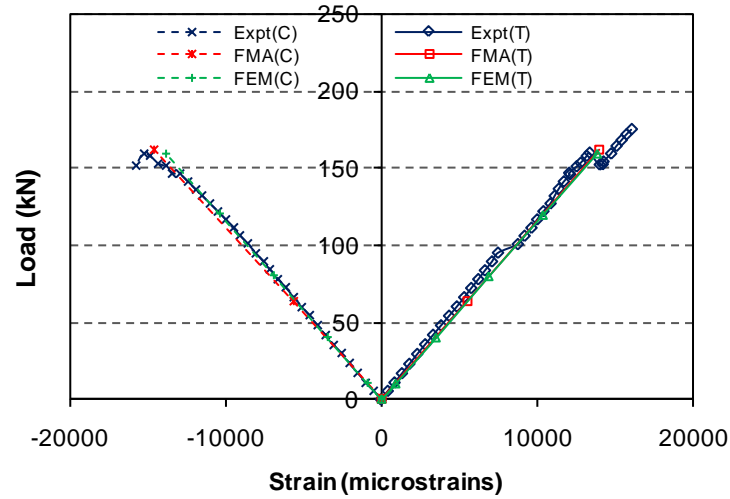
Figure 8.22 Load and longitudinal strain relationship of specimen 4F-TS-F
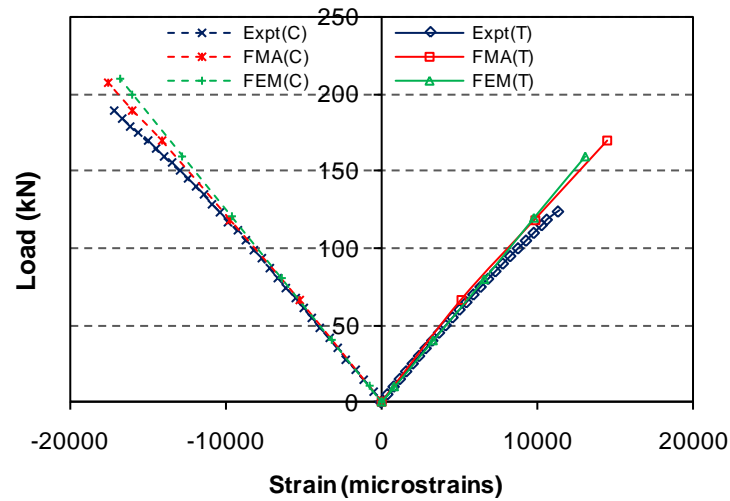
Figure 8.23 Load and longitudinal strain relationship of specimen 4F-TS-E
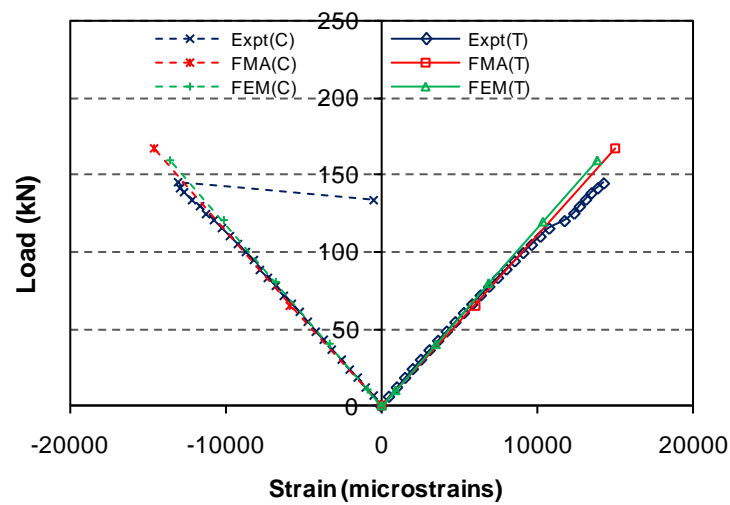
Figure 8.24 Load and longitudinal strain relationship of specimen 4F-TS-C

8.7.2.3 Predicted failure behaviour

The flexural stress contours of the full-scale sandwich beams under static 4-point bending test determined from FEM simulations are shown in Figures 8.25 to 8.27. The predicted failure mechanisms of the sandwich beams showed a good agreement with the experimental results. The actual failure mode in the experimental work consisted of the compressive failure of the topmost skins due to beam bending for specimens AF-TS-F and 4F-TS-C while a simultaneous compressive and tensile failure of the skins for specimen 4F-TS-E. Based on the FEM simulations, the specimen 4F-TS-F and 4F-TS-C will fail due to compressive failure of the topmost skins at the region of maximum bending moment at a load of 160 kN (Figures 8.25 and 8.27, respectively) while the specimen 4F-TS-E will fail at a load of 210 kN due to simultaneous compressive and tensile failure of the inner and bonded fibre composite skin at any point between the loading rollers (Figure 8.26). It appears in the figures that the maximum stress contour of the composite sandwich beams at failure is very similar to the observed failure behaviour in Figures 8.8 to 8.10. Thus, the FEM prediction on the failure location and mechanisms is consistent with the experimental observations.
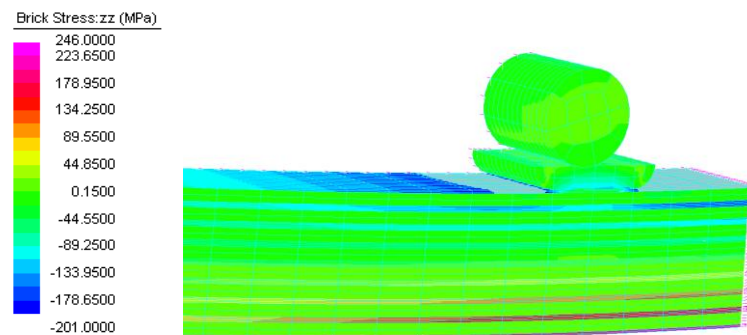
Figure 8.25 Predicted failure behaviour of specimen 4F-TS-F
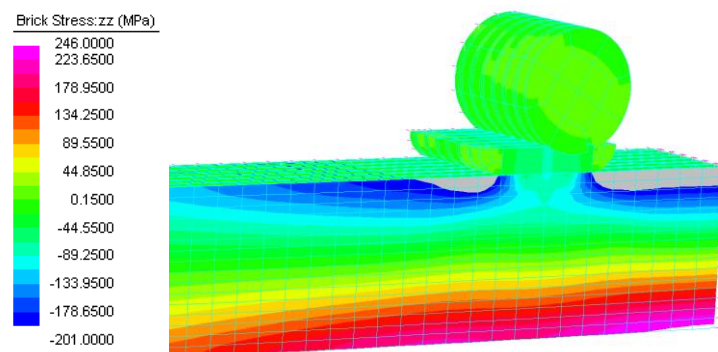
Figure 8.26 Predicted failure behaviour of specimen 4F-TS-E
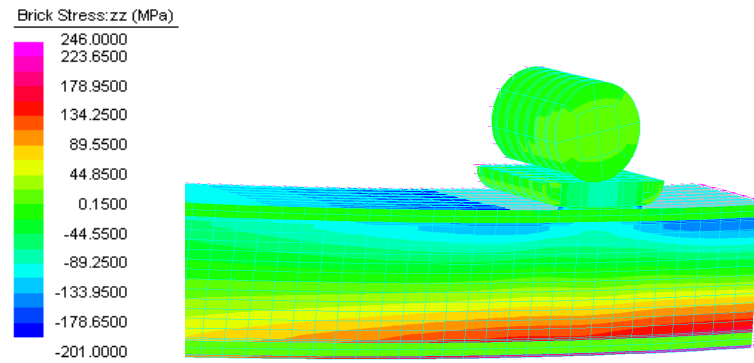
Figure 8.27 Predicted failure behaviour of specimen 4F-TS-C

8.7.3 Predicted behaviour in shear

8.7.3.1 Load and shear-strain behaviour

The load and shear strain relationship of the full-scale glue-laminated sandwich beams without fibre wraps is shown in Figure 8.28. As can be seen in the figure, a good agreement between the predicted values using FEM and the experimental results was observed only at the initial linear portion of the load and shear strain curve. The linear behaviour occurred up to a shear strain level of around 8000 microstrains, after which the actual specimens behaved non-linearly and does not follow the anticipated strain. This nonlinear behaviour can be due to the core material starting to fail in shear at this level of strain. Similarly, this softening behaviour before reaching the maximum load in actual specimens could be due to the non-linear behaviour of the fibre composite skins in shear and the core going into non-linear region in compression zone. This behaviour could not be modelled accurately due to the limitations of the Strand7 in handling non-linear behaviour of materials in shear, thus only the shear modulus value at the linear elastic behaviour of the skin and the core could be accounted for in the analysis. However, the FE model using Strand7 can reasonably predict the shear strength and failure mechanisms of the glue-laminated composite sandwich beams using the maximum stress criteria of the constituent materials. In comparison to the experimental results, the predicted failure load under asymmetrical beam shear test of glue-laminated composite sandwich beams is only 2-5% lower. Considering the uncertainties and assumptions regarding the exactness of the modelling, the results of the elastic FEM simulation of the shear behaviour for glue-laminated composite sandwich beam can be acceptable.
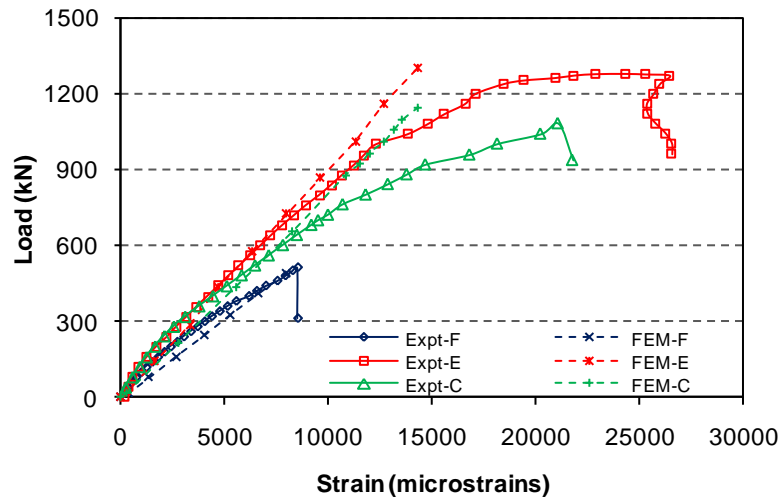
Figure 8.28 Load and shear strain relationship of full-scale sandwich beams

8.7.3.2 Predicted failure behaviour in shear

The failure behaviour of full-scale sandwich beams under asymmetrical beam shear test based on the FEM simulations is illustrated in Figures 8.29 to 8.31. A high principal shear stress around the mid-height of the specimens at the location of maximum shear is clearly observed from the shear stress contour. As expected, the shear failure of the beams originates from this portion of the specimens. In specimen AS-TS-F, the sandwich beams failed due to shear failure of the core in all sandwich laminations (Figure 8.31). This is very similar to the failure behaviour observed in the experimental investigation where the shear failure of the core occurred simultaneously in all laminations after the appearance of the first shear crack.

The predicted failure mode is shear failure of the vertical skins in specimen AS-TS-E (Figure 8.32). Some indentation failure on the loading points and at the supports is also observed. Similar to specimen AS-TS-E, the predicted failure of specimen AS-TS-C is due to shear failure of the vertical skins at the edgewise laminations (Figure 8.33). In the experiment, the final failure of specimen AS-TS-C is a shear failure of the vertical skins followed by the debonding failure of the flatwise laminations. The debonding failure in specimen AS-TS-C could not be represented in the FE model due to the integrity of the bond between the adjacent brick elements. It should be pointed out however that at the same load level where the vertical skin fails in shear, the stress contours indicates that the shear stress within the adhesive layers between the flatwise and edgewise laminations is almost 20 MPa. Since this level of shear stress will cause debonding failure of adhesives,

then the numerical results imply that epoxy debonding is a potential failure in this location. These results provide evidence that the failure mechanisms of sandwich beams under asymmetrical beam shear test could be predicted using FE models well.
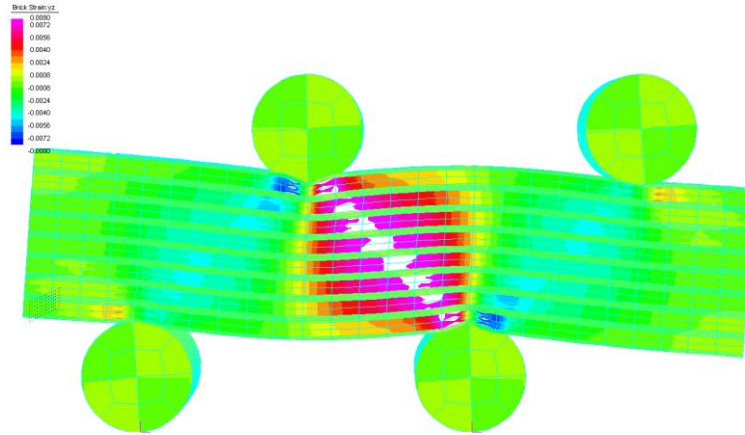
Figure 8.29 Predicted failure behaviour of specimen AS-TS-F
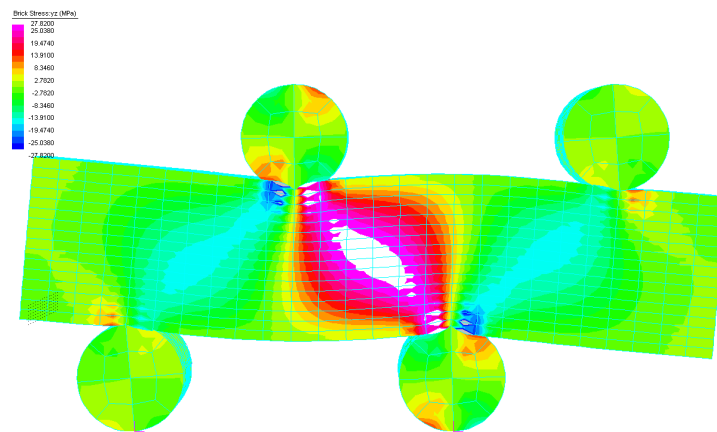
Figure 8.30 Predicted failure behaviour of specimen AS-TS-E
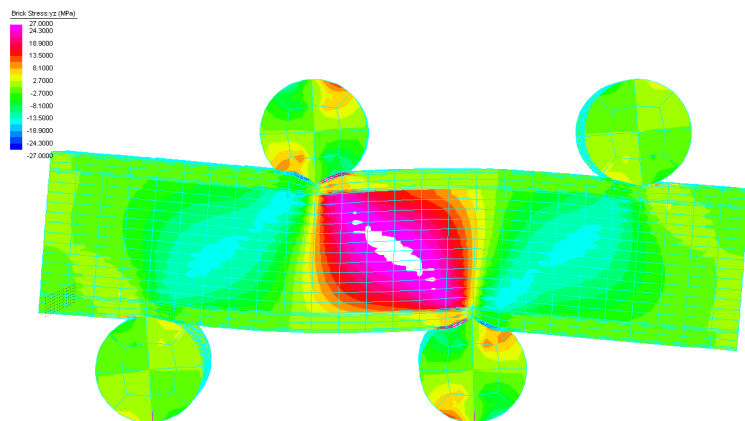
Figure 8.31 Predicted failure behaviour of specimen AS-TS-C

8.8   Conclusions

This chapter presents the performance evaluation of a full-scale fibre composite turnout sleeper made from glue-laminated sandwich beams. The structural behaviour of these beams was verified through practical experimentation and was evaluated against technical and performance benchmarks for sleeper application. The results suggest that the glue-laminated composite sandwich beams have the strength and the stiffness suitable for turnout sleeper application. This fibre composite turnout sleeper has better mechanical properties than most of the commercially available composite sleepers and showed compatible performance with timber turnout sleepers.

The orientation of the sandwich laminations has a significant effect on the structural behaviour of the full-scale sandwich beams. The addition of one layer of fibre wraps resulted in only 10% increase in shear strength and did not contribute much to the overall behaviour of the beams. The sandwich beams with laminations in the edgewise position showed the most efficient section in terms of strength and stiffness among the investigated sandwich beam configurations. This sandwich beam presented the appropriate strength and stiffness for turnout sleepers and the high resistance to hold screw spikes. Thus, this section configuration can form the basis for the development of prototypes for on-site performance evaluation.

The simplified analyses models and numerical simulations using the established mechanical properties of the materials and the observed behaviour in individual and small scale glue-laminated sandwich beams predicted the behaviour of full-scale beams reasonably well. This agreement shows that these analyses methods are important complement to experimental investigations for assessing the reliability and providing a better understanding of the behaviour of the glue-laminated composite sandwich beams. Such analyses methods would allow the efficient use of composite materials with a high degree of confidence.

The results of this study can be applied and extended to the analysis and design of glue-laminated beams consisting of composite sandwich structures. The sandwich beams considered in this study can efficiently be used in structural applications, particularly in turnout railway sleepers where there is a high demand for a suitable alternative to hardwood timber sleepers. The successful determination of the structural behaviour of the full-scale sandwich beams suggests the high feasibility of producing prototypes for in-track performance and durability testing. This endeavour will further increase the acceptance and use of fibre composites to railway sleepers.

Chapter 9

Conclusions

9.1 Summary

The widespread deterioration of most timber sleepers and the declining supply of quality timber resulted in many railway industries relying on alternative materials for sleeper replacement to maintain the functionality and safety of railway structures. Conventional sleeper materials like concrete and steel have not proven reliable alternatives as they have mechanical properties incompatible with that of existing timber sleepers. The recent developments in fibre composites now suggest their use as alternative material for railway sleepers. Fibre composites could be a viable alternative in specific applications such as railway turnouts where larger, longer, stronger, and more expensive timber sleepers are required.

A comprehensive review of literature suggested that the key performance issues of the currently used railway sleeper materials can be simulated using fibre composites. Fibre composites can be designed to behave like hardwood timber. They are almost maintenance free and are more environmentally sustainable than steel and concrete. They have similar installation requirements to those of timber sleepers which reduces labour costs. Most importantly, fibre composite materials use less amounts of energy and release small amounts of greenhouse gases.

This study was the first to investigate the concept of glue-laminated composite sandwich beams for railway turnout sleepers. The building block of this innovative beam is a novel composite sandwich structure made up of glass fibre composite skins and phenolic core material. There are several challenges needed to overcome for fibre composite sandwich structure to become a viable alternative to timber railway turnout sleepers, which is the main focus of this study. The conclusions gathered from the various studies conducted towards understanding the behaviour of the composite sandwich structure and investigating the suitability of this construction system for replacement railway sleepers are presented in this chapter. Further research works are suggested to facilitate the adoption of this composite material for replacement railway sleeper application.

9.2 Major conclusions from the study

9.2.1 Behaviour of composite sandwich structure with high strength core material

This study has investigated the behaviour of a structural composite sandwich panel with fibre composite skins and a modified phenolic core material using a combination of experimental, analytical and numerical simulations. Based on the results of this investigation, the following conclusions are drawn:

- As a general behaviour, the glass fibre composite skins behaved linearly elastic up to failure in both tension and compression with the tensile strength much higher than the compressive strength. On the other hand, the modified phenolic core behaved linearly elastic in tension but exhibited non-linear behaviour in compression. Hence the core can be modelled by bi-linear and the skin with linear behaviour for analytical purposes.

- The modified phenolic core material exhibited higher strength and modulus in shear and compression compared to the traditional core material systems. The significant improvement in the mechanical properties of the core structure combined with the high-strength and lightweight fibre composite skins suggest a high potential of the composite sandwich panel for structural applications.

- The composite sandwich structures exhibited different failure behaviour under flexural loading in the flatwise and the edgewise positions. The sandwich structures in the flatwise position failed due to compressive failure of the skin followed by the debonding between the skin and the core. The sandwich structures in the edgewise position behaved in a more ductile manner due to the progressive failure of the skin in compression followed by tensile failure of the skin. The better structural performance in the edgewise position than in the flatwise position suggests that the strength of the composite sandwich structures is significantly improved by the introduction of the vertical skins.

- The shear behaviour of the composite sandwich structures in the flatwise position is governed by the shear strength of the phenolic core material while the shear behaviour in the edgewise position is significantly influenced by the shear strength and modulus of the fibre composite skins. The presence of the vertical skins adds to its overall strength and delayed the shear failure of the beam until all the fibres crossing the cracked core material failed.

9.2.2 Behaviour of glue-laminated composite sandwich structures

The behaviour of the glue-laminated composite sandwich beams with different orientations of sandwich laminations was evaluated to determine the most effective use of this material for structural beam application. The conclusions related to this study are summarised as follows:

- Gluing the composite sandwich beams together resulted in a stronger and more stable section than individual sandwich beams alone. The glue-laminated sandwich beams in the edgewise position resulted in an increase of at least 25% in bending strength and over 20% in shear strength compared to that of the individual sandwich beam.

- The bending stiffness of the glue-laminated sandwich beams in the flatwise position decreases with increasing sandwich laminations while the bending stiffness of the glued sandwich beam in the edgewise position is almost equal to that of the individual sandwich beam. The bending stiffness of the glue-laminated sandwich beam in the flatwise position converges to that of the glued sandwich beam in the edgewise position with increasing sandwich laminations. It is better to glue together composite sandwich structures in the edgewise position as these beams will result in higher strength and a ductile failure behaviour.

- The flexural behaviour of the glue-laminated composite sandwich beams in the flatwise position is governed by the compressive properties of the fibre composite skin while the glue-laminated sandwich beams in the edgewise position continued to carry load even after the outermost fibre composite skins failed in compression as the load was shed to the inner bonded sandwich laminations. This load sharing mechanism leads to a better performance of the beams with edgewise sandwich laminations. The final failure of these sandwich beams is a simultaneous compressive failure of the inner skins, crushing of the core and tensile failure of the fibre composite skins. This mode of failure showed that the strength of the skins and the core material are efficiently utilised, suggesting the optimal utilisation of the fibre composite sandwich structures.

- The number and orientation of sandwich laminations has no significant effect on the shear strength of the glued composite sandwich beams tested in the flatwise position. In this position, the shear strength of the glued sandwich beam is governed by the shear strength of the core material regardless of how many laminations are there in a beam section.

- The higher shear strength of the glue-laminated sandwich beams in the edgewise position is due to the contribution of the vertical fibre composite skins in carrying the shear. In this position, the fibre composite skins carries almost 60% of the applied load compared to the flatwise position where the skin carries only 20%. The glued composite sandwich beam in the edgewise position achieved over 200% shear strength than beams in the flatwise position.

- Wrapping with 1 layer of tri-axial glass fibres has shown some positive effects on the behaviour of glue-laminated composite sandwich beams. In all the experimental cases, there was a nominal increase in the bending strength and stiffness of the wrapped sandwich beams than the beams without fibre wraps. The additional layers of glass fibres on both sides of the sandwich beams have resulted in a 10% increase in the shear strength.

9.2.3 Prediction of structural behaviour of composite sandwich beams

A simple prediction equation was established to describe the approximate behaviour and the governing failure mechanisms of the structural composite sandwich beams. This was verified through numerical simulations using Strand7 finite element program. The conclusions of the theoretical prediction and numerical simulation of the composite sandwich beam behaviour are summarised below:

- The simplified Fibre Model Analysis (FMA) gives a preliminary indication of the flexural behaviour of the composite sandwich beam structure. This simplified model was able to predict accurately the behaviour of the sandwich beams until the maximum load which was used to safely carry out the experimental investigation. However, the evaluation of the complex behaviour exhibited by the composite sandwich beam in the edgewise position is beyond the capabilities of this simplified model due to the progressive failure of the skin after the peak load. This nonlinear behaviour is not of significant

importance as only the behaviour up to the peak load is more of a concern in the design and analysis of most fibre composite structures.

- The conversion of the fibre composite sandwich section into an equivalent core material gives a good estimate of the shear strength of the sandwich beam in the flatwise position. The homogenisation of the composite section into an equivalent skin material accurately predicted the shear strength of the individual sandwich beam in the edgewise position. The predicted load close to the actual failure load can be obtained if the increase in shear strength caused by the gluing the sandwich beams together in the edgewise position would be accounted for.

- The accuracy of the finite element (FE) model using brick elements was determined by comparing the experimental results with numerical predictions. The FE simulation predicted the flexural behaviour of the sandwich beams reasonably well, however the non-linear behaviour in shear was not predicted accurately. The numerical results further suggest that the model is appropriate for predicting the failure load and mechanisms.

9.2.4 Application to railway turnout sleepers

A simplified three dimensional grillage beam model was used to investigate the behaviour of sleepers with different moduli of elasticity resting on different support moduli in a complex railway turnout structure. The conclusions related to this analysis are summarised as follows:

- The behaviour of sleepers in a railway turnout is most critical between the switch and the frog in all the scenarios investigated. The bending moment, shear and vertical deflection are highest in this region with a magnitude of almost 180%, 250% and 120% respectively, compared to that of the transition sleepers.

- The changes in the modulus of elasticity and the ballast/subgrade stiffness have a significant influence on the behaviour of railway turnout sleepers. The increase in the support modulus resulted in a reduction in the bending moment while the increase in sleeper stiffness has resulted in an increase in the bending moment. The shear force in turnout railway sleepers is not sensitive to both the

changes of the modulus of elasticity and the sleeper support modulus while the sleeper with a lower modulus of elasticity and support modulus tend to undergo greater settlement into the ballast.

- The modulus of elasticity for the development of a fibre composite sleeper alternative can be as low as 4 GPa provided that the support modulus is at least 20 MPa from the consideration of sleeper/ballast pressure and the requirement for a maximum vertical deflection. There were no significant variations in the behaviour of railway turnout sleepers with this modulus of elasticity.

The structural behaviour of the full-size glue-laminated composite sandwich beams was verified. The conclusions drawn from this study are summarised below:

- A design concept of the glue-laminated sandwich structure that includes the verification of serviceability and structural safety is proposed for railway turnout sleeper application, although this concept can also be used for structural beam applications. The mechanical properties of this innovative sandwich beam concept are far better than most of the available composite railway sleepers and are comparable with the existing timber turnout sleepers.

- The results of this study can be applied and extended to the analysis and design of glue-laminated beams consisting of composite sandwich structures. The glue-laminated sandwich beams considered in this study can be efficiently used in structural applications, particularly in turnout railway sleepers wherein there is a high demand for a suitable alternative to timber sleepers.

9.3 Proposals for future research

The following aspects need to be further studied in more detail for a widespread application of the glue-laminated composite sandwich beam concept for railway turnout sleepers and to pave the way in the development of structural components for civil engineering applications:

- The similarity of the behaviour of the phenolic core with the well known behaviour of concrete suggests the great potential of using the simplified material model for concrete in predicting the behaviour of fibre composite sandwich structures. The suitability of this simplified approach should be investigated to increase the confidence of design engineers in designing fibre

composite sandwich structures for a wide range of civil engineering applications.

- Predicting the shear behaviour of the glue-laminated sandwich structure is far more complex and could probably be best approached with a more powerful finite element software, using non-linear analysis. Developing a simplified model to predict the shear behaviour, especially for edgewise position is also important.

- The capability of fibre composite railway turnout sleepers of being installed on track without errors and being fitted with fastening component should be determined. Further research related to the further understanding of the long term performance and safety issues arising from the properties like fatigue, sleeper-ballast interaction, spike loosening, and durability should be conducted. The deterioration of the mechanical properties of the fibre composite sleepers due to environmental exposures should be also investigated. This is a key issue especially if the fibre composite sleepers do not provide significant improvement in durability over traditional sleeper materials; their market will likely be limited.

- Continuous research and development are essential to develop the market and increase the confidence in using this alternative material. Field trials and in-service performance evaluation will be very valuable in achieving this goal. Finally, the development of national and international standards will encourage the adoption of the fibre composites as an alternative railway sleeper material.

- The continued efforts to improve the performance and further innovations around optimising the fibre composite materials with an automated manufacturing process should make the fibre composite turnout sleepers a suitable solution and cost effective alternative to existing timber sleepers. Similarly, cost analysis which considers the life-cycle cost of the fibre composite railway sleeper should be undertaken and should be compared to the cost of the currently available railway sleepers.

References

Abdalla, M.A.A. and Sekino, N. (2006). Veneer strand flanged I-beams with MDF or particleboard as web material IV: effect of web material types and flange density on the basic properties. *Journal of Wood Science,* 52, 167-172.

ACI-ASCE Committee 426 (1973). *Shear strength of reinforced concrete members.* ACI-ASCE 426, 99(6), 1091-1187.

ACI Committee 318 (1995). Building code requirements for reinforced concrete. *ACI 318-95 and commentary 318R-95.* American Concrete Institute, Farmington Hills, MI.

ACI Committee 440R (2007). Report on fibre reinforced polymers (FRP) reinforcement for concrete structures. *ACI 440R-2007,* American Concrete Institute, Farmington Hills, MI.

Adams, D.O., Moriarty, J.M., Gallegos, A.M., and Adams, D.F. (2007). The V-notched rail shear test. *Journal of Composite Materials*, 41(3), 281-297.

Adams, J.C.B. (1991). Cost effective strategy for track stability and extended asset life through planned sleeper retention. *Demand Management of Assets National Conference Publication*, Institution of Engineers, Australia, 145-152.

Adhikary, B.B. and Mutsuyoshi, H. (2006). Shear strengthening of RC beams with web-bonded continuous steel plates. *Construction and Building Materials*, 20, 296-307.

Australian Greenhouse Office (2006). *AGO Factors and Methods Workbook*, Department of the Environment and Heritage, Australia.

Allen, H. (1969). *Analysis and design of structural sandwich panels*, Oxford Pergamon Press, New York.

Al-Saidy, A.H., Klaiber, F.W., Wipf, T.J., Al-Jabri, K.S., and Al-Nuaimi, A.S. (2008). Parametric study on the behaviour of short span composite bridge girders strengthened with carbon fibre reinforced polymer plates. *Construction and Building Materials*, 22, 729-737.

Al-Sulaimani, G.J., Sharif, A., Basunbul, I.A., Baluch, M.H., and Ghaleb, B.N. (1994). Shear repair for reinforced concrete by fibreglass plate bonding. *ACI Structural Journal*, 91(3), 458-464.

American Plywood Association (APA) – The Engineered Wood Association (1995). *Design and fabrication of all-plywood beams – plywood design specifications*, APA – The Engineered Wood Association, Tacoma, Washington.

Andersson, C. and Dahlberg, T. (1998). Wheel/rail impacts at a railway turnout crossing. *Proceedings of the Institution of Mechanical Engineers, Part F: Journal of Rail and Rapid Transit*, 212(2), 123-134.

Anonymous (2004). Polyurethane replaces wooden sleepers. *Reinforced Plastics,* 48(9), 9.

Aravinthan, T., Manalo, A.C. and Douglas, S. (2010). Development of a fibre composite turnout sleeper. *Proceedings of the 5th Civil Engineering Conference*

in the Asian Region and Australasian Structural Engineering Conference (CECAR 5/ASEC), 8-12 August, Sydney, Australia.

Aref, A.J., Alampalli, S. and He, Y. (2005). Performance of a fibre reinforced web core skew bridge superstructure. Part I: field testing and finite element simulations. *Composite Structures,* 69, 491-499.

AREMA (2003a). *Basic track components*. Viewed 22 May 2008, <http://www.arema.org/eseries/scriptcontent/custom/e_arema/Practical_Guide/PGChapter3.pdf.>

AREMA (2003b). *Chapter 30, Section 5, Engineered composite ties*, *Manual for Railway Engineering*, American Railway Engineering and Maintenance-of-Way Association, Maryland, USA.

Ashby, M.F., Evans, A.G., Fleck, N.A., Gibson, L.J., Hutchinson, J.W., and Wadley, H.N.G. (2000). *Metal foams: a design guide*, Elsevier.

ASTM Standard C39 (2005). Standard test method for compressive strength of cylindrical concrete specimens. *ASTM C39/C39M-05e1*, ASTM International, West Conshohocken, Philadelphia, Pa 19103.

ASTM Standard C274 (1999). ASTM standard terminology of structural sandwich constructions. *ASTM C274-99,* ASTM International, West Conshohocken, Philadelphia, Pa 19103.

ASTM Standard C297 (1994). Standard test method for flatwise tensile strength of sandwich constructions. *ASTM C297-94*, ASTM International, Philadelphia, Pa 19103.

ASTM Standard C365 (1994). Standard test method for flatwise compressive properties of sandwich cores. *ASTM C365-94*, ASTM International, Philadelphia, Pa 19103.

ASTM Standard C393 (2000). Standard test method for flexural properties of sandwich constructions. *ASTM C393-00*. ASTM International, Philadelphia, Pa 19103.

ASTM Standard D245 (2006). Standard practice for establishing structural grades and related allowable properties for visually graded lumber. *ASTM D245-06*, ASTM International, Philadelphia, Pa 19103.

ASTM Standard D638 (1991), Standard test method for tensile properties of plastics. *ASTM D638-91*, ASTM International, Philadelphia, Pa 19103.

ASTM Standard D4255 (2001). Standard test method for in-plane shear properties of polymer matrix composite materials by the rail shear method. *ASTM Standard D4255 /D4255M-01*, ASTM International, Philadelphia, Pa 19103.

ASTM Standard D5379 (1993). Standard test method for shear properties of composite materials by the V-notched beam method. *ASTM D5379/D5379M-93*. ASTM International, Philadelphia, Pa 19103.

ASTM Standard D5868-01 (2008) Standard test method for lap shear adhesion for fibre reinforced plastic (FRP) bonding. *ASTM D5868 - 01*. ASTM International, Philadelphia, Pa 19103.

References

ASTM Standard D7078 (2005). Standard test method for shear properties of composite materials by the V-notched rail shear method. *ASTM D 7078/ D7078-05*, ASTM International, Philadelphia, Pa 19103.

Australasian Railway Association. (2002). *Code of practice for the defined interstate rail network - Common Requirements*, Australasian Railway Association, Canberra, Australia.

Australian Rail Track Corporation (2007a). *Engineering (Track and Civil) Standard, ETA-04-01 Ballast specification*, Australian Rail Track Corporation Ltd. Viewed 30 September 2008. <http://extranet.artc.com.au/docs/engineering/common_standards/track/eta_04 _01_ballast_specification.pdf>

Australian Rail Track Corporation (2007b). *Engineering (Track and Civil) Standard, ETA-02-01 Timber sleeper, turnout and bridge transom specification*, Australian Rail Track Corporation Ltd. Viewed 07 October 2008. <extranet.artc.com.au/docs/engineering/common_standards/track/eta_02_01_ti mber_sleeper_turnout_and_bridge_transom_spec.pdf>

Baggott, M. McGrath, M. and Wong, J. (2006). *Maintenance cost benchmarking for the Victorian Freight Network*, Worley Parsons Services Pty Ltd, Australia.

Bakis, C.E., Bank, L.C., Brown, V.L., Cosenza, E., Davalos, J.F., Lesko, J.J., Machida, A., Rizkalla, S.H., and Triantafillou, T.C. (2002). FRP composites in construction – state of the art review. *ASCE Composite for Construction Journal*, 6(2), 78-87.

Bank, L.C. (2006). *Composites for construction: Structural design with FRP materials*, John Wiley and Sons, Inc., New Jersey.

Bank, L.C., Gentry, T.R. and Nadipelli, M. (1996). Local buckling of pultruded FRP beams - Analysis and design. *Journal of Reinforced Plastics and Composites*, 15(3), 283- 294.

Bank, L.C., Gentry, T.R., Thompson, B.P., and Russel, J.S. (2003). A model specification for FRP composites for civil engineering structures. *Construction and Building Materials*, 17, 405-437.

Barbero, E.J. (1999). *Introduction to composite materials design*, Taylor and Francis Group, New York.

Beckwith, S.W. (2008). Sandwich core materials and technologies – Part I. *SAMPE Journal*, 44(4), 30-31.

Bekuit, J.R.B., Oguamanam, D.C.D. and Damisa, O. (2007). A quasi-2D finite element formulation for the analysis of sandwich beams. *Finite Elements in Analysis and Design*, 43, 1099-1107.

Belouettar, S., Abbadi, A., Azari, Z., Belouettar, R., and Freres, P. (2009). Experimental investigation of static and fatigue behaviour of composite honeycomb materials using four point bending tests. *Composite Structures*, 87(3), 265-273.

Bendsten, B. and Porter, S. (1978). Comparison of results from standard 2-inch and 1½-inch shear block test. *Forest Products Journal*, 40(3), 9-14.

BHP Institute of Railway Industry - Monash University (2008). *Advancing the railway industry through technology*. Viewed 02 October 2008, <www.eng.monash.edu.au/railway>.

Birks, F.J., Tew, G.P. and Chitty, G.B. (1989). Narrow gauge track with interspersed steel sleepers. *The Fourth International Heavy Haul Railway Conference, Institution of Engineers*, Brisbane, Australia, 297-302.

Bootle, K.R. (1983). *Wood in Australia: Types, properties and uses*, McGraw-Hill Book Company, Sydney, Australia.

Borsellino, C., Calabrese., L. and Valenza, A. (2004). Experimental and numerical evaluation of sandwich composite structures. *Composite Science and Technology*, 64, 1709-1715.

Boughton, G.N. and Crews, K.I. (1998). Timber design handbook. *HB 108-1998*, Sydney.

Bowles, K.J. and Vanucci, R.D. (1986). *Mechanical properties characterisation of composite sandwich materials intended for space antenna applications*, NASA Technical Memorandum 88893, Phoenix, Arizona.

Bradtmueller, J., Hunt, M. and Shook, S.M. (1998). Mechanical properties of laminated veneer lumber via five-point bending test. *Journal of Testing and Evaluation*, 26(2), 132-137.

British Standard (1996). Plastics – Determination of tensile properties. Part 1: General principles. *BS EN ISO 527:1996*.

Brocca, M., Bazant, Z.P. and Daniel, I.M. (2001). Microplane model for stiff foams and finite element analysis of sandwich failure by core indentation. *International Journal of Solids and Structures*, 38, 8111-8132.

Brough, M., Stirling, A., Ghataorab, G., and Madelin, K. (2003). Evaluation of railway trackbed and formation: a case study. *NDT&E International,* 36, 145-156.

Buekett, J. and Conquergood, S.J. (1989). Requirements for prestressed concrete tie performance. *Proceedings of the Fourth International Heavy Haul railway Conference*, Brisbane, Australia, 291-296.

Burdurlu, E., Kilic, M., Ilce, A.C., and Ozunkavak, O. (2007). The effects of ply organisations and loading direction on bending strength and modulus of elasticity in laminated veneer lumber (LVL) obtained from beech (Fagus orientalis L.) and Lombardy poplar (Populus nigra L.). *Construction and Building Materials*, 21: 1720-1725.

Cabrera, N.O., Alcock, B. and Peijs, T. (2008). Design and manufacture of all-PP sandwich panels based on co-extruded polypropylene tapes. *Composites: Part B*, 39, 1183-1195.

Canning, L., Hollaway, L. and Thorne, A.M. (1999). Manufacture, testing and numerical analysis of an innovative polymer composite/concrete structural unit. *Proceedings of the Institution of Civil Engineering Structures and Buildings*, 134, 231-241.

References

Chattree, R., Manoharan, S. and Satyanarayana, P. (n.d.). *Composite sleepers for bridges: progress till date and road ahead*, Indian Railway Institute of Civil Engineering, Pune. Viewed: 02 December 2008, <http://iricen.gov.in/IRICEN1/projects/722/Composite%20Sleepers.pdf>

Chow, P. (2007). *Test report on mechanical properties with eight IntegriCo composite crossties*, University of Illinois, Chicago.

Cope, D.L. and Ellis, J.B. (2001). *Plain line maintenance*, British Railway Track, The Permanent Way Institution, England.

Cox, J. (1995). Deflection of sleeper in ballast. *Vehicle System Dynamics,* 24(1), 146–153.

Cromberge, P. (2005). *Polymer rail sleepers being tested for the mining industry*. Viewed: 04 November 2008, <http://www.miningweekly.com/article.php?a_id>.

Dahlberg, T. (2001). Some railroad settlement models – a critical review. *Proceedings of the Institution of Mechanical Engineers, Part F, Journal of Rail and Rapid Transit,* 215(4), 289–300.

Dai, J. and Thomas Hahn, H. (2003). Flexural behaviour of sandwich beams fabricated by vacuum-assisted resin transfer moulding. *Composite Structures,* 61, 247-253.

Daniel, I.M. and Abot, J.L. (2000). Fabrication, testing and analysis of composite sandwich beams. *Composites Science and Technology*, 60, 2455-2463.

Davalos, J., Kim, J. and Barbero, E. (1994). Analysis of laminated beams with layer-wise constant shear theory. *Composite Structures*, 28: 241-253.

Davalos, J.F., Qiao, P., Xu, X.F., Robinson, J., and Barth, K.E. (2001). Modelling and characterisation of fibre-reinforced plastic honeycomb sandwich panels for highway bridge applications. *Composite Structures*, 52, 441-452.

Davalos, J.F, Salim, H.A., Qiao, P., Lopez-Anido, R., and Barbero, E.J. (1996). Analysis and design of pultruded FRP shapes under bending. *Composites: Part B*, 27, 295-305.

Davalos, J.F, Zipfel, M.G. and Qiao, P. (1999). Feasibility study of prototype GFRP-reinforced wood railroad crosstie. *Journal of Composites for Construction*, 3(2), 92-99.

Demelio, G., Genovese, K. and Pappalettere, C. (2001). An experimental investigation of static and fatigue behaviour of sandwich composite panels joined by fasteners. *Composites: Part B,* 32, 299-308.

De Souza, F., del Menezzi, C.H.S. and Bortoletto, G., Jr. (2010). Material properties and non-destructive evaluation of laminated veneer lumber (LVL) made from *Pinus oocarpa* and *P. kesiya*. *European Journal of Wood and Wood Products*, Springer.

DIAB (2001). *Sandwich concept*, DIAB sandwich handbook. Available from: www.diabgroup.com

Doyle, N.F. (1980). *Railway track design: a review of current practice*, Bureau of Transport Economics, Australia Government Publishing Service, Canberra.

Duthin, D. and Starnes, M. (2004). Strength and ductility of concrete beams reinforced with carbon fibre-reinforced polymer plates and steel. *ASCE Journal of Composites for Construction*, 8(1), 59-69.

Dutton, S. and Cartwright, B. (2001). *Findings of a study into the feasibility of building a polymer composite bridge as a technology demonstrator project*, Technology Diffusion Program, Final Report, CRC-ACS.

Dweib, M.A., Hu, B., O'Donnel, A., Shenton, H.W., and Wool, R.P. (2004). All natural composite sandwich beams for structural applications. *Composite Structures,* 63, 147-157.

Dynamic Composites LLC – *Engineered composite railroad ties*. Viewed: 10 December 2009, <http://www.dynamic-cci.com/product.htm>

Eamon, C.D. and Nowak, A.S. (2004). Effect of secondary elements on bridge structural system reliability considering moment capacity. *Structural Safety*, 26, 29-47.

El-Hacha, R., Rizkalla, S.H., and Kotynia, R. (2005). Modelling of reinforced concrete flexural members strengthened with near-surface mounted FRP reinforcement. *Proceedings of the 7th International Symposium on Fibre Reinforced Polymer for Reinforced Concrete Structures (FRPRCS-7)*, New Orleans, Louisiana, USA, 7-10 December, 1681-1700.

Elkins, J.A., Handal, S.N. and Reinschmidt, A.J. (1989). Reducing turnout component deterioration: An analytical assessment. *Proceedings of the 4th International Heavy Haul Railway Conference*, 11-15 September, Brisbane, Australia, 46-50.

Ellis, D.C. (2001). *Track Terminology*, British Railway Track, The Permanent Way, Institution, England.

El-Sayed, A. K., El-Salakawy, E. F. and Benmokrane, B. (2006). Shear Strength of FRP-Reinforced Concrete Beams without Transverse Reinforcement. *ACI Structural Journal*, 103(2), 235-243.

Eshani, M.R., Saadatmanesh, H. and Al-Saidy, A. (1997). Shear behaviour of URM retrofitted with FRP overlays. *ASCE Journal of Composites for Construction*, 1(1), 17-25.

Ets Rothlisberger (2008). *History and development of wooden sleeper*. Viewed: 20 October 2008, < http://www.corbat-holding.ch/documents/showFile.asp >

European Rail Infrastructure Managers (EIM) Newsletter (2008). *A ban on the use of creosote: Possible consequences for the railway sector*, Brussels, Belgium.

Evans, A. and Evans, R. (2006). *Rubber/plastic composite rail sleepers*, The Waste & Resources Action Programme, Tyres report no: TYR0009-27, Oxfordshire, United Kingdom.

Feichtinger, K., Ma, W. and Elkin, R. (2006). Properties of structural sandwich core materials: Hand lay-up vs. vacuum-infusion processing, *American Composites Manufacturers Association*, St. Louis, USA.

Fujikubo, M. (2005). Structural analysis for the design of VLFS. *Marine Structures*, 18, 201-226.

Galletti, G.G., Vinquist, C. and Es-Said, O.S. (2008). Theoretical design and analysis of a honeycomb sandwich structure loaded in pure bending. *Engineering Failure Analysis,* 15, 555-562.

GangaRao, H.V.S., Taly, N. and Vijay, P.V. (2007). *Reinforced concrete design with FRP composites*, CRC Press, Taylor and Francis Group, Florida.

Gaudenzi, P., Pascucci, A., Barboni, R., and Horoschenkoff, A. (1997). Analysis of a glass fibre sandwich panel for car body constructions. *Composite Structures*, 38 (1-4), 421-433.

Gay, D. and Hoa, S.V. (2007). *Composite Materials: Design and applications*, Second edition, CRC Press, New York.

Gdoutos, E.E. and Daniel, I.M. (2008a). Failure modes of composite sandwich beams. *Theoretical Applied Mechanics*, 35(1-3), 105-118.

Gdoutos, E.E. and Daniel, I.M. (2008b). Nonlinear stress and deformation behaviour of composite sandwich beams. *Applied Mechanics and Materials*, 13, 91-98.

Geimer, R.L. (1982). *Feasibility of producing reconstituted railroad ties on commercials scale*, Research paper FPL 411, Forest Products Laboratory, 7 p.

Gezer, H. and Aydemir, B. (2010). The effect of wrapped carbon fibre reinforced polymer material on fir and pine woods. *Materials and Design*, 31: 3564-3567.

Gibson, R.F. (2007). *Principles of composite materials mechanics*, Second edition, CRC Press, Taylor and Francis Group, Florida.

Gonzalez-Nicieza, C., Alvarez-Fernandez, M.I., Menendez-Diaz, A., Alvarez-Vigil, A.E., and Ariznavarreta-Fernandez, F. (2008). Failure analysis of concrete sleepers in heavy haul railway tracks. *Engineering Failure Analysis*, 15, 90-117.

Grassie, S.L. and Cox, S.J. (1984). The dynamic response of railway track with flexible sleepers to high frequency vertical excitation. *Proceedings of the Institution of Mechanical Engineers, Part D: Transport Engineering*, 198, 117-124.

Grenestedt, J.L. and Bekisli, B. (2003). Analyses and preliminary tests of a balsa sandwich core with improved shear properties. *International Journal of Mechanical Sciences*, 45, 1327-1346.

Grimes, G.A. and Barkan, C.P.L. (2006). Cost-effectiveness of railway infrastructure renewal maintenance. *ASCE Journal of Transportation Engineering,* 132(8), 601-607.

Gruber, J. (1998). Making supply equal demand. *Railway Track and Structures, 17-23.*

Gupta, R. and Siller, T. (2005a). Shear strength of structural composite lumber using torsion test. *Journal of Testing and Evaluation*, 33(2), 110-117.

Gupta, R. and Siller, T. (2005b). A comparison of the shear strength of structural composite lumber using torsion and shear block tests. *Forest Products Journal*, 55(12), 29-34.

Hagaman, B.R. and McAlphine, R.J. (1991). ROA timber sleeper development project. *Proceedings of the Eight International Rail Track Conference*, Rail Track Association of Australia, 233-237.

Haj-Ali, R. and Kilic, H. (2002). Nonlinear behaviour of pultruded FRP composites. *Composites: Part B*, 33, 171-191.

Hardwicke, L. (2005). *Australian Infrastructure Report Card*, Engineers Australia, Barton, ACT, Australia.

He, M. and Hu, W. (2008). A study on composite honeycomb sandwich panel structure. *Material and Design,* 29, 709-713.

Health and Safety Executive (2006). *Rail track and associated equipment for use underground in mines: Guidance on selection, installation and maintenance*. Viewed: 20 October 2008, <http://www.hse.gov.uk/pubns/mines06.pdf>

Hearsch, J. (2008). *Rail CRC research helps save old-growth forests*. Viewed: 27 October 2008. <http://www.railinnovation.com.au/news/softwood_sleepers.html>

Herakovich, C.T. and Mirzadeh, F. (1991). Properties of pultruded graphite/epoxy. *Journal on Reinforced Plastics Composites*, 10, 2-28.

Hernandez, R., Davalos, J.F., Sonti, S.S., Kim, Y., and Moody, R.C. (1997). *Strength and stiffness of reinforced Yellow-Poplar glued-laminated beams*, Res. Pap. FPL-RP-554. Madison, WI: US Department of Agriculture, Forest Service, Forest Products Laboratory, 28 p.

Hetenyi, K. (1976). *Beams on elastic foundation: theory with applications in the field of civil and mechanical engineering*, University of Michigan Press, Michigan, USA.

Hibbeler, R.C. (2004). *Statics and mechanics of materials*, SI edition, Prentice Hall, Singapore.

Hoger, D.I. (2000). *Fibre composite railway sleepers*, University of Southern Queensland, Toowoomba, Queensland, Australia.

Hollaway, L.C. and Head, P.R. (2001). *Advanced polymer composites and polymers in the civil infrastructure*, Elsevier Science Ltd., Oxford, UK.

Hollaway, L.C. (2003). The evolution of and the way forward for advanced polymer composites in the civil infrastructure. *Construction and Building Materials*, 17, 365-378.

Honinger, H., Ridzewski, J. and Hoffman, T. (2007). Compression testing of fibre-reinforced plastics. *JEC Composites Magazine*, 32.

Howe, J.P. (1996). Look for wood in crossties. *Forest Products Journal 1*, 14-16.

Huang, H. (1989). *Static and dynamic analysis of plates and shells: Theory, software and applications*, Springer-Verlag, London.

Humpreys, M.F. and Francey, K.L. (2004). *An investigation into the rehabilitation of timber structures with fibre composite materials*, Queensland University of Technology, Australia.

Humpreys, M.F., Van Erp, G.M. and Tranberg, C. (1999). The structural behaviour of monocoque fibre composite truss joints. *Advanced Composite Letters,* 8(4),

173-180.

Hunt, G.A. (2005). *Review of the effect of track stiffness on track performance*, Report to the Rail Safety and Standards Board, London, NW1, 27 p.

International Standard (1981). Cellular plastics – Determination of shear strength of rigid materials. *ISO 1922:1981*.

International Standard (1995). Plastics - Determination of tensile properties - Part 1: General principles. *ISO 527-1:1995*.

International Standard (1996). Textile-glass-reinforced plastics – Prepregs, moulding compounds and laminates - Determination of the textile glass and mineral-filler content – calcination methods. *ISO 1172:1996*.

International Standard (1998). Fibre-reinforced plastic composites – Determination of flexural properties. *ISO 14125:1998*.

International Standard (1999). Fibre-reinforced plastic composites – Determination of compressive properties in the in-plane direction. *ISO 14126:1999*.

Iosipescu, N. (1967). New accurate procedure for single shear testing of metals. *Journal of Materials*, 2(3), 537-566.

Issa, C.A. and Kmeid, Z. (2005). Advanced wood engineering: glulam beams. *Construction and Building Materials*, 19(2), 99-106.

Iwnicki, S. (2006). *Handbook on railway vehicle dynamics*, CRC Taylor and Francis Group, New York.

Jacob, A. (2004). Indian composites industry set to take off. *Reinforced Plastics*, 34-39.

Jeffs, T. and Tew, G.P. (1991). A review of track design procedures: Volume 2 – Sleepers and ballast, *Railways of Australia*, Melbourne, Australia.

Jen, Y.M. and Chang, L.Y. (2008). Evaluating bending fatigue strength of aluminium honeycomb sandwich beams using local parameters. *International Journal of Fatigue,* 30, 1103-1114.

Johnson, K.A. (2002). *Timber bridge decks: comparison of types and evolution of design*, Wheeler Consolidated, Inc, St Louis Park, Minnesota.

Jordan, R. and Morris, G. (2006). *The feasibility of recycled plastic railway sleepers*, Project report PPR 094, Testing Research Laboratory, United Kingdom.

Kaewunruen, S. and Remennikov, A.M. (2009). Impact capacity of railway prestressed concrete sleepers. *Engineering failure analysis*, 16(5), 1520-1532.

Kalny, O., Peterman, R.J., Ramirez, G., Cai, C.S. and Meggers, D. (2003). *Evaluation of size effect and wrap strengthening on structural performance of FRP honeycombed sandwich panels,* TRB 2003 Annual meeting, Kansas State University.

Kamala, B.S., Kuman, P., Rao R.V. and Sharman S.N. (1999). Performance test of laminated veneer lumber (LVL) from laminated veneer lumber (LVL) from rubberwood from different physical and mechanical properties. *Holz als Roh- und Werkstoff*, 57: 114-116.

Kampner, M. and Grenestedt, J.L. (2007). On using corrugated skins to carry shear in sandwich beams. *Composite Structures*, 85, 139-148.

Karbhari, V.M. and Seible, F. (2000). Fibre reinforced composites – advanced materials for renewal of civil infrastructure. *Applied Composite Material,* 7, 95-124.

Karlsson, K.F. and Astrom, B.T. (1997). Manufacturing and applications of structural sandwich components. *Composites Part A,* 28, 97-111.

Kassa, E. and Nielsen, J.C. (2008). Dynamic interaction between train and railway turnout: full-scale field tests and validation of simulation models. *Vehicle System Dynamics,* 46(1), 521-534.

Kawasaki, T., Hwang, K., Komatsu, K., and Kawai, S. (2003). In-plane shear properties of the wood-based sandwich panel as a small shear wall evaluated by the shear test method using tie-rods. *Journal of Wood Science*, 49, 199-209.

Keller, T. (2006). *Material tailored use of FRP composites in bridge and building construction*, Swiss Federal Institute of Technology Lausanne, Switzerland.

Kemp, M. (2008). Use of pultruded sections in civil infrastructure. *Proceedings of the International Workshop on Fibre Composites in Civil Infrastructure – Past, Present and Future*, 1-2 December, University of Southern Queensland, Toowoomba, Queensland, Australia, 29-35.

Kohoutek, R. (1991). Dynamic and static performance of interspersed railway track. *Railway Engineering Conference*, Adelaide, Australia.

Kohoutek, R. and Campbell, K.D. (1989). Analysis of spot replacement sleepers. *The Fourth International Heavy Haul Railway Conference*, Institution of Engineers, Brisbane, Australia, 316-321.

Koller, G. (2009). The use of sleepers made of FFU synthetic wood in Europe. Viewed: 12 December 2009, <http://www.eurailpress.de/fileadmin/user_upload.pdf>

Kooistra, G.W. and Wadley, H.N.G. (2007). Lattice truss structures from expanded metal sheet. *Materials and Design*, 28, 507-514.

Kumar, P., Chandrashekhara, K. and Nanni, A. (2003). Testing and evaluation of components for a composite bridge decks. *Journal of Reinforced Plastics and Composites*, 22, 441-461.

Kumar, P., Chandrashekhara, K. and Nanni, A. (2004). Structural performance of a FRP bridge deck. *Construction and Building Materials*, 18, 35–47.

Kwak, K.H., Choi, D.H., Jang, H.S., Kim, H.O., and Yang, D.O. (2009). An experimental study on compressive strength of FRP modular members. *Proceedings of the 2nd Asia-Pacific on FRP in Structures (APFIS)*, Seoul Korea, 9-11 December, 209-213.

Lampo, R. (2002). *Recycled plastic composite railroad crossties*. Viewed: 06 November 2008, <http://www.cif.org/Nom2002/Nom13_02.pdf>

Lampo, R., Nosker, T., and Sullivan, H. (2003). *Development, Testing, and Applications of Recycled Plastic Composite Cross Ties*, US Army Engineer Research and Development Centre, Champaign, Illinois.

References

Lascoup, B., Aboura., Z., Khellil, K., and Benzeggagh, M. (2006). On the mechanical effect of stitch addition in sandwich panel. *Composites Science and Technology*, 66, 1385-1398.

Lebrun, R., Bureau, M.N. and Denault, J. (2003). Evaluation of bias-extension and picture-frame test methods for the measurement of intraply shear properties of PP/glass commingled fabrics. *Composite Structures*, 61(4), 341-352.

Leichti, R.J., Falk, R.H. and Laufenberg, T.L. (1990). Prefabricated wood composite I-beams: A literature review. *Wood and Fibre Science*, 2(1), 62-79.

Leong, J. (2007). Development of a limit state design methodology for railway track, *Master of Engineering Thesis*, Queensland University of Technology, Queensland, Australia.

Lingard, J.R. (1993). Optimising foam sandwich composites for ship superstructure applications. *Proceedings of Shipshape 2000. Tenth International Maritime and Shipping Symposium*, 8-9 November, 653-670.

Lopez-Anido, R. and Xu, H. (2002). Structural characterization of hybrid fibre-reinforced polymer-glulam panels for bridge decks. *Journal of Composite for Construction*, 6(3), 194-203.

Lundqvist, A. and Dahlderg, T. (2005). Load impact on railway track due to unsupported sleepers. *Proceedings of Institution of Mechanical Engineers Part F: Journal of Rail and Rapid Transit*, 219, 67-77.

Mahfuz, H., Islam, M.S., Rangari, V.K., Saha, M.C., and Jeelani, S. (2004). Response of sandwich composites with nanophased cores under flexural loading. *Composites: Part B*, 35, 543-550.

Mai, S.P., Fleck, N.A. and Lu, T.J. (2007). Optimal design of box-section sandwich beams in three-point bending. *International Journal of Solids and Structures*, 44, 4742-4769.

Mamalis, A.G., Spentzas, K.N., Pantelelis, N.G., Manolakos, D.E., and Ioannidis, M.B. (2008). A new hybrid concept for sandwich structures. *Composite Structures*, 83, 335-340.

Marsh, G. (2007). Augmenting core values. *Reinforced plastics*. Viewed: 21 October 2008, < http://www.reinforcedplastics.com/view/3729/augmenting-core-values-/>

McCarthy, K. and Cookson, L. (2008). *Natural durability of five Eucalypt species suitable for low rainfall areas - Sugar gum, spotted gum, red ironbark, yellow gum and swamp yate*. Rural Industries Research and Development Corporation Publication No 08/162, Project No CSF-61A, Australia, 16 p.

Miller, R. (2007). *Rail and tramway sleepers: Product recognition, identification and presentation,* viewed 29 May 2008, <http://www.cqfa.com.au/documents/1181619278_sleepers_fact_sheet.pdf>

Mirsayah, A.A. and Banthia, N. (2002). Shear strength of steel fibre reinforced concrete. *ACI Materials Journal*, 99(5), 473-479.

Mitchell, R., Baggott, M.G. and Birks, J. (1987). Steel sleepers – An engineering approach to improved productivity. *Conference on Railway Engineering*, Perth, Australia.

Miura, S., Takai, H., Uchida, M., and Fukuda, Y. (1998). The mechanism of railway tracks. *Japan Railway and Transport Review*, 38-45.

Moody, R. and Vizzini, A.J. (2000). *Damage tolerance of composite sandwich structures*, National Technical Information Service, Springfield, Virginia.

Moody, R., Hernandez, R. and Liu, J. (1999). *Wood handbook - Wood as an engineering material, Chapter 11 – Glued structural members*, Gen. Tech. Rep. FPL GTR–113, Madison, WI: U.S. Department of Agriculture, Forest Service, Forest Products Laboratory, 463 p.

Morris, T. (2008). Poisonous railway sleepers pose health risk, The Greens Tasmania, Media release, viewed: 08 October 2008, <http://www.abc.net.au/news/stories/2008/10/02/2380183.htm?site=news>

Mouritz, A.P. and Thomson, R.S. (1999). Compression, flexure and shear properties of a sandwich composite containing defects. *Composite Structures*, 44, 263-278.

Namura, A., Kohata., Y. and Miura, A. (2004). Effect of sleeper size on ballasted track settlement. *Railway Technical Research Report*, 45(3), 156-161.

Natterer J. and Hoeft, M. (1987). *Load-carrying behaviour of timber-concrete-composite constructions*, Research Report CERS No. 1345, Laboratory of Timber Construction, Swiss Federal Institute of Technology Lausanne.

New South Wales Environment Protection Agency Assessment (2004). *Classification and management of liquid and non-liquid wastes*. Department of Environment and Conservation (NSW), Sydney, 121 p.

Ng, S.T.K. and Soudki, K. (2010). Shear behaviour of externally prestressed beams with carbon fibre-reinforced polymer tendons. *ACI Structural Journal*, 107(4), 443-450.

Norton, J. (1998). *Safety and the use of CCA-treated timber*, Queensland Department of Primary Industries, Timber Research and Development Advisory Council, Timber Note 13.

Omar, T. (2008). *Multi-pultrusion fibre composite truss systems for deployable shelters*, PhD dissertation, University of Southern Queensland, Toowoomba, Queensland, Australia.

Optimat Ltd. and MERL Ltd. (2003). *Wood plastic composites study – technologies and UK market opportunities*, The Waste and Resource Action Programme, UK.

Papanicolaou, C.G., Triantafillou, T.C., Karlos, K., and Papathanasiou, M. (2007). Textile-reinforced mortar (TRM) versus FRP as strengthening material of URM walls: in-plane cyclic loading. *Materials and Structures*, 40, 1081–1097.

Park, R. and Paulay, T. (1975). *Reinforced Concrete Structures*, John Wiley and Sons Ltd.

Pattamaprom, C., Dechojarassri, D., Sirisinha, C., and Kanok-Nukulchai, W. (2005). *Natural rubber composites for railway sleepers: A feasibility study*, Thammasat University, Thailand.

References

Pfeil, H. and Broadley, J.R. (1991). Turnouts – "The hungry asset". *Railway Engineering Conference*, Adelaide, Australia, 176-184.

Pitarresi, G., Carruthers, J.J., Robinson, A.M., Torre, G., Kenny, J.M., Ingleton, S., Velecela, O., and Found, M.S. (2007). A comparative evaluation of crashworthy composite sandwich structures. *Composite Structures,* 78*,* 34-44.

Prasad, P. (2008). Fibre composite railway transom. *Proceedings of the International Workshop on Fibre Composites in Civil Infrastructure – Past, present and future*, University of Southern Queensland, Toowoomba, Australia, December 2008, 67-71.

Primi, S., Areiza, M., Bansal, A., and Gonzalez, A. (2009). New design and construction of road bridge in composites materials in Spain: Sustainability applied to civil works. *Proceedings of the 9th International Symposium on Fibre-reinforced polymer for concrete structures (FRPRCS-9)*, 13-15 July, Sydney, Australia.

Pruszinski, A. (1999). *Review of the landfill disposal risks and the potential for recovery and recycling of preservative treated timber*, Environmental Protection Agency Report, South Australia.

Qiao, P., Davalos, J.F. and Zipfel, M.G. (1998). Modelling and optimal design of composite-reinforced wood railroad crosstie. *Composite Structures,* 41, 87-96.

Quante, F. (2001). *Innovative track systems technical construction*. Viewed 11 November 2008, <http://www.promain.org/images/counsil/09_Track_Construction.pdf>

Queensland Government – Department of Infrastructure and Planning (2008). *Queensland Input for the COAG National Infrastructure Audit*, Part A – Sectoral Analysis Report, 110 p.

Railway Technical Society of Australasia (2008). *Engineers Australia Newsletter 10*, North Adelaide, South Australia.

Railway Track and Structures (2008). *Boost rail infrastructure*, Simmons-Boardman Publishing, Viewed: 02 June 2008, <http://www.nxtbook.com/nxtbooks/sb/rts0108/index.php>

Rammer, D.R. (1996). *Shear strength of glued-laminated timber beams and panels*. Forest Products Laboratory, USDA Forest Service, pp. 192-201.

Reis, E.M. and Rizkalla, S.H. (2008). Material characteristics of 3-D FRP sandwich panels. *Construction and Building Materials,* 22, 1009-1018.

Remmenikov, A.M. and Kaewunruen, S. (2008). A review on loading conditions for railway track structures due to wheel and rail vertical interactions. *Structural Control Health Monitoring*, 15, 207–234.

Rocca, S.V. and Nanni, A. (2005). Mechanical characterization of sandwich structure comprised of glass fibre reinforced core: Part I. *Composites in Construction 2005 – Third International Conference*, Lyon, France.

Rocla concrete sleepers. Viewed: 12 November 2008, <http://www.rocla.com.au/Drawings/Sleepers_guide_-_technical_info.pdf >

Rogers, D. (2004). *Characterisation of Hyrez 201 laminating resin*. Polymer Testing Laboratory, University of Southern Queensland, Toowoomba, Australia.

Russo, A. and Zuccarello, B. (2007). Experimental and numerical evaluation of the mechanical behaviour of GFRP sandwich panels. *Composite Structures,* 81, 575-586.

Sadeghi, J. (2001). Investigation on modelling of railway track system. *Scientia Iranica*, 8(1), 76-79.

Sandie, R. (1987). The flexural behaviour of nailed vertically-laminated hardwood beams. *First National Structural Engineering Conference*, Melbourne, 26-28 August, 330-334.

Santos-Neto, A.S. and La Rovere, H.L. (2007). Flexural stiffness characterization of fibre reinforced plastic (FRP) pultruded beams. *Composite Structures*, 81, 274-282.

Shahin, M.A. (2008). Investigation into some design aspects of ballasted railway track substructure. *Proceedings of the Conference on Railway Engineering*, 7-10 September, Perth, Australia, 617-623.

Shahu, J.T., Kaweswara, R.N.S. and Yudhbir, V. (1999). Parametric study of resilient response of tracks with sub-ballast layer. *Canadian Geotechnical Journal*, 36(6), 1137-1150.

Shahu, J.T., Sharma, A. and Sharma, K.G. (2008). Numerical modelling of railway tracks with ballast and sub-ballast layers using critical state parameters. *Proceedings of the International Conference of International Association for Computer Methods and Advances in Geomechanics (ICMAG)*, 1-6 October, Goa, India, 4400-4408.

Shenhar, Y., Frostig, Y. and Altus, E. (1996). Stresses and failure patterns in the bending of sandwich beams with transversely flexible cores and laminated composite skins. *Composite Structures,* 35, 143-152.

Shokrieh, M.M. and Rahmat, M. (2006). On the reinforcement of concrete sleepers by composite materials. *Composite Structures,* 76, 326-337.

Shokrieh, M.M. and Rahmat, M. (2007). Effects of Young's modulus on response of railway sleeper. *Applied Mathematical Modelling*, 31, 700-711.

Smith, R.L. and Shiau, R.J. (1998). An industry evaluation of the reuse, recycling and reduction of spent CCA wood products. *Forest Products Journal*, 48 (2), 44-48.

Smith, S.T. (2006). *Economics of treated wood used in aquatic applications*, Report prepared for the Western Wood Preservers Institute, viewed 16 August 2009, <http://www.wwpinstitute.org/>

Sokolinsky, V.S., Shen, H., Vaikhanski, L., and Nutt, S.R. (2003). Experimental and analytical study of nonlinear bending response of sandwich beams. *Composite Structures,* 60, 219-229.

Soltis, L. and Rammer, D. (1994). Shear strength of unchecked glued-laminated beams. *Forest Products Journal*, 44(1), 51-57.

Song, K., Choi, J.Y., Kweon, J.H., Choi, J.H., and Kim, K.S. (2008). An experimental study of the insert joint strength of composite sandwich structures. *Composite Structures,* 86, 107-113.

Standards Australia (1996). Aggregates and rock for engineering purposes, Part 7: Railway ballast. *AS2758.7-1996*, Sydney.

Standards Australia (1997). Timber structures – Design methods. *AS1720.1-1997*, Sydney.

Standards Australia (2002a). Railway track material, Part 1: Steel rails. *AS1085.1-2002*, Sydney.

Standards Australia (2002b). Railway track material, Part 3: Sleeper plates. *AS 1085.3- 2002*, Sydney.

Standards Australia (2003a). Railway track material, Part 14: Prestressed concrete sleepers. *AS1085.14-2003*, Sydney.

Standards Australia (2003b). Railway track material, Part 17: Steel sleepers. *AS 1085.17-2003*, Sydney.

Standards Australia (2003c). Railway track material, Part 18: Screw spikes and threaded inserts. *AS 1085.18-2003*, Sydney.

Standards Australia (2004). Timber- heavy structural products- visually graded: Part 2: Railway track sleepers. *AS3818.2-2004*, Sydney.

Steffens, D. and Murray, M. (2005). Establishing meaningful results from models of railway track dynamic behaviour. *Proceedings 8th International Heavy Haul Conference*, Rio de Janeiro, Brazil, 41-50.

Steeves, C.A. and Fleck, N.A. (2004). Collapse of sandwich beams with composite face sheets and a polymer foam core: experiment versus theory. *International Journal of Mechanical Science*, 46(4), 585-608.

Stevens, N. and Dux, P. (2008). *Case study: Design of new prestressed concrete railway sleepers*. Viewed 28 October 2008, <http://www.uniquest.com.au/index.php?sectionID=669>..

Stoll, F., Banerjee, R., Campbell, S., and Day, S. (2001). Manufacture of fibre-reinforced-foam composite structures. *ASC 16th Annual Technical Conference*, Blacksburg, VA.

Stonebraker, D.J., Brown, D.L. and Dolan, C.W. (2008). Effect of web bonded CFRP shear reinforcement on internal steel stress. *Proceedings of the Fourth International Conference on FRP Composites in Civil Engineering (CICE2008)*, 22-24 July, Zurich, Switzerland.

Strand7 (2005). *Strand7 Release 2.3.7 finite element analysis system*, Sydney, Australia.

Styles, M., Compton, P. and Kalyanasundaram, S. (2007). The effect of core thickness on the flexural behaviour of aluminium foam sandwich structures. *Composite Structures,* 80, 532-538.

Tan, G.H., Brameld, G.H. and Thambiratnam, D.P. (1998). Development of an analytical model for treating bridge-vehicle interaction. *Engineering Structures*, 20(1-2), 54-61.

Tew, G.P. (1991), A review of track design procedures: Volume 1 – Rails, *Railways of Australia*, Melbourne, Australia.

Thierfelder, T. and Sandstrom, E. (2008). The creosote content of used railway crossties as compared with European stipulations for hazardous waste. *Science of the Total Environment*, 402, 106-112.

Thompson, D.J. and Verheij, J.W. (1997). The dynamic behaviour of rail fasteners at high frequencies. *Applied Acoustics*, 52(1), 1-17.

Ticoalu, A.N.E. (2008). *Investigation on fibre composite turnout sleepers*, Master of Engineering dissertation, University of Southern Queensland, Toowoomba, Queensland, Australia.

TieTek composite crossties technical data. Viewed: 11 December 2009, <http://www.tietek.com/specsheets.php>

Tong, P. (1969). Exact solutions of certain problems by finite element method. *American Institute of Aeronautics and Astronautics Journal*, 7, 178-180.

Torre, L. and Kenny, J.M. (2000). Impact testing and simulation of composite sandwich structures for civil transportation. *Composite Structures,* 50, 257-267.

Transportation Technology Centre (2005). *Fibreglass wrapped tie performance evaluation report*, Office and Research and Development, Federal Railroad Administration, US Department of Transportation, Washington, D.C.

Triantafillou, T.C. (1997). Shear reinforcement of wood using FRP materials. *ASCE Journal of Materials in Civil Engineering*, 9(2), 65-69.

Triantafillou, T.C. (1998). Composites: A new possibility for the shear strengthening of concrete, masonry and wood. *Composite Science and Technology*, 58, 1285-1295.

Van Erp, G., Cattell, C. and Heldt, T. (2005). Fibre composite structures in Australia's civil engineering market: an anatomy of innovation. *Progress in Structural Engineering Materials,* 7, 150-160.

Van Erp, G., Cattell, C. and Huang, D. (2006). *Fibre composite innovations in Australia's construction industry*, CRC for Construction Innovation, Australia.

Van Erp, G. and Rogers, D. (2008). A highly sustainable fibre composite building panel. *Proceedings of the International Workshop on Fibre Composites in Civil Infrastructure – Past, Present and Future*, 1-2 December, University of Southern Queensland, Toowoomba, Queensland, Australia.

Vermaak, G.S. and Quinn, P. (1983). Laminated pine railway sleepers. *South African Forestry Journal*, 126(1), 60-65.

Vinden, P., Torgovnikov, G. and Hann, J. (2010). Microwave modification of radiate pine railway sleepers for preservative treatment. *European Journal of Wood and Wood Product*, Springer Berlin/Heidelberg.

Vinson, J.R. (1999). *The behaviour of sandwich structures of isotropic and composite materials,* Technomic, Lancaster, Pa.

Walrath, D.F. and Adams, D.E. (1987). Current status of the Iosipescu shear test method. *Journal of Composite Materials*, 21(6), 494-507.

Wang, X., Ross, R.J., Brashaw, B.K., Verhey, S.A., Forsman, J.W., and Erickson, J.R. (2003). *Flexural properties of laminated veneer lumber manufactured from ultrasonically rated red maple veneer: A pilot study*, Res. Note FPL-RN-

0288. Madison, WI: US Department of Agriculture, Forest Service, Forest Products Laboratory, 5 p.

Wang Y. and Zureick, A. (1994). Characterization of the longitudinal tensile behaviour of pultruded I-shape members using coupon specimens. *Composite Structures*, 29, 463-472.

Wicks, N. and Hutchinson, J.W. (2001). Optimal truss plates. *International Journal of Solids and Structures,* 38, 5165-5183.

Williams, B., Shehata, E. and Rizkalla, S. (2003). Filament-wound glass fibre reinforced polymer bridge deck modules. *ASCE Journal of Composite for Construction*, 7(3), 266-276.

Woidasky, J. (2008). *Railwaste – production of railway sleepers by mixed plastic waste*, SUSPRISE Joint Call Evaluation Workshop, Berlin, Germany.

Yamane, C., Masuda, M. and Murata, K. (2000). Influence of the overhangs on the failure property of short span beams. *Proceedings of the 50th Annual Meeting of the Japanese Wood Research Society*, 120 p.

Yildiz, H. and Sarikarat, M. (2001). Finite-element analysis of thick composite beams and plates. *Composite Science and Technology*, 61, 1723-1727.

Yoshihara, H. and Furushima, T. (2003). Shear strength of wood measured by various short beam shear test methods. *Wood Science and Technology,* 37, 189-197.

Yun, W.Y. and Ferreira, L. (2003). Prediction of the demand of the railway sleepers: A simulation model for the replacement strategies. *International Journal of Production Economics,* 81-82, 589-595.

Zakeri, J. and Sadeghi, J. (2007). Field investigation on load distribution and deflections of railway track sleepers. *Journal of Mechanical Science and Technology*, 21, 1984-1956.

Zarembski, A.M. (1993). Concrete vs. wood ties: Making the economic choice. *Conference on Maintaining Railway Track: Determining Cost and Allocating Resources*, Arlington, VA.

Zenkert, D. (1995). *An introduction to sandwich construction*, Engineering Materials Advisory Services Ltd, UK.

Zhang, Y.J., Murray, M.H. and Ferreira, L. (2000). Modelling of rail track performance: An integrated approach. *Transport Journal*, 187-194.

Zhang, S., Xiao, X., Wen, Z., and Jin, X. (2008). Effect of unsupported sleepers on wheel/rail normal load. *Soil Dynamics and Earthquake Engineering*, 28, 662-673.

Zhao, J., Chan, A.H.C. and Burrow, M.P.N. (2007). Reliability analysis and maintenance decision for railway sleepers using track condition information. *Journal of the Operational Research Society,* 58, 1047-1055.

Zhou, G., Green, E.R. and Morrison, C. (1995). In-plane and interlaminar shear properties of carbon/epoxy laminates. *Composite Science and Technology*, 55, 187–193.

Appendix A – Derivation of equation for estimation of failure load

The derivations of equations 4.1 to 4.9 are presented here. In the estimation of the failure load and mechanisms of the fibre composite sandwich beams, the skin and the core material are assumed to behave linearly elastic up to failure.

A.1 Skin and core failure in bending

In the engineering theory of sandwich beams, the axial strain is assumed to vary linearly over the cross-section of the beam as in Euler-Bernoulli theory (Zenkert, 1995). The classic formula for determining the bending stress in a beam under simple bending is given by:

$$\sigma = \frac{My}{I}$$

(A.1)

where σ is the bending stress, M is the moment about the neutral axis, y is the perpendicular distance to the neutral axis, and I is the second moment of area about the neutral axis. Due to assumptions (sections remain plane and perpendicular to the centroidal axis) this theory for engineering stresses in beams can be used in determining the stresses in a composite sandwich beam, with a few modifications (DIAB, 2001). Since the top skin is under compression, the failure of the sandwich beam due to compressive failure of the skin is calculated by equating the moments within the sandwich beam to the applied external bending moment. This gives a relation:

$$\sigma_{sc} = \frac{MD}{2EI} E_s$$

(A.2)

In this relation, the flexural stiffness EI depends on the position of the sandwich beam as given in equations 4.2 and 4.3 for flatwise and edgewise, respectively. In specimen 4FSW-I, the maximum bending moment at midspan due to the applied load P_{sf} is $P_{sf}L_T/6$ while the maximum bending moment at midspan of specimen 4FSW-II is $P_{sf}L_T/5$. Introducing a constant C of 1/6 and 1/5 for specimens 4FSW-I and 4FSW-II, respectively and rearranging with P_{sf} at the left hand side of the equation gives:

$$P_{sf} = \frac{2(EI)\sigma_{sc}}{CL_T E_s D}$$

(A.3)

A.2 Core shear failure

The maximum shear stress τ in a beam occurs at the neutral axis and is zero at both the top and bottom surface of the beam and can be determined using the relation:

$$\tau = \frac{VQ}{IB} \tag{A.4}$$

where V is the transverse shear force at the section of the beam considered and Q is the first moment of area (section above area of interest). For a sandwich beam, the shear force at the section under consideration can be determined by accounting the different materials of the sandwich beam cross section (Triantafillou, 1998). This relation can be written as:

$$\tau = \frac{V}{(EI)B} \sum (SE) \tag{A.5}$$

In this expression, (EI) is the flexural rigidity of the entire beam section and $\Sigma(SE)$ represents the sum of the products of S and E of all parts of the beam section where S is the first moment of area and E is the corresponding elastic modulus. Base on Figure 4.8, the $\Sigma(SE)$ for composite sandwich beam section in the flatwise and in edgewise positions can be calculated as equations A.6 and A.7, respectively.

$$\sum (SE) = E_s \frac{Bt_s d}{2} + E_c B\left(\frac{t_c}{2}\right)\left(\frac{t_c}{4}\right) \tag{A.6}$$

$$\sum (SE) = 2E_s t_s \frac{D}{2}\frac{D}{4} + E_c t_c \left(\frac{D}{2}\right)\left(\frac{D}{4}\right) \tag{A.7}$$

Equations A.6 and A.7 can then be simplified to A.8 and A.9, respectively.

$$\sum (SE) = B\left(E_s \frac{t_s d}{2} + E_c \frac{t_c^2}{8}\right) \tag{A.8}$$

$$\sum (SE) = \frac{D^2}{8}\left(2t_s + t_c \frac{E_c}{E_s}\right) \tag{A.9}$$

In a simply supported beam, the maximum force to cause shear failure along the beam section is half the applied load, P_{cs}. In the flatwise position, the composite sandwich beam is expected to fail when the maximum shear stress in the phenolic core material τ_c is reached. Substituting equation A.8 to A.5 gives:

$$\tau_c = \frac{P_{cs}}{2(EI)B} B\left(E_s \frac{t_s d}{2} + E_c \frac{t_c^2}{8} \right) \tag{A.10}$$

solving for P_{cs} gives:

$$P_{cs(flat)} = \frac{2\tau_c (EI)}{(E_s t_s d / 2 + E_c t_c^2 / 8)} \tag{A.11}$$

In the edgewise position, the section of the sandwich beam under the maximum shear stress is a combination of two skins and the core. The shear failure of the composite sandwich beam in this position is expected to occur when the maximum shear stress becomes equal to the shear strength of the skin τ_s, the core material in the sandwich beam section is transformed into an equivalent skin using the ratio of the modulus of elasticity of the materials, i.e. the width of the beam under maximum shear is $(2t_s + t_c E_c / E_s)$. Substituting (A.9) and the EI of beam in the edgewise position (equation 4.2) to equation A.5 gives:

$$\tau_s = \frac{\dfrac{P_{cs}}{2} \dfrac{D^2}{8} \left(2t_s + t_c \dfrac{E_c}{E_s} \right)}{\dfrac{D^3}{12} \left(2t_s + t_c \dfrac{E_c}{E_s} \right)\left(2t_s + t_c \dfrac{E_c}{E_s} \right)} \tag{A.12}$$

transposing P_{cs} on the left of the equation gives:

$$P_{cs(edge)} = \frac{4\tau_s D}{3} \left(2t_s + t_c \frac{E_c}{E_s} \right) \tag{A.13}$$

Equations (A.11) and (A.13) are similar to the relation used in predicting the peak shear strength P_{csG} (in equations 4.8 and 4.9) for composite sandwich beams in the flatwise and in the edgewise positions with the modulus of elasticity of materials, E_s and E_c replaced with shear modulus G_s and G_c, respectively.

A.3 Sandwich beam deflection

The total deflection at the midspan of the composite sandwich beam is the sum of the flexural and shear deformation.

$$\Delta_{total} = \int_0^L \frac{M_u M_L}{EI} dx + \int_0^L \frac{V_u V_L}{kGA} \tag{A.14}$$

For a simply supported beam under 4-point static bending with an applied load of P and shear span a, the deflection at the midspan of the beam due to unit and actual bending moments can be calculated by integrating the deflection from the support to the loading point ($0 \leq x \leq a$) and from the loading point to the midspan ($a \leq x \leq L/2$). This relation can be written as:

$$\Delta_b = 2\left[\int_0^a \left(\frac{M_L}{(EI)_1} \cdot \frac{x}{a}\right) \cdot \frac{x}{2} dx + \int_a^{L/2} \frac{M_L}{(EI)_2} \cdot \frac{x}{2} dx\right] \tag{A.15}$$

where EI_1 is the flexural stiffness for ($0 \leq x \leq a$) and EI_2 is the flexural stiffness for ($a \leq x \leq L/2$) or at the constant moment region. In relation A.3, M_L is common for both terms and simplifying gives:

$$\Delta_b = M_L\left[\int_0^a \frac{x^2}{a(EI)_1} dx + \int_a^{L/2} \frac{x}{(EI)_2} dx\right] \tag{A.16}$$

Integrating the equation gives:

$$\Delta_b = M_L\left[\left.\frac{x^3}{3a(EI)_1}\right|_0^a + \left.\frac{x^2}{2(EI)_2}\right|_a^{L/2}\right] \tag{A.17}$$

Simplifying this equation gives:

$$\Delta_b = M_L\left[\frac{a^2}{3(EI)_1} + \frac{1}{2(EI)_2}\left(\frac{L^2}{4} - a^2\right)\right] \tag{A.18}$$

For specimen 4FSW-I, $a = L/3$, $M_L = PL/6$ and assuming that only a single cross-section over the whole length of the beam similar to that of Natterer and Hoeft (1987), thus $EI_1 = EI_2$. This relation gives:

$$\Delta_b = \frac{PL}{6}\left[\frac{(L/3)^2}{3(EI)} + \frac{1}{2(EI)}\left(\frac{L^2}{4} - (L/3)^2\right)\right] \tag{A.19}$$

$$\Delta_b = \frac{23PL^3}{1296EI} \tag{A.20}$$

For specimen 4FSW-II, $a = 0.4L$ and $M_L = PL/5$ and assuming that $EI_1 = EI_2$ gives:

$$\Delta_b = \frac{PL}{5}\left[\frac{(0.4L)^2}{3(EI)} + \frac{1}{2(EI)}\left(\frac{L^2}{4} - (0.4L)^2\right)\right] \tag{A.21}$$

$$\Delta_b = \frac{59PL^3}{3000EI} \tag{A.22}$$

For a simply supported beam, the shear displacement diagram is the same as the bending moment diagram, with a factor $1/kAG$ applied to it, with AG often referred to as the shear stiffness of the sandwich beams (DIAB, 2001) and k is the shear correction factor (Bank, 2006). The maximum bending moment occurs at the midspan of the beam (at $x = L/2$). Consequently, the shear deformation at this location can be calculated as:

$$\Delta_s = 2\left[\int_0^a \frac{(P/2)(1/2)}{(kGA)_1}dx + \int_a^{L/2} \frac{0(1/2)}{(kGA)_2}dx\right] \tag{A.23}$$

Simplifying equation A.23 and integrating in terms of x gives:

$$\Delta_s = \frac{1}{2kGA}\left|Px + C\right|_0^a \tag{A.24}$$

At the support ($x = 0$), there is no deflection thus, $C = 0$. For specimen 4FSW-I, $a = L/3$ while for specimen 4FSW-II, $a = 2L/5$. The total deflection at the midspan for specimen 4FSW-I can then be obtained by combining the relations A.20 and A.24 while the total deflection at the midspan for specimen 4FSW-II can be calculated by combining A.22 and A.24. This results to relations A.25 and A.26, respectively:

$$\Delta_{4FSW-I} = \frac{23PL^3}{1296EI} + \frac{PL}{6kGA} \tag{A.25}$$

$$\Delta_{4FSW-II} = \frac{59PL^3}{3000EI} + \frac{PL}{5kGA} \tag{A.26}$$

Appendix B - Effect of plate width on the shear strength

The shear strength of the sandwich structures tested in the edgewise position is expected to be higher than that of sandwich structures tested in the flatwise position, making load introduction into the specimen problematic. The higher shear load required to fail the fibre composite sandwich structures in this position could result to compression and/or indentation failure under the load rollers and at the supports. The determination of a sufficient plate width that prevented the premature failure on sandwich beams under asymmetrical beam shear in Chapter 5 is presented here.

In sandwich structures, compression and indentation failure occurs when load is highly localised and arises because the stress immediately under the loading point is greater than the crushing strength of the core material (Dai and Thomas Hahn, 2003). In order to prevent this type of failure, sufficient area of load transfer needs to be provided during testing. Previous investigations on composite sandwich structures have used wide roller plates rather than rollers to obtain a core shear failure than indentation failure (Steeves and Fleck, 2004). In studying the effects of pure bending, Gdoutus and Daniel (2008b) provided special reinforcement at the outer section of the sandwich structures to prevent premature shear failure. In the preparation of their test specimen, the fibre composite skins directly under the concentrated loads were reinforced with additional layers of carbon/epoxy fibres to suppress and prevent indentation failure. These earlier studies suggest that providing steel plates on the loading points and at the supports could minimise or prevent localised failure and could result to a shear failure for sandwich beam specimens.

An expression for peak load in ductile indentation of sandwich structures in the flatwise position was presented by Ashby et al. (2000). This expression is relevant to sandwich beams with metal foam cores and ductile skins where the skins are assumed to form plastic hinges at the boundaries of the indentation region. Since the result of the material characterisation showed that the modified phenolic core material has strength and stiffness comparable to that of the metal foam cores, this relation is considered in the calculation of the indentation failure load for composite sandwich beams. The load to cause indentation failure, P_{id} into the composite sandwich structures can be calculated by:

$$P_{id} = 2Bt_s(\sigma_{cc}\sigma_{cs})^{1/2} \tag{B.1}$$

where t_s is the thickness of the skin, σ_{cc} is the compressive strength of the core and σ_{cs} is the compressive strength of the skin. Using this relation and the nominal thickness of the skin of 1.8 mm, width of 50 mm and the compressive properties of the core and the skin listed in Tables 3.3 and 3.4, respectively the indentation failure for composite sandwich beam with a modified phenolic foam core in the flatwise position is around 12.26 kN. Galleti et al. (2008) suggested that the load at which local core crushing, P_{lc} on composite sandwich structures can be calculated by:

$$P_{lc} = \sigma_{cc} A_c \qquad\qquad\qquad (B.2)$$

where A_c is the area of the plates in contact with the sandwich specimen. Steeves and Fleck (2004) suggested that in composite sandwich structure, the core crush mode entails the upper and lower face sheets behaving as rigid platens with the core crushing between them. Following this relation and a shear span of 80 mm, then the minimum point load required for local crushing of the core to occur would be 92 kN. A load of this magnitude would cause shear failure of the core for specimen AS-SW-F before compressive failure occurs. However, for specimen AS-SW-E, there is no horizontal fibre composite skin to distribute the applied load and the area that will support the load is greatly reduced as the load is applied in the in-plane direction of the sandwich beams. It is more likely therefore that in this position, the specimen will not fail in shear without producing any localised failures at the loading points and the roller supports.

In an attempt to minimise the effect of load concentration, the influence of the beam support conditions, specifically, the width of the steel plate used to distribute the load at the loading points and supports is investigated. Different width of steel plates were provided at each loading and reaction points to determine the minimum size of steel plates which can be use during testing to prevent compression and indentation failure without changing the overall behaviour of the composite sandwich beam. A 3 mm thick steel plate was used covering the full thickness of the sandwich beams. The results of this investigation is summarised in Table B.1.

The results show that for all sandwich beams tested in the flatwise position, the failure load under asymmetrical beam shear test is nearly equal for the different plate widths investigated. All the specimens failed at an applied load of around 11 kN. Within the results of the experiment, the composite sandwich beams tested in the edgewise position failed at a higher load for wider steel plates. For specimens tested

with no or lesser width steel plates, the localised stress concentration under the loading points and the supports resulted to a lower failure load due to indentation and compressive failure. However, there is no significant increase in the failure load of sandwich beams tested with plate widths of 30, 40 and 50 mm. This result suggests that the provision of steel plates of at least 30 mm width on the loading points and at the supports improves the uniformity of load distribution on the specimen reducing the stress concentration and preventing premature local failure.

Table B.1 Failure load of sandwich beams with different plate widths

Plate width (mm)	AS-SW-F			AS-SW-E		
	Depth (mm)	Width (mm)	Failure load (kN)	Depth (mm)	Width (mm)	Failure load (kN)
Rollers	19.88	48.58	10.78	49.16	19.70	7.58
10	19.79	49.74	10.75	49.73	19.49	9.23
20	19.95	49.67	10.85	49.67	19.93	15.89
30	20.13	49.71	10.63	49.72	19.56	17.60
40	20.03	49.42	11.16	49.64	19.87	17.46
50	20.20	49.91	10.69	49.23	19.91	18.51

Figure B.1 shows the failure mode of the specimen AS-SW-F with different plate widths tested under asymmetrical beam shear. The results show that the failure mechanisms do not vary substantially for specimens in the flatwise position. Even without steel plates under the loading points and at the supports, there is no any skin indentation failure or local core crushing observed on the beams. The presence of the stiffer glass fibre composite skins throughout the width of the beams spreads out the compressive stresses under the loading area to a lesser stiff modified phenolic core preventing any localised failure. All specimens failed with a sudden brittle type core shear failure without any failure warning in the form of minute cracks or stiffness reduction. At failure, a major shear crack (oriented at approximately 45° to the beam axis) propagated throughout the depth of the core was observed, then immediately followed by core-skin debonding. This shear crack occurred either under the loading point or at the roller support and propagated towards the edges of the specimens.

Figure B.2 shows the failure mode of specimen AS-SW-E. The figure shows that the sandwich structures loaded in-plane are more prone to local crushing and indentation due to its higher shear strength than specimen AS-SW-F. Excessive

compressive failure under the loading point and the support was observed for specimens tested without and with 10 mm width steel plates (Figures B.2a and B.2b). Signs of localised failure were still noticeable for specimens tested with 20 mm width steel plates (Figure B.2c) but none were observed for specimens with 30 mm width steel plates (Figure B.2d). This result suggests that a 30 mm width steel plate is sufficient to prevent local indentation and compressive failure in the composite sandwich structures. Similarly, there is no change in the shear failure mechanism for plate widths of 30, 40 and 50 mm. The actual shear failure criterion for sandwich structures provided with wider steel plates is the formation of a diagonal tension crack between the supports and the loading points. This has provided the basis for providing 30 mm width steel plates on the loading points and at the support of sandwich structures under asymmetrical beam shear test when loaded in-plane.

| (a) No plate | (b) 10 mm plate | (c) 20 mm plate |

Figure B.1 Failure of composite sandwich structures in the flatwise position
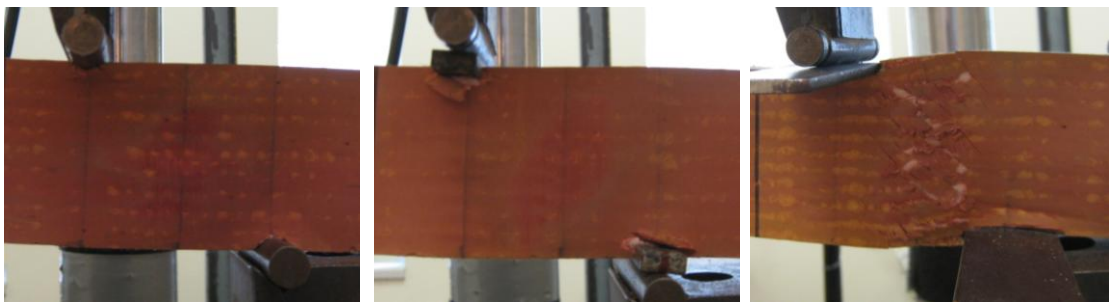
| (a) No plate | (b) 10 mm plate | (c) 20 mm plate |

| (d) 30 mm plate | (e) 40 mm plate | (f) 50 mm plate |

Figure B.2 Failure of composite sandwich structures in the edgewise position

Appendix C - Behaviour of glued sandwich beams with fibre wraps

The behaviour of glue-laminated sandwich beams in Chapter 6 wrapped with one layer of tri-axial glass fibre composite is presented here. The effect of fibre wraps on stiffness, strength and failure mechanisms of the glued composite sandwich beams under 4-point static bending test are discussed and the comparison with the behaviour of their unwrapped beam counterparts was conducted.

C.1 Effect of fibre wrapping on stiffness and strength

The comparison of the load-deflection relation of glue-laminated composite sandwich beams with and without fibre wraps are shown in Figures C.1 and C.2. The figures show that the initial load-deflection behaviour of all specimens was linear and became non-linear with a reduced stiffness up to failure. As expected, the specimen with fibre wraps behaved slightly stiffer and failed at a higher load compared to specimen without wraps. The higher stiffness of the wrapped specimen became more apparent when cracking of the core occurs and until final failure. This could be due to the bridging effect provided by the fibre wraps on the local defects in the specimen. Similarly, the composite sandwich beams with fibre wraps tested in flatwise position behaved slightly stiffer than the specimens in edgewise position.

The behaviour of specimen with fibre wraps tested in the flatwise position is similar to the specimen without wraps before cracking of the core. In specimens 3LSW-F and 4LSW-F, a big drop in the load was observed when compressive failure of the skin occurred. On the other hand, compressive failure of the skins and cracking of the core in specimens 3LSW-WF and 4LSW-WF are represented by smaller load drops. Interestingly, the first load drop occurred at almost the same level of applied load and deflection for both wrapped and unwrapped specimens. As loading continues, the load starts to rise again but with a reduced stiffness as shown in the load-deflection curve. The wrapped specimen failed at 18-35% higher load and a higher deflection than the unwrapped specimens, thus more ductile. However, the results also showed that the fibre wraps could not prevent or delay the compressive failure of the fibre composite skin. The fibre wraps only held the composite sandwich laminations together thereby preventing the separation between the skins and the core and increasing the failure strength.

In the edgewise position, the fibre composite wraps acted as a load distributing element which resulted to a more ductile load-deflection behaviour. For specimens 3LSW-E and 4LSW-E, the progressive failure of the fibre composite skin is represented by small load drops similar to a saw-tooth pattern. As a consequence of wrapping, the progressive failure of the fibre composite skins in specimens 3LSW-WE and 4LSW-WE is characterised by a decreasing capacity but with a smoother non-linear load-deflection curve. Similarly, the progressive failure of the fibre wraps did not create visible load drops due to small percentage of additional fibres (single wrap). The non-linear load-deflection response was terminated by a sudden drop in the load as a result of the composite sandwich beam failure. The increase in failure load of specimen with fibre wraps is in the order of 10-15% compared to specimens without wraps. Noticeably, both the specimens with and without fibre wraps failed at almost the same amount of deflection. This result showed that the strength and ductility of the glue-laminated composite sandwich beams are controlled primarily by the composite sandwich beams and not that of the fibre wraps. Nevertheless, the fibre wraps provided additional load sharing mechanism amongst the bonded composite sandwich beams. The presence of fibre wraps prevented the compressive buckling and debonding of the outermost fibre composite skins. This resulted in a wrapped glue-laminated composite sandwich beams tested in the edgewise position to fail in a more ductile behaviour than the unwrapped specimens.
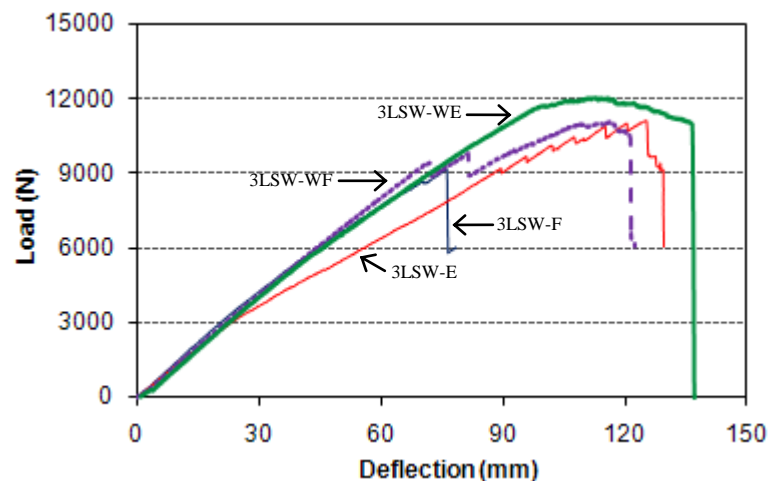

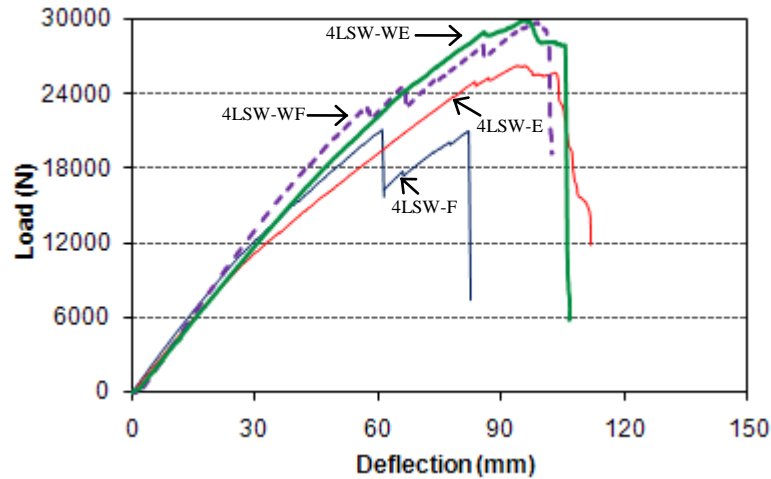Figure C.1 Load-midspan deflection relation of specimens 3LSW and 3LSW-W

Figure C.2 Load-midspan deflection relation of specimens 4LSW and 4LSW-W

In general, the maximum load recorded for beams with fibre wraps were almost the same in the flatwise and edgewise positions. If the first initiation of damage (represented by a drop in the load) is considered as the failure, the sandwich beams in the flatwise position has a 20-25% lower capacity than the specimen in the edgewise position. This difference in strength between wrapped specimens in the edgewise and flatwise positions is similar to the unwrapped specimens. Finally, the increase in stiffness and strength is due to additional reinforcement provided by the fibre wraps and not the confining effect.
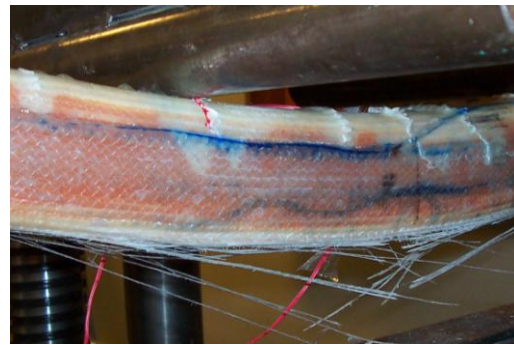
C.2 Effect of wrapping on failure behaviour

The failure modes of glue-laminated sandwich beams with fibre wraps are shown in Figure C.3. The results show that fibre wrap has some significant effects on the failure behaviour of the composite sandwich beams. The presence of fibre wraps prevented the immediate failure of the specimen as it held up the glue-laminated sandwich beams together which resulted to a higher strength before failure.

At the early stage of loading, the noise related to micro-cracking of the core was evident. Prior to failure, the cracking noise are more frequently heard. In all specimens, the failure of the glue-laminated composite sandwich beams with fibre wraps was initiated at the compressive part at the constant moment region. This failure mechanism is similar to what was observed in the specimen without fibre wraps. Also, the failure mechanisms of wrapped specimens indicated that very little confining effect was provided by the fibre wrap. After compressive failure of the

skin in the composite sandwich beams was detected, progressive failure of the fibre wraps immediately followed. Several points of debonding failure were observed between the fibre wraps and the specimen at the compressive side followed by splitting of the fibre wraps in tension. Thus, it was concluded that the failure of glue-laminated composite sandwich beams is governed by the strength of the composite sandwich beams and not that of the fibre wraps. However, the wrapped specimen failed with more ductility than the specimen without wrap.
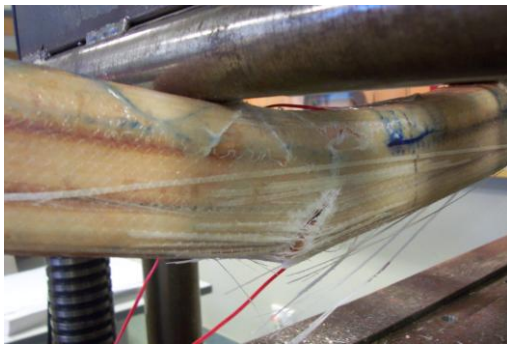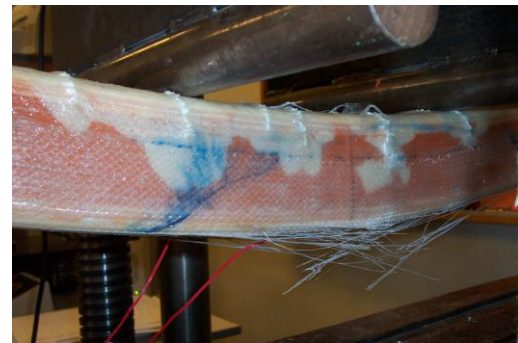

(a) Specimen 3LSW-WF   (b) Specimen 3LSW-WE
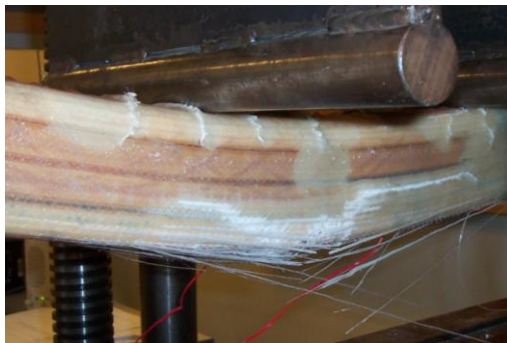
(c) Specimen 4LSW-WF   (d) Specimen 4LSW-WE

Figure C.3 Failure of glue-laminated sandwich beams with fibre wraps

The test results have shown some positive effects of fibre wrapping on the flexural behaviour of glue-laminated composite sandwich beams. In all of the experimental cases, there was considerable amount of increase in the strength and stiffness of the wrapped sandwich beam specimens compared to specimens without fibre wraps. More effective results could be obtained on specimen with more layers of fibre wrapping but increasing the number of fibre composite wraps would definitely entail higher cost.

Appendix D - Bond quality between sandwich laminations

The major advantage of a glue-laminated beam is its ability to resist bending forces with the increase in cross-sectional moment of inertia (Rammer, 1996). Full-moment resistance may only be accomplished if shear forces are transferred completely through the cross section. The inability to transfer shear in one lamination will lead to substantially reduced inertia values. Thus, a very good adhesion between the layers of composite sandwich panels has to be ensured for a better performance of the glue-laminated sandwich beams. The bond quality provided by the Techniglue-HP structural epoxy resin between layers of the glue-laminated sandwich beams in Chapters 6 and 8 are determined and presented in this section.

An initial investigation was conducted to assess the quality of bond provided by the structural epoxy using a lap shear test. Figures D.1a and D.1b show the dimensions of the specimens and the actual test set-up, respectively. Five specimens with single-lap-joints was prepared and tested following the ASTM D5868-1 (2008) test standards. In the preparation of the specimens, the sandwich panels are bonded together with epoxy adhesive and cured. The test specimens are placed in the grips of a universal testing machine and pulled at a loading rate of 1.3 mm/min until failure.

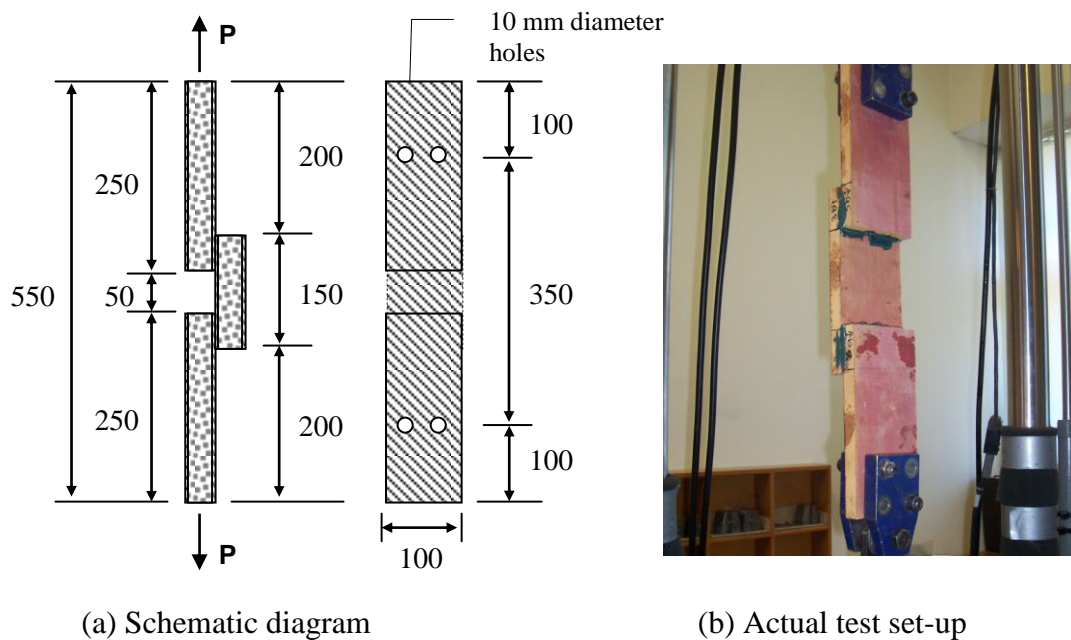(a) Schematic diagram   (b) Actual test set-up

Figure D.1 Lap shear test of laminated composite sandwich beam

The results of the bond quality test showed that the failure of epoxy bonded sandwich panels occur in the skins and not on the gluelines. A closer observation revealed that the failure of the lap joints was associated with peel-off of the skins and not due to interfacial bond failure of the epoxy as shown in Figure D.2. Similar failure mechanism was observed in the earlier studies on direct shear strength of core and flatwise tensile test, where the composite sandwich panel with high strength core material failed by debonding between the skin-core interface (Omar, 2008). The bond (lap shear) strength of the structural epoxy adhesives was found to be around 20 MPa with a standard deviation of 0.9 MPa. The summary of the results for the single lap shear test is listed in Table D.1. In the table, the shear strength is determined as the average over the bonded area. This bond strength is more than the shear strength of the core, thus, it was expected that the core will fail in shear before any debonding failure occurs at the gluelines. In effect, no debonding failure was observed in the gluelines of glued sandwich beams subjected to static bending test. This suggests that the quality of bond provided by the epoxy adhesives is sufficient to develop full composite action for sandwich beams. Furthermore, the high strength of the epoxy bonds leads to the development of the full strength of the beams.
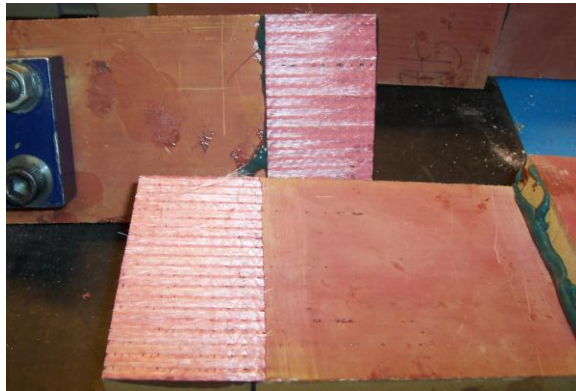

Figure D.2 Failure mode of lap shear test

Table D.1 Results of the lap shear test

Specimen number	Lap area (mm^2)	Peak load (N)	Shear stress (MPa)
1	9574.5	206100.8	21.5
2	9873.4	203016.6	20.6
3	9563.2	193585.1	20.2
4	9683.7	184154.2	19.1
5	9805.6	194723.6	19.8
Average	9700.1	196315.1	20.2
St. Dev.	137.8	8639.9	0.9

Appendix E – FE model for glue-laminated sandwich beams

The finite element (FE) model developed to verify the structural behaviour of the glue-laminated composite sandwich beams in Chapters 6 and 8 is presented here.

E.1 FE model for small scale glue-laminated sandwich beams

The FE model for composite sandwich beams bonded together in Chapter 6 is analysed by modelling the skin and the core as 20-node hexahedron (Hexa20) brick elements with aspects ratios of 1.4 to 1.9. In flexure, only a quarter of the specimen is modelled (symmetry along the XY and YZ plane) while half of the composite sandwich beam is modelled in asymmetrical beam shear (symmetry along the XY plane only) to reduce the computational time. Tables E.1 and E.2 list the number of Hexa20 bricks, nodes and the computation time for the FE model of the glue-laminated composite sandwich beams in flexure and shear, respectively. Figures E.1 to E.3 show the numerical model to simulate the behaviour of the glue-laminated sandwich beams in the flatwise and edgewise positions in flexure and shear.

Table E.1 FE model for glued sandwich beam under static 4-point bending

Specimen	Hexa20 bricks	Nodes	CPU time (sec)
2LSW-F	3120	15553	3869
2LSW-E	2060	10709	3647
3LSW-F	16344	77081	18211
3LSW-E	10944	52712	16783
4LSW-F	28992	131589	28703
4LSW-E	19344	89197	25034

Table E.2 FE model for glued sandwich beam under asymmetrical beam shear

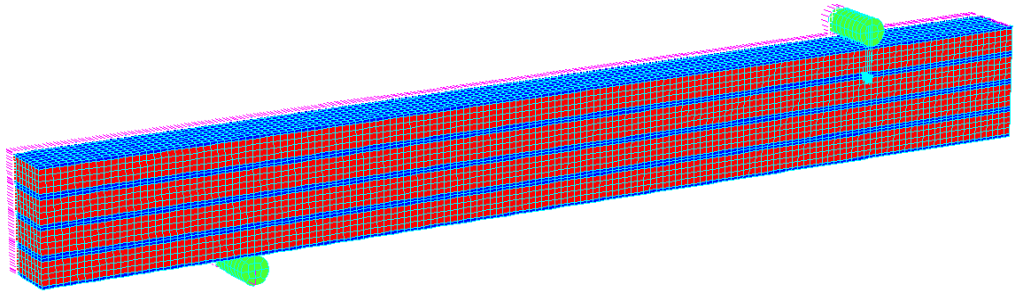| Specimen	Hexa20 bricks	Nodes	CPU time (sec)
AS-2LSW-F	8598	39156	2874
AS-2LSW-E	9032	41071	3207
AS-3LSW-F	14616	66564	3996
AS-3LSW-E	15534	70643	3502
AS-4LSW-F	25248	111876	7095
AS-4LSW-E	26472	117329	7922

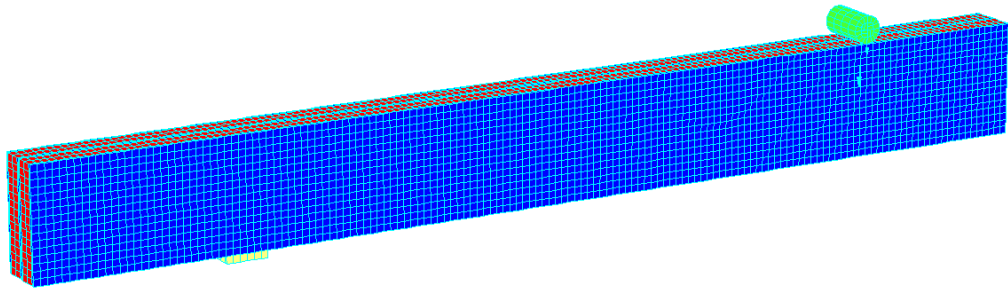Figure E.1 FE model for glued sandwich beam in flatwise position under bending

Figure E.2 FE model for glued sandwich beam in edgewise position under bending
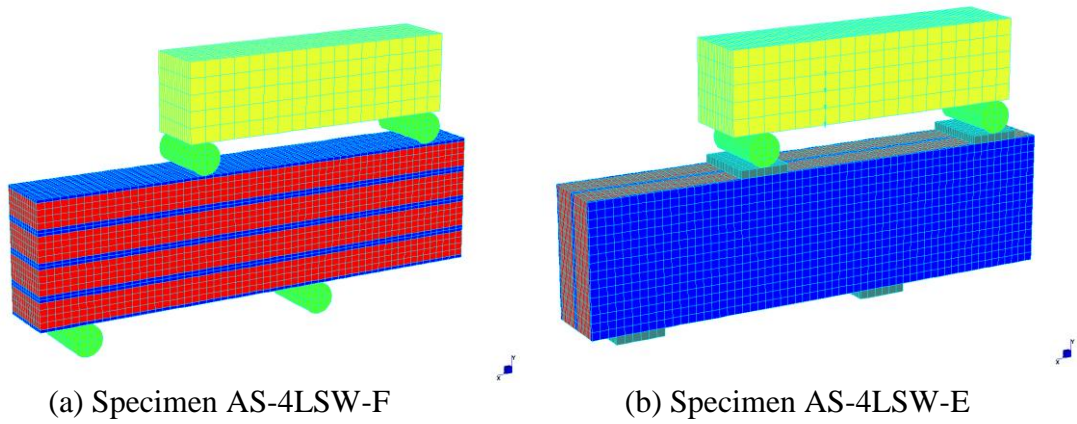

(a) Specimen AS-4LSW-F   (b) Specimen AS-4LSW-E

Figure E.3 FE model for glued sandwich beam under asymmetrical beam shear test

E.2 FE model for full-scale glue-laminated sandwich beams

Several assumptions were made to simplify the analysis in the development of the numerical model for the full-scale glue-laminated sandwich beams in Chapter 8. The main components of the innovative glue laminated beam section are the composite sandwich panels and the structural epoxy adhesives used to bind the sandwich laminations. In all the beams investigated in Chapter 6, no failure was observed in the adhesive layers at the ultimate capacity even at final failure. In addition, the epoxy adhesives only made limited contribution to the strength and stiffness of the glue-laminated sandwich beams due to the low modulus of the adhesives compared to the composite sandwich structure. Therefore the first simplification considered was ignoring the effect of the adhesive layers. Yildiz and Sarikanat (2001) suggested taking an average value for the element material properties in finite element analysis in order to determine the material constants of a multi-layered composite element. Similarly, Davalos et al. (2001) used the equivalent elastic properties for a honeycomb core with sinusoidal wave configuration to simplify the model of a fibre-reinforced composite highway bridge. The results of both analyses showed that the simplified analytical prediction using the effective properties of the materials correlated very well with the experimental values. Accordingly, the second simplification was to assume that the skin and the core of the sandwich sections are materials with equivalent elastic properties. These equivalent properties were determined from the test of coupon specimens listed in Tables 3.3, 3.4 and G.1. Table E.3 lists the number of Hexa20 brick elements, nodes and computation time for the FE model of the full-scale glue-laminated sandwich beams while the actual configuration of the FE model of the specimen with combined sandwich laminations in flexure and shear are shown in Figures E.4 and E.5, respectively. The nonlinear static analysis was performed under static bending while linear static analysis was conducted for sandwich beams under asymmetrical beam shear test.

Table E.3 FE model for full-size glue-laminated sandwich beams

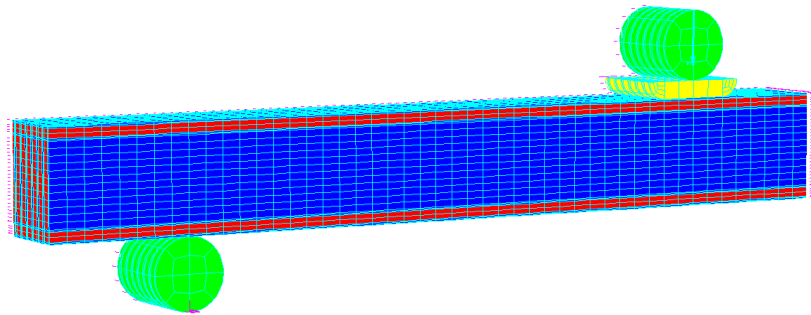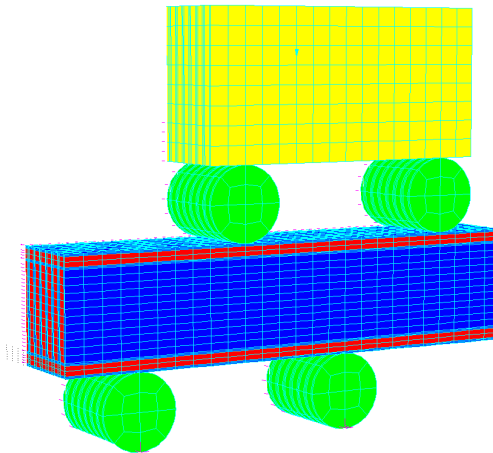| Specimen	Hexa20 bricks	Nodes	CPU time (sec)
4F-TS-F	25470	115974	17364
4F-TS-E	21320	101798	13012
4F-TS-C	23840	104495	14086
AS-TS-F	17680	76161	8629
AS-TS-E	14840	64220	7855
AS-TS-C	16000	71980	8214

Figure E.4 FE model for specimen 4F-TS-C

Figure E.5 FE model for specimen AS-TS-C

Appendix F – Influence of train route and steel distance blocks

The behaviour of sleepers in Chapter 7 when the train passed through the railway turnout in both the through (main) and the diverging tracks and the effects of steel distance blocks at crossing are discussed. Similarly, the negative bending moments and shear forces in the turnout sleepers with different $E_{sleeper}$ and U_s are presented.

F.1 Influence of train route on turnout sleeper behaviour

The influence of train route in the magnitude and position of the maximum bending moment in railway turnout sleeper is investigated. The wheel load is passed through the railway turnout in both the through (main) and the diverging tracks to determine if there is significant difference on the behavior of the railway sleepers when the wheel load passed through either of the two routes. Figure F.1 shows the maximum positive bending moment in sleepers along the through and diverging routes for sleepers with $E_{sleeper}$ = 10 GPa resting on U_s = 10 MPa. In the figure, Case 1 represents the envelope of the maximum bending moment in sleepers when the wheel load is passing through the main track while Case 2 is when the train is passing through the diverging track.
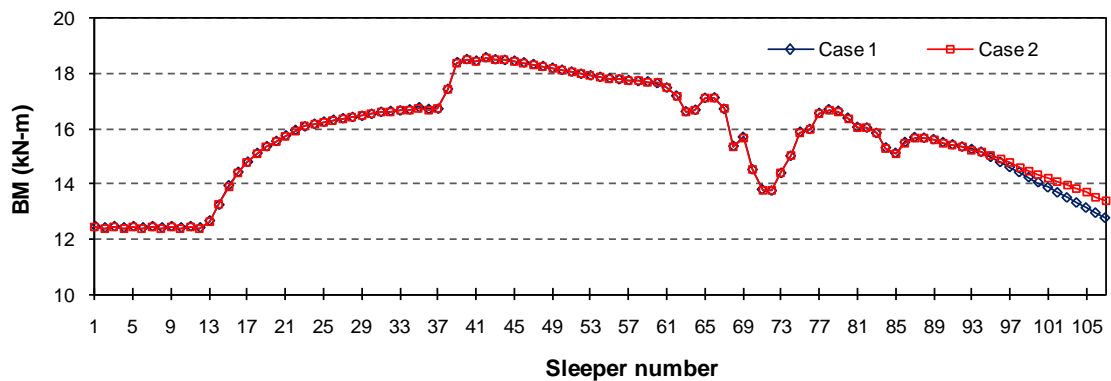

Figure F.1 Bending moments on sleepers for different train routes

The results of the numerical simulations show that the turnout sleepers are subjected to an almost similar magnitude of maximum bending moments for both train routes. This is due to the arrangement of rails with respect to the sleeper essentially symmetric when the wheel load is placed either in the main or in the diverging tracks. A slightly higher bending moment was however observed on the transition sleepers after the wheel load has passed the longest sleeper for the

diverging route compared to the main route which could be due to the curve rails supporting the sleepers. After the longest sleeper, the symmetry of the track is lost, implying that the tracks at the main and the diverging routes will have different stiffness. In general, the difference in the influence of train routes on the behavior of sleepers is relatively small for both the main and the diverging routes. Thus, the parametric investigation to determine the effects of the different elastic and subgrade moduli on the behavior of turnout sleepers was conducted only for the model when the train is passing through the diverging tracks.

F.2 Effects of steel distance blocks at crossing

At the point of the crossing (frog), the rails are very close together and joined by steel distance blocks. These distance blocks are welded to the web of the rail which extend up to a distance of 3 sleepers away from the frog to resist the high wheel forces at the crossing. In order to determine the effects of these distance blocks on the behavior of sleepers, two grillage beam models of the railway turnout system were prepared; a model without distance blocks (Model 1) and a model with additional beams representing the distance blocks (Model 2). Figure F.2 shows the actual and the FEM model for the steel distance blocks at the crossing. The additional steel beams in Model 2 have dimensions of 60 mm x 80 mm.
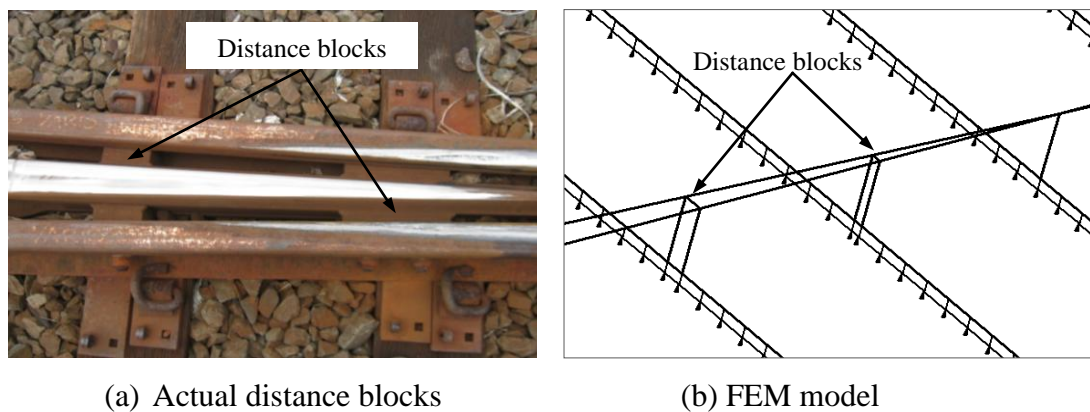

(a) Actual distance blocks   (b) FEM model

Figure F.2 Details of steel distance blocks at the crossing

Figures F.3 and F.4 show the behavior of sleepers in both models when $E_{sleeper}$ = 10 GPa and resting on U_s = 10 MPa. The results show that by installing additional beam elements to model the distance blocks increased its stiffness and increased the load-distributing effect of the rails, resulting in a slightly lower bending moment in

sleepers near the location of the frog (Figure F.3). In Figure F.4, Model 1 shows that the shear forces in sleepers when the wheel load is placed in the frog results in a shear force almost equal to that of sleepers at the switch. However, the provision of additional rails in Model 2 resulted in a significant reduction in the shear forces in the sleepers at the frog. The magnitude of the maximum shear force in sleeper 72 is around 143.3 kN for Model 1 but decreases to 53.9 kN for Model 2. It can also be noticed in Figures F.3 and F.4 that the effect of additional beams extends only up to 10 sleepers before and after the frog.
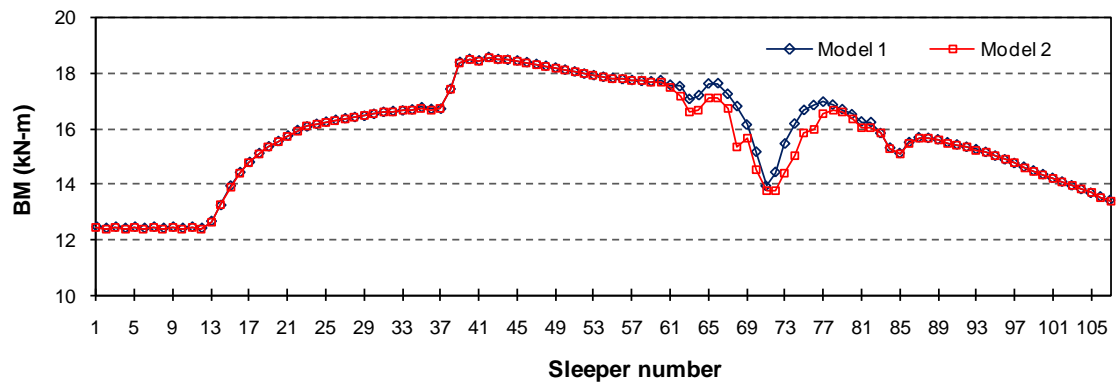

Figure F.3 Bending moments on sleepers when $E_{sleeper} = 10$ GPa and $U_s = 10$ MPa
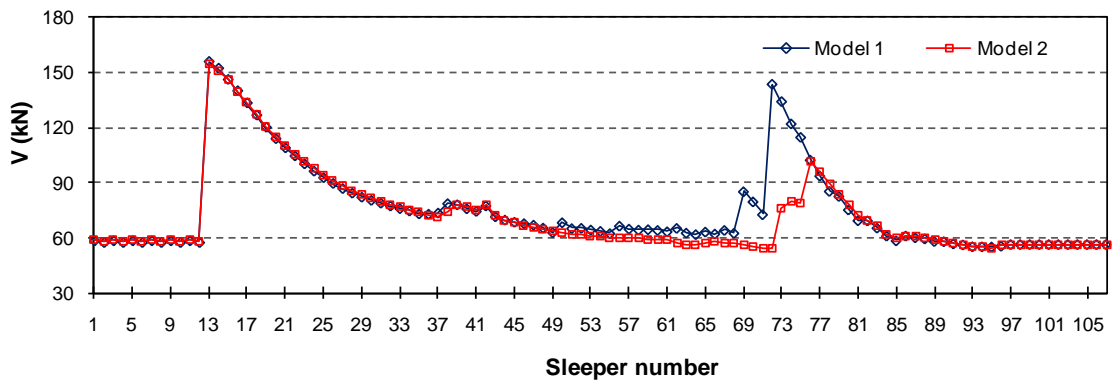

Figure F.4 Shear forces on sleepers when $E_{sleeper} = 10$ GPa and $U_s = 10$ MPa

F.3 Effects of $E_{sleeper}$ on negative bending moment and shear

Figures F.5 and F.6 show the maximum negative bending moment in turnout sleepers for all $E_{sleeper}$ with U_s of 10 and 40 MPa, respectively. The results show that there is an increase in the negative bending moment when $E_{sleeper}$ increases. On the other hand, the difference in negative bending moment decreases with increasing $E_{sleeper}$. Interestingly, the maximum negative bending moment can be at the rail centre or any place along the sleeper. The location of the maximum negative bending moment

occurred at the rail centre for transition sleepers and for turnout sleepers before the wheel load passed through the frog. Just before passing and after the frog, the maximum negative bending moment in the turnout sleepers occurred under the rail seat of the through tracks. This could be due to the presence of the continuous rails which act as fixed supports to the other sleeper ends creating negative bending moment. The maximum negative bending moment was again observed at the rail seat centre when the wheel load passed through the longest turnout sleeper.
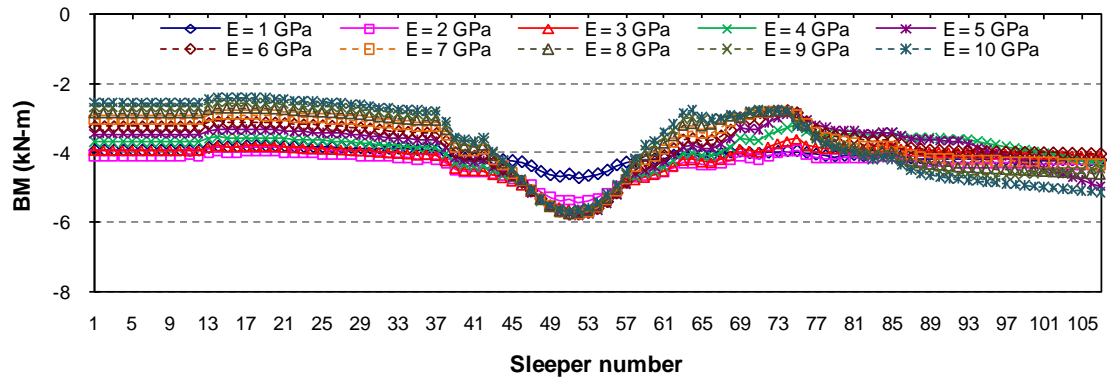

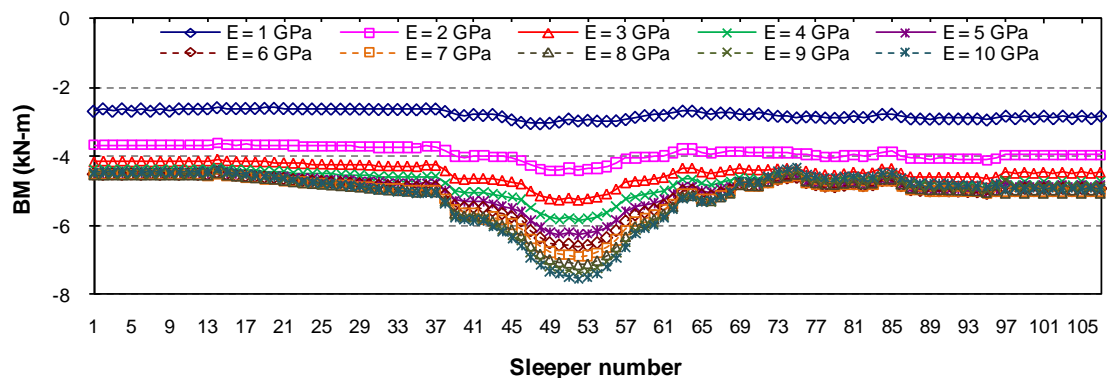Figure F.5 Negative bending moment on turnout sleepers when $U_s = 10$ MPa

Figure F.6 Negative bending moment on turnout sleepers when $U_s = 40$ MPa

At $U_s = 10$ MPa, the negative bending moment in the transition sleepers is around 3.9 kN-m for $E_{sleeper} = 1$ GPa and around 2.5 kN-m for $E_{sleeper} = 10$ GPa (Figure F.5) while the maximum negative bending moment in the turnout sleepers is 4.7 kN-m for $E_{sleeper} = 1$ GPa and 5.7 kN-m for $E_{sleeper} = 10$ GPa. A higher negative bending moment was observed for higher $E_{sleeper}$ when the wheel load was placed after the frog as one end of the sleeper is restrained by the continuous rails while the wheel load is placed on the other end of the sleeper. For lower $E_{sleeper}$, the load is carried mostly by the stiffer rail and not the sleepers resulting in a lower negative bending moment while the higher $E_{sleeper}$ resulted in a higher moment due to the load being carried only by a fewer sleepers. At $U_s = 40$ MPa, a more uniform negative

bending moment was observed for lower $E_{sleeper}$ but a noticeable difference for higher $E_{sleeper}$ (Figure F.6). The negative bending moment on the transition sleepers ranges from 2.7 kN-m to 4.4 kN-m for the different $E_{sleeper}$ investigated. These values of the negative bending moment increases to 3.1 kN-m for $E_{sleeper}$ =1 GPa and 7.5 kN-m for $E_{sleeper}$ =10 GPa when the wheel load entered the switch of the turnout.

Figures F.7 and F.8 show negative shear force in the turnout sleepers for all $E_{sleeper}$ with U_s = 1 MPa and 10 MPa, respectively. The results show that there is no significant difference on the magnitude of negative shear forces in the transition sleepers for both sleeper support moduli. The negative shear forces in the transition sleepers is around 50 kN for U_s = 10 MPa and around 53 to 59 kN for U_s = 40 MPa. After passing the switch, an increasing magnitude of negative shear was observed in the sleepers up to sleeper 68. This negative shear force is around 94 kN for $E_{sleeper}$ = 1 GPa and around 129 kN for $E_{sleeper}$ = 10 GPa. This high magnitude of negative shear force in the sleeper occurs at the sleeper region between the inner rails of the through and the divergent tracks. A decreasing magnitude of the negative shear force was then observed after the wheel load has passed the frog to a magnitude similar to that of transition sleepers before the wheel load enters the turnout.
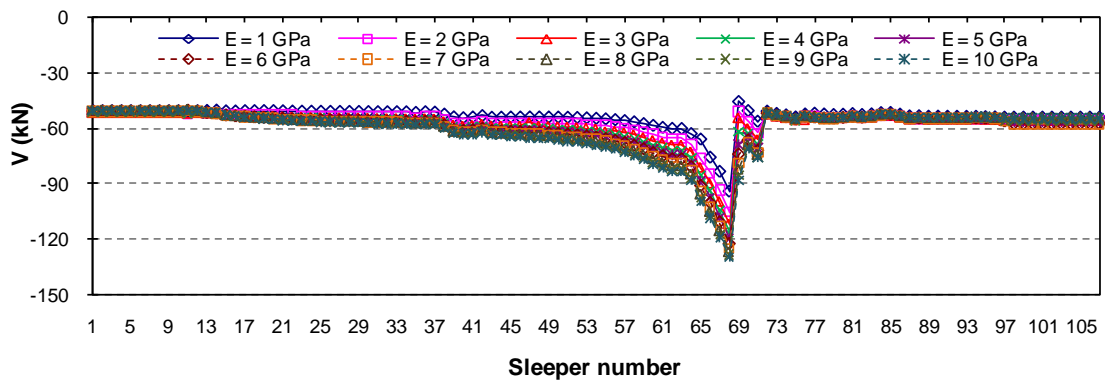

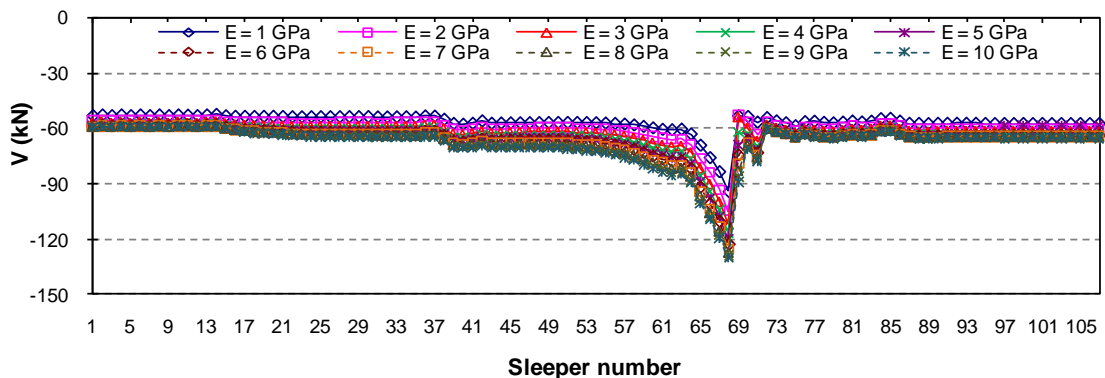Figure F.7 Maximum negative shear on turnout sleepers when U_s = 10 MPa

Figure F.8 Maximum negative shear on turnout sleepers when U_s = 40MPa

F.4 Effects of U_s on negative bending moment and shear

Figures F.9 and F.10 show the influence of the support modulus on the magnitude of negative bending moment in railway turnout sleepers. The results show that there is no significant difference on the values of negative bending moment at lower $E_{sleeper}$ but increases at higher $E_{sleeper}$ for all the investigated U_s. A higher negative bending moment was observed for lower U_s when $E_{sleeper}$ = 1 GPa (Figure F.9). The magnitude of the negative bending moment at the transition sleepers is around 3.93 kN-m for U_s = 10 MPa and around 2.67 kN-m for U_s = 40 MPa while the magnitude of the highest negative bending moment in the turnout sleeper is around 4.74 kN-m for U_s = 10 MPa and around 3.04 kN-m for U_s = 40 MPa. The negative bending moment at the transition sleepers ranges from 2.54 kN-m to 4.46 kN-m when $E_{sleeper}$ =10 GPa (Figure F.10). The negative bending moment on the sleepers increases when the wheel load enters the turnout. The magnitude of the negative bending moment increases to 5.69 kN-m for U_s = 10 MPa to 7.54 MPa for U_s = 40 MPa.
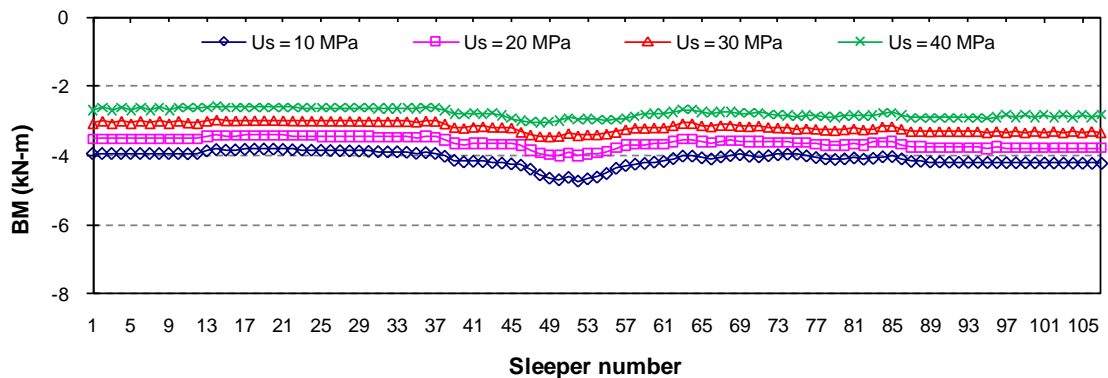

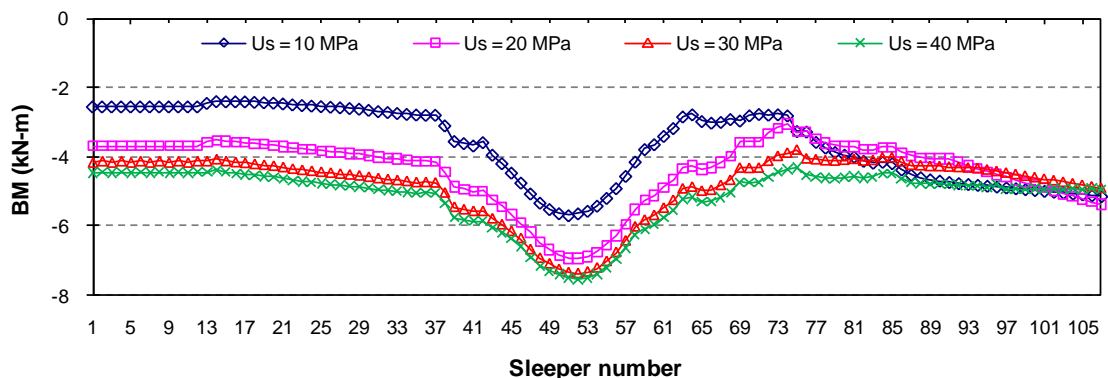Figure F.9 Maximum negative bending moment of sleeper when $E_{sleeper}$ = 1 GPa

Figure F.10 Maximum negative bending moment of sleeper when $E_{sleeper}$ = 10 GPa

Figures F.11 and 7.12 show the results of the FEM analyses on the maximum negative shear force in the turnout sleepers for all U_s considered and with $E_{sleeper} = 1$ GPa and 10 GPa, respectively. The results show that there is no significant difference on the magnitude of the highest negative shear force in all sleeper support moduli investigated. After passing the switch, an increasing magnitude of maximum shear force was observed in the turnout sleepers. In both $E_{sleeper} = 1$ GPa and 10 GPa, the maximum negative shear force occurred at sleeper 68. Figure F.11 indicates that the maximum negative shear at the transition sleepers is around 59 kN while in the turnout sleepers is around 103 kN when $E_{sleeper} = 1$ GPa. The higher modulus of elasticity of the sleepers resulted to the wheel load distributed to only a few sleepers generating a higher shear force to the supporting sleepers. The maximum negative shear at the transition sleepers is around 53 kN while the maximum negative force in the turnout sleepers is around 94 kN when $E_{sleeper} = 10$ GPa (Figure F.12). A decreasing magnitude of the maximum negative shear force was then observed after the wheel load has passed sleeper 68 to a magnitude similar to that of the transition sleepers before the wheel load enters the turnout.
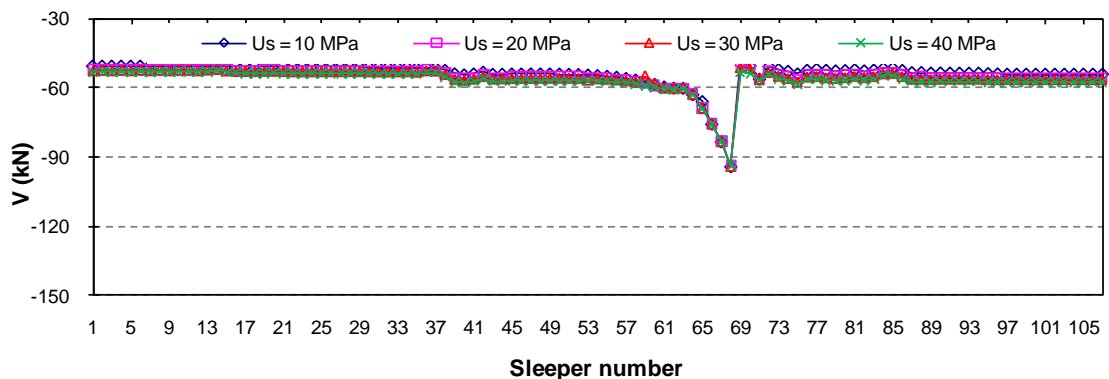

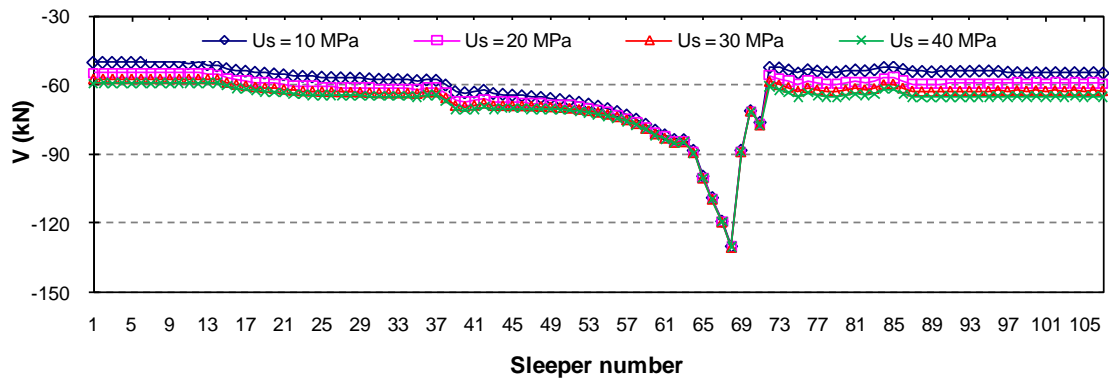Figure F.11 Maximum negative shear on sleeper when $E_{sleeper} = 1$ GPa

Figure F.12 Maximum negative shear on sleeper when $E_{sleeper} = 10$ GPa

Appendix G – Behaviour of new composite sandwich panels

There have been some recent developments in the sandwich panel used in the production of the full-scale glue-laminated sandwich beams in Chapter 8. In Chapters 4 to 6, the investigated sandwich panel has a nominal thickness of 20 mm with fibre composite skins of around 1.8 mm thick while the new sandwich panel in Chapter 8 is only 18 mm thick with 3 mm thick top and bottom skins. Thus, the behaviour of the new sandwich structure was verified to have a reasonable estimation of the failure load and prediction of the behaviour of the full-scale glue-laminated composite sandwich beams. The behaviour in flexure and shear of the individual composite sandwich structures from the new panels are presented in this section.

G.1 Material properties of skins of new composite sandwich structures

The new composite sandwich panel has 2 layers of bi-axial $[0^{o}/90^{o}]$ glass fibres with a chopped strand mat (CSM) and has a total nominal thickness of 3 mm. The CSM was introduced to improve the bonding of the skin to the phenolic core material. The phenolic core material used for both composite sandwich panels has the same mechanical properties. Investigation showed that the skins of the new sandwich panels have similar strength but slightly lower stiffness compared to that of the previous panels. The reduced stiffness of the new skins could be due to the lower stiffness of the fibreglass mat. Table E.1 lists the stiffness and elastic properties of skin of the new composite sandwich panels.

Table G.1 Elastic properties of a 3 mm thick bi-axial glass fibre with mat

Property	Skin
Elastic modulus (MPa)	12,820.51
Tensile strength (MPa)	247.24
Compressive strength (MPa)	201.75

G.2 Flexural behaviour

The new sandwich structures were tested under static 4-point bending following the test set-up in Figure 4.1. The specimens were cut directly from the new sandwich panel with length and width similar to that of specimen 4FSW-II in Chapter 4. The

flexural behaviour of the new sandwich structures both in flatwise and edgewise positions was determined and reported in this section.

G.2.1 Load-deflection behaviour

Figure G.1 shows the typical load and midspan deflection behaviour of the new sandwich structures tested in the flatwise and the edgewise positions. The load-deflection of specimen 4FSW-II in Chapter 4 was included for comparison. In the figure, specimen 4F-18 corresponds to the beam from the new sandwich panels. The results show that the sandwich beams in the flatwise position behaved linearly elastic until failure while the beams in the edgewise position showed a non-linear load and midspan deflection curve due to the progressive failure of the skins. The results also show that the new sandwich beams failed at a significantly higher load than the specimen 4FSW-II. In the flatwise position, the specimen 4F-18-F failed at an applied load of around 5140 N while specimen 4FSW-II-F failed at an applied load of 4534 N. On the other hand, the specimen 4F-18-E failed at an applied load of 7442 N while specimen 4FSW-II-E failed at an applied load of 5567 N. The combination of the thicker skins and core for the new panel resulted in a flexural stiffness similar to that of the previously tested panel with relatively higher strength. Calculating the apparent bending strength and assuming that the composite sandwich beams acted as a solid section suggested that the new sandwich beams have over 30% and 50% higher strength than the previously tested beams in the flatwise and edgewise positions, respectively. This information is used in the theoretical and numerical investigations of the behaviour of the full-scale glued sandwich beams.
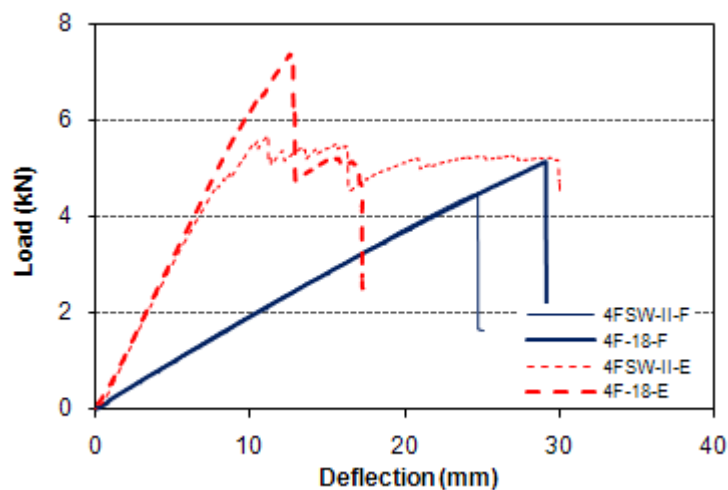

Figure G.1 Load and midspan deflection of new sandwich structures

G.2.2 Longitudinal stress-strain behaviour of fibre composite skins

The longitudinal stress-strain relationship of the topmost and the bottommost skins of the sandwich beam is shown in Figure G.2. In the figure, the stress in the skin was calculated using equation 6.4 while the strains were determined from the strain gauges attached to the composite sandwich specimen. The experimental results show an almost linear stress-strain relation in the fibre composite skins (both in tension and compression) before any failure was observed. At a stress of around 157 MPa and strain of 12200 microstrains, the strain gauge at the tension side of specimen 4F-18-F broke indicating the development of flexural cracks in the core material. The specimen then failed at a compressive stress of 205 MPa and a strain of around 16000 microstrains. On the other hand, the failure in specimen 4F-18-E was initiated at a stress of around 200 MPa due to compressive failure of the skin. However, the sandwich beam continued to carry load up to a stress of around 238 MPa, which is almost similar to the failure strength of the fibre composite skins in tension. Thus, it was concluded that the sandwich beams tested in the flatwise position will fail due to compressive failure of the skin at a stress level of around 200 MPa while failure of the sandwich beam in the edgewise position occurs when the tensile stress at the bottommost skin layer reaches 240 MPa. These failure stress limits were used in both the theoretical and numerical strength predictions of the full-scale glued composite sandwich beams.
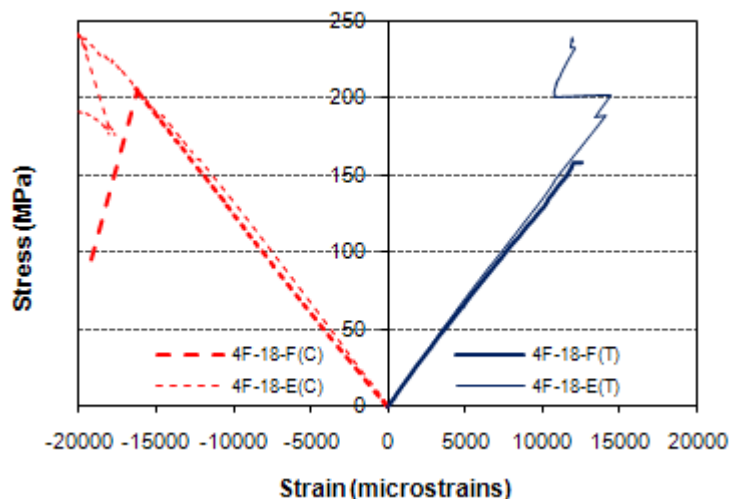

Figure G.2 Stress-strain behaviour of new sandwich structures in flexure

G.2.3 Failure behaviour

Similar failure behaviour was observed on the new sandwich structures to that of the specimen 4FSW-II. The specimen 4F-18-F failed due to the compressive failure of the fibre composite skins (Figure G.3a) while tensile cracking of the phenolic core was observed at the lower level of applied load for specimen 4F-18-E. The vertical fibre composite skins on the other hand prevented the crack width from increasing to cause failure. The specimen failed progressively due to the compressive failure of the skin followed by the tensile failure of the fibre composite skin (Figure G.3b). These observed failure behaviours were considered in the prediction of the structural behaviour of the full-scale glue-laminated composite sandwich beams.
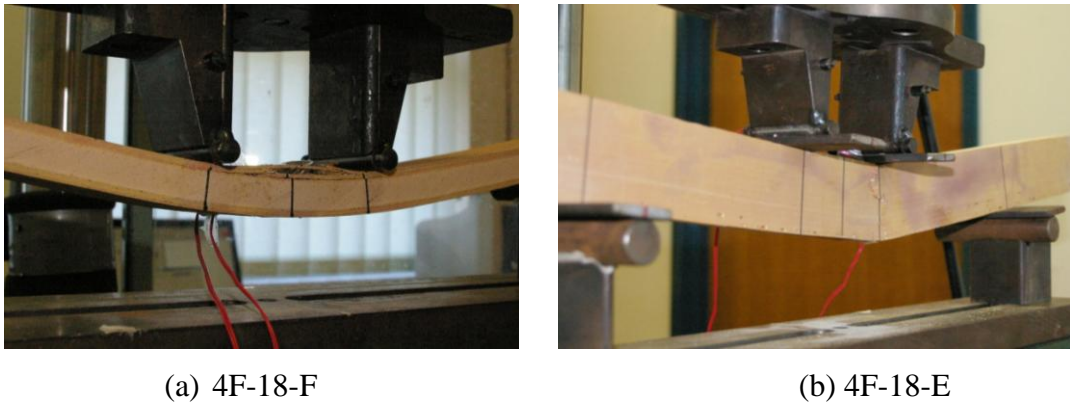

(a) 4F-18-F   (b) 4F-18-E

Figure G.3 Failure behaviour of new sandwich structures in flexure

G.3 Shear behaviour

The shear behaviour of the new sandwich structures was determined under asymmetrical beam shear test. In this section, the shear strength and failure mechanisms of this sandwich structure were presented and comparison with the previously investigated sandwich panels was made.

G.3.1 Load and crosshead displacement behaviour

The typical load and crosshead displacement behaviour of the new composite sandwich beams (AS-18) under asymmetrical beam shear test throughout the loading regime is shown in Figure G.4. In this figure, the load and crosshead displacement behaviour of the sandwich panels (AS-SW) tested in Chapter 5 is included for comparison. The figure indicates that the applied load on the sandwich beams tested in the flatwise position increases almost linearly with the crosshead displacement of

the testing machine. A sudden drop in the load was then observed indicating the failure of the sandwich beam specimen. For specimen tested in the edgewise position, a linear load-crosshead displacement relation occurred up to the shear cracking of the core material. Before the ultimate failure, significant shear cracks were observed in the fibre composite skins and an increased amount of deflection even without an increase in the applied load.
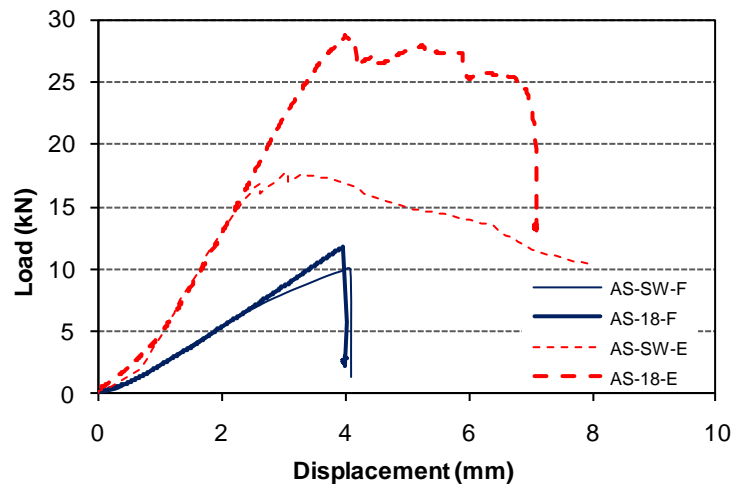

Figure G.4 Load-crosshead displacement relationship of new sandwich structures

As indicated in Figure G.4, the specimen AS-18 failed at a higher load compared to specimen AS-SW. In the flatwise position, the new sandwich panels failed at an applied load of 11.57 kN while the specimen tested in the edgewise position failed an applied load of 28.27 kN. These correspond to a 10% higher failure load in the flatwise position and over 60% higher failure load in the edgewise position than specimens AS-SW. The higher failure load is expected for the new sandwich panel as it has thicker fibre composite skins compared to the previously tested sandwich panels. However, the results indicate that the effective modulus of rigidity is similar for both specimens AS-18 and AS-SW. This information suggests that the shear modulus of the fibre composite skins of the new sandwich panels can be estimated by correlating it with the shear properties of the previously tested sandwich structure. Furthermore, the results verified that there is no significant difference in the mechanical properties of the phenolic core material for both composite sandwich structures as failure load and the type of failure is similar.

The shear modulus of the fibre composite skin of the new sandwich panel was estimated using equation 5.5 for effective modulus of rigidity as suggested by APA

(1995). The calculation gives an effective shear modulus of around 1574 MPa. Based on the failure load of the new sandwich beams tested under asymmetrical beam shear in the edgewise position, it was also estimated that the shear strength of the skin material is approximately 27.8 MPa These effective properties of the fibre composite skin in shear were used in the analytical and numerical evaluations of the behaviour of the full-scale composite sandwich beams.

G.3.2 Failure behaviour

Figure G.5 shows the failure behaviour of the new composite sandwich panels under asymmetrical beam shear test. In specimen AS-18-F, the sandwich beam failed in a brittle manner due to shear failure of the core followed by debonding between the skin and the core (Figure G.5a). In specimen AS-18-E, the sandwich beam failed due to progressive shear failure of the fibre composite skins (Figure G.5b). The different failure behaviour of sandwich beams in the flatwise and the edgewise positions demonstrates the necessity of considering this behaviour in the evaluation of their failure strength. Since similar failure behaviour was observed for specimen AS-18 to that of specimen AS-SW, it was concluded that the proposed theoretical prediction of the strength based on the shear properties of the constituent materials in Chapter 5 can be used in the estimation of the failure load the full-scale glue-laminated composite sandwich beams.
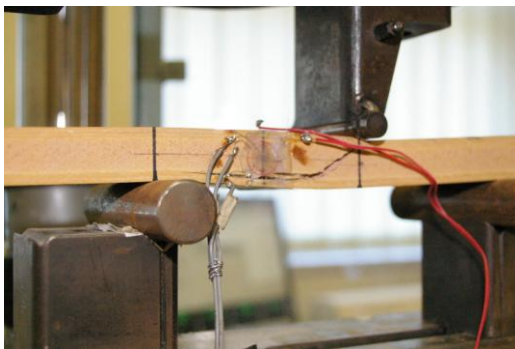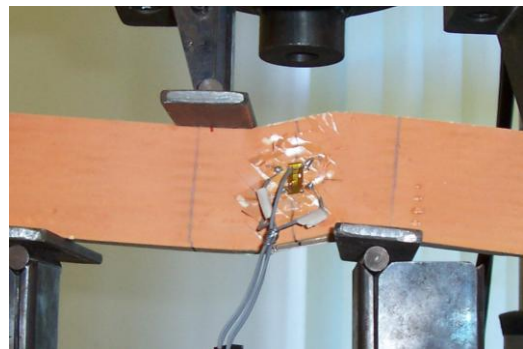
| (a) AS-18-F | (b) AS-18-E |

Figure G.5 Failure behaviour of the new sandwich structures in shear

Appendix H – Screw holding capacity of glued sandwich beams

The low pull-out force of the mechanical connection in most fibre composite sleepers is considered the most likely reason for sudden catastrophic failure of the track system with composite sleepers due to derailments (Lampo et al., 2003). Thus, the pull-out capacity of screw spikes on the full-scale glue-laminated composite sandwich beams in Chapter 8 is investigated in this section.

Moody et al. (1999) suggested that some of the most persistent difficulties in the used of sandwich structure are caused by the necessity of introducing inserts and connectors. While the innovative composite sandwich structure used in this study have high specific stiffness and strength, most sandwich structures have weakness related to joining. The core of sandwich structure is normally light, soft and weak in order to lessen the weight. Accordingly, it cannot support mechanical joints such as screws and spikes. Song et al. (2008) reinforced the core of a sandwich structure with potting materials and inserts to sustain the mechanical fasteners. In their study, aluminium insert and Hysol EA9394 was used as insert potting material. This localised strengthening increased the rigidity of the sandwich beams, but the addition of high stiffness inserts complicates the manufacturing process of the sandwich structure. Similarly, this approach is difficult for turnout application as the location of the spikes and screws vary within the sleepers. Apparently, not much information has been collected to date on the fastener pull-out force for composite railway sleepers (Lampo et al., 2003). There is a need therefore to determine if the glued composite sandwich beams have adequate resistance to hold rail spikes and screws.

H.1 Test of mechanical fasteners

Preliminary investigation on the holding resistance of the glue-laminated composite sandwich beams to a 24 mm diameter and 165 mm long 'R' type screw-spike is evaluated through direct withdrawal test. Clearance holes measuring 17 mm in diameter were drilled through the depth of 100 mm into the specimens. The screw spikes were then screwed into these holes until the clearance under the head was approximately 45 mm. A loading head and jig was used to pull-out the screw spikes from the sandwich beam specimens. Figure H.1 shows the test set-up and the position of the holes in specimen for the screw-spike withdrawal resistance.
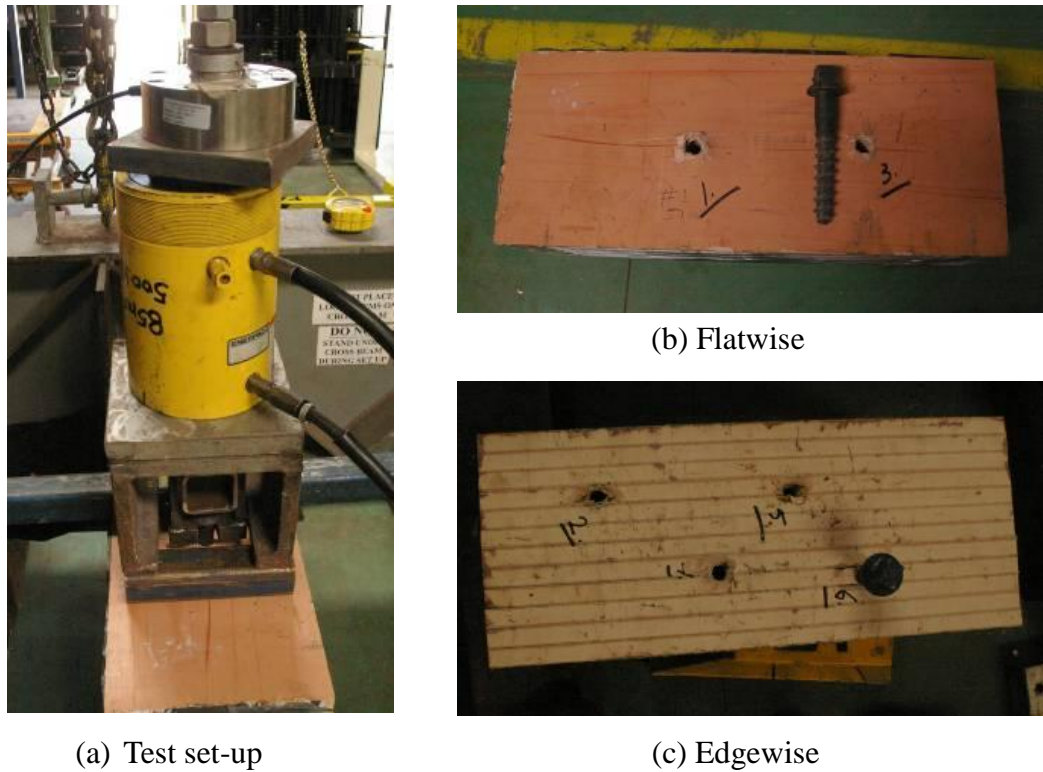
(b) Flatwise

(a) Test set-up　　　　　　　　　　　　　　　(c) Edgewise

Figure H.1 Test set-up and specimen for screw-spike withdrawal resistance

H.2 Screw-spike resistance

The screw-spikes remained in the specimens throughout the test; however the force simply decreased after reaching the maximum value as the screw spike was pulled out of the specimens. Table H.1 summarises the results of the pull-out test of screw spikes. The screw-spike withdrawal resistance in glue-laminated sandwich beams varies between 62 and 68 kN for those with edgewise laminations and between 60 and 64 kN with flatwise laminations. This shows that the presence of horizontal skins did not significantly contribute to the mechanical holding resistance of the beams. This could be due to the relative thinness of the skin compared to the phenolic core.

Table H.1 Results of the pull-out test of screw spikes

Test number	Sample orientation	Hole location	Peak load (kN)
1	Flatwise	Skin	63.91
2	Edgewise	Core	64.85
3	Flatwise	Skin	60.31
4	Edgewise	Skin	62.61
5	Edgewise	Skin	68.83
6	Edgewise	Core	62.47

H.3 Effect of orientation of sandwich laminations on screw-spike resistance

The results of the test showed that the resistance to hold screw-spike was quite high for both fibre composite turnout sleeper configurations with the level of load to pull-out the screw-spike is almost the same. The main reason could be that this resistance to hold mechanical connections was provided mainly by the core material with minimal contribution from the skin as the fibre composite skin is relatively thin compared to the phenolic core. The results showed that the modified phenolic core material has sufficient strength to hold mechanical connections as the screw-spike withdrawal resistance of fibre composite sandwich sleeper is higher compared to that of the usual Red Oak hardwood sleeper which has only around 38 kN (Chattree et al., n.d.). This is also much higher than the required pull-out force in most fibre composite sleepers of only 15.6 kN (Lampo et al., 2003). Conversely, the high resistance to pull-out screw spikes from glued sandwich beams can address the inability of most composite sleepers to meet the performance requirement for mechanical connections and show that it can provide a comfort level to installing these types of spikes in field trials. However, tests on other types of fastening inserts such as dog spikes and dog screw spikes should be conducted to determine the safest and most reliable railway fasteners to fibre composite sleepers. The method of installation and removal of these railway fasteners are different which may cause splitting and/or damage to the glue-laminated composite sandwich beams. Similarly, dynamic test on these different mechanical fasteners is necessary.